POLYMER/FIBER MODIFIED ASPHALT FRACTURE MECHANISMS AND MICROSTRUCTURE RELATIONSHIPS TO DISTRESSES AND ENVIRONMENTAL FACTORS

By

Edward Burton Scott

A THESIS

Submitted to
Michigan State University
in partial fulfillment of the requirements
for the degree of

MASTER OF SCIENCE

Department of Chemical Engineering

1993

ABSTRACT

POLYMER/FIBER MODIFIED ASPHALT FRACTURE MECHANISMS AND MICROSTRUCTURE RELATIONSHIPS TO DISTRESSES AND ENVIRONMENTAL FACTORS

By

Edward Burton Scott

Asphalt concrete pavements have been showing signs of early distress in areas of thermal cracking, aging, fatigue cracking, rutting, and ravelling/stripping which are diminishing pavement performance. Therefore, the focus of the research in this thesis is a determination of the role of polymer modifiers on the properties of asphalt cement and performance of asphalt concrete. The key to establishing this linkage is a fundamental understanding of the microstructure, morphology, adhesion, locus of fracture, and fracture toughness of polymer modified asphalt (PMA).

Tests were developed for microscopic, image, and fracture analyses enabling microstructural and morphological investigation and examination of crack propagation, fracture mechanisms, and locus of fracture. The general failure mechanisms seen in asphalt specimens through fracture analysis were yielding, crazing causing the formation of microvoids and fibrils, and ultimate failure. Tests have also been proposed for adhesion and fracture toughness evaluation of PMA and polymer modified asphalt cement (PMAC).

To my patient and loving wife, Debra Lynn,

and

in loving memory of my God Father, Ron Dean,

December 6, 1946 - September 28, 1992.

ACKNOWLEDGEMENTS

This thesis would have be unattainable if it were not for the help of many others. I, the author wish to thank the many University Staff, CMSC Staff, and fellow graduate students for those invaluable bits of information given. Special thanks goes to my wife, and Jeff Shull on their comments for improvement. I wish to thank my committee Dr. Lawrence Drzal, Dr. Martin Hawley, and Dr. Gilbert Baladi for their time at inopportune moments, and a truly special thanks to Dr. Drzal for his many comments, guidance, and abilities that have helped me develop and grow with an understanding of research and development.

Portions of this work were supported by the Michigan Department of Transportation.

TABLE OF CONTENTS

LIST OF TABLES

LIST OF FIGURES

Chapter One

Introduction

Our nation's, as well as the State of Michigan's, infrastructure of asphalt concrete pavements are showing signs of early distress. New goals for the Federal and State Departments of Transportation are to increase the performance and lifetime of asphalt concrete pavements, thereby, reducing the overall cost. In recent studies from the Strategic Highway Research Program (SHRP), there has been an indication that polymer modification of asphalt with the proper additives will increase the performance and lifetime of asphalt concrete pavement.

Asphalt cement is primarily a mixture of hydrocarbons left over from the refining of crude oil. It is characterized as a black liquid having a high viscosity that changes with temperature. Since asphalt is made up of the last remaining fractions of processed crude oil significant variations are possible in asphalt cement. Each of these differences complicate the selection of polymeric compatible modifiers since being able to find one compatible modifier for one asphalt type does not necessarily mean it will work for another asphalt type.

Asphalt cement mixed with aggregate forms asphalt concrete. Therefore, the mixture is a composite made of asphalt cement, aggregate, and various added modifiers. Modifiers are added to alter or enhance desirable properties in asphalt concrete to overcome asphalt pavement distresses.

The prevalent pavement distresses found in asphalt are thermal cracking, aging,

fatigue cracking, rutting, and ravelling/stripping. The main causes for pavement distresses are summarized in Table 1.1. Thermal cracking can be the result of three fracture mechanisms. Materials having different coefficients of thermal expansion lead to strains that cause crack failure. The presence of water in voids and existing cracks causes fracture upon freeze/thaw cycling during Michigan winters by expanding and increasing crack propagation. Asphalt concrete becomes brittle in cold weather being more susceptible to fracture initiation and cracking with applied load. Aging has a similar embrittlement effect from oxidation and evaporation of increasing the viscosity in the top layer allowing fracture by load and environmental effects [1].

Table 1.1 - Pavement Distress

Thermal Cracking	-	fracture due to coefficient of thermal expansion (CTE) differences
	-	fracture due to H_2O freeze/thaw cycling
	-	fracture due to low temperature embrittlement
Aging	-	fracture caused by embrittlement
Fatigue Cracking	-	fracture due to tensile failure
Rutting	-	microstructural rearrangement due to asphalt plasticity under load
Ravelling/Stripping	-	adhesive fracture due to low adhesion

Fatigue cracking is failure due to tensile stresses. The failure is initiated at the bottom of the asphaltic layers where the tensile strain is the greatest. Rutting is a failure due to the microstructural rearrangement of the aggregate and asphalt cement due to

plastic deformation under load. Modifiers can help stabilize the mixture reducing the deformation. The last distress, ravelling/stripping is a failure due to loss in the adhesive strength of the bond between the aggregate/fiber/rubber particle and asphalt cement. Polymer modification offers the possibility of increasing and optimizing the adhesion; thus, reducing failure during initiation and propagation.

The desired properties that polymers and other modifiers offer to overcome asphalt distresses are dependent on the modifiers used. The desired properties are reduced creep at high temperatures, less brittleness at low temperatures, better impact properties at intermediate temperatures [2], increased toughness, higher elongation (ductility), increased adhesion and cohesion, higher moisture resistance, less temperature susceptibility, to increase mix viscosity allowing for the use of softer asphalts, and reduced apparent age hardening. Polymers themselves may modify the binder properties through the complex modulus, ductility, temperature susceptibility, air permeability, adhesion at the interface, and cohesion while fibers and particles offer improved properties of the asphalt concrete through their bulk properties.

In most cases the complex modulus of the binder, G*, is the most useful parameter to characterize the asphalt binder. The complex modulus can be broken down into two components; elastic modulus, G', and viscous modulus, G". G' and G" at the crack tip in asphalt concrete characterize the fracture and deformation possibilities. In modifying the asphalt with polymers, G' and G" change. Polymers can increase the elastic modulus, G', which is important at low temperatures to stop fracture by absorbing energy elastically. Polymers can also increase the viscous modulus, G", at high temperatures leading to a decrease in rutting.

The aggregate is another very important aspect of the asphalt concrete. Course aggregate should be crushed stone so the compacted aggregate structure in the roads will support applied loads. The fine aggregate may be natural sand, but if heavy traffic is expected manufactured sand with cleaved edges should be used. This also allows the fine aggregate to help support the load and reduce rutting. The gradation of the aggregate should follow a smooth curve above or below, and not criss-crossing a 0.45 power gradation chart [3].

The effect of voids (size, distribution, and density) is also an important aspect in pavement performance. Void microstructure and morphology relates to initiation of crack failure and crack propagation.

Performance of asphalt concrete is ultimately judged based on failure criteria. A review of the morphological literature on asphalt concrete suggests that the main root of pavement distress is fracture by various mechanisms. Polymer, fiber, and rubber particle modifiers have the capability to affect asphalt concrete failure by altering the mechanisms of fracture initiation and crack propagation. Therefore, polymer modification could be the key to successfully creating a better pavement through enhancement of asphalt concrete properties.

Asphalt modifiers can be catalogued into five types: dispersed thermoplastic polymers, network thermoplastic polymers, reacting polymers, polymeric and organic fibers, and rubber particles. Based on the microstructure of these five types, the polymer modified asphalts can be catalogued into three morphological types: Type H, Type F, and Type P. Type H refers to homogeneous asphalts, such as dispersed thermoplastic polymer modified asphalts, network thermoplastic polymer modified asphalts, and reactive polymer

modified asphalts. Figure 1.1 is a drawing of type H polymer modified asphalt (PMA). Type F refers to fiber modified asphalts and Figure 1.2 is a drawing of type F PMA. Type P refers to rubber particle modified asphalts and a drawing of this type is shown in Figure 1.3.

To summarize, polymer/fiber/particle modification may be beneficial in alleviating the prevalent pavement distresses found in the State of Michigan's infrastructure of asphalt concrete pavements. Modifications have shown better fatigue cracking resistance, permanent deformation resistance, lower temperature susceptibility, thermally induced cracking resistance, improved impact resistance, less run-off in open-graded mixes, less moisture sensitivity, and reduced apparent age hardening in asphalt pavements. These modifications change the binder properties effecting microstructure, morphology, adhesion, and fracture properties, thereby, effecting the pavement performance.

The focus of the research in this thesis is a determination of the role of polymer modifiers in the properties of asphalt cement and performance of asphalt concrete. The key to establishing this linkage is a fundamental understanding of the microstructure, morphology, adhesion, and fracture of polymer modified asphalt. Chapter Two presents a review of the literature including: the molecular make up of asphalt showing the significant chemical variations; asphalt modifier classification; concepts of adhesion; morphology and microstructure of polymer modified asphalt; pavement distresses; and fiber toughening in fracture and failure modes. Chapter Three covers the five categorized types of polymer modified asphalts, three categorized microstructure modified asphalts, crack growth mechanisms, relates the need for microscopic testing, and presents fracture toughness related to asphalt concrete. Chapter Four presents the sample preparation,

PMA Microstructure TYPE H

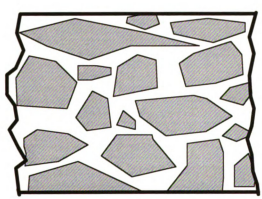

Conventional Aggregate
Acceptable Void Content
Homogeneous Asphalt
Polymer Modifiers
Dispersed Thermoplastics
Network Thermoplastics
Reactive Polymers

PMA is HOMOGENEOUS in Microstructure at the MICROSCOPIC LEVEL

Figure 1.1 - Type H PMA Microstructure

PMA Microstructure TYPE F

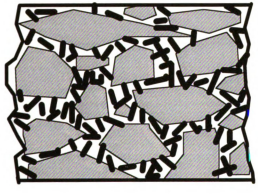

Conventional Aggregate
Acceptable Void Content
Homogeneous Asphalt
FIBERS
Polymer
Inorganic

FIBERS are UNIFORMLY dispersed throughout the Asphalt phase.

Figure 1.2 - Type F PMA Microstructure

PMA Microstructure TYPE P

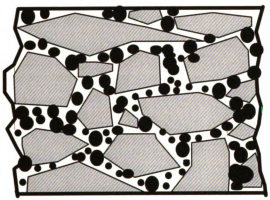

Conventional Aggregate
Acceptable Void Content
Homogeneous Asphalt
Dispersed Rubber Particles

PMA has Rubber Particles UNIFORMLY dispersed throughout the Asphalt phase.

Figure 1.3 - Type P PMA Microstructure

mechanical testing, microscopic crack analysis, and image analysis of voids including data refinement. Chapter Five presents current results for morphological and microstructural analysis, image analysis, crack propagation, and microscopic analysis for straight asphalt concrete. Chapter Six proposes future experimentation for the study of polymer modified asphalt concrete in the areas of adhesion and fracture toughness. Chapter Seven recommends characterization and evaluation tests for polymer modified asphalt cement (PMAC) and polymer modified asphalt concrete (PMA).

Chapter Two

Review of the Literature

Microstructure, morphology, adhesion, and fracture of polymer-asphalt-aggregate mixes and the mechanisms by which the addition of polymer, fiber, and particle additives to asphalt concrete improve the mix properties, hence the pavement performance has been reviewed. Additional potential beneficial property improvements such as crack blunting and microcrack toughening mechanisms have been identified to be brought about by the addition of polymer, particulate polymers, and/or fibrous materials to asphalt.

One important rule that does not change even with polymer modification is: "A pavement is only as good as the materials and workmanship that go into it [4]."

2.1 Molecular make up of asphalt

Asphalt cement is primarily a mixture of hydrocarbons left over from the refining of crude oil. It is characterized as a black liquid having a high viscosity that changes with temperature. Since asphalt is made up of the last remaining fractions of processed crude oil significant variations are possible in asphalt cement. Table 2.1 contains elemental analyses of different asphalt cements differing primarily in their viscosity each a little different from the other. Each of these differences complicate the selection of polymeric compatible modifiers since being able to find one compatible modifier for one asphalt type does not necessarily mean it will work for another asphalt type.

The average molecular weight of asphalt cement varies from 500 to 5000 grams

Table 2.1 - Elemental analysis of asphalt cements [5].

	AC-5	AC-10	AC-20
Carbon, %	85.7	82.3	84.5
Hydrogen, %	10.6	10.6	10.4
Oxygen, %	---	0.8	1.1
Nitrogen, %	0.54	0.54	0.55
Sulfur, %	5.4	4.7	3.4
Vanadium, ppm	163	220	87
Nickel, ppm	36	56	35
Iron, ppm	---	16	100
Aromatic C, %	32.5	31.9	32.8
Aromatic H, %	7.24	7.12	8.66
Molecular Weight (Toluene)	570-890	810-930	840-1300

per mole [5]. Figure 2.1 is a typical representation of an asphalt molecule which contains linear and complex organic ring structures. The ring structures are generally naphthenic and aromatic. Naphthenic compounds are simple or complex saturated rings that have a large number of side chains. Aromatic compounds are heavier molecules that consist of stable six atom rings with few side chains [6].

Asphalt has also been represented by a two phase model. Figure 2.2 shows the model as a combination of asphaltene/resin/oil. Asphaltenes are the highest molecular weight compounds with aromatic ring structures, a few side chains, a carbon/hydrogen ratio greater than 0.8, and form one phase of the model. Oils are the second phase with the lowest molecular weight materials containing large numbers of side chains and a few rings. Resins are polar molecules enabling the two phases to be held together. These resins are intermediate molecular weight compounds with a carbon to hydrogen ratio

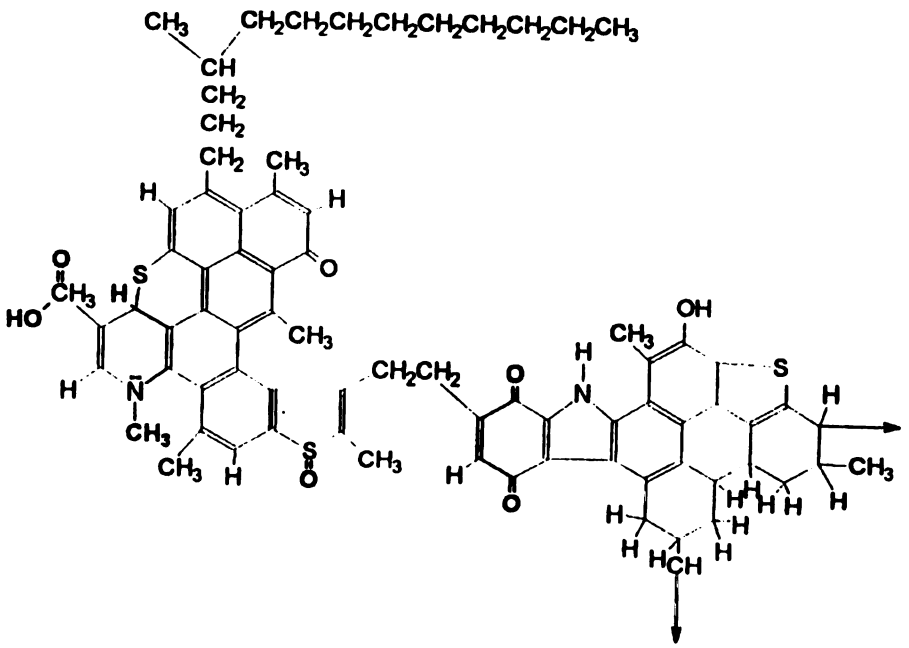

Figure 2.1 - Theoretical structure of an asphalt molecule [6].

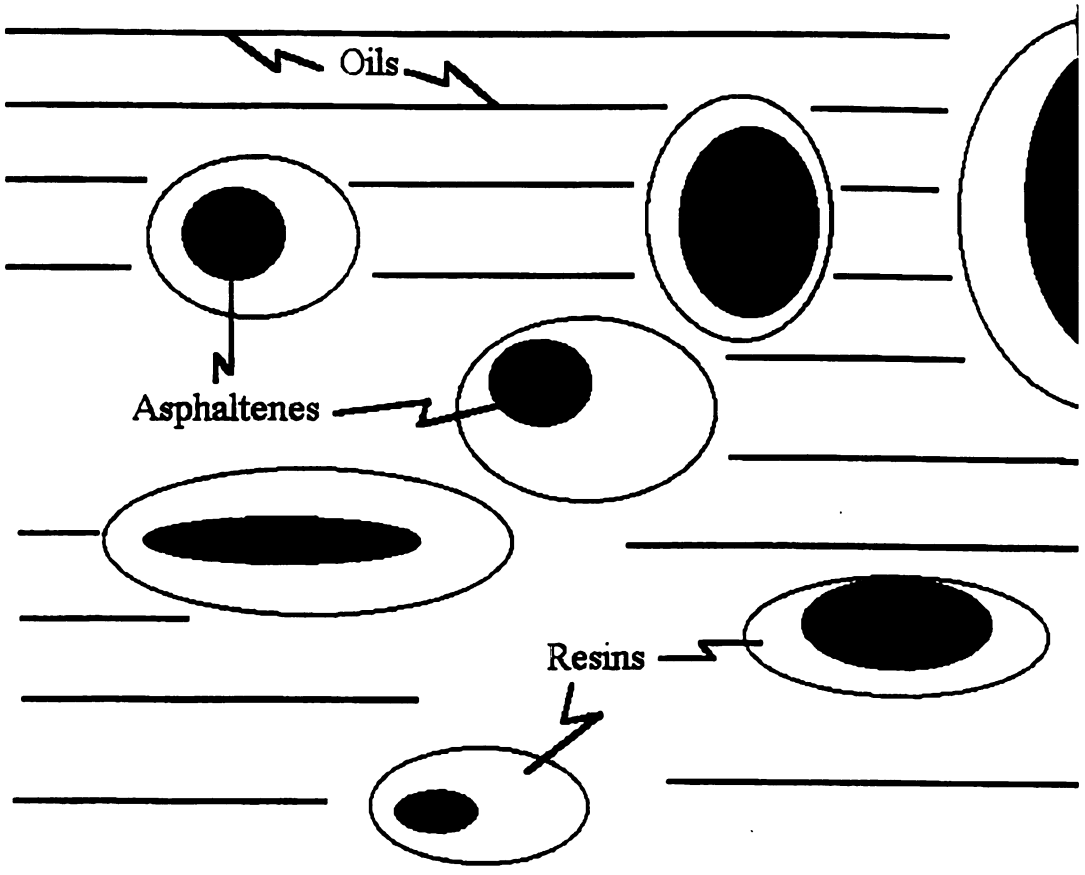

Figure 2.2 - Two Phase Asphalt Model, phase 1 = asphaltenes + resins (assemblies), phase 2 = oils (solvent) [6].

between 0.6 and 0.8. The model depicts the asphaltenes and resins forming assemblies in one phase and the oils as the solvent and second phase [6].

2.2 Microstructural effects of modifiers in asphalt

2.2.1 Modifier classification

Inorganic and polymer modifiers for asphalts can be categorized into five types; dispersed thermoplastic polymers, network thermoplastic polymers, reacting polymers, polymeric and inorganic fibers, and rubber particles. These five types have been reviewed and descriptions of each with examples are presented.

2.2.2 Dispersed thermoplastic polymers

Dispersed thermoplastic polymers behave like asphaltenes, the high molecular weight compounds in asphalt that increase the viscosity and give resilient properties. Normally dispersed thermoplastic polymers require peptizing agents, like resins mentioned in the introduction, to stabilize the modified systems. These resins are polar molecules that enable the dispersed thermoplastic polymers to be stabilized in the oils of asphalt, thereby not coalescing. Dispersed thermoplastic polymer concentrations can also be increased to form a network structure. The formation of a network structure in asphalt concrete increases the capabilities for relief from pavement distresses by allowing energy and load transfer to the network, therefore giving the greatest pavement performance benefits when a network is present. Usually, a considerable amount of thermoplastic polymer, six percent or more, must be added before a macrostructural network forms.

Dispersed thermoplastic polymer modifiers that improved low temperature susceptibility of asphalts include ethylene acrylic copolymer [7], hydroxylterminated polybutadiene (HTPB) [8], and polypropylene wax (PPW) [8]. Those modifiers that improved the fatigue cracking resistance included hydroxylterminated polybutadiene (HTPB) [8], and polypropylene wax (PPW) [8]. When polyethylene (PE) was used to modify AC-20 asphalt, the modified binder had higher resistance to permanent deformation and thermal cracking [8-10].

Previous studies show PE to have the best performance for the dispersed thermoplastic polymer modified asphalts, but PE can also coagulate and separate easily if not handled properly. For example, PE will coagulate and separate from the asphalt phase in half an hour at 160°C after mixing stops if no stabilization technique was introduced. This instability comes from a low glass transition temperature range for PE from -130°C to -15°C allowing it to behave as fluid and its insolubility in asphalts. A commercial company called Novophalt has circumvented the problem of coagulation and separation by having the asphalt continually shear mixed in trucks on site until ready for immediate application. Another modified asphalt not yet commercially available called Polyphalt is in the process of being patented. This modified asphalt circumvents the problem by a proprietary stabilization technique.

2.2.3 Network thermoplastic polymers

Network thermoplastic polymers form a network by bonding with themselves throughout the asphalt forming a network when enough polymer is present. In network thermoplastic polymers it generally takes between two to seven weight percent of the

binder to form a network.

Network thermoplastic modifiers that increase the binder resistance to rutting include styrene-butadiene-styrene (SBS) [8, 11-14], styrene-ethylene-butadiene-styrene (SEBS) [12, 13], styrene-butadiene copolymer (SBR) [11, 14, 15], and styrene-butadiene latex [7, 16]. These polymers have also lowered the cracking temperature from 32°F to -10°F. The styrene in the copolymer strengthens the mix and increases the viscosity at high temperatures increasing rut resistance while the butadiene in the copolymer boosts the material's flexibility lowering the fracture temperature [17]. Styrene-butadiene copolymer (SBR) modified asphalt also reduced fatigue cracking [11, 14, 15]. Ethylene vinyl acetate (EVA), ethylene acrylic acid, and acrylic ester copolymers increase the softening point 10°F to 15°F making the asphalt more rigid during hot weather, thus increasing rut resistance [17]. However, ethylene-vinyl acetate (EVA) modified asphalt (AC-20) has displayed increased rutting and fatigue cracking as well as a tendency to produce stripping effects [8, 12, 14, 15, 18]. Stripping is caused by a weakening of the adhesive bond between the aggregate and polymer modified asphalt allowing failure to occur at this interface.

Reviews on previous studies show SBS/SEBS and SBR latex offer the greatest potential benefits and ability to work as asphalt modifiers of the network thermoplastic polymers. SBR modifier is usually used in a latex form, a polymer/water mixture. SBR latex is manufactured at temperatures of 100°F - 110°F with a resulting polymer size of 0.1 micron and an overall solid weight percentage of 31 percent. Mechanical agglomeration is used to concentrate the latex and the final commercial product is 70 weight percent solids with a polymer size of half a micron. Generally, a homogeneous

blend is desired with either polymer or asphalt as the continuous phase. In SBR modified asphalt, asphalt is the continuous phase if SBR concentration is below seven weight percent. Molecular weight distribution and average polymer size in the latex are the two variables that can be adjusted to increase compatibility between asphalts and polymers. When using a SBR modifier, SBR of different molecular weight are used to match asphalts having different properties. Typically, enough latex is added to produce a three to five weight percent solid SBR in the asphalt.

2.2.4 Reacting polymers

Reacting polymers are those that chemically bond themselves to asphalt. This increases the polymer stability reducing the need for continuous high speed stirring and immediate application. The polymers normally chemically bond to the asphaltene molecules and when enough polymer is present a network of continuous polymer will form. Reacting polymers require even smaller quantities of polymer than network polymers to form polymer networks, typically below three weight percent of the binder.

For reacting polymers, epoxy [19] and ELVALOY® AM [20] modified asphalts show reduced rutting, thermal cracking, and temperature susceptibility. Furfural [18, 21] modified asphalts have lower temperature susceptibility, higher resistance to rutting and low temperature cracking, higher freeze-thaw resistance, and better adhesion, but lower cohesion. Maleic anhydride (MAH) [22] modified asphalts have lower temperature susceptibility, higher resistance to rutting and low temperature cracking, and better adhesion, but lower cohesion.

ELVALOY® AM is a reactive thermoplastic polymer containing an epoxide group

that can chemically link to asphalt. ELVALOY® AM is a random copolymer of ethylene, n-butyl acrylate, and glycidyl methacrylate (E/nBA/GMA) [20]. The glycidyl methacrylate monomer contains the epoxide group that can chemically link to asphalt. In the final form of the polymer the epoxide is at the end of a side chain allowing for easy access and reaction with the asphalt. This allows the polymer to form a network and at greater concentrations forms a gel. The recommended network concentration in asphalt mixtures is approximately 2.5 weight percent [23]. Greater concentrations such as three weight percent of the binder have formed gels which cause problems in the equipment. ELVALOY® AM is mixed with asphalt at 350°F in a sealed tank for two to 48 hours to complete the reaction of the epoxy groups with the asphalt constituents. Oxidation is kept to a minimum through the use of the sealed tank [24].

2.2.5 Fibers

Some fibers offer good methods of asphalt concrete modification. Studies show that different fibers offer different sets of toughening mechanisms to strengthen the asphalt composite and slow crack growth including: debonding, pullout, and deformation and failure of the fiber. Fibers act as bridges across cracks where energy is required to extend the cracks to overcome the toughening mechanisms. Fibers also increase the available wetting surface area and behave as binder thickeners which reduces asphalt bleeding and adds fiber toughening mechanisms. Organic fibers offer the largest reduction of crack growth by debonding, pullout, deformation (yielding), and fracture of the fiber. Inorganic fibers reduce crack propagation by debonding, pullout, and fracture, but are the least effective due to smaller surface area and no yielding effect. Aramid (Kevlar) fibers have

been reported to offer good properties as asphalt modifiers, but polyethylene fibers did not due to their low melting temperature (325°F) [25, 26].

Cellulose, mineral, glass, and polyester fibers have been used in asphalt modification [27]. In the study by Peltonen a multiple role was suggested for fibers. It was determined that fibers increase the viscosity and toughness of bitumen mixtures. The elongation of the mix samples and their toughness were analyzed through strain curves. Table 2.2 is a display of the mixes used and the numerical data for Figures 2.2 and 2.3 [27]. Figures 2.2 and 2.3 are graphical displays of the strain curves for the fiber modified asphalts at 7°C and after the samples had been cooled to -10°C and then tested at 7°C, respectively. This data indicates that the polyester fibers gave the best increase in total energy or toughness and the maximum force needed for failure in both cases. Therefore, polyester fiber would be a good reinforcement and offer asphalt a higher strength level. Cellulose fibers also increase the total energy a small amount, but their main role is stability of the bitumen (asphalt cement).

2.2.6 Particles

The current hypothesis for rutting reduction by particles in particle modified asphalts is that particles offer an increased ability to stabilize the asphalt mix and prevent asphalt bleeding. This effect is largely due to the adhesive effects from the particles bonding to the asphalt and being able to transfer energy between the particles and asphalt cement. Particles also take up space between the aggregate reducing the amount of asphalt cement needed and available for bleeding. Particles behave as aggregates if their sizes are large and behave as dispersed thermoplastic polymers if their sizes are small

Table 2.2 - Test results of the elongation tests of the different fiber-bitumen blends [27].

	Sample	Amount (wt%)		Amount (vol%)		Max. Force (N)		Strain at max. stress (mm)		Breaking strain (mm)		Total Energy (N mm)	
#	Temp. (°C)	7	-10	7	-10	7	-10	7	-10	7	-10	7	-10
1	Bitumen	-	-	-	-	52	280	8	7	-	62	17.1	35.8
2	Cellulose 1	5.0	5.0	3.4	3.4	102	230	15	10	42	27	25.0	37.8
3	Cellulose 2	5.0	5.0	3.4	3.4	92	220	16	8	32	27	17.0	32.8
4	Cellulose 3	5.0	-	3.4	-	130	-	17	-	35	-	30.0	-
5	Mineral M-P	5.0	-	1.8	-	196	-	8	-	37	-	34.0	-
6	Polyester	5.0	4.6	3.6	3.4	335	530	22	26	27	30	54.4	99.5
7	Mineral M-D2	-	4.0	-	1.7	-	314	-	8	-	27	-	44.3
8	Glass L-W	-	4.0	-	1.7	-	256	-	7	-	18	-	26.9

Legend for Figure 2.3

#	Fiber Modifier
1	straight bitumen B-120
2	cellulose 1
3	cellulose 2
4	cellulose 3
5	mineral M-P
6	polyester

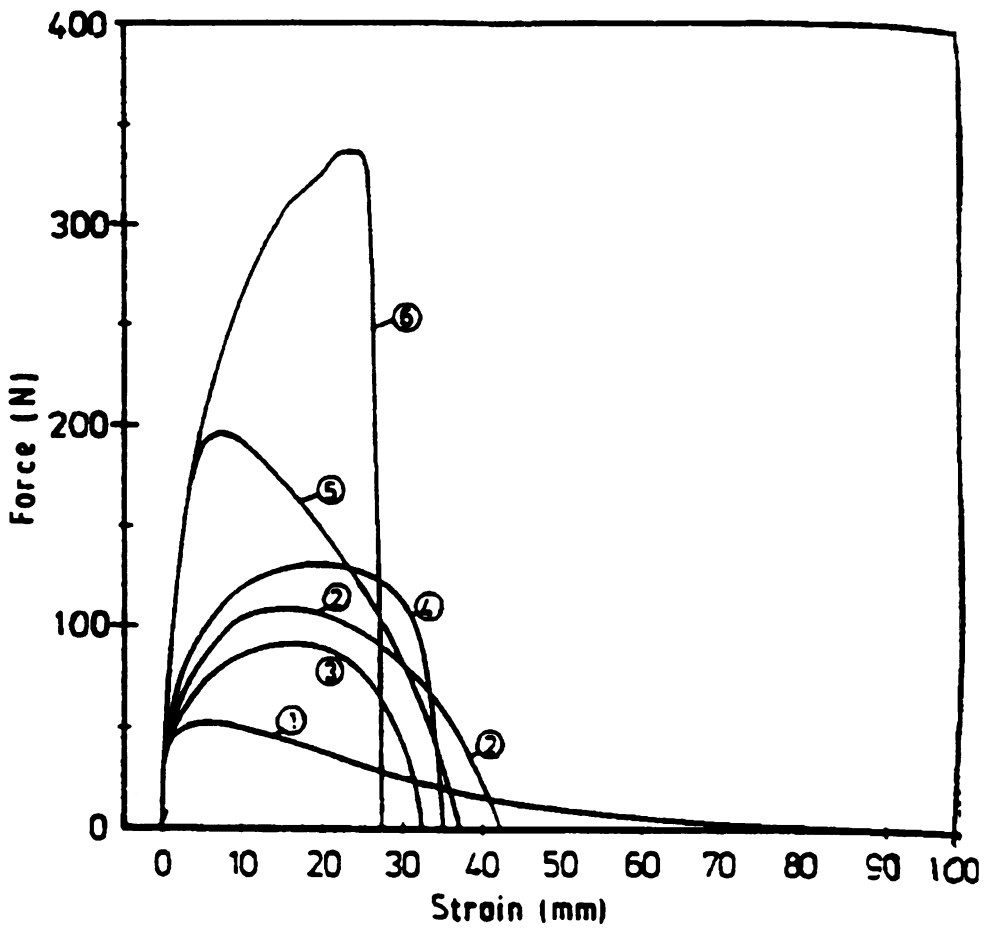

Figure 2.3 - Strain (elongation) test curves of different fiber bitumen blends at 7±1°C [27].

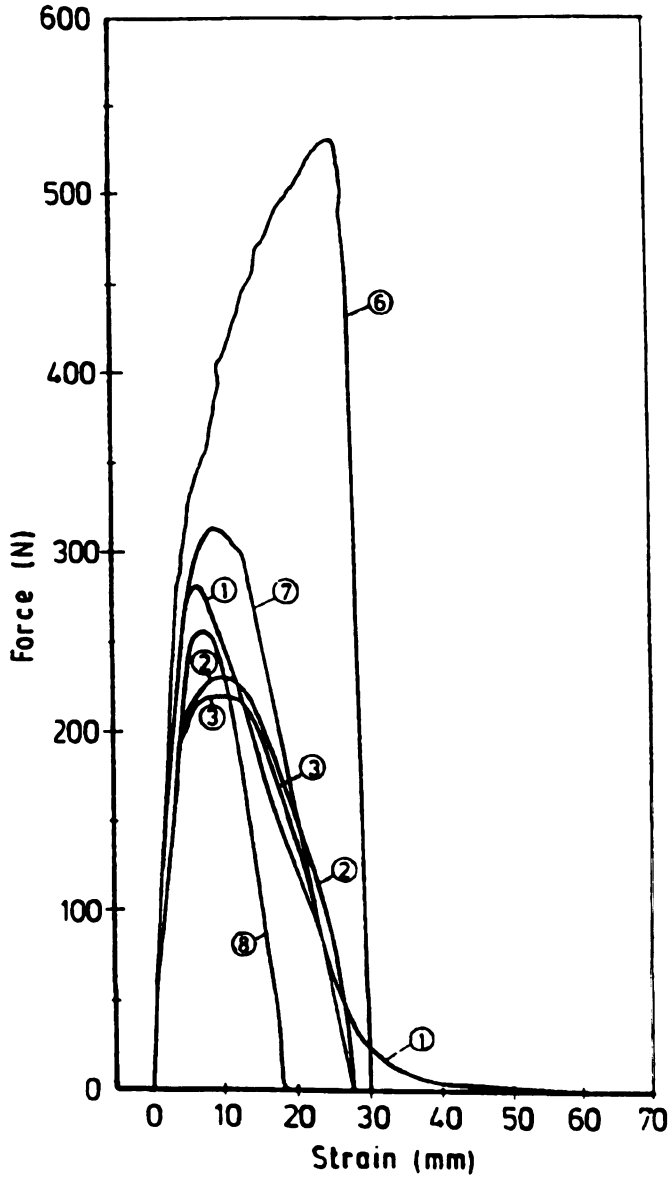

Legend

for Figure 2.4

#	Fiber Modifier
1	straight bitumen B-120
2	cellulose 1
3	cellulose 2
6	polyester
7	mineral M-D2
8	glass fiber L-W

Figure 2.4 - Strain (elongation) curves of the different fiber bitumen composites measured after cooling the blends at -10°C before normal straining at 7°C [27].

(below 100 μm).

In order to relate microstructure to performance, the effects of modifiers need to be understood. Khosla [28] looked at straight asphalt, asphalt with carbon particles, and asphalt with styrene butadiene (SB) polymer. Performance test results showed that the polymer modified asphalt offered the greatest fatigue cracking resistance followed by the carbon particle modified asphalt and then straight asphalt [28]. However, the test results were not related to the fundamental asphalt microstructure. In an earlier study [29], it was also shown that particle (MICROFIL8) modified asphalt lasted longer than straight asphalt.

Carbon black has been used in a great many asphalts with good field results [28-30]. Where as rubber particle modified asphalt concrete has had good pavement performance [31, 32] and bad pavement performance [26, 28, 33]. The bad pavement performance showed severe aging, lower tensile and shear strength, reflective cracking, and ravelling (crumb rubber loss).

Crumb rubber modified (CRM) asphalt does not seem to pose a problem with the standard handling, mixing, or construction practices even though the mix is a little stiffer [34]. But ravelling/stripping of crumb rubber modifier has been a problem [33, 35]. In practice, some CRM modified mixes have experienced a pick up problem during the pneumatic rolling stage. The pick up problem showed characteristics of adhesive failure between the mix and crumb rubber. This problem could be a result of extender oils added to lower the viscosity because CRM stiffens asphalt concrete. Extender oils are commonly used to plasticize rubber polymers making them softer and lowering the melt viscosity for easier processing [36]. The extender oils may also create a thin, low

viscosity boundary layer around the crumb rubber particle giving poor adhesive characteristics, hence a low fracture energy characteristic of adhesive failure. A reaction between rubber particles and asphalt could solve this problem and has been claimed by some, but no reaction has been found between the rubber particles and asphalt [35].

Since, the use of CRM asphalt is being mandated by law the amount of crumb rubber added to asphalt is a concern. In a study [35], it was determined the crumb rubber content should fall below three percent of the mix depending on the size of the particles.

2.3 Microstructural effects of particles in similar composite materials

In other areas of polymer and composites, surface treatments have been used successfully to increase the adhesive bond between materials. One of the possible surface treatments is sulfonation of crumb rubber or polymer particle surfaces. This modification of the surface may enhance the adhesive properties of the CRM, hence increasing the adhesive strength between the CRM and asphalt leading to the elimination of stripping failure.

RT-PMMA is polymethylmethacrylate that has rubber particles of a core-shell structure dispersed throughout. The rubber particles have a core of styrene and butylacrylate copolymer, 241 nm in diameter, grafted to a PMMA shell giving a final rubber particle diameter of 271 nm [37]. Morphological parameters were found to govern the toughness of rubber toughened polymethylmethacrylate. These parameters are: rubber volume fraction, matrix rubber adhesion, particle size, and interparticle distance.

The deformation behavior of rubber toughened polymethylmethacrylate (RT-

PMMA) was investigated with respect to plasticity. The results of two parameters, work-hardening rate, K and critical stress intensity, K_{IC}, show a sharp transition in the materials ability for shear band nucleation from difficult to easy as the critical rubber volume fraction increases. The main deformation mechanism was shear banding at moderate strains and shear rates. The work-hardening rate parameter was developed in a constant strain rate test to be a sensitive method to measure the nonelastic deformation (plasticity) of solid polymers. The measure of this parameter seems very similar to modulus as it is the differential stress over the differential strain. This parameter can then be used to quantify contributions of plastic deformation to toughness.

RT-PMMA exhibits good adhesive bonding [37] and gives hope to higher levels of recycled rubber in asphalt, if a good adhesive bond can be created between the asphalt and crumb rubber. Results showed little to no effect on the materials behavior with rubber particle volume fractions at less than 20 percent after which a large beneficial change occurred which seemed to plateau at 40 percent volume fraction. Testing was performed at 0.05, 0.10, 0.15, 0.20, 0.30, 0.40, and 0.45 particle volume fractions. At the highest particle volume fractions of 0.40 and 0.45 notable shear banding was achieved. This means an increase in the materials ability to nucleate plasticity and increased toughness was achieved [37].

2.4 Morphology of straight and polymer modified asphalt/aggregate mixtures

2.4.1 Networks

Network structures formed in polymer modified asphalts are essential for property enhancement. Previous studies showed that there were no significant improvements in properties of modified asphalt at concentrations below that required to form the network. Because of the different network formation mechanisms, the amount of material required to form a network is a strongly dependent on the modifier type. General concentrations ranges for network formation of dispersed thermoplastic polymers, network thermoplastic polymers, and reacting polymers are greater than six weight percent, two to seven weight percent, and less than three weight percent, respectively. Depending on the paving situation, any of these modifiers may be the appropriate choice, however only limited and inconclusive field data are available. Even though laboratory tests on binders imply improved properties, a model to quantitatively predict field performance and thereby predict the economic benefit of adding modifiers is not available.

Some polymer/asphalt systems, such as polyethylene-asphalt emulsions, form network structures, as shown in Figure 2.5 in which the physical and mechanical properties of the mix are enhanced [9]. This polymer network is known as a spherulitic structure, an intricate structure of molecules that develop forming crystalline and amorphous regions having the microscopic appearance of round objects or spheres. The polymer network is the subject of continuing investigation because it is believed that the network structure is closely related to the pavement performance. The polymer network structure improves creep performance at high temperatures as well as elastic

Figure 2.5 - Spherulitic structure in polyethylene modified asphalt cement [9].

behavior of the asphalt binder (the ability to store deformation energy) [12]. The polymer network may also increase the rutting resistance and high temperature stiffness without losing low temperature flexibility. Literature on dispersed polymers support this hypothesis [10, 38].

2.4.2 Binder characterization

The complex modulus of the binder, G^*, has been studied as an intrinsic parameter to characterize polymer modified asphalt cement [39-41]. The complex modulus, G^* is determined by dynamic mechanical testing. In dynamic mechanical testing, oscillatory strain is applied to a sample which in turn produces a resulting sinusoidal stress which is measured and correlated to the input strain. The complex modulus, G* is obtained by dividing this stress by the strain. G* represents the total amount of energy to deform a material and is the vector sum of G' and G". The storage modulus, G', is the in phase component of the stress obtained by multiplying G* by the cosine of the phase angle. The phase angle is the shift between the sinusoidal stress and strain curves. G' is also proportional to the energy stored in the material elastically. The loss modulus, G", is the out of phase component of the stress obtained by multiplying G* by the sine of the phase angle. G" is also proportional to the energy lost to viscous dissipation.

G* has been used to characterize the amount of polymer in polymer modified asphalts. This technique requires polymer concentration high enough to effect the modulus of the polymer modified asphalt. This polymer concentration is dependent on each specific type of polymer modifier and asphalt cement mixed.

The most significant effect of polymer on asphalt properties seems to be on its

improved elastic behavior. The elastic behavior can be characterized though the use of loss tangent or tan δ values. Tan δ is the tangent of the phase angle between the stress and strain and is represented by the ratio of G" over G'. Polymer modified binders show much smaller loss tangent values at high temperatures than straight (unmodified) asphalts as shown in Figure 2.6 [30]. Smaller loss tangent values show an increase in G', the amount of energy that was stored elastically, thereby, a greater elastic response in the sample being tested. Elsewhere, Bouldin and Collins [2] showed that at 60°C, both the storage modulus, G', and the complex modulus, G^*, of the polymer modified binders are substantially higher than those of the straight binders. These indicate that polymer modified binders have more ability to recover through their elastic storage (higher G'), and are more resistant to permanent deformation (higher G^*) than the straight binders, thereby better rutting resistance than the straight asphalt.

Asphalt-aggregate mixture properties were also tested to verify the binder results by axial dynamic testing [30]. Polymer modified asphalt mixtures proved to have less accumulation of plastic strain under the action of repetitive loading when compared to straight mixes indicating an increase in elastic behavior, thus better rut resistance.

2.4.3 Network formation

Finding the starting polymer network concentration, C*, in amorphous asphalt cement can be done by dynamic mechanical testing when applying Time Temperature Superposition. Time Temperature Superposition is a shifting procedure for stress/strain data done at short testing times, increased frequencies, and higher temperatures to form a complete master curve based on temperature and time relaxation. The master curve is

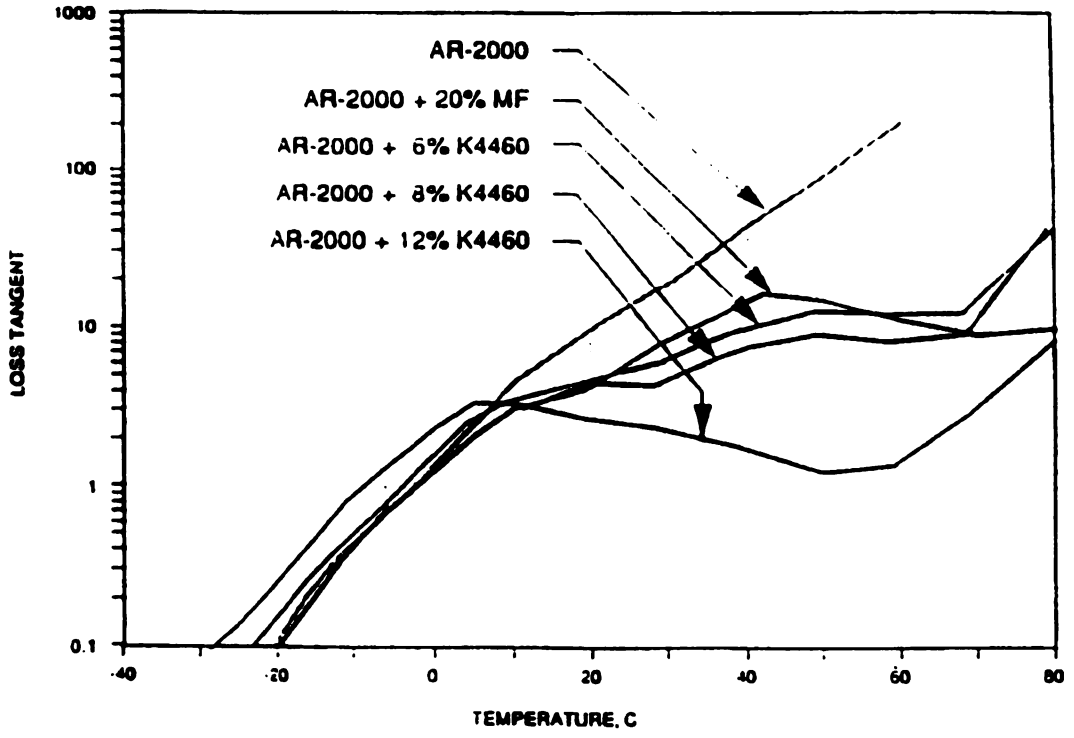

Figure 2.6 - Loss Tangent vs. Temperature (rate-0.1 rad/sec) measured by dynamic mechanical testing shows increased polymer modification lowers the loss tangent [30].

representative of a long time frame at a single temperature. Therefore, long term data can be predicted from short time data obtained at elevated temperatures and frequencies over a short time period. The two principles this theory is based on are Boltzmann Superposition Principle and Time Temperature Equivalence. Boltzmann Superposition Principle states that strain is a linear function of stress allowing all strains to be applied separately and summed together giving a strain that would be equivalent to that of a single stress with all the strain done at one time. Time Temperature Equivalence states that system equilibrium will be achieved more rapidly with an increase in temperature due to the accelerated molecular and segmental motion [42]. The time for this accelerated equilibrium is based on the temperature and relaxation time of the polymer. Generally related through a_T called a shift factor. a_T is a ratio of the relaxation time at a desired temperature to that of the relaxation time at a reference temperature. An empirical representation of a_T in terms of the materials glass transition temperature or a reference temperature has been done by Williams, Landel, and Ferry in the WLF equation [43].

$$\log a_T = \frac{-17.44(T-T_g)}{51.6 + (T-T_g)} \qquad \textbf{2.1 WLF Equation}$$

Despite the molecular structure dependence this equation holds over a temperature range from T_g to 100 K above the materials T_g [43].

Time and temperature affect the viscoelasticity of a material through a_T, but a_T does not vary with response time. Therefore, changes in temperature shift the relaxation times to represent all possible molecular responses of the system. The shift is represented

by multiplying a_T by the frequency, ω, of the test. Thus, putting the two principles together a master curve of long time creep data at a single temperature can be obtained from short time dynamic stress/strain tests done over a range of temperatures and frequencies by superimposing and shifting the data to create a master curve. Figure 2.7 is an example of asphalt data and then shifted data making a master curve is shown in Figure 2.8 [41]. The original data was taken at -28, -23, -14, -10, -5, 0, 5, 10, 20, 29, 39, 50, 60, 69, and 80°C. In making the master curve the original data was moved along the horizontal axis until the regions of modulus overlapped. This type of test is also frequently used in the polymer and adhesive industry [43].

The asphalt industry identifies the starting polymer network concentration, C*, through Time Temperature Superposition. Moduli G' and G" are plotted against log a_T*ω which can be correlated to temperature as previously stated. In straight asphalts, G" is the dominate modulus and G" and G' do not cross, therefore the behavior is dominated by viscous forces all of the time. In polymer modification G' can plateau crossing G". This plateau is indicative of a polymer network and the crossing changes the governing behavior of the asphalt to elastic forces. Figure 2.9, a) shows the straight Deer Park AC-5 where G' and G" do not cross. Both SBR b) and SBS modified c) at four weight percent, respectively, show a crossing of G' and G" curves indicating the start of network formation. Note the region between 65°C and 80°C in c) the four weight percent SBS modified Deer Park AC-5. This region indicates the start of the formation of a polymer network while four weight percent SBR modified Deer Park AC-5 b) has not formed a network at four percent.

Some critical concentrations for the start of network formation, C*, for SBS

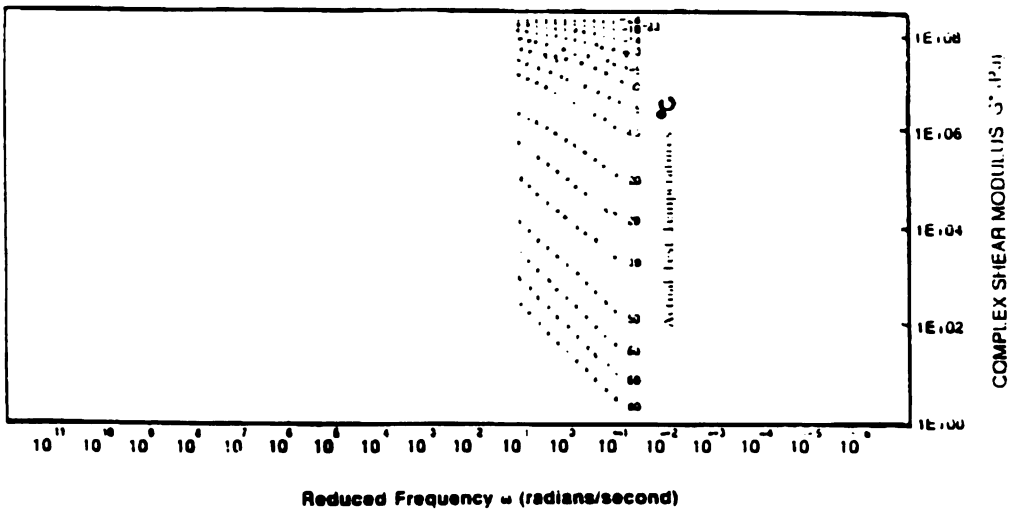

Figure 2.7 - Original asphalt data from frequency sweeps at 16 temperatures [41].

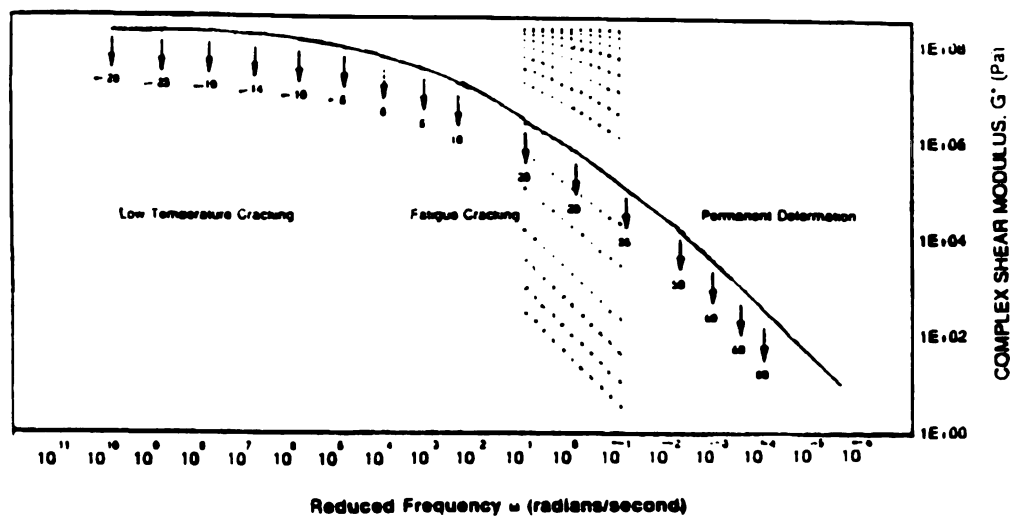

Figure 2.8 - A master curve for asphalt by shifting the data from the original data along the original axis and superimposing them in regions of modulus overlap [41].

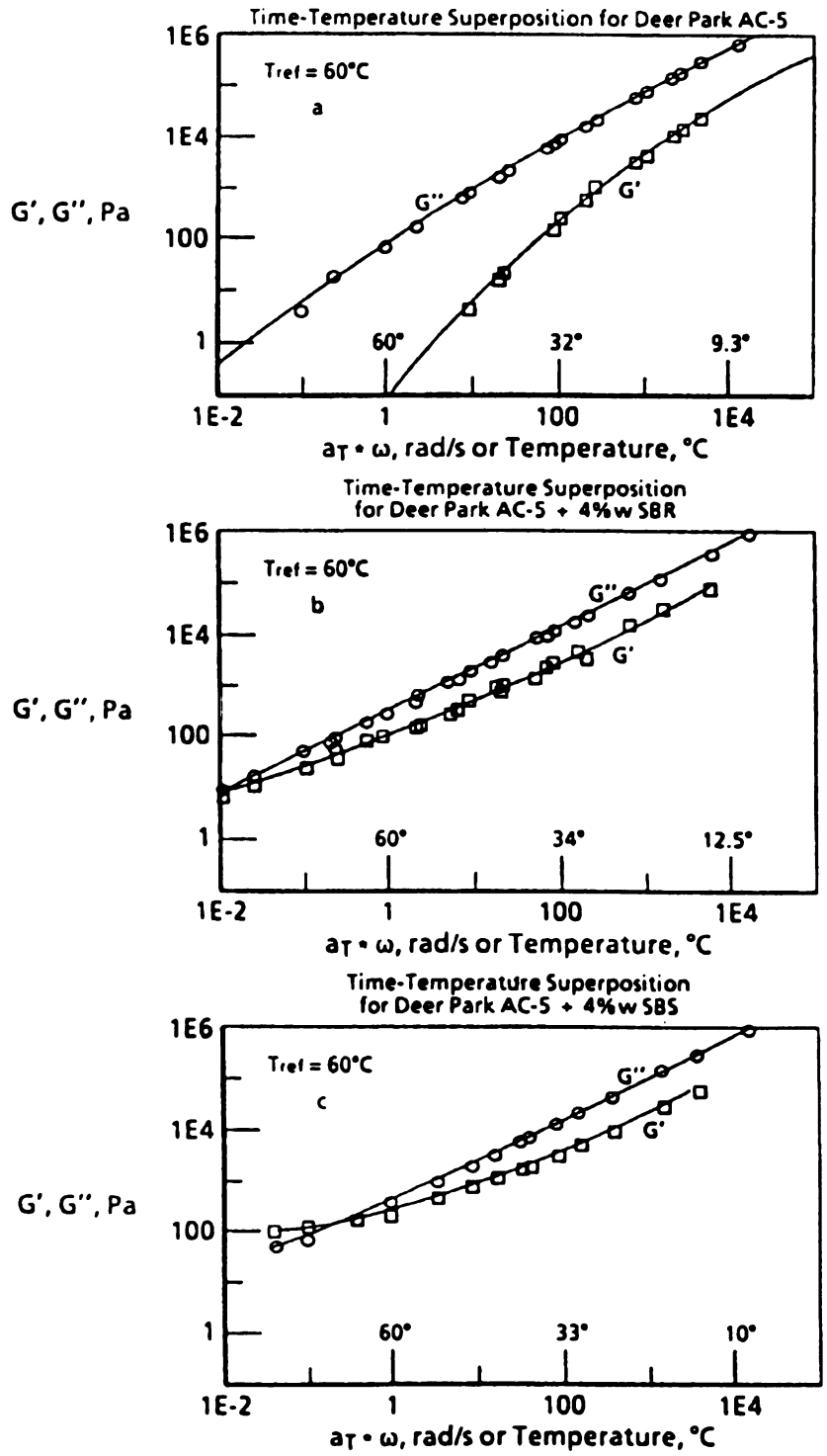

Figure 2.9 - PMA and straight asphalt moduli comparison for network formation [2].

(styrene-butadiene-styrene) and SBR (styrene-butadiene rubber) have been measured in different asphalts and are listed in Table 2.3 [2]. These networks were also identified visually at 50,000 magnification. Lower magnification was insufficient to identify the networks. Collins also claims a polymer network with a micellar structure was formed in EVA (ethylene-vinyl-acetate) modified asphalt [2].

Table 2.3 - Polymer critical concentrations for network formation in various polymer modified asphalt cements [2].

Asphalt	Polymer	C^*, wt %
MAR	SBS	~2
BOS	SBS	>4
DPAC-5	SBS	~3
DPAC-5	SBR	~4

MAR - Shell Martinez asphalt, AR1000
BOS - Boscan asphalt, AC-6
DPAC-5 - Deer Park asphalt, AC-5
SBS - Kraton® D1101, Shell Chemical Company
SBR - SBR latex, Ultrapave 70, Goodyear

2.4.4 Network Stability

At network concentrations however, thermoplastic polymer networks have a potential problem. Gross separation may occur between the two interpenetrating continuous phases resulting in the formation of two separate phases. To prevent separation the network needs to be stabilized. A stable network will increase rutting resistance, decrease low temperature cracking, and elevate tensile strength. Stability can

usually be achieved through modification of the microstructure. Many approaches have been proposed for increasing stability including [2]; adding inorganic or organic fillers, the use of organic gelling agents, using block and random copolymers with greater compatibility, formation of cationic emulsions, polymer oxidation, the use of peptizing agents, steric stabilization by random block copolymers, polymer chlorination, the addition of ester groups to the polymer, and the use of amphifatic block copolymer or comb type graft-copolymers. Of these possible approaches, the most promising solutions appear to be: addition of organic fibers if the small cracks are self healing; steric stabilization by the addition of amphifatic polymers if creaming can be stopped; and steric stabilization with ester groups if the wetting of the aggregate is enough to overcome the disadvantage of the formation of amorphous micellar structures [9]. Amorphous micellar structures are not rigid and will not hold their shape. In steric stabilization, PE coalescence is prevented using a form of steric barrier to keep the particles far enough apart so that Van der Waals attractions can be overcome by thermal forces. The steric barrier must be partially soluble in asphalt and reactive with PE. Stabilizers studied were styrene-butadiene rubber, Kraton G1652, and styrene hydrogenated butadiene-styrene tri-block copolymer.

LDPE (low density polyethylene), a thermoplastic polymer, has been studied as a modifier in a commercial product marketed under the name Novophalt. Novophalt is a biphase binder of LDPE and asphalt blended through a patented high shear blender at the mix site. Separation can be a problem, but if mixed and stored properly LDPE modified asphalt can give good pavement performance. This mixing and storage encompasses the use of huge mixing trucks on construction sites so the asphalt cement and LDPE stay dispersed until lay down. Usually, the smaller the particle size the better

the performance of the polymer modified asphalt [44]. In the laboratory, the optimum polymer content was 4.8 to 5.0 percent of the binder when the particles were below 100 μm. Novophalt was found to offer better resistance to fracture (reflective cracking and thermal cracking). Better durability was also found due to thicker asphalt films that reduce air and water permeability, hence reducing aging and stripping [10]. In another study [38], polyethylene chlorinated to less than 15 weight percent of the polymer and polyethylene maleated to less than four weight percent also gave improved properties. Chlorination and malleation helped stabilize the polyethylene by increasing the compatibility between the polymer and asphalt allowing the beneficial properties of the polyethylene to appear.

Another form of PE modified asphalt will be available as a commercial product in the future under the name Polyphalt. Polyphalt is a stabilized binder of LDPE and asphalt. The process is currently being patented and knowledge of the system and exact means of stabilization has remained proprietary. Research has indicated particles between 1-5 μm in diameter are required for good steric stability [44].

2.5 Morphology through fractography

The morphology of sulfur modified asphalt was investigated through the use of energy dispersive x-ray spectroscopy (EDS) and backscattered electrons (BE) images. Energy dispersive x-ray spectroscopy makes dot maps based on the release of x-rays from the surface after being excited by electrons. In sulfur modified asphalt, the sulfur will release a specific x-ray. The intensity and location of the x-ray emission is converted to

a dot map showing sulfur distribution and morphology. Backscattered electron images show the three dimensional morphology with more clarity. Four fractographs, two from EDS and two from BE of sulfur modified asphalt are presented here. A fractograph is a micrograph of a fractured surface. Figures 2.10 and 2.11 are shown at 118X and Figures 2.12 and 2.13 at 1176X [45]. Figures 2.10 and 2.12 are the energy dispersive x-ray maps showing the sulfur distribution. Figures 2.11 and 2.13 are the backscattered electron images revealing the surface morphology. Figures 2.10 and 2.11 show that the sulfur has formed crystalline faceted needles during their unconfined growth in the void regions. Whereas in the confined regions, spherical sulfur particles were formed as presented in Figures 2.12 and 2.13.

2.6 Microstructural and morphology effects of air voids

The occurrence of air voids in the microstructure is an important aspect of asphalt mixes and its performance as pavement. Low air void content can lead to load sensitive asphalt with a tendency to bleed at high temperatures. Bleeding is the rise of asphalt cement to the surface through the aggregate structure. Too high an air void content can lead to accelerated aging, fatigue cracking, and damage from moisture if the voids are interconnected. The ideal air void content suggested by the Shell Oil Company is 4.9 percent determined empirically through laboratory and field experimentation.

In polyethylene modified asphalt, air void content has been acceptable from 1.8 percent up to eight percent of the binder with good performance below three percent air voids[10]. This differs slightly with the earlier cited value by the Shell Oil Company of

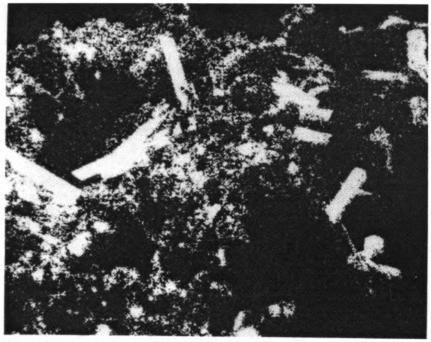

Figure 2.10 - Energy dispersive x-ray spectroscopy fractograph showing the distribution of sulfur in asphalt at 118X [45].

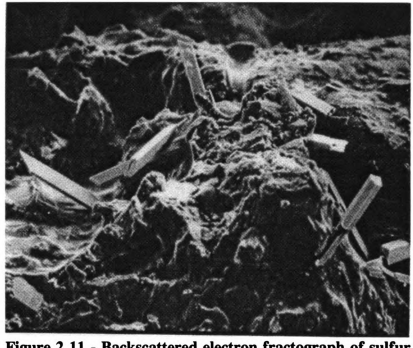

Figure 2.11 - Backscattered electron fractograph of sulfur modified asphalt showing the morphology of the crystalline sulfur at 118X [45].

Figures printed with permission from ASM International.

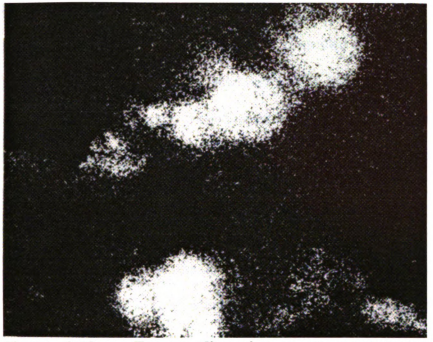

Figure 2.12 - Energy dispersive x-ray spectroscopy fractograph showing the spherical formation of sulfur in asphalt under confined growth at 1176X [45].

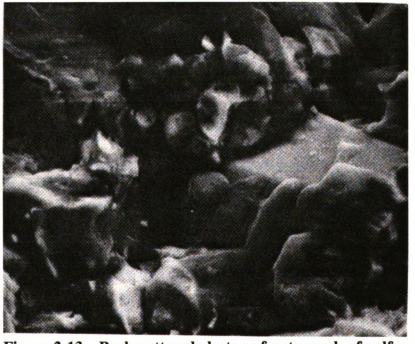

Figure 2.13 - Backscattered electron fractograph of sulfur modified asphalt showing the morphology of the crystalline sulfur at 1176X [45].

Figures printed with permission from ASM International.

4.9 percent air void content being optimum. According to the National Center for Asphalt Technology, the air void content should be closely controlled between three to four percent [35]. In a study of crumb rubber modified asphalt [46], four percent air void content was found to be the optimum. Four percent air voids has also been interpreted as the maximum threshold value in asphalt concrete in a previous literature review [47].

On Murphy road in Oregon in 1989, test sections were laid down by the ODOT (Oregon Department of Transportation) with rather large void content measured in field cores of 14.5 and 17.6 percent [15]. As of 1990 the roads were showing no pavement distresses. These values are believed questionably high because other roads that the Shell Oil Company has monitored having such high void contents have failed prematurely.

Little [10] related higher void contents to a decrease in fracture toughness of gravel sand asphalt mixes at four temperatures. Fracture toughness is represented by the area under a stress/strain curve analyzed through indirect tensile testing and is a measure of the materials overall strength. Figure 2.14 shows fracture toughness decreases with increasing air void content. Although the higher regions were not tested, the data trend seems to show higher air void contents would offer reduced benefits.

2.6.1 Void theory

Additional work has been done in the area of air void morphology by Terrel and Al-Swailmi [48] who formulated the theory of "pessimum" voids. The theory proposes that three distinct void morphologies exist: impermeable, "pessimum" voids, and free drainage. Literature data supports such categorizing and a diagram of their theory relating mix strength to void content is presented in Figure 2.15. The theory suggests

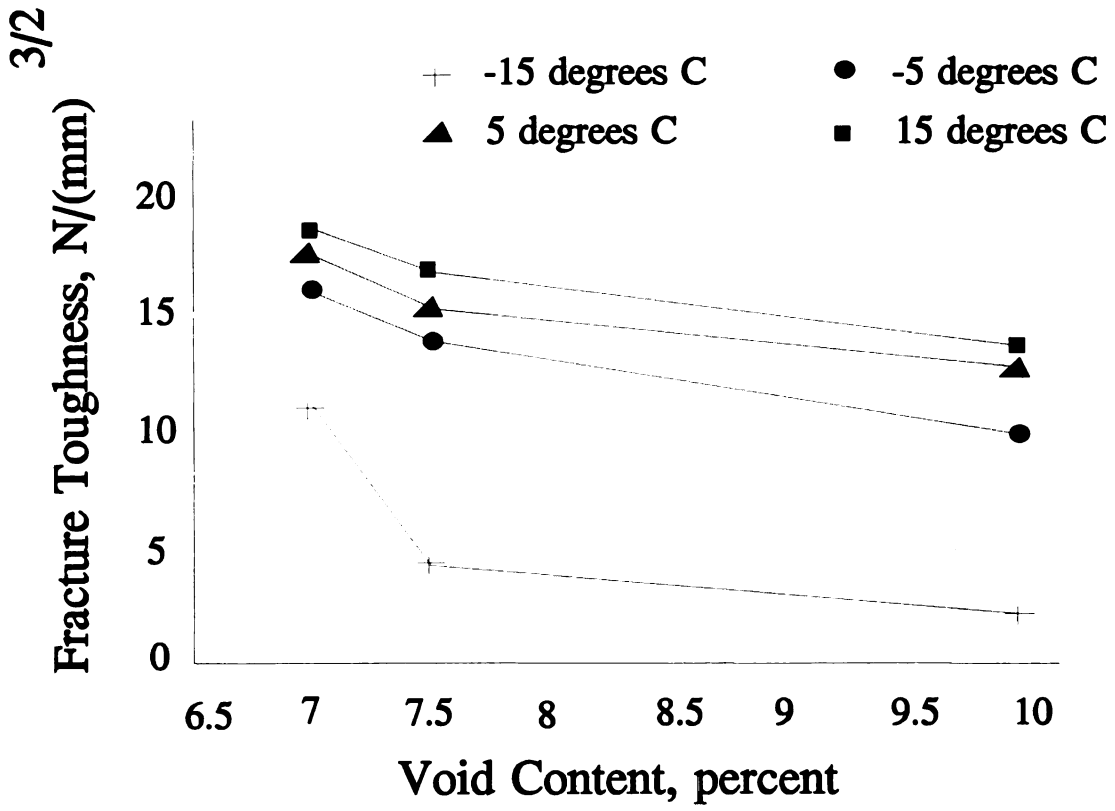

Figure 2.14 - Influence of void content and temperature on fracture toughness of gravel sand asphalt mixes [10].

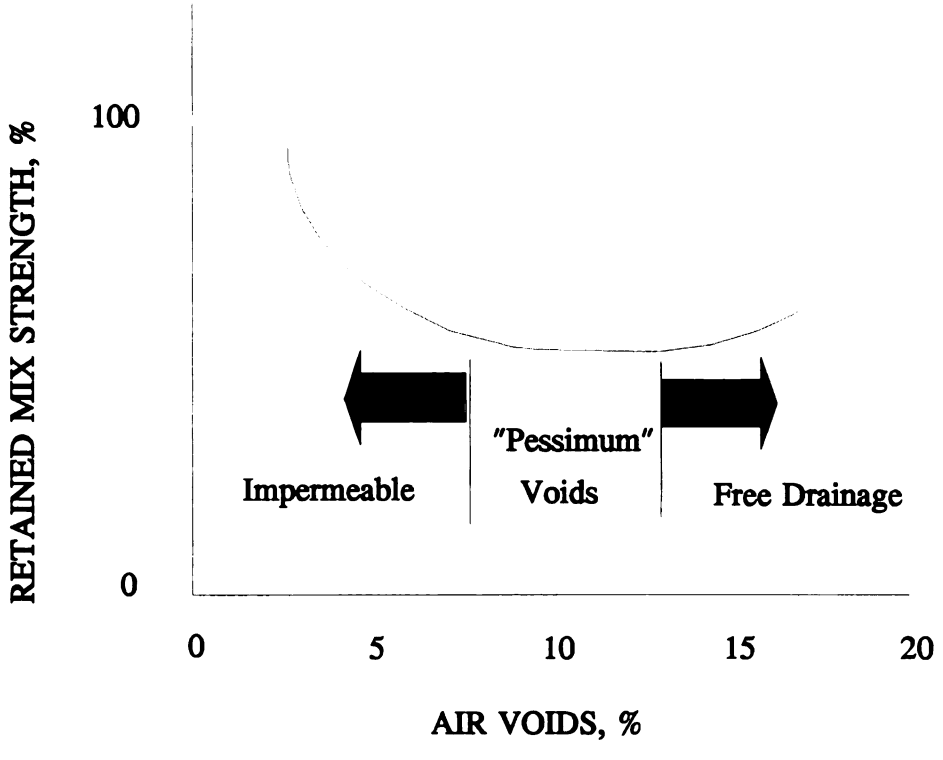

Figure 2.15 - The Relative Strength of Mixtures May Depend on the Access to Water in the Void System [48].

impermeable, and free drainage give better retained strength than the "pessimum" voids. Impermeable means not allowing the water to penetrate the asphalt and air voids range from zero to approximately seven percent. The air voids in impermeable have a closed void morphology. Free drainage is where the water is free to move down through the asphalt and into the ground [48]. The void morphology in free drainage is open and interconnected. The drainage would be similar to that of a packed bed or a sieve. "Pessimum" voids are partially interconnected, but not fully open voids, that allow for the slow diffusion of water into the asphalt. The "pessimum" range of air void content is between approximately seven to 13 percent. It is proposed that in the "pessimum" void region water penetrates and is trapped in the asphalt to cause detrimental effects such as stripping and freeze-thaw cracking [48]. Therefore, "pessimum" void morphology is not desired, as well free drain would probably not be acceptable in Michigan with the high humidity and rainfall in combination with freezing weather.

2.6.2 Void morphology

Air voids have also been studied as part of the Strategic Highway Research Program (SHRP). The study followed and modified cement concrete technologies from the past 20 years in the area of air void characterization for asphalt concrete [49]. Microscopic analysis using automated image analysis of thin and plane asphalt sections was used to characterize air void content, sizes, forms, and distribution. The study [50] investigated the air void characteristics as they were related to compaction method, mix type, and compaction temperature. The study consisted of preparation of thin and plane asphalt sections. These sections were carefully prepared by filling the voids through

vacuum impregnation with an epoxy containing a fluorescent dye. The epoxy served two purposes: it filled the voids allowing the specimen to be cut and polished without breaking up and served as a medium to hold the dye which was used to detect the size, shape, and distribution of the voids [51, 52]. Air void content results obtain through plane section image analysis were comparable to the current dry methods. The problem with image analysis is that it is a 2-dimensional technique, therefore not accounting for possible interconnections of the air voids in three dimension [53]. Bulk gas measurement of the air voids has potential to solve this three dimensional interconnection problem, but has not been established. Percolation theories suggest that when the porosity is 27±5 percent, the air void morphology will shift from separated (closed) to interconnected (open) [49].

To attain good pavement performance a homogenous air void content is desired in asphalt pavement. This study showed not all laboratory compaction methods were the same and all had some form of difficulty representing the field mixtures that generally gave a homogenous void distribution [53]. Of all the laboratory molded samples, the gyratory compacted samples gave the most homogenous air void distributions with only problems along the sides of the molded specimen.

An illustration of the plane section work is presented in Figure 2.16 [49]. This picture was obtained with two plane section samples placed under UV-illumination and photographed. The plane sections were approximately 90 mm wide by 110 mm high and the top surface is the top of the photograph. The lines marked at the sides represent the division of the compacted layers. The light grey to white areas are the voids fluorescing under the UV light. The solid colored objects, generally medium size are aggregate, and

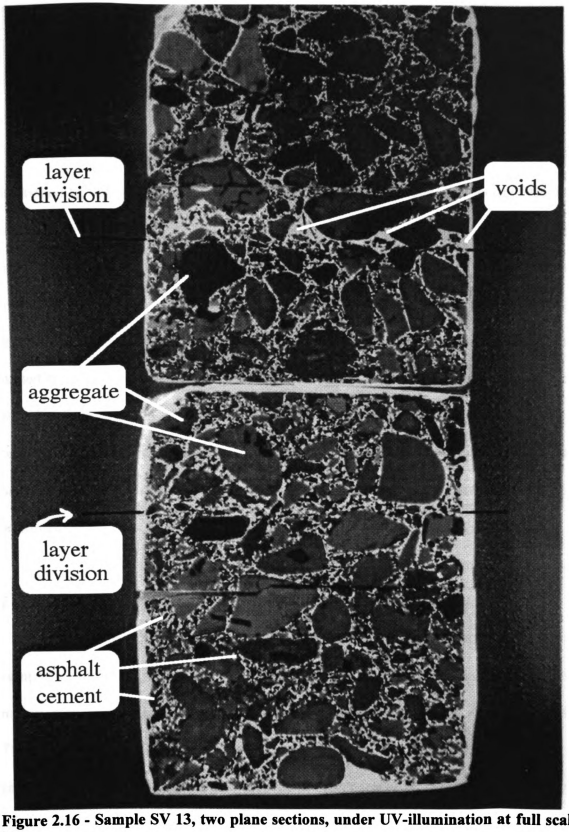

Figure 2.16 - Sample SV 13, two plane sections, under UV-illumination at full scale [49].

the small speckled black areas are asphalt cement, see figure with labeled details.

2.7 Fracture and failure mode of conventional and modified asphalt/aggregate mixtures

Morphology and microstructure are the heart of fracture mechanics. An understanding of the these two items enable the fracture mechanisms and locus of fracture to be determined giving insight to the performance of materials. The strategy is to apply the knowledge of polymer composites to the composite macrostructure of asphalt concrete and polymer modified asphalt concrete. Polymer composites have been studied from the fracture mechanics point of view for a much longer time than asphalt which has only started fracture mechanic analysis in the last few years. Due to this, limited theoretical work has been found in the literature for asphalt fracture mechanics. The application of polymer, composite, and adhesive theory can give insight for the development of the fundamental relationships between morphology and microstructure to pavement performance.

2.7.1 Composite theory

Composite theory helps explain the failure mechanisms in asphalt concrete. The composite interphase is defined as the region between fiber/rubber/aggregate and the matrix, asphalt cement, where both the chemical and physical properties are different [54]. The interface also influences to some extent the mechanical and thermal properties of composites. It has been found that the fracture locus could be at the interface region. Therefore, an understanding of the mechanisms of adhesion would be useful. The

microstructural bonding aspects of polymer-polymer adhesion and the macrostructural properties effecting adhesive strength have been summarized by Kalantar [54]. These aspects of adhesion/ cohesion are also important in asphalt/aggregate mixes as shown in previously conducted tests.

2.7.2 Mechanisms of adhesion

In asphalt, adhesion is an important concept when investigating fracture. Adhesion is the measure of the ability of two surfaces to stay together. In asphalt many factors appear to govern adhesion including; surface tension of the asphalt cement and aggregate, chemical composition of the asphalt and aggregate, asphalt viscosity, surface texture of the aggregate, aggregate porosity, aggregate cleanliness, and aggregate moisture content and temperature at the time of mixing with asphalt cement [48]. The concept of adhesion is explained through four microstructural mechanisms involving combinations of physical and chemical interactions. These mechanisms are: mechanical adhesion, chemical reaction, surface energy, and molecular orientation [48].

Mechanical adhesion is the interpenetration of surface irregularities and molecular contacts to act as mechanical anchors. This mechanical interlocking between aggregate and asphalt is strongest when the aggregate is rough and porous. For smooth surfaces, mechanical adhesion does not play a significant roll, thus the need for crushed and not smooth aggregate.

Chemical reaction is the mechanism of absorption interactions where the molecules of one phase such as asphalt are attracted to the molecules in the other phase, aggregate, fibers, and/or particles. These interactions originate from basic chemical interactions,

covalent chemical bonds, and secondary interactions. Covalent bonding is the sharing of electrons among atoms and is the primary form of chemical interactions [54]. When forming a stable interface the formation of these covalent bonds at the interface are very desirable. To form covalent bonds intimate physical contact must be achieved to which secondary interactions are a prerequisite. Secondary interactions form over greater atomic distances not requiring physical contact and include non polar dispersion forces (Van der Waals forces), polar dipole interactions, and polar Lewis acid/base interactions which includes hydrogen bonding. These chemical interactions are those responsible for better adhesion between asphalt and basic aggregates as compared to that of acidic aggregates [48].

Surface energy is the sum of the dispersive attractions across an interface. These interactions are generally small, but the surface can be modified to increase the attractive forces. The surface energy difference between the adherent and adhesive is responsible for wetting. Wetting is needed in asphalt for the asphalt cement to coat the aggregate forming a good bond.

Molecular orientation is the alignment of molecules at an interface. The extent of alignment depends on the mutual molecular affinities. The attraction of asphalt to aggregate molecules is low compared to the attraction of water to the aggregate. Therefore, water has a stronger attraction to the aggregate surface. This mechanism causes the wicking of water that occurs in small cracks and fractures created between the asphalt and aggregate and is the mechanism of stripping.

2.7.3 Macroscopic failure mechanisms

The study of fracture mechanics of asphalt mixes has been concentrated on macroscopic properties which can be seen with the naked eye and under low magnification. Hugo and Kennedy published a list of general failure mechanisms as follows [1]:

1. Excessive hardening of the binder.
2. Excessive stresses due to external loads or temperature changes.
3. Excessive volume change of the asphalt.
4. Excessive loss of subgrade support.
5. Excessive volume change of non-asphalt components of the pavement structure.
6. Excessive post construction compaction.

These macroscopic failure mechanisms are good for classification, but microscopic failure mechanisms are needed to provide the basis for solutions.

2.7.4 Microscopic failure mechanisms

Macroscopic failure mechanisms or pavement distresses have been related and categorized into microscopic failure mechanisms and are presented in Table 2.4. These pavement distresses are: thermal cracking, aging, fatigue cracking, rutting, and ravelling/stripping. The majority of distresses are seen to be related to fracture in various ways. Pavement ingredients with different coefficients of thermal expansion cause failure

stresses. Cyclic temperatures due to the environment cause freezing and thawing of water in seams, holes, and cracks which create and propagate fracture. Embrittlement of the asphalt concrete caused by both low temperature and aging increases the viscosity. Therefore, the resulting failure occurs at low strain as a brittle fracture rather than a ductile fracture [55].

Table 2.4 - Pavement Distress

Thermal Cracking	-	fracture due to thermal expansion differences
	-	fracture due to water freeze/thaw cycling
	-	fracture due to low temperature embrittlement
Aging	-	fracture caused by embrittlement of the asphalt binder
Fatigue Cracking	-	fracture due to tensile failure
Rutting	-	microstructural rearrangement due to asphalt plasticity under load
Ravelling/Stripping	-	adhesive fracture due to low adhesion

2.7.5 Thermal Cracking

Many mechanisms have been reported in the literature as being responsible for the thermal cracking problem. Binder stiffness was one of the most common criteria mentioned in the literature in controlling thermal cracking. Compared to straight asphalts,

SBS (styrene-butadiene-styrene) copolymer and styrene-butadiene block copolymer modified asphalts have reduced stiffness (i.e. less thermal cracking potential) while EVA (ethylene-vinyl acetate) modified asphalts have higher stiffness at low temperatures [56]. The "limiting stiffness" or "defined asphalt stiffness modulus" are the value above which pavement cracking is imminent [57], and has been reported by many researchers [58-60]. They range from 20,000 to 70,000 psi at a loading time of 10,000 seconds and SHRP has proposed 29,000 psi (200 MPa) at a loading time of 60 seconds for the bending beam stiffness test. This SHRP specification followed the work previously developed for the critical stress value based on thermal stresses. It should be noted that these values might not be applicable for polymer/fiber/aggregate modified binders. Tensile properties are also important parameters in controlling thermal cracking.

In order to quantify the improvement in thermal cracking resistance, the concept of cracking temperature was introduced and defined in two different manners. First, the temperature at which the stiffness reaches the critical value of "limiting stiffness" can be considered to predict the "cracking temperature." Bitumen stiffness has been used as a fundamental indicator of asphalt cement performance [61]. Second, the temperature at which the failure strain is one percent when a tensile strain of one millimeter per minute is applied is also called the "cracking temperature."

Fraass brittleness tests were also reported in the literature to characterize the possible benefits of adding polymer to improve low temperature cracking resistance. The Fraass brittleness temperature is where a crack forms in a thin film of asphalt which has been subjected to tensile stresses while being cooled at a rate of one degree celsius per minute. Polymer modification was found to lower the Fraass brittleness temperature with

increasing polymer concentration [8, 11, 15, 62] as shown in Figure 2.17. European bitumen specifications use the Fraass brittleness temperature as an indication of low temperature cracking performance [63].

Polymer modified binders were reported to have a higher penetration than straight binders and less temperature susceptibility [8, 11, 62]. Temperature susceptibility is defined as the change in consistency of penetration or viscosity of asphalt over a temperature change. This indicates that modified binders are softer and therefore, have less thermal cracking potential than straight binders at low temperatures. It has been reported that polymer modification is more effective in reducing thermal cracking when used with soft-grade asphalts [28].

The ability of asphalt mixes to resist thermal cracking has often been examined using indirect tensile testing at low temperatures. It has been found polymer modified mixtures offer higher tensile strength at low temperatures [7] thereby, better thermal cracking resistance as compared to straight mixtures.

Indirect tensile testing applies a compressive load to an asphalt core or Marshall sample measuring the force and deformation involved to relate them to the tensile and compressive strengths of the asphalt sample. The indirect compressive and tensile strengths are dependent on test temperature, angularity, kinematic viscosity (centistoke), and air voids.

Past indirect tensile tests have given data that is not strongly reproducible due to sloppiness of the equipment, equipment configuration allowing the sample to move during testing, specimen positioning, and lack of measurement capabilities. The development of a new indirect tensile test has overcome these problems with the development of a unique

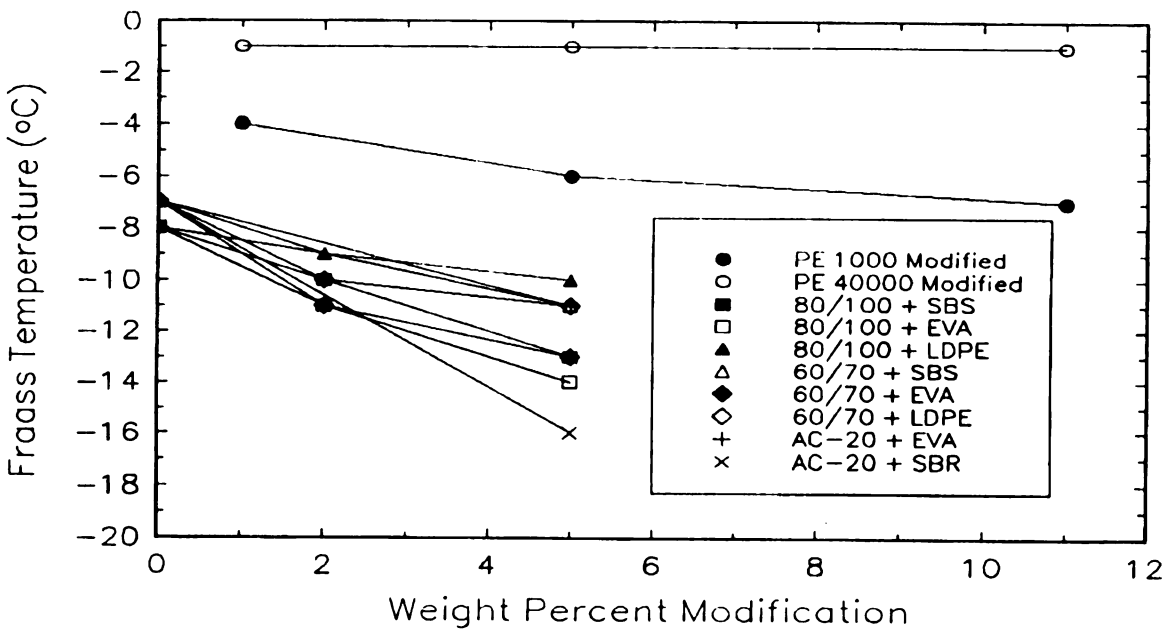

Figure 2.17 - Fraass Temperature vs. Polymer Content, data compilation [8, 11, 15, 62].

frame to transfer an applied force to an asphalt sample with reproducible results. Figure 2.18 [3] presents two general views of the new indirect tensile testing frame where the circular holding device on the bottom can be seen. This frame can be placed under a compressive load that can be applied by a variety of equipment depending on the test to be conducted. Figure 2.19 [3] shows the new frame in a standard Marshall test frame used to perform indirect tensile tests to failure with a constant load. Cyclic loading requires the use different equipment such as a MTS hydraulic system where a compressive load can be applied twice every second for a duration of 0.1 seconds.

Practical asphalt parameters to characterize the binder are the viscosity and temperature susceptibility. These parameters have the greatest effect in predicting cracking temperature through thermal analysis [64]. Ruth *et. al.* proposed a predictive method for thermal and load induced pavement cracking using the concept when an asphalt concrete pavement meets a critical condition cracking occurs. Critical condition was defined as "any combination of materials, environmental, and loading characteristics which produced stresses or strains equivalent to those required for fracture [64]." Currently, fatigue concepts are not like this and in most cases are inadequate pavement life predictions. Current fatigue concepts are to repeat stress and/or loading cycles until failure occurs building on the past stresses in the material. Ruth *et. al.* [64] believe the high temperatures, which lower the viscosity, and traffic that asphalt pavements endure during the summer months eliminates prior stress history.

The cracking criteria was based on incremental creep strain limits of failure stress, fracture energy, and mix stiffness concepts. The computer program developed included the thermal coefficients of contraction to account for their moderate effects on the asphalt

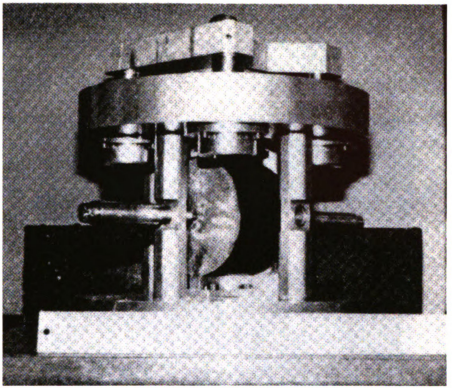

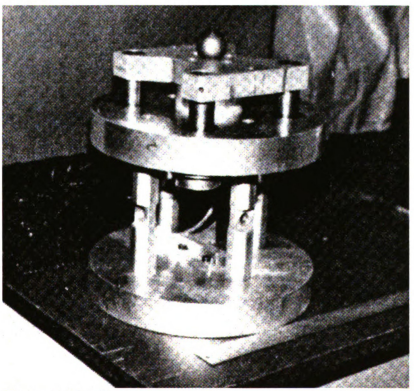

Figure 2.18 - General views of the new indirect tensile test frame [3].

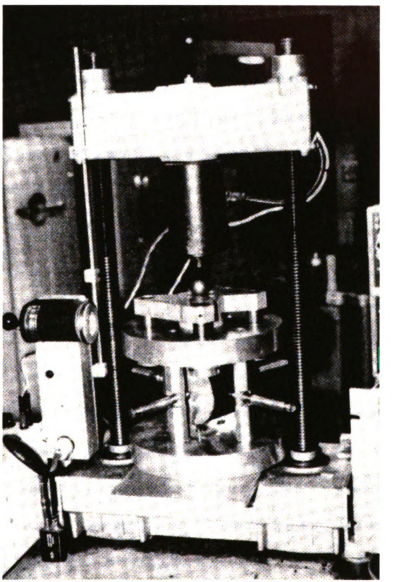

Figure 2.19 - The new indirect tensile frame in a standard Marshall test frame [3].

cracking temperature. The larger the thermal coefficient the higher the cracking temperature predicted. The most realistic failure values for predicting cracking temperatures were obtained through the fracture energy ratio obtained through thermal analysis. This was believed best because the values were calculated using both stress and creep strain [64].

A similar concept was developed in Lausanne and Urbana discussed in Kausch *et. al.* [65] where two cracked surfaces were brought together above their glass transition temperatures, T_g, where interpenetration of molecular coils occurred. This interpenetration caused healing effects where the original strength could be obtained in a finite amount of time. Others have also looked into this entanglement healing based on similar considerations [65].

2.7.6 Aging

Aging is a pavement distress which causes cracking. The fracture of the pavement occurs when the viscosity of the pavement increases to the extent it is no longer flexible. The increase in viscosity at the surface is due to the evaporation of the lower molecular weight materials and the oxidation/polymerization of asphalt molecules at the surface. Low air void contents of two percent have allowed negligible field aging below the surface after 11 to 13 years where as greater than two percent increases hardening of the asphalt [47]. Hugo and Kennedy compiled their viscosity work and have related it to cracking. Figure 2.20 presents typical examples of viscosity-depth profiles of uncracked pavements showing a high increase in viscosity as the surface was approached. These sites were in southern Africa and were; Johannesburg, P68/1, site B and Durban, R2/27

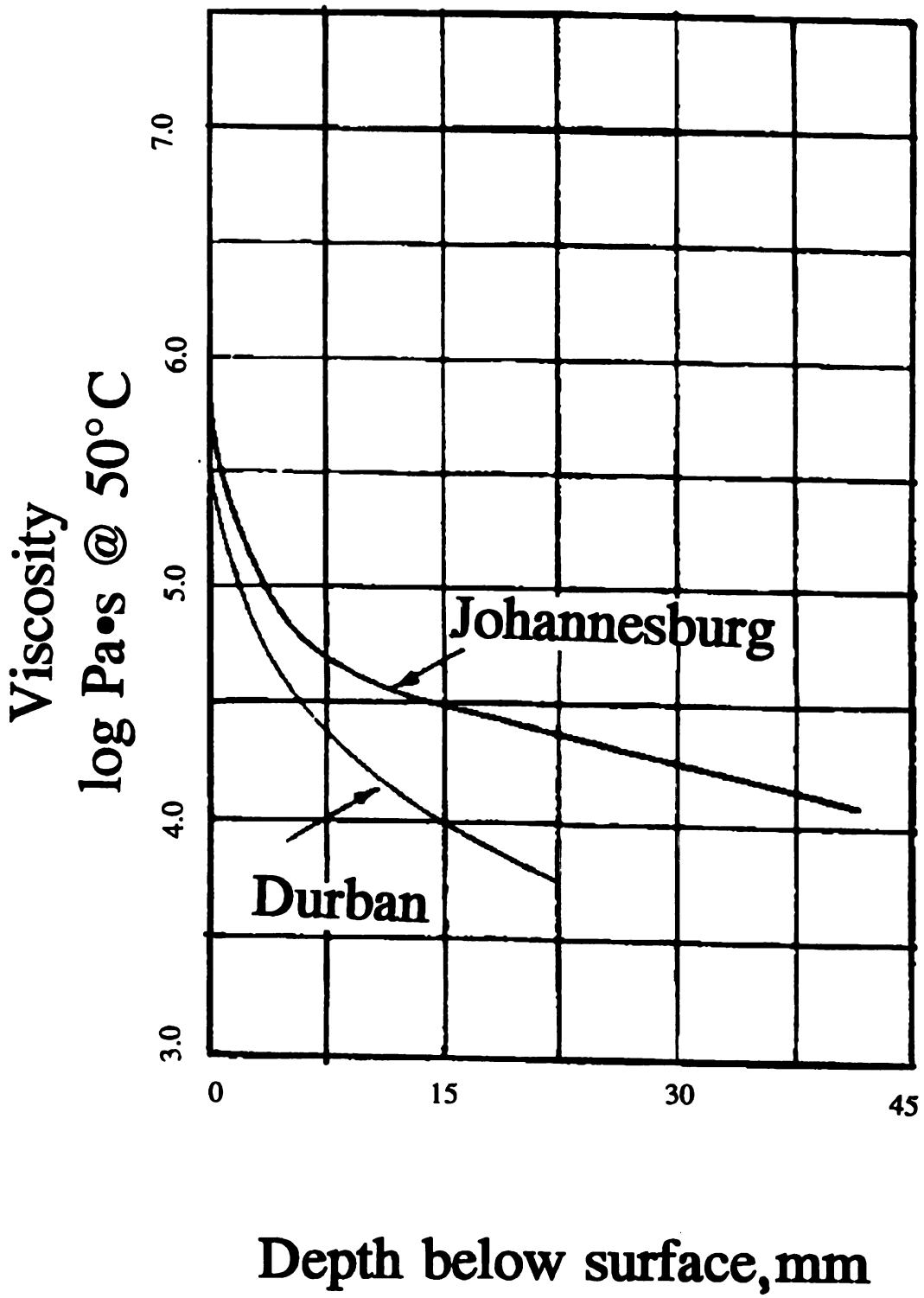

Figure 2.20 - Viscosity-Depth Profiles of Uncracked Pavements [1].

(Natal). Figure 2.21 shows a comparison of viscosity between cracked and uncracked asphalt pavements [1]. As the viscosity rose a critical viscosity was achieved and the plastic deformation of the asphalt could no longer compete with the applied stress/strains of the environment ending in crack failure. Evaluation of viscosity has also been applied to fatigue life by others [3].

Short term aging due to a higher processing temperatures can also be a problem. Crumb rubber and other polymer modified asphalts often need increased processing temperatures. It was found an increase in the mix temperature of 20°F, doubles the oxidation rate during processing [34].

2.7.7 Fatigue Cracking

Fatigue cracking damage is related to rheological properties of asphalt binder and is the least understood pavement distress mode because the results of fatigue testing are dependent on the testing mode. Fatigue cracking is caused by tensile deformation and strains in asphalt concrete from applied loads [3]. Fatigue analysis has been usually studied by two approaches; phenomenological approach, using the flexural fatigue or the diametral fatigue tests, and mechanistic approach using fracture mechanic principles to estimate the period of time during which damage grows from an initial state to a critical and final state [66]. Polymer modification provided asphalt mixtures with a superior fatigue life as determined by the flexural beam fatigue test [8], and diametral fatigue test [15, 29].

Laboratory investigation [67] on polymer modified asphalts reported the fatigue cracking resistance increased with polymer modification. Due to proprietary rights the

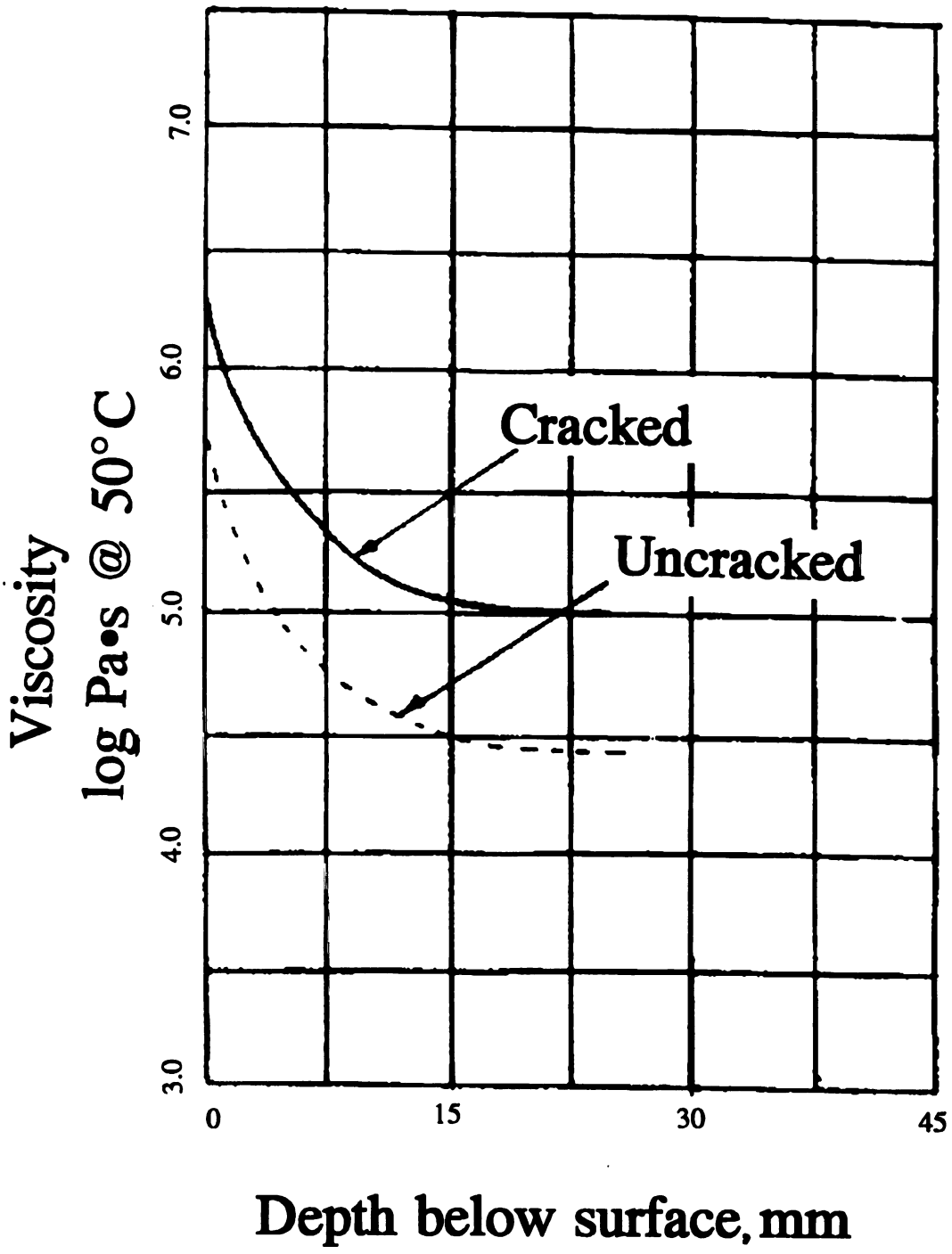

Figure 2.21 - Comparison of Viscosity-Depth Envelopes with and without Cracks [1].

exact modifiers were not reported, but some generic polymers reported were styrene-butadiene copolymer and ethylene copolymer. The importance of polymer modified asphalts is shown in Figure 2.22 [67] where most of the polymer modified asphalts show better fatigue cracking resistance than the straight asphalt, AC-20L and AC20S. Failure was measured in kilocycles to failure with the polymer modified asphalts sometimes being better by an order of magnitude at the smaller initial stains. The fatigue cracking resistance was measured through the push-pull fatigue test were tensile and compressive loads were applied to the sample at 10 Hz and 10°C until failure occurred. The asphalts were labeled with L, S, A showing different additives and sample preparation. L stands for the test run on a level-up mix. S is for the test run on a surface mix, and A refers to an antistrip additive [67].

In another laboratory study [29], fatigue cracking of straight asphalts (AC-5, AC-10, and AC-20), modified asphalt with carbon black filler (MICROFIL8), and styrene butadiene (SB) copolymer (Styrelf) modified asphalt were tested, analyzed, and fit to a cracking index. The index predicts and extrapolates using time temperature superposition techniques and extreme forethought should be exercised when using it. But, it does give some useful insight matching what would be predicted by composite fracture mechanics. The cracking index was subdivided into four different seasonal regions. These regions are presented in Table 2.5 [29].

The fatigue cracking damage index is a computer formulation for the expected fatigue cracking based on the response properties, traffic, pavement temperatures, and layer thickness. An index number of one corresponds to fatigue cracking just initiated at the bottom of the asphaltic layer and with increasing value increasing crack damage.

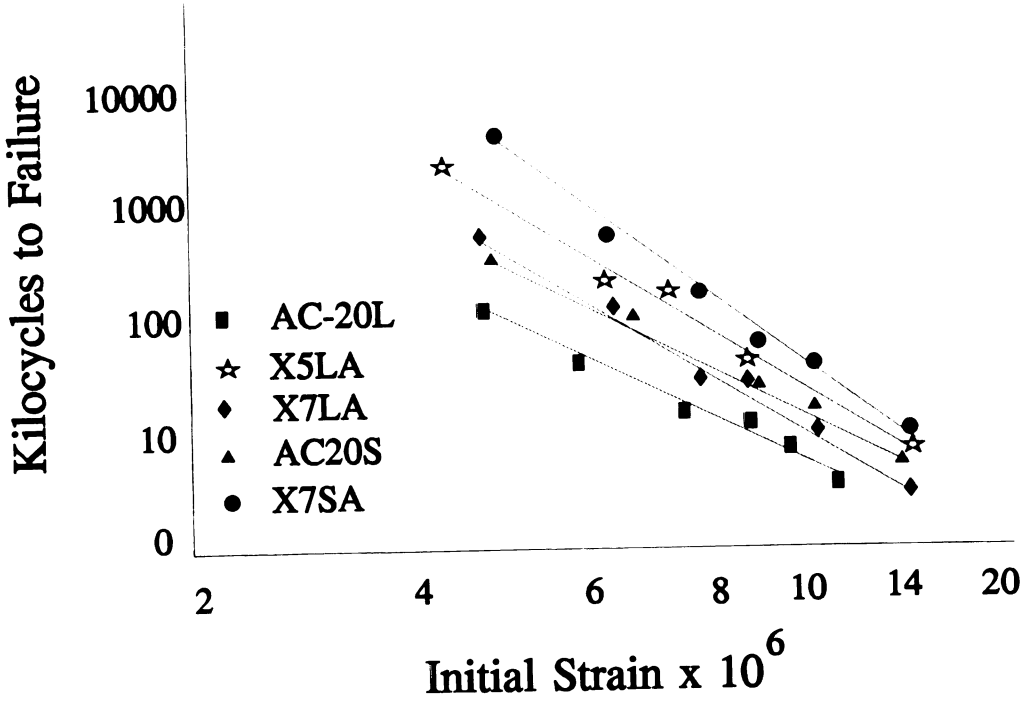

Figure 2.22 - Fatigue Resistance Test Results [67].

Table 2.5 - Seasonal Temperature Regions in Degrees Fahrenheit [29].

Region	Winter	Spring	Summer	Fall
1	0	40	90	70
2	40	70	90	70
3	40	70	120	70
4	40	70	140	90

Figure 2.23 predictions suggest straight asphalt would fail first followed by the filled asphalt and finally the polymer modified asphalt. Table A-1 of the appendix has the numerical data for these graphs. This would suggest the polymer modified asphalt has better ways to absorb the fatigue energy put into the asphalt. The modifier used was styrene-butadiene, an elastomer, which could absorb load energy in the form of stretching and releasing it back in the form of heat after the load is removed and the elastomer returns to its original shape minus any plastic deformation. These polymer particle modifiers are also known to stop cracking by means of crack blunting and microcrack toughen mechanisms in polymer composite materials. The carbon fill also has an additional mechanism for energy absorption the particle-asphalt interface. The addition energy is absorbed fracturing the interface slowing the crack growth and allows reduced cracking.

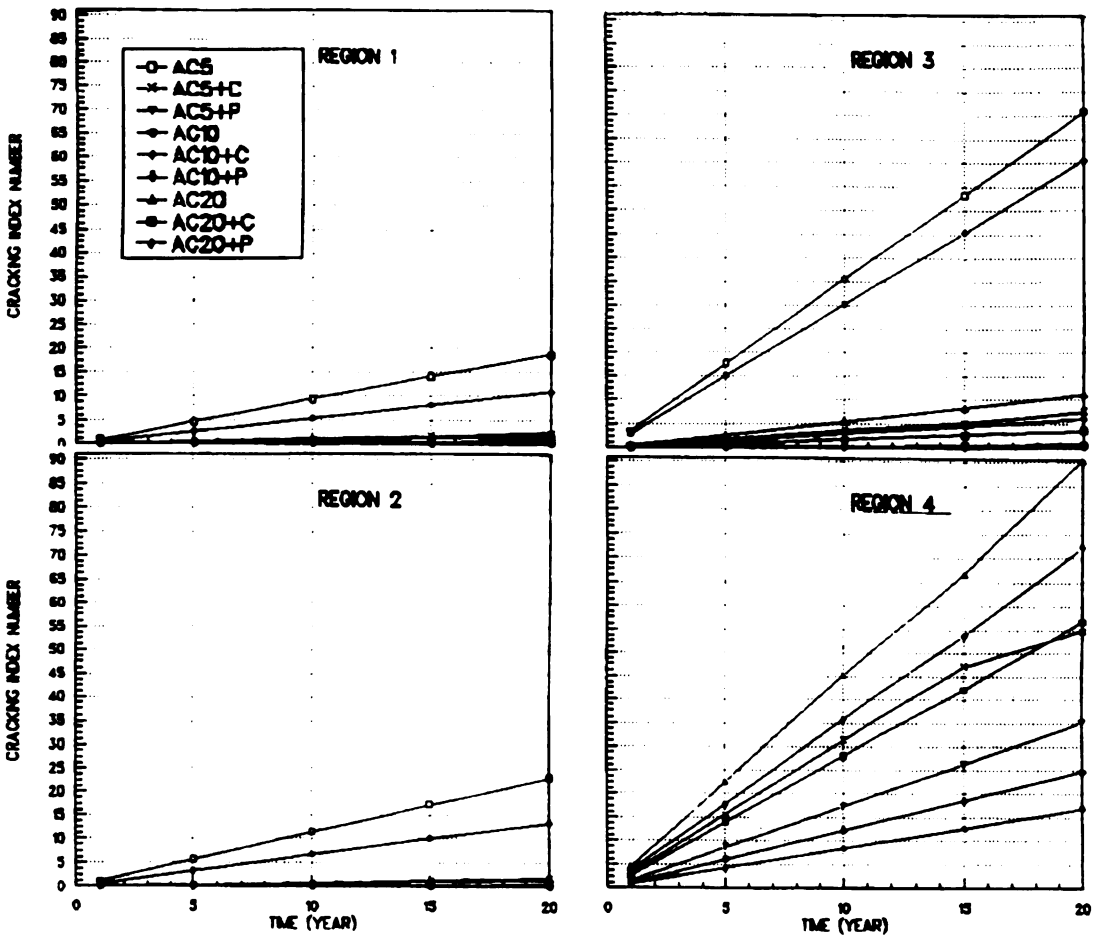

Figure 2.23 - Fatigue Cracking Damage Index for Four Climatic Regions [29].

2.7.8 Rutting

Rutting, a major distress, is the plastic deformation sustained by the asphalt/aggregate matrix while supporting applied loads. It happens when the elasticity and rigidity of the road are not resilient enough to withstand the applied loads.

Laboratory investigation on rutting deformation of different concentrations of polyethylene modified asphalt (Novophalt) were reported to have larger values of fracture toughness than straight asphalts. The greater the concentration of polyethylene (Novophalt), the better the resistance to rutting deformation. Figure 2.24 shows with increased polymer content better resistance to rutting deformation was achieved [10]. Similar results were obtained in another study [67] with a variety of modifiers. The creep resistance, the ability to with stand movement under applied load over long periods of time, was measured for several modified hot mix asphalts over a range of temperatures from 80°F to 120°F. The creep test was run under purely compressive sinusoidal axial stress with a constant isotropic stress to represent pavement confinement found in a road. Due to proprietary rights the exact modifiers were not reported, but some generic polymers reported were styrene-butadiene copolymer and ethylene copolymer. The importance of polymer modified asphalts is shown in Figure 2.25 [67] where all of the modified asphalts show better creep resistance than the straight asphalt, AC-20.

In the same laboratory investigation [29] where the fatigue cracking index was developed, a rut depth damage index was developed for straight asphalts (AC-5, AC-10, and AC-20), modified asphalt with carbon black filler (MICROFIL8), and styrene butadiene copolymer (Styrelf) modified asphalt. This index also predicts and extrapolates using time temperature superposition techniques and should be used with extreme

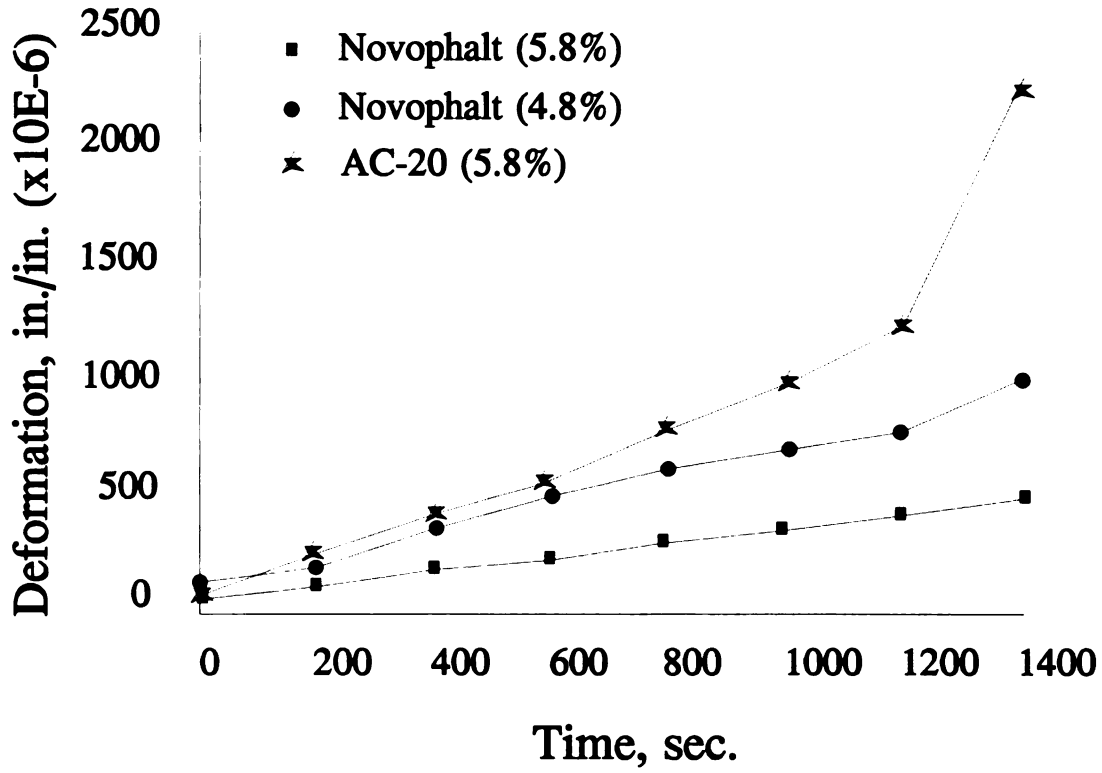

Figure 2.24 - Indirect tensile creep data at 77°F, 20 psi stress level, comparing optimally designed and binder-rich Novophalt mixtures and unmodified AC-20 [10].

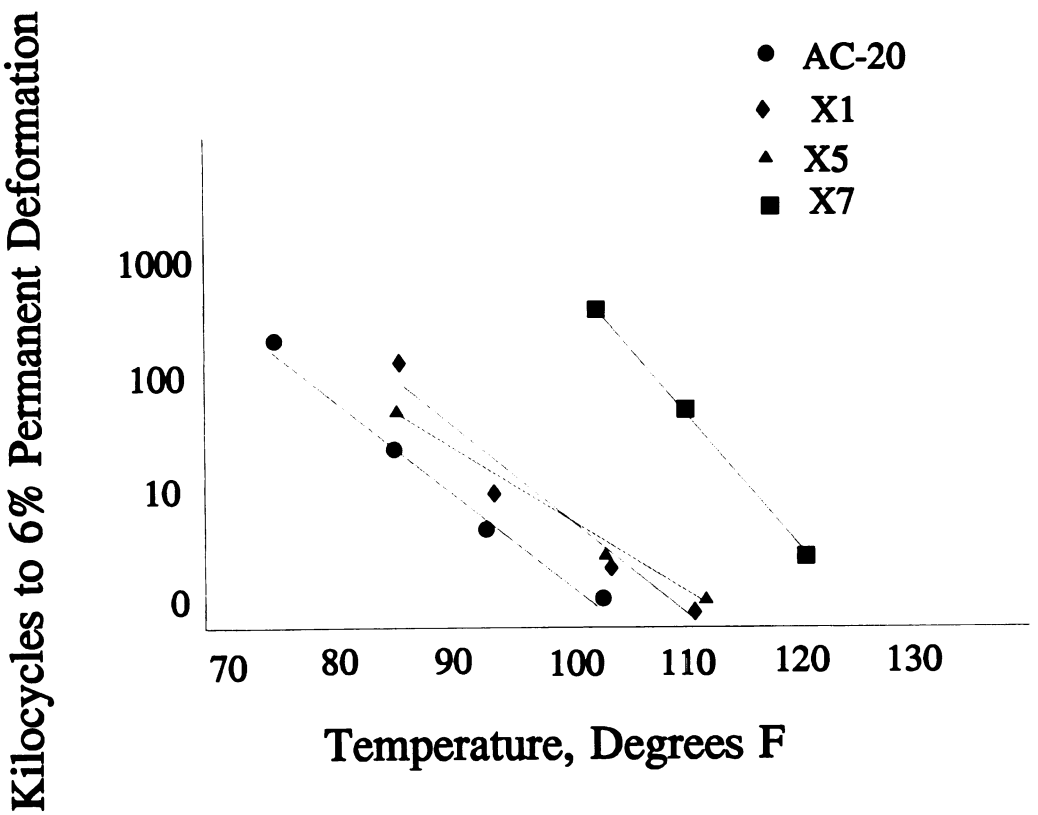

Figure 2.25 - Creep resistance of hot mix asphalts[67].

forethought. Again the index gives useful insight matching what would be predicted by composite fracture mechanics. The damage index was subdivided into the same four seasonal regions found in Table 2.5 [29].

Rut depth which is a measure of the permanent deformation in the wheel path has been predicted by the rut depth index and is presented in Figure 2.26. Table A-2 presents the numerical data for the graphs in Figure 2.26 and are located in the appendix. The predicted values are dependent on; permanent deformation characteristics, stiffness of the materials in the pavement, and traffic. The rut depth was reported in inches with the failure limit considered to be 0.6 inches.

The carbon particle modified asphalt was predicted to be the best in rut resistance followed by the styrene butadiene copolymer modified asphalt and then the straight asphalt with service lives of 10 to 12 years, 8 to 10 years, and 4 to 6 years, respectively [29]. The carbon particle modified asphalt out-performed the polymer modified asphalt because of its additional ability to help support the applied load where the polymer modified asphalt was better at stopping cracks because it had better modulus characteristics in the plastic zone. The plastic zone is defined as the region in the front and around a crack tip where the stresses change from elastic to plastic allowing for plastic yielding. The Irwin model of the plastic zone suggests a small circular area in front of the crack tip would have the same stress distribution in it as would the real crack [68]. Others have defined it as more like a dumbbell or double lobes for plane strain with the crack intersecting their middle. In plane stress, the area is almost circular like a balloon was being pushed over a straight edge creating an indentation at the crack tip [69].

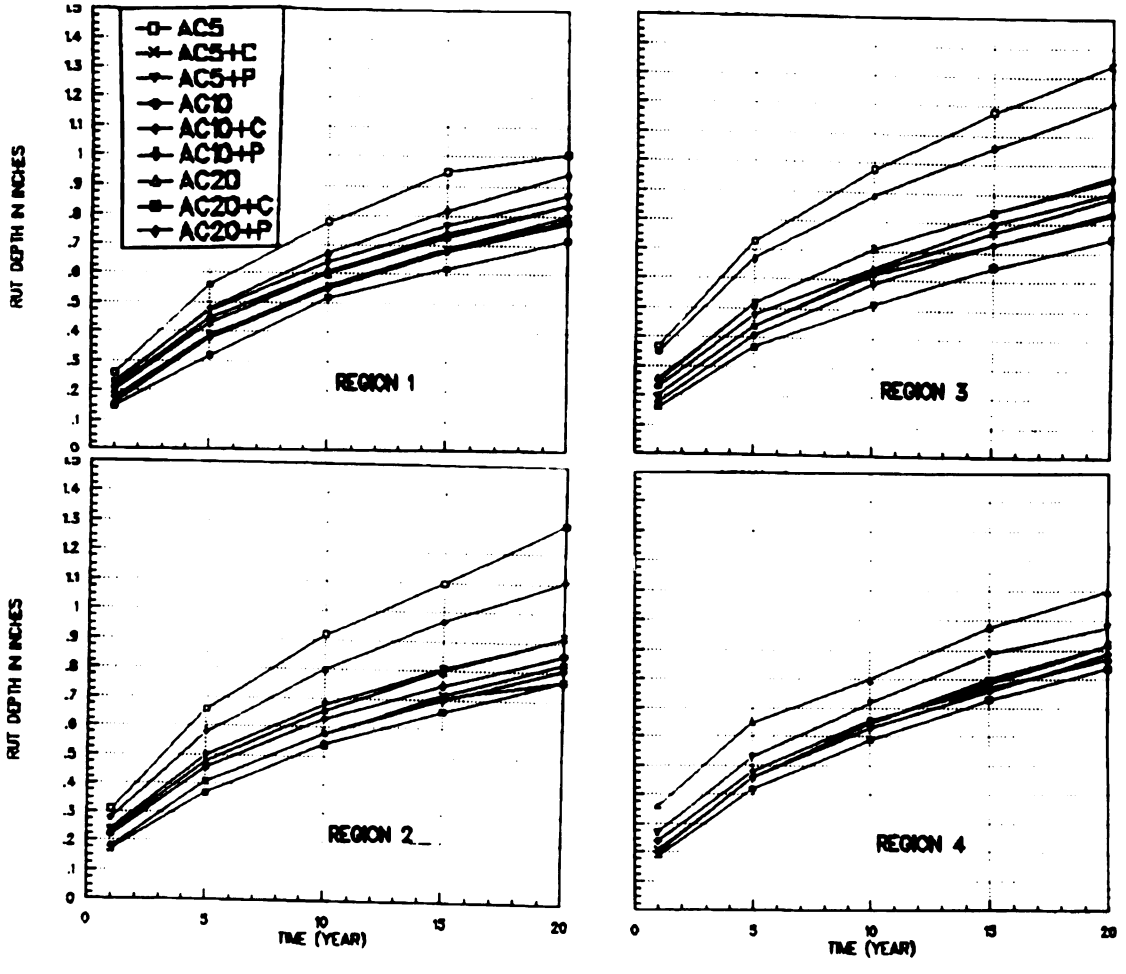

Figure 2.26 - Rut Depth for Four Climatic Regions [29].

In most of these cases the binder modulus is an important factor in fracture. G' and G" at the crack tip characterize fracture and deformation possibilities. In modifying asphalt with polymers, G' and G" are changed. Polymers can increase the elastic modulus, G', which is important at low temperatures to stop fracture by absorbing energy elastically. Polymers can also increase the viscous modulus, G", at high temperatures lending to the decreasing of rutting. This allows for the use of softer asphalts that are less susceptible to low temperatures [24].

2.7.9 Ravelling/Stripping

The other major distresses, ravelling/stripping, are fractures at the interface between the asphalt and aggregate. Ravelling is the characteristic name for the failure at the top surface while stripping is the failure that starts at the base of the asphalt layers. Both are a result of poor adhesive strength known to be caused by the wicking of water between the asphalt and aggregate creating poor adhesive characteristics and adhesive fracture. Altering the aggregate surface chemistry has reduced ravelling/stripping with additives such as lime and calcium carbonate [24, 70].

2.7.10 Surface Cracking

Another macroscopic classification others have done is categorizing cracking into six different types; transverse, longitudinal, skew, block, crazy, and crocodile cracking [1]. Figure 2.27 shows these classifications. This type of categorizing helps distinguish the extent of cracking, but not the failure mechanisms or locus of fracture. Similarly, these types of cracking can be broken down into their microscopic failure mechanisms, those

associated with thermal cracking, aging, and fatigue cracking.

2.7.11 Fracture Toughness

Fracture toughness is a measure of the ability of something not to fracture or up until fracture. Fracture toughness is the total energy for failure of a specimen calculated by determining the area under a stress/strain curve. The importance of fracture toughness is in its ability to be a predictive tool for future pavement performance. An example of the importance of fracture toughness occurred after a mistake during the paving process at an airport in Texas where the incorrect amount of LDPE was mixed into the asphalt concrete. To determine the potential problems, the asphalt was tested and many benefits were revealed from the mistake. The mixture had a LDPE content of 5.8 weight percent of the binder, instead of 4.8 percent which was originally designed. A comparison of the fracture toughness of the two concentrations of LDPE modified asphalt at three temperatures, 33°F, 77°F, and 104°F, was completed using indirect tensile testing. Their data showed the 5.8 percent modified binder gave higher toughness values than the 4.8 percent modified binder at all three temperatures tested and are presented in Figure 2.28 [10].

2.7.12 Fracture with fiber modification

Fibers have been studied as asphalt modifiers to enhance pavement performance with respect to fracture. Fibers improve the mechanical properties of composite materials with increased toughness and tensile strength, as well as the flexural and impact strength. These properties are offered through the three fiber toughening mechanisms: fiber-asphalt

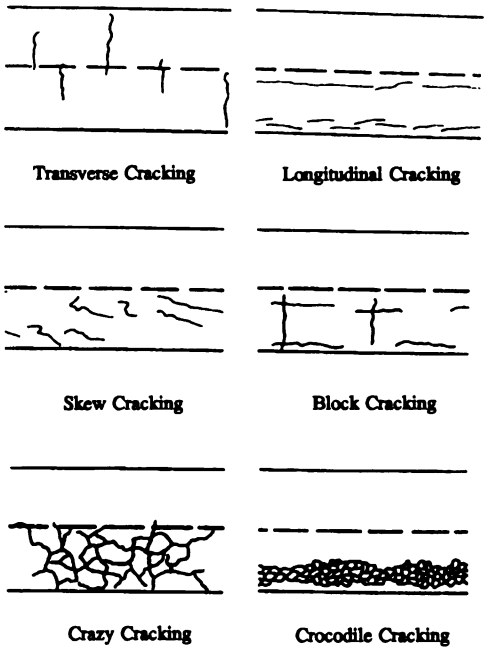

Figure 2.27 - Graphic Description of Cracks for Conditions [1].

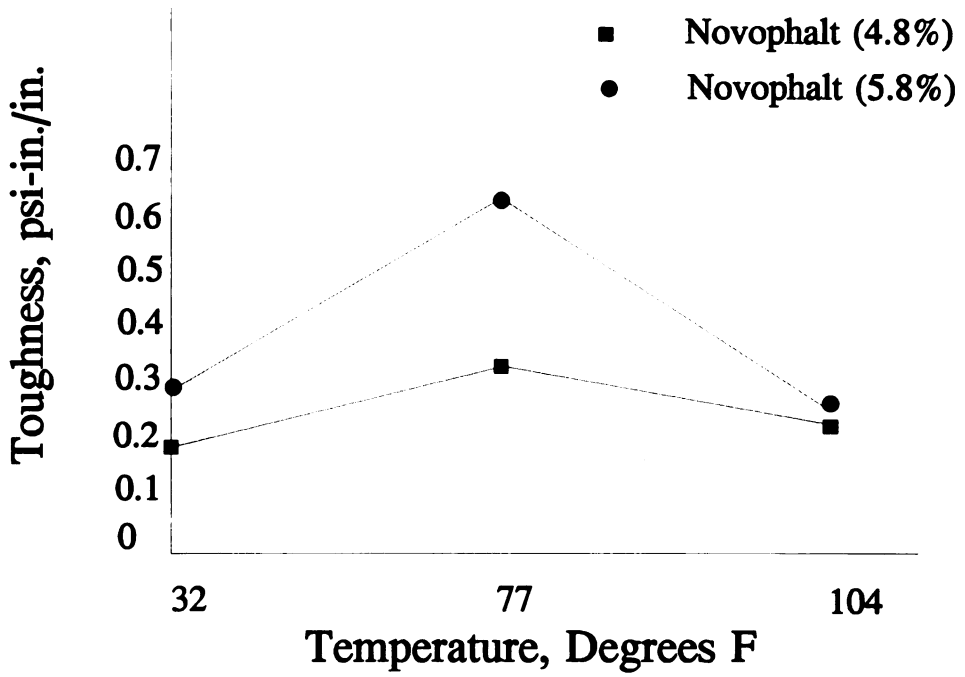

Figure 2.28 - Comparison of toughness for Novophalt mixtures determined from indirect tension testing at 32, 77, and 104°F [10].

debonding, fiber pullout, and fiber deformation and failure, as shown in Figure 2.29. Debonding is energy lost during adhesive failure between the fiber and matrix generally occurring around the fiber break point. Fiber pullout is the mechanism of energy lost to over come frictional resistance [71]. Fiber deformation and failure is the energy lost to yielding and fiber breakage. Organic fibers have the ability to reduce crack propagation and add strength to the system by providing the crack blunting and microcrack toughening mechanisms. Organic cellulose fibers are currently being used at 0.3 weight percent by BASF in their cellulose modified asphalt for stabilization. The stability is offered through a large fiber surface area allowing the bitumen to stay in place due to wetting the fiber surfaces, thereby reducing bleeding. Inorganic fibers may reduce the performance by acting as Griffith crack initiators due to their length to width ratio. However, inorganic fibers have been used as storage stabilizers [9] to slow down phase separation.

2.8 Fiber morphology and microstructure in other composite materials

Portland cement, also being a composite road material, provides some generic information that can be applied to asphalt composites. The cement industry has studied the added benefits of fiber reinforcement from 0.05 to 5.0 weight percent of steel, glass, polypropylene, polyethylene, aramids, cellulose, acrylic, fiberglass, carbon, and nylon fibers.

Fibers have been shown to increase the compressive strength of concrete up to 10 times over that of concrete without fibers [72]. Polypropylene fibers have doubled concrete strength with pullout being the main fiber failure mechanism [73]. Steel fibers

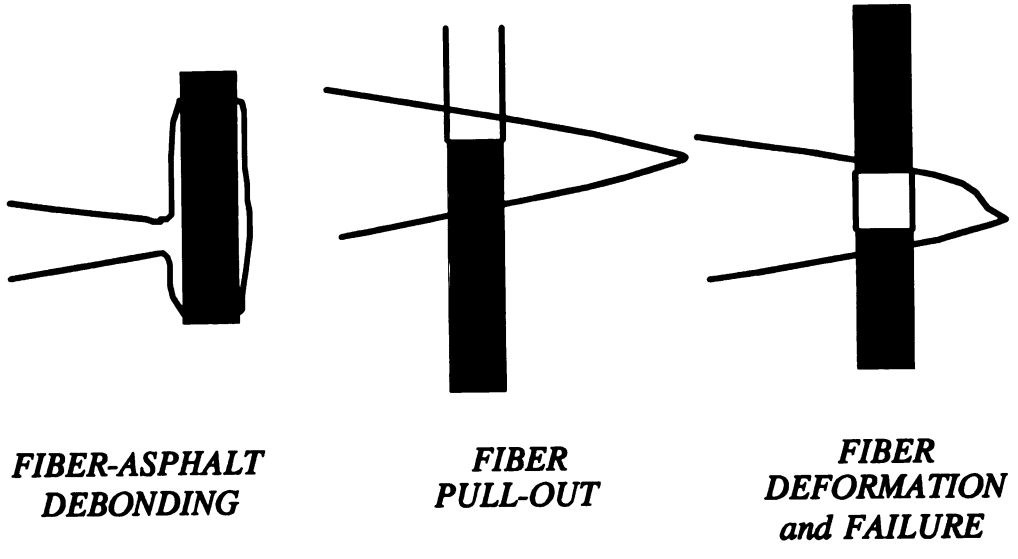

Figure 2.29 - Fiber Toughening Mechanisms

in concrete also fail by pullout [74, 75]. In other cement concrete studies carbon fibers show a great increase in the flexural strength and toughness. The addition of carbon fibers increases the toughness from 0.28 MPa*mm to 1.3 MPa*mm and the flexural strength from 1.4 MPa to 8.3 MPa. Additional additives, such as latex, and curing processes can increase these properties even more with the fiber failure mechanism still being pullout [76]. Figure 2.30 is a single carbon fiber from a pullout failure of portland cement concrete. The micrograph was taken with SEM (secondary electron microscopy) at 5 kV and 1000 magnification. The adhesive bond strength is the weakest failure mechanism and is shown by very little cement sticking to the fiber. The addition of latex increased the fiber bond strength between the cement and fiber from 2.1 MPa to greater than 5.9 MPa. The latex allows for a thin coating of polymer on the fiber and aggregate. This thin film of latex increases the fiber/cement and cement/aggregate bond and can be seen in a close up under the SEM in Figure 2.31. This picture was taken at 5 kV and at a magnification of 3500 [76]. In corrosive conditions, carbon fibers have been found to perform best [72].

ESEM (environmental scanning electron microscopy) investigation enabled the cement industry to examine the cement microstructure, thereby identifying embrittlement problems and their failure mechanisms during curing [72]. This is possible because the ESEM allows samples to be in a liquid environment and under a low vacuum instead of a dry, ultra high vacuum.

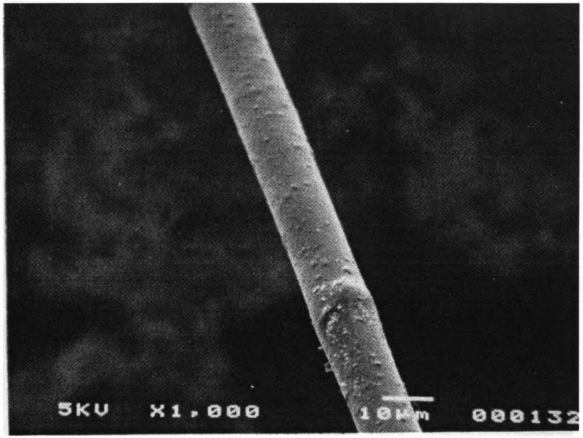

Figure 2.30 - Carbon fiber pulled out of cement concrete [76].

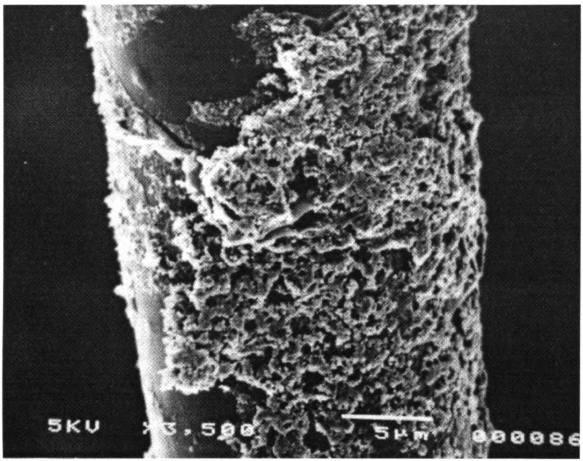

Figure 2.31 - Carbon fiber pulled out from latex-modified cement concrete [76].

2.9 Summary

Polymer modified asphalts increase pavement performance when used with properly constructed asphalt concrete pavements. Polymer modifiers have improved the creep resistance and fatigue resistance of hot mix asphalt at normal and high temperatures by as much as an order of magnitude over straight asphalt [67]. Polymers like ethylene-vinyl acetate can reduce rutting. Elastomeric polymers, SBS and SBR, can lower the cracking temperature by as much as 13°F [17].

The greatest benefit of polymer modification is their ability to form polymer network structures that can improve pavement performance. Polymer networks transfer and distribute applied stresses to reduce creep at high temperatures, increase rutting resistance, and gain high temperature stiffness without loosing low temperature flexibility.

Cellulose fibers offer good characteristics for asphalt modification, larger surface area to help stabilize and low expense. Polyester fibers offered the highest strength of those fibers reviewed in fiber modified asphalt.

Rubber particle modified asphalts were noted to under go adhesive fracture, a ravelling/stripping problem. In the composite industry, surface treatments have helped reduce and eliminate similar problems of adhesive fracture.

Air voids are an important aspect in pavement performance. Terrel and Al-Swailmi [48] proposed an air void theory with three regions of which the lower range from zero to approximately seven percent void content, the impermeable region, is best in humid, freezing climates such as Michigan. The optimum air void content range being between 3 and 4.9 percent in straight and polymer modified asphalts. Smaller amounts

can have bleeding problems and greater void contents can lead to accelerated fatigue crack, aging, and moisture damage.

Fracture toughness of a material represents a measure of the total energy for material failure. It has been shown fracture toughness of PE modified asphalt goes down with increased air void content (between seven and ten percent) at four tested temperatures, -15, -5, 5, and 15°C. An improvement in the toughness of PE modified asphalt has been shown with the use of 5.8 weight percent PE modified binder over 4.8 weight percent. This improvement may not be large enough to justify the added expense, but does show an operating window for the binder content.

Laboratory tests and computer modeling has predicted better pavement performance for carbon black and polymer modified (SB) asphalt over straight asphalts [28].

Understanding fracture mechanics and the locus of fracture of polymer modified asphalts is essential to relate PMA composition to pavement performance. Microscopic failure mechanisms are needed for this relationship, but macroscopic failure mechanisms of asphalt concrete constitute the majority of past work. The two key microscopic failure mechanisms are fracture and deformation. Knowledge in these two areas will accelerate pavement performance improvement.

Chapter Three

Problem Refinement

3.1 Problem statement

Asphalt concrete pavements have been showing signs of early distress in areas of thermal cracking, aging, fatigue cracking, rutting, and ravelling/stripping diminishing pavement performance. Microstructure, morphology, adhesion, and fracture are key factors influencing all these distress areas and are the focus of work contained in this thesis. Tests were developed to investigate the relationships between pavement performance and these key factors. Pavement performance is directly related to fracture of the pavement while fracture is governed by the microstructure and morphology of the asphalt concrete. Additional investigation of asphalt concrete shows microstructure and morphology are governed by the mix ingredients. This is where polymer modifiers can have large effects, thereby showing a direct correlation between polymer modification and pavement performance. The tested developed were: microscopic and image analysis of thin asphalt concrete thin and plane sections enabling microstructural and morphological investigation and fracture testing of thin asphalt samples allowing crack propagation, fracture mechanisms, and locus of fracture to be investigated. Additional tests are proposed for adhesion and fracture toughness. Therefore, existing and proposed tests will allow characterization and evaluation of polymer modified asphalt cement and concrete.

3.2 Microstructure and crack growth

Categorization of modifiers and microstructure is a necessary organizational step in order to understand the role of polymer modifiers on failure mechanisms. Therefore, asphalt modifiers are catalogued into five types: dispersed thermoplastic polymers, network thermoplastic polymers, reacting polymers, polymeric and organic fibers, and rubber particles as discussed in Chapter Two. It is further desired to categorize these five types by their microstructure for analysis of crack growth and fracture mechanisms. Since fracture and crack growth mechanisms are inherent functions of microstructure. Therefore based on the microstructure, three morphological types have been determined: Type H, Type F, and Type P.

3.2.1 Type H

Type H refers to asphalt concrete with homogeneous asphalt cement, conventional aggregate, and acceptable void content. The asphalt cement being homogenous at the microscopic level. The majority of polymer modified asphalt cements are of this type and include; dispersed thermoplastic polymer modified asphalts, network thermoplastic polymer modified asphalts, and reactive polymer modified asphalts. Conventional asphalts are also included in this category. Figure 3.1 is a drawing of Type H polymer modified asphalt (PMA) showing their general characteristics.

For Type H polymer modified asphalts, the tip crack growth is a function of asphalt-aggregate adhesion [77-81], properties of asphalt at the crack tip[82-87], plastic zone size [68, 69, 88-95], and void content [77, 78, 96-98], as shown in Figure 3.2. The

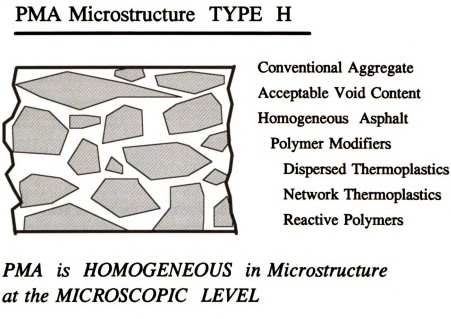

Figure 3.1 - Type H PMA microstructure

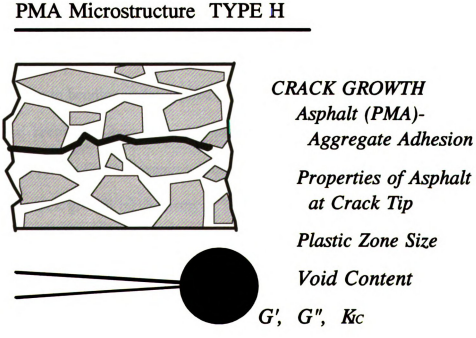

Figure 3.2 - Type H PMA microstructure crack mechanisms

critical stress intensity factor, K_{IC}, a characteristic within the plastic zone, has been found to measure crack blunting [99]. K_{IC} is a measure of stresses and strains inside the plastic zone when fracture occurs which can be used to measure the crack resistance of a material [100].

3.2.2 Type F

Type F refers to asphalt concretes similar to Type H except with the addition of fibers to form fiber modified asphalts. The fibers can be of either polymeric or inorganic in nature. Figure 3.3 is a drawing of Type F PMA with their general characteristics. Fibers are added as reinforcements leading to superior mechanical properties.

Type F PMA exhibits the same crack growth mechanisms as Type H, plus those related to fibers. Fibers contribute to improving the asphalt crack growth performance by adding three fiber toughening mechanisms [101]; fiber-asphalt debonding, fiber pullout, and fiber deformation. These mechanisms must function individually and collectively for the composite to give improved properties. Fibers contribute high strength and modulus to resist breakage in bending under applied load while the matrix transfers the stresses to the fibers and keeps the fibers separated and orientated. The matrix also serves as a protective layer for the fibers preventing abrasion and decomposition. Figure 3.4 presents the important crack growth mechanisms of Type F PMA where crack growth rate is a function of asphalt binder-fiber adhesions [77, 79, 97, 101-104], binder-aggregate adhesions [77, 79, 81, 102], fiber properties [102-107, Kinloch, 1983 #466], and void content [77, 96-98, 108].

PMA Microstructure TYPE F

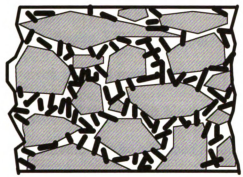

Conventional Aggregate
Acceptable Void Content
Homogeneous Asphalt
FIBERS
Polymer
Inorganic

FIBERS are UNIFORMLY dispersed throughout the Asphalt phase.

Figure 3.3 - Type F PMA microstructure

PMA Microstructure TYPE F

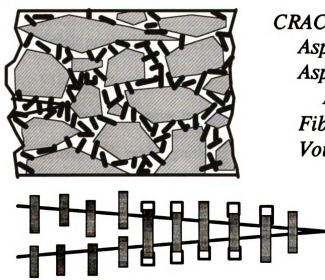

CRACK GROWTH
Asphalt -Fiber
Asphalt-Aggregate Adhesion
Fiber Properties
Void Content

Figure 3.4 - Type F PMA microstructure crack mechanisms

3.2.3 Type P

Type P refers to asphalt concretes similar to Type H except with rubber particle modification. Rubber particles for asphalt modification come from ground up passenger and truck tires. Figure 3.5 is a drawing of Type P PMA microstructure.

The crack growth mechanisms in Type P are similar to those of Type H, plus those associated with the asphalt binder-rubber particle interactions. These interactions allow energy of fracture to be adsorbed reducing crack growth through ductile tearing and debonding of the rubber particles [109, 110]. Rubber particles can toughen materials through a mechanism called toughening. Rubber toughening is the incorporation of a soft rubbery phase into the brittle polymer matrix asphalt at low temperatures. This can activate multiple shear yielding as the toughening mechanism in the material [111, 112]. Shear yielding is a ductile failure mechanism that takes place in highly localized shear bands or diffuse shear deformation zones. Figure 3.6 displays the important crack growth mechanisms of Type P PMA microstructure where the crack growth rate is a function of binder-rubber adhesion [79, 80, 110, 111, 113, 114], rubber particle size [85, 102, 110, 112, 114-116], particle properties [112, 117, 118], rubber content [80, 115, 119], and void content [77, 96-98].

A variety of polymers have benefitted from the addition of rubber particles. Epoxy resins modified with rubber particles showed an increase in fracture toughness. This considerable increase in toughness only reduces other properties a small amount [113]. In high impact polystyrene (HIPS) dispersed rubber particles of one micron in diameter were found to increase the impact behavior by ten percent when simple blending was used. If the rubber particles were added during polymerization greater benefit was

PMA Microstructure TYPE P

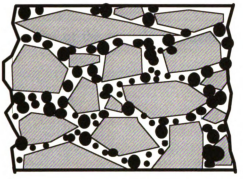

Conventional Aggregate
Acceptable Void Content
Homogeneous Asphalt
Dispersed Rubber Particles

PMA has Rubber Particles UNIFORMLY dispersed throughout the Asphalt phase.

Figure 3.5 - Type P PMA microstructure

PMA Microstructure TYPE P

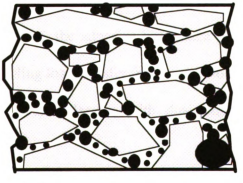

CRACK GROWTH
Asphalt-Rubber Adhesion
Rubber Particle Size
Void Content
Rubber Content
Particle Properties

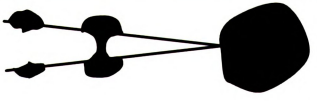

Figure 3.6 - Type P PMA microstructure crack mechanisms

achieved. The addition during polymerization increases the chemical compatibility of the rubber particles to the matrix, thereby increasing the adhesive bond which serves as an energy sink during fracture [115]. This bond is also dependent on both the elastic and adhesive properties of the particle and matrix.

3.3 Fracture

In order to determine the role of polymer modifiers in asphalt concrete fracture an understanding of adhesion, deformation, fibril bridging, and fracture toughness are essential.

3.3.1 Adhesion

The fiber/particle-matrix bond is generally the site for premature failure of composites due to high localized stresses in this region. Differential thermal expansion is one of the causes of localized stresses between the fiber and matrix that adhesion must resist. Therefore, the adhesive bond must possess the necessary chemical and physical features enabling load transfer from matrix to fiber or particle reinforcement. Frequently, coupling agents, molecules with dual functionality, are used to improve adhesive properties.

There are many coupling agents used in the treatment of fibers and particles. Coupling agent molecules must possess the ability to bond to both the matrix and the fiber/particle of a system. Therefore, a coupling agent must be properly selected for each specific fiber/particle-matrix system. The advantage of pretreatment with a coupling agent

can be illustrated by the application of one percent aminosilane (Union Carbide A-1100) to glass spheres in Nylon 6 [120]. Figures 3.7 and 3.8 are SEM (secondary electron microscope) micrographs at 1400 magnification showing glass sphere filled Nylon 6 without and with coupling agent, respectively. Figure 3.8 definitely shows the better bonding capabilities of coupling agent pretreatment where the Nylon 6 strongly adheres to the glass sphere instead of separating under stress and creating a void at the bond as shown in Figure 3.7. Coupling agents may be useful in this application enabling the aggregate and crumb rubber adhesive bond to be strengthened reducing stripping effects.

3.3.2 Deformation and fibril bridging

Asphalt cement is an amorphous polymer with glassy behavior at cold temperatures. Most amorphous glassy polymers are brittle in tension, but yield and flow (plastic deformation) under high strains in compression or pure shear when there is no overall hydrostatic tensile stress [121]. Plastic deformation and crazing have a strong relationship in the fracture of amorphous thermoplastics and asphalt. Both plastic deformation and crazing are processes of energy dissipation. Crazing is the development of concentrated bands of microvoids where fibrils are formed between the voids [122]. Normally crazing leads to brittle fracture, but with multiple crazing general yielding results and acts as a toughening mechanism. A second phase, such as fibers, particles, and/or a network, is needed to take full advantage of this toughening mechanism [121].

Plasticized fibrils increase the drawing of craze fibrils, but if crazed fibrils become plasticized by the environment, i.e. introduction of water, then the crazing can turn into a crack. This is dependent on molecular weight and molecular weight degradation of the

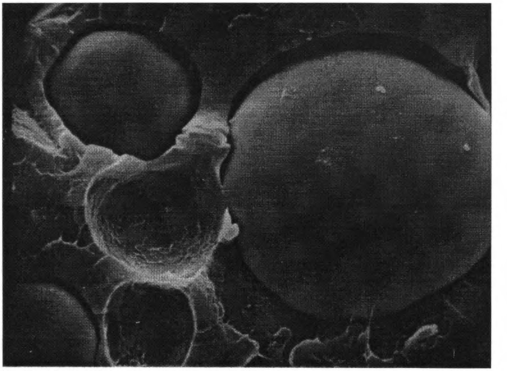

Figure 3.7 - Fracture surface of glass sphere filled Nylon 6 without coupling agent at 1400 X [120]. Printed with permission from Chapman & Hall.

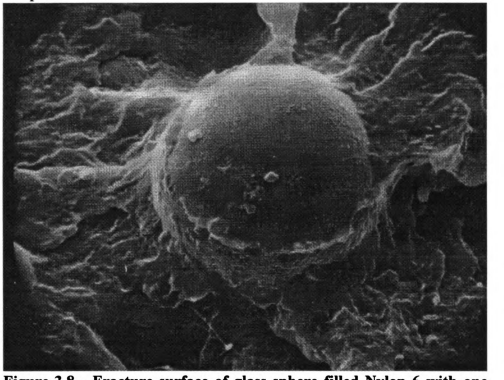

Figure 3.8 - Fracture surface of glass sphere filled Nylon 6 with one percent aminosilane at 1400 X [120]. Printed with permission from Chapman & Hall.

fibrils [123].

3.3.3 Fracture strength and toughness

Fracture strength can be used to determine the effects of flaws when modulus and fracture energy (toughness) are held constant for a given set of testing conditions. Fracture strength, σ, is the stress to failure and is controlled by the size of the largest cracks and flaws. Fracture energy, G, or fracture toughness is the total amount of energy dissipated during crack growth. The "inherent flaw size" of a material determines its strength and toughness. These "inherent flaw size" effects are those flaws created during loading from nucleation, growth, and breakdown of crazes [124]. A special property of fracture toughness is its independence of testing geometry. Investigation [78] of adhesive joints, aluminum-epoxy-aluminum, were used to determine this geometric independence using single edge notch (SEN) and tapered double cantilever beam (DCB) geometries.

Fracture toughness can also be used for pavement performance evaluation. Although fracture toughness is not fully accepted by industry, academia uses it with favorable results when comparing toughness of modified asphalts and asphalt pavements. The asphalt binder toughness can be measured by proven and accepted direct tensile strain methods being a homogenous material. Two accepted theories are Griffith criterion and stress intensity factor.

The basis of Griffith criterion was developed in 1921 to overcome the infinite stress concentration at the crack tip. Griffith used an energy balance approach equating the elastic energy, U, and the energy required for crack growth, W [125].

$$\frac{dU}{da} = \frac{dW}{da} \qquad \textbf{3.1 energy balance}$$

Using this approach he derived equation 3.2 relating the energy required to make a crack, to the energy it took to create a new surface [124]:

$$\sigma = \left(\frac{2\,E\,\gamma}{\pi\,a}\right)^{1/2} \qquad \textbf{3.2}$$

where σ = fracture stress required to fracture a crack of size 2a

E = Young's Modulus

γ = surface free-energy

a = half the length of the crack developed

Fracture stress measurements using this equation worked well for glassy polymers, but when measuring lower modulus materials higher surface free energy values were determined. This was due to the high degree of local plastic deformation at the crack tip which dissipated energy to a greater extent. Therefore, equation 3.3 was developed replacing 2γ with the fracture energy, G, representing the total amount of energy dissipated during crack growth under plane stress. The units of G are force per unit crack extension.

$$\sigma = \left(\frac{E\,G}{\pi\,a}\right)^{1/2} \qquad \textbf{3.3}$$

This allows a fracture energy or toughness to be calculated from the fracture stress and modulus of a material.

Stress intensity factor, K_I , is a means of measuring crack resistance under plane strain. K_I is similar to Griffith fracture, but a more characteristic measure of the plastic zone's stresses and strains [100]. The stress intensity factor value (fracture toughness) reflective of an infinite crack plate is:

$$K_I = \sigma\sqrt{\pi\, a} \qquad \textbf{3.4}$$

Where σ is the fracture strain.

When the plate is of finite size the stress intensity factor becomes a function of the crack size, a, to plate width, W, as below:

$$K_I = \sigma\sqrt{\pi\, a}\, f(\frac{a}{W}) \qquad \textbf{3.5}$$

This relationship can then be used to estimate the plastic zone size through the yield stress, σ_{ys} once the function of crack size to plate width is determined for the system.

$$\sigma_{ys} = \frac{K_I}{\sqrt{2\ \pi\ r_p^*}} \qquad \textbf{3.6}$$

Where r_p^* is the diameter of the plastic zone in front of the crack. Therefore, r_p^* can be

defined as:

$$r_p^* = \frac{K_I^2}{2\ \pi\ \sigma_{ys}^2} = \frac{\sigma^2\ a}{2\ \sigma_{ys}^2} \qquad 3.7$$

For heterogenous materials the stress intensity factor is still not fully defined and direct tensile testing for Griffith criterion is not acceptable with the shear forces in asphalt concrete pavements. Accepting this, the asphalt industry has done work in the area of fracture toughness for asphalt pavements. Three methods of testing have been triaxial, indirect tensile, and flexural beam in a variety of configurations including compression, creep, and constant and variable cyclic loading. Recent developments in indirect tensile testing offer data that has a greater reproducibility [3], that could lead to industrial acceptance. Plotting stress (Y-axis) and strain (X-axis) measurements obtained through indirect tensile testing allows for fracture toughness (the area under the curve) to be determined. The slope of the plot is also important indicating the rate of energy dissipation. The greater the slope the faster the rate of dissipation and the lower the fracture potential. This is also a valid statement for indirect tensile creep data where deformation (Y-axis) is plotted versus time (X-axis) [10].

In the adhesive industry, it has been found the maximum adhesive fracture energy, G, was obtained when the adhesive layer thickness and the plastic zone were approximately equal [68]. This finding may give the greatest benefit to asphalt concrete when asphalt cement film thickness on the aggregate is equal to the plastic zone size.

In thick fracture specimens, shear yielding and crazing are favored under plane

strain conditions. Both these mechanisms cause extensive plastic deformation at the crack tip giving a greater fracture energy. These are important features when determining the sample thickness for testing since to thin a testing sample may not be representative of the pavement.

3.4 Summary

Microstructure, morphology, adhesion, and fracture are essential areas related to pavement distresses. Fracture of asphalt concrete occurs by a variety of mechanisms including adhesive failure, properties at the crack tip, plastic zone size, void content, and material properties all of which are included in fracture toughness. Fracture toughness is dependent on the fracture strength and therefore dependent on the cracks and flaws in the material. Therefore, knowledge of the crack size and propagation are of fundamental importance. A fundamental understanding of the failure mechanisms of the three types of microstructure; Type H, Type F, and Type P will serve as the foundation for evaluation and optimization of polymers as modifiers to asphalt concrete and for the improvement in asphalt pavement performance.

Chapter Four and Six will present existing and proposed testing techniques for microstructural, morphological, adhesion, and fracture investigations of asphalt concrete. Specifically, thin asphalt concrete plane sections are required for the morphological and microstructural investigation of air void shape, size, distribution, and density. The use of a fracture test will make it possible to observe the crack formation mechanisms and their propagation.

Chapter Four

Experimental Details

Four experimental methods have been developed for characterization of asphalt binder and asphalt concrete. They are: thin section specimens for void morphology, plane section specimens for void image analysis, fracture specimens for crack propagation and fracture mechanism, and failed fracture specimens for determining locus of fracture.

4.1 Sample Preparation

In each test the initial preparation was the same. A core sample from an existing pavement or a Marshall sample was sectioned using a diamond blade saw. The Composite Materials and Structure Center (CMSC) at Michigan State University has a Felker 41-AR rotating saw which was used to cut the Marshall and core samples. The first cuts were done with a large rough cut blade and consecutive cuts were made with a fine diamond blade containing mechanically embedded diamonds. For better cutting, the Felker 41-AR water bath was filled with ice to keep the asphalt sample and saw blade cool. The colder temperature stiffened the asphalt sample and kept the saw blade pores from filling up with asphalt. For the thin section and fracture samples, the Marshall and core samples were cut into specimens with approximate dimensions of 11 x 15 x 40 mm. For the plane sections, the samples were cut into specimens with dimensions of 15 x 50 x 70 mm. Figure 4.1 shows a core cut into thin (1-6) and plane (7-8) sections as prepared by Kirsten Eriksen [49]. Similar cuts were made in the Marshall and core samples.

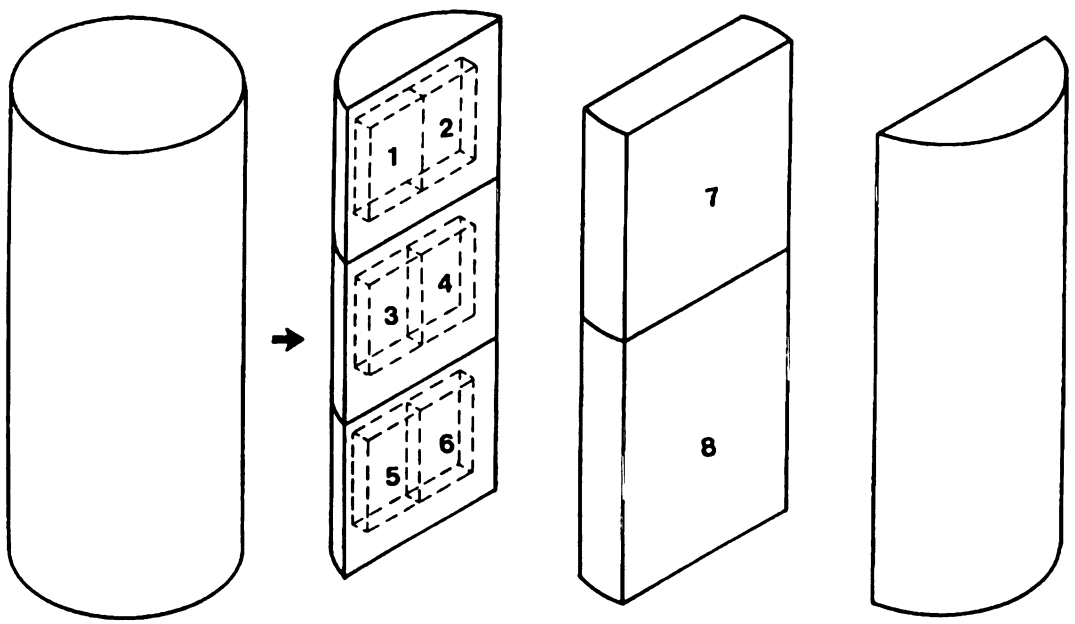

Figure 4.1 - Divisioning of samples for plane sections [49].

The sample type and traffic direction were recorded directly on the material for identification. The direction indicates the traffic flow on the pavement surface. In the case of a Marshall sample marking the top or the bottom was sufficient.

4.1.1 Cleaning

After the samples were cut they required cleaning. Cleaning the samples was accomplished by rinsing them under running tap water. The cut samples were then placed in beakers containing clean water (deionized water at the CMSC) which were placed in an ultrasonic bath for 2 minutes. A Bransonic ultrasonic cleaner made by Fisher Scientific was utilized taking care not to leave the specimens in too long to prevent the aggregate and asphalt from separating. The asphalt specimens were rinsed with deionized water twice and placed on towels to partially air dry. The samples were then placed in a timer controlled oven, Fisher Isotemp oven model 230F, to control the drying at a maximum temperature of 30°C for 6 to 8 hours. The oven was regulated by a Wahl RS210 controller. After oven drying the samples were placed in a desiccator for one day.

4.1.2 Impregnation

Impregnation of the dried samples was accomplished using a two component low viscosity epoxy embedded with a fluorescent dye before mixing. The system used was HQ Epofix Resin and HQ Epofix Hardener from Struers. The dye used was EPODYE (Hudson Yellow) also from Struers. This dye fluoresces at approximately 440 nm in visible light and in the ultraviolet region between 256 nm and 285 nm. Fluorescence emission occurs at 530 nm making the impregnated voids detectable through a filter

system. Filling the voids also helped keep the samples intact when polished to the fine finish that was needed for viewing the thin and plane sections under the microscope. When impregnation was not done, as with some of the fracture samples to enable seeing the effects of filling the voids, it lead to some crumbling problems during cutting and polishing of the samples. The main crumbling problems were from core 1-29-5F(core 1 from section 29 site 5) which showed signs of stripping.

The samples for impregnation were prepared by putting them in a disposable tray, handmade from aluminum foil. As the manufacturer suggested, one liter of the Epofix resin and five grams of EPODYE dye were mixed. The Epofix impregnation medium was then mixed at a ratio of 30 ml Epofix Resin/dye to 4 ml Epofix Hardener. A pasteur pipet was used to measure four milliliters, approximately 180 drops, although each pipet differed. The mixture was stirred for approximately two minutes ensuring complete mixing. The mixture was poured into the foil tray. Samples were positioned to insure that the bottom of the specimens were well covered. The tray was immediately placed in a vacuum oven and pumped down to -0.97 bar. The VWR 1410 vacuum oven with Sargent-Welch DIRECTORR vacuum pump by General Electric was used. It took approximately 2 to 2.5 minutes to reach a pressure of -0.97 bar which was held for 2 to 3 minutes. Outgassing of the sample occurred and foam overflowed the trays, therefore, an overflow sheet under the tray was used to keep the vacuum oven clean. Briefly letting some air in once when the samples were foaming heavily helped break down the bubbles and kept the tray overflow to a minimum. The chamber was then pressurized over a course of one to two minutes by venting the vacuum oven to the atmosphere. The impregnated samples were taken out of the oven, removed from the trays, and placed on

a flat silicone mold for easy removal upon curing.

4.1.3 Curing

The samples were placed in a hood at room temperature for at least 24 hours. During curing, the epoxy hardener will absorb water and be deactivated creating a sticky film on the uncovered surfaces. Therefore, the samples were covered as much as possible to keep moisture away from the surface. After curing, rough sanding using the Leco water cooled Belt Grinder BG-20 removed any sticky film on the samples.

4.1.4 Pre-polishing

The excess epoxy and a thin layer of asphalt from the impregnated side of the samples had to be removed before polishing. This was accomplished with the Felker 41-AR diamond saw cutting approximately two millimeters off the samples thickness or the belt grinder was used to grind it off. Thin sections and fracture samples were made best with the diamond saw in sets of five or six samples all of the same thickness. The same thickness proved to be very helpful during polishing. The best method to pre-polish the plane sections was to do one at a time grinding the impregnated side on the belt grinder.

4.1.5 Polishing

The samples were prepared for polishing by affixing a strip of one inch double sided Scotch tape to the cut side after it had dried. One strip of tape for the thin and fracture samples and two strips for the plane sections were used to cover the entire sample to keep the samples on the polishing wheel and from breaking during polishing. The

polishing wheel was from the Struers Abramin Automated polisher and made out of aluminum. Either, one plane section was mounted in the center or five to six thin or fracture samples were mounted and evenly distributed in a circle pattern on the polishing wheel. The first grinding was to level the specimens using 120 grit silicon carbide abrasive paper. The time this step took depended on the thickness variability of the samples attained during the pre-polishing step. Experience suggests cutting the samples with even thickness is best. The pressure setting during polishing on the Abramin was approximately 3 Nx10, although higher settings were used. When these higher pressure settings were used, the samples would not always level. Once the samples were level they were taken off the polishing wheel, turned over, dried, taped, and fixed to the wheel again for the polishing of the first finished side of the sample. Since polishing took more than a few seconds, a block of ice was polished at the same time as the asphalt specimens keeping the surfaces cool and the asphalt behavior glassy. The first polishing was started with 120 grit and cycled through 240, 320, 600, 1000, 2400, and 4000 grit wet or dry abrasive paper at two minute intervals. Water was always used during polishing to lubricate the surfaces. After polishing with the 120 grit the samples were checked for levelness by visual observation. Polishing was continued at 120 grit until all samples were level. When the abrasive paper was changed the samples and the sanding wheel were thoroughly rinsed. The samples were placed under running tap water and the sanding wheel was rinsed utilizing its water outlet. After polishing with the 240 grit paper, the samples were examined to insure that less than five percent of the surface showed empty air voids. If the surface showed a larger void concentration the impregnation process was completed again. During a second impregnation process upon

reaching the pre-polishing step, grinding was done instead of cutting the specimens were there was a better chance of having the voids filled because only a thin layer of asphalt was removed. Upon completion of the 4000 grit paper the samples were removed, rinsed, and air dried for 30 minutes. The specimens were then dried overnight in a desiccator.

4.1.6 Mounting

The specimens were affixed to their respective mounting plates. The thin sections were affixed to glass petrographic slides with dimensions of 27 x 46 mm. The plane sections were affixed to glass petrographic slides with dimensions of 51 x 75 mm. The glass slides were purchased from Hugh Courtright and Co. LTD. The fracture samples were affixed to a strip of 0.01 inch thick polycarbonate film, Lexan 8010, with approximate dimensions of 35 x 100 mm. The polycarbonate film was purchased from Cadillac Plastics and Chemical Company. The petrographic slides were ground to a level finish prior to use. A *Buehler Petro-Thin* Thin Sectioning System was used to grind each slide to a ±5 micron finish. This equipment is maintained by Robert Harris and located at the Michigan State University, Geological Science's Thin Section Laboratory in the Natural Science building, room 6. The laboratory phone number is (517) 353-7235. The finish was achieved by removing approximately the top 50 microns giving a ground glass appearance. The adhering agent used to affix the samples was EPON 828 (bisphenol A/ epichlorohydrin) with a V-40 curing agent (dimer fatty acid/ polyethylene polyamine based polyamide) from Shell Oil Company. The samples were cured at room temperature for four or more days. The manufacture suggests four to seven days for curing to full strength. The mixture proportions used were 50/50 resin and hardener and mixed well.

The amount of epoxy needed at a time was only about five milliliters, but consistent formulation and mixing was better attained with about ten milliliters of each. The epoxy mixture was applied in a very thin layer through the use of a tongue depressor. In thin and plane section preparation the entire sample was adhered with epoxy. In fracture samples epoxy was only applied to a small part of each end was insuring no epoxy got on the center of the sample where fracture occurs later. To eliminate all of the air voids, the sample and its respective mounting plate were pressed together creating a very thin even film of epoxy. Dead weight loading of the samples during the cure helped create a thin even film also. A 100 gram weight was sufficient. Curing was performed in a hood on a level surface to keep the samples from sliding off their plates.

4.1.7 Thin sectioning

The samples were cut thin and polished on the *Buehler Petro-Thin* Thin Sectioning System. Figure 4.2 is a photograph of the thin sectioning system and viewer. The system was designed for metal thin sectioning, but worked well in this application. A vacuum held one slide in place at a time while a rotating diamond blade cut the sample. The cutting speed was hand controlled. This speed was slow and steady ensuring the blade did not drift and start cutting at an angle. The samples were cut around one millimeter thick. After cutting, a sample was polished to a thin and even surface with a diamond grinding wheel in the same device. Again the entry speed of the sample was controlled by hand giving the best results when slow and steady. Grinding at fast speeds caused the sample to be thicker in the middle and lead to excessive material removal at the end edges due to the way the sample entered the grinding wheel. The system was water cooled.

Figure 4.2 - *Buehler Petro-Thin* thin sectioning system and viewer.

The thin and plane sections were cut and polished to 20 to 30 μm, while the fracture samples were left at approximately 1 to 1.5 mm thick polishing only enough to level the samples. The system has the capability of controlling polishing to ± 5 μm through the use of a micrometer. For thin and plane sections, sample thickness was attained using a *Buehler Petro-Thin* Thin Section Viewer in combination with the thin sectioning system. The viewer uses polarized light and the principles of refraction to allow a user to determine specimen thickness. This is done through the use of a Michel-Levy Chart and quartz, a common rock also found in the asphalt concrete. A Michel-Levy Chart is a color chart relating aggregate thickness to refracted light colors for 66 aggregates. The samples were visually polished down to approximately 50 to 100 microns in 100 micron steps using the micrometer. The samples were then polished 20 microns at a time removing the sample each time and placing it under the viewer to observe the bright colors from light diffraction through the aggregate. When the quartz aggregate no longer deflected the light the sample generally took on a grey color indicative of the first order region and approximately 20 to 30 μm thick. Thin and plane sections were also made at approximately 50, 100, and 150 microns for comparative testing.

When the fracture samples were cut the polycarbonate film did not vacuum seal as well as the glass slides and had to be kept in place by hand due to the high shear forces applied to the sample. This was the reason for the large film size. The protective polyethylene film over the polycarbonate was removed before placing the sample on the vacuum port for cutting. The first cut was made through half to three-quarters of the specimen after which it was turned around and the cut finished. The vacuum was sufficient to hold the sample in place during the following polishing procedure. During

cutting and polishing the vacuum system must be rinsed frequently with large amounts of water to keep the line free of asphalt particles. The small asphalt particles can plug up the vacuum line stopping the experiment for a three or more hour repair when the line is not rinsed frequently.

4.1.8 Converting to a tensile specimen

The fracture samples were turned into dogbone samples and holes drilled in the ends for mounting in the tensile frame. The steps are outlined in Figure 4.3. First, the long sides of the polycarbonate film were cut down to within 5 mm of the asphalt specimen with a trimming board. A dogbone sample was then created by cutting out the center region, where the EPON 828 was not applied, with a TensilKut made by Sieburg Industries located in the CMSC. The sample was mounted in a preformed dogbone sample guide to assist in the cutting. Following this the ends were cut down with a razor blade or trimming board leaving approximately 2 cm. The screw holes for mounting in the tensile frame were then marked and drilled. The excess polycarbonate left on the edges during drilling and dogbone preparation was trimmed as final sample preparation.

4.2 Mechanical testing of the fracture samples

The fracture samples were strained to determine crack propagation, fracture mechanism, and locus of fracture. For tensile testing, a sample was mounted in a tensile frame for hand straining. The tensile frame has a 200 lb strain capacity. This frame was then mounted in an anvil to keep the sample in place for video recording during straining.

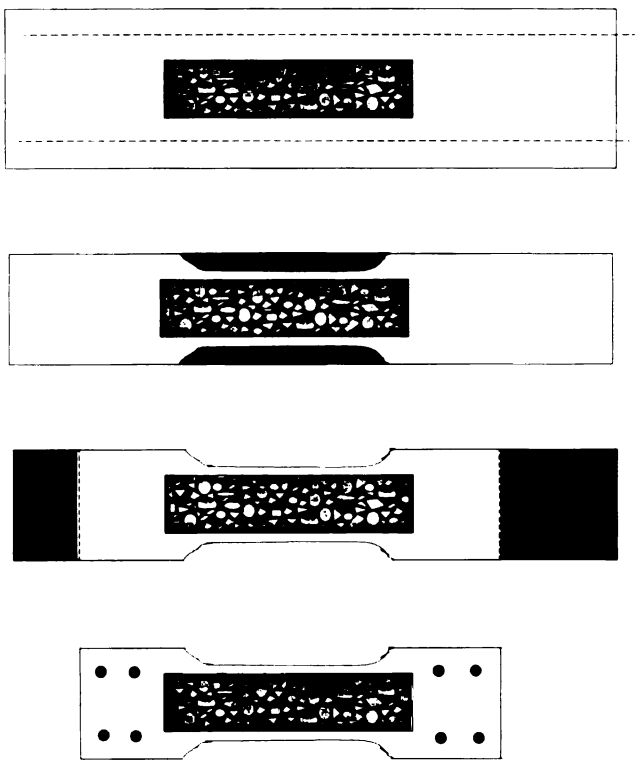

Figure 4.3 - Steps to final preparation of the fracture samples.

4.2.1 Recording system

Straining was performed in front of a 200 mm zoom lens hooked to a high speed camera, Kodak EKTAPRO 1000 Motion Analyzer. Figure 4.4 [126] shows the manual's diagram of the camera equipment while Figure 4.5 is a photograph of the experimental setup. The high speed camera has the capabilities to take pictures of events from 50 to 6000 frames per second of which 125 frames per second was deemed sufficient. This gave a 13.1 second time period to capture pictures of the failure. The time period of the pictures is based on the ability of the computer to store 1637 frames. These frames can then be played back at speeds ranging from one per second to 480 frames per second allowing for slow close up images to investigate crack propagation and the failure mechanisms. Tests were conducted at room temperature.

4.2.2 Lighting

Good lighting was essential for viewing the asphalt fracture sample. Two lights were utilized one on each side of the sample for oblique lighting. Oblique lighting offered the highest contrast between the aggregate and asphalt cement. Dye coated and gold coated samples were also made and tested, but the non coated fracture samples gave the best contrast. A goose neck halogen light was also used behind the specimen to highlight the voids and cracks as they developed.

4.2.3 Recording

Recording was done in a couple of different ways; start recording or stop recording. Start recording is normal recording when the record button is pushed. Stop

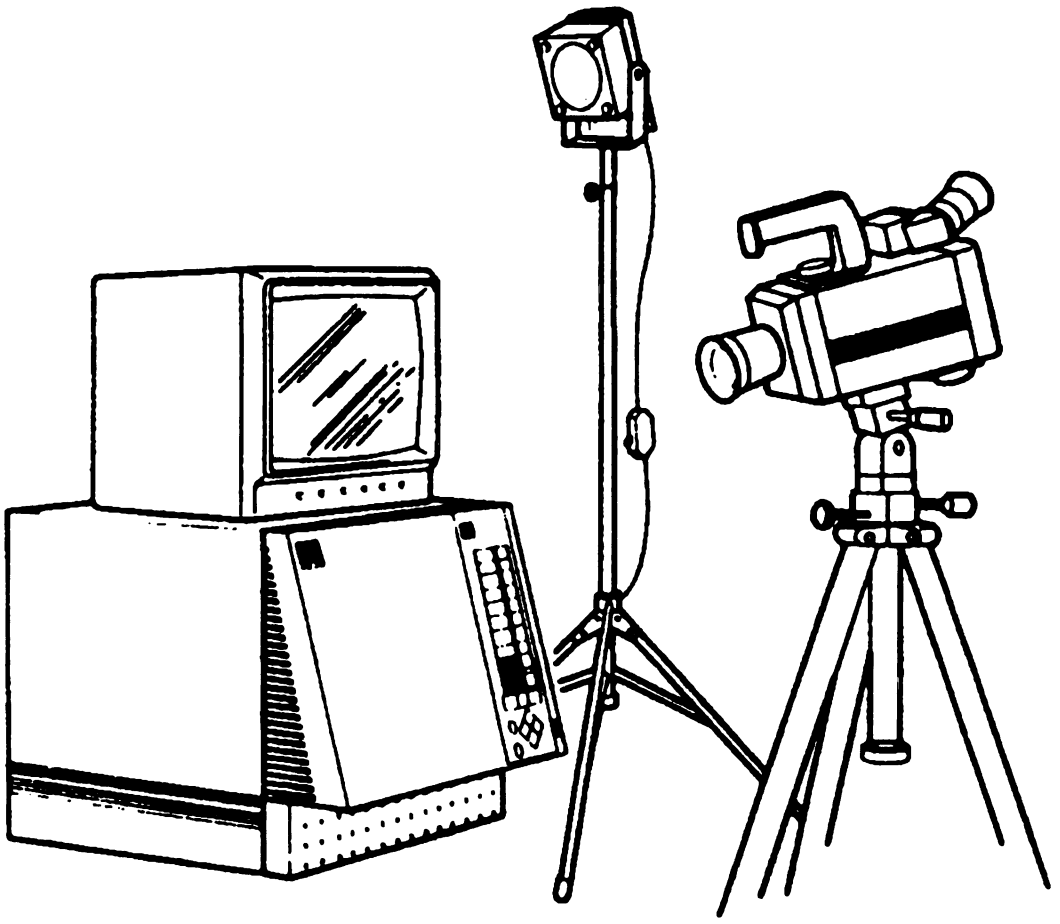

Figure 4.4 - Kodak EKTAPRO 1000 Motion Analyzer [126].

Figure 4.5 - Experimental setup of the Kodak EKTAPRO 1000 Motion Analyzer.

recording records the past 1637 frame after the recording is stopped. This can be done because the computer memory can be thought of as a wheel that continually stores images replacing the oldest with the new until told to stop. The last method, called stop recording, was used most of the time so rushing at the beginning was not an issue because upon failure of the sample the test was stopped capturing the fracture. Whereas, the fracture process was just starting generally when the recording was stopped automatically after filling 1637 frames using the regular recording mode.

Before actually starting the recording of the test, the lights and camera settings were adjusted with the image on the screen in the live mode. When everything was set, the computer was prompted into the ready mode, record was pressed in the stop record mode, and the sample was strained by hand. Upon failure, the stop button was pressed storing the images in the computer for visual observation. The stored images were then down loaded onto super and/or regular VHS tape for storage, presentation, and later analysis. Super VHS gave better resolution and is the choice media with the exception of presentations where most places do not have direct access to super VHS players. When down loading onto a tape the play back speed of the recording was set at 5 or 7 frames per second while the video recorder recorded at its predetermined setting of 30 frames per second. This recording rate allowed better photographic and viewing capabilities. A thermal printer was available for a quick print of the screen image. This picture is rather small, 2.25 X 2.75 inches, having good print quality with a good grey scale although somewhat darker than desired at times. These thermal prints make excellent laser scanned images with computer enhancement for enlarging. A picture of the screen can also be taken with a 35 mm camera and a Screenshooter. A Screenshooter is a product of NPC

Photo Division which acts as a light funnel and camera mount enabling pictures to be taken of a monitor screen. For comparison, Figures 4.6 and 4.7 present a thermal print image and a 35 mm photograph, respectively. The 35 mm prints offer better handling and visual characterization away from the computer, but lack in a full grey scale.

4.3 Microscopic Analysis

4.3.1 Thin and plane section samples

Morphology and microstructure of thin and plane sections were observed under a BH-2 Olympus optical microscope with reflected light. Void analysis uses the fluorescent dye that has been impregnated in the asphalt samples. The impregnation medium fluorescence was visible through a set of two filters. The two filters were purchased from Scientific Supply Company, an exciter filter cutting off light above 515 nm (45 mm in diameter) and a banded barrier filter at 530 nm (20 mm in diameter). A 100 watt TH3 Olympus power source with halogen bulb illuminated the dye embedded regions allowing the void size, shape, and distribution to be seen. The exciter filter was placed straight up and down in the light path between the light source and the main body in the slot just after the light source. The barrier filter was placed between the sample and the eyepiece or camera in the polarizer slot in the front of the microscope. This same fluorescent filter setup was utilized for the image analysis of the plane sections, discussed later.

The micrograph system used was a Polaroid 545 land film holder with light funnel (PM-10ADS) and an AD system Exposure Control Unit PM-CBSP by Olympus allowing the use of Polaroid high speed 4 x 5 instant sheet film. Type 57 film, ISO 3000/36° with

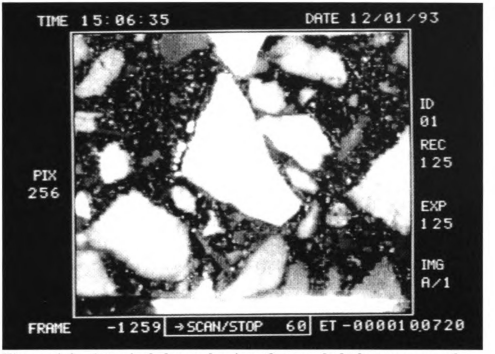

Figure 4.6 - A typical thermal print of an asphalt fracture sample.

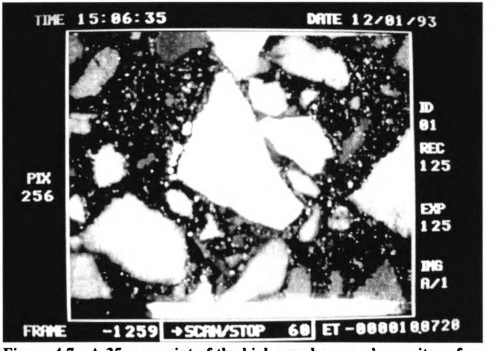

Figure 4.7 - A 35 mm print of the high speed camera's monitor of an asphalt fracture sample.

low light capabilities was needed. The exposure control unit settings were set on; format, L, ISO/ASA, 3200, reciprocity, 4, exposure adjust, 1, and auto exposure. Some micrographs had a better grey scale contrast when slightly under exposed using the exposure setting and manually reducing the exposure time. This was due to the film being ISO 3000 and having to set the speed at the predetermined setting of 3200 in the Exposure Control Unit. The final magnification on the micrographs with a 5X objective lens, a 2.5X photo relay lens, and 3X light funnel magnification was determined to be 38X through the use of a calibration slide. A typical picture of an observed void field is displayed in Figure 4.8. The light areas are voids and the speckles are reflected light off the aggregate.

4.3.2 Fracture samples

The microscope was also utilized to observe the failed surfaces of the fracture samples after mechanical testing. The failed samples' aggregate surfaces were observed under a magnification of 50X. Some fracture samples were mounted, while others were hand held for viewing. Holding the samples by hand at 50X created a shaky view, but allowed quick, easy viewing. When magnification greater than 50X was used or when micrographs were taken, the samples were mounted and placed on the stage. Both cohesive and adhesive failure were observed on the fractured surfaces. When both sides of a fracture are covered with asphalt cement it indicates a cohesive failure. Those failures between the asphalt cement and aggregate where no asphalt cement is on the aggregate indicates an adhesive failure at the interface. Observing just one of these kinds of failure is very rare, if ever. Usually failed samples have both cohesive and adhesive

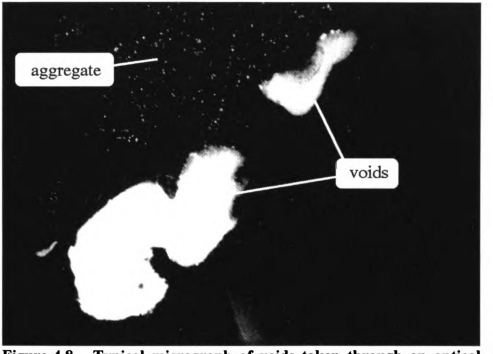

Figure 4.8 - Typical micrograph of voids taken through an optical microscope with reflective lighting represented here at 43X.

failure and are categorized depending on the degree of each type of failure. Of the asphalt samples tested, those exhibiting good adhesion had little adhesive failure and those with poor adhesive properties like asphalt samples showing signs of stripping exhibited a majority of adhesive failure. Later work through ESEM will quantify the degree of each failure type.

4.4 Image analysis of plane sections

Image analysis was performed on plane section samples to determine the void size, shape, distribution, and density. Following the work of Kirsten Eriksen [50], the void area, perimeter, and Ferret diameters were easily determined as well as additional parameters through the use of the CUE-2 image analyzer by Olympus. Figure 4.9 [127] shows the operating manual's system configuration composed of a microscope setup, CCD video camera, image monitor, and computer with monitor. Figure 4.10 is a photograph of the experimental setup consisting of a microscope setup as described previously, CCD video camera model XC-57, Sony Trinitron color video monitor, Galai camera power supply, and Zenith 386/20 computer with monitor capable of EGA graphics. In past work [50] the magnification ranged between 25 to 50X. Currently, the CMSC has reflective light magnification capabilities down to 38X through the use of a 2.5X objective lens and 1.67X photo relay lens in the image analysis system. The additional magnification comes from the internal optics of the camera and camera attachment.

The CUE-2 system analyzes objects through a black and white system upon calibration of the system. Initially the camera image was digitized into a 256 grey scale

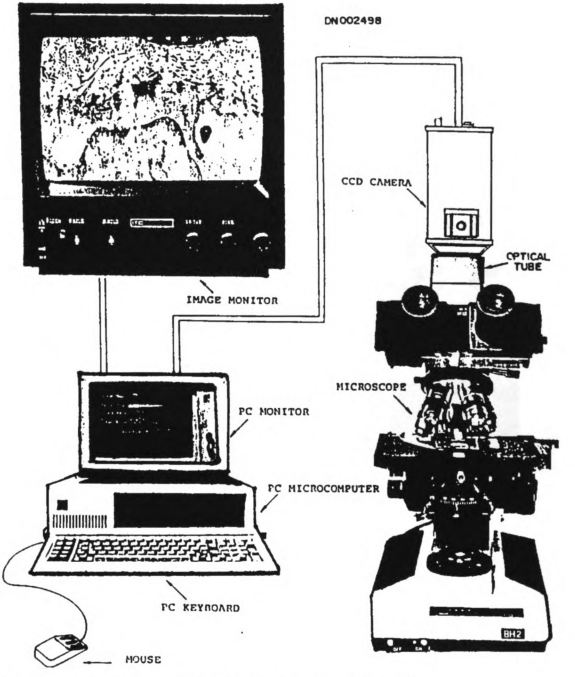

Figure 4.9 - Auto Image Analysis System Configuration [127].

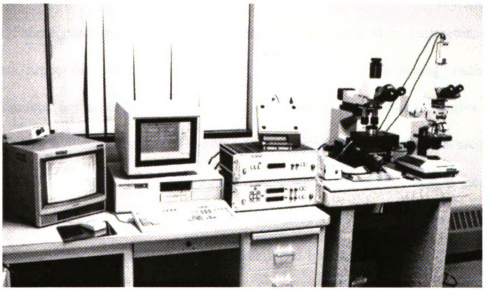

Figure 4.10 - Experimental Auto Image Analysis System.

image that was enhanced to determine the break points, or dividing regions, where the image was converted to a black and white image. It was important to have the camera settings of GAMMA and A.G.C. (automatic gain control) in the on positions. This offered a better grey scale image to initially digitize the asphalt samples. Computer analysis of the image gave the following parameters for each object in the digitized image or set of images; area, perimeter, convexity, center of gravity, Ferret's diameters, orientation, aspect ratio, shape factor, specific length, hole area, hole area: object area, areafract, mnlinintc, meanchord, anisotrpy, closeappr, areafill, avrg radius, and Martin's radii. Of these parameters the following ones were recorded; area, perimeter, Ferret's diameters, aspect ratio, shape factor, specific length, areafract, and average radius. The Ferret diameter is the projection of the object measured at predetermined angles through the center of gravity to the edges of the object. The Ferret diameter was measured at four angles, but can be measured at up to 32 different angles. The aspect ratio is the ratio of minimum Ferret diameter to the maximum Ferret diameter. Shape factor is a measurement of the sharpness of an object calculated by multiplying the area by 4π and then dividing by the perimeter. A shape factor of one refers to a circle and zero to that of a straight line. The specific length is the total length of an object similar to that of the Ferret diameter, but not measured at specific angles or necessarily through the center of gravity. Areafract is the ratio of the area of an object over the total frame analyzed area. Average radius is the mean of the eight Martin Radii, where a Martin radius is the distance from the center of gravity to the object edge at predetermined angles of 0, 45, 90, 135, 180, and 225 degrees.

Image analysis was done through digitizing a set of images for each plane section

sample. The image analysis measured area of the section should be at least 500 mm^2 spread over a total test area of 7,000 mm^2 according to Kirsten Eriksen [50]. The plane section samples each had a maximum area of 3825 mm^2, the area of our largest petrographic slide useable with the equipment available. Therefore, the results of two slides were combined or in some cases a smaller total test area was used. At the start of an analysis run, a plane section sample was placed under the microscope and an image focused. Next, the autoroute was defined through a number of predetermined steps. The steps used for the analyses included: image stretching, clear small objects, pause, fill holes, total image statistics, add to data base, and store lotus file. Upon defining the autoroute, a manual enhancement and preprocessing was done to set the parameters for the computer to follow. By pressing the <F1> key, the enhancement and preprocessing step was started where a picture sketching was conducted via a grey scale histogram by pressing <F2>. For the images analyzed a dividing low value of 40 and high value of 41 worked well. These values did vary day to day dependent on the lighting conditions. The dividing values converted the grey scale pixels assigned values ≤ 40 to 0 the value for black pixels and those pixels with values ≥ 41 were converted to white pixels. Thus, a black and white image was formed. This ended the manual operation and the original picture was returned to for start of the autoroute. At this point the user was prompted for the number of images to be analyzed. The number of images needed for analysis depends on the field image size (area of the frame), which depends on the magnification. At 38X, at least 29 images need to be analyzed. This number was determined by dividing 500 mm^2 by the field image size of 17.5 mm^2.

It is important to note that the raw data file being stored in the form of a lotus file

can be added to as long as the parameters being collected during tests are the same. This allows testing to be stopped and restarted during an image analysis data set collection.

The pause was placed in the autoroute before the total image analysis to take a negative of the image, switching the black and white pixels. This was because the computer only analyzes black images and the voids were white before taking the negative. To take a negative simply press <n> when the autoroute stops, wait for the image to appear, and when prompted press the <esc> key to restart the autoroute. After each image was analyzed the computer prompted the user to change the image position manually and continue the program by pressing <y> when the new image was ready or to discontinue by pressing <n>.

Selection of the image position for analysis was done systematically to avoid bias. The plane sections were analyzed every 10 increments in the X direction and then every 5 in the Y direction avoiding the use of the edges where artifacts of sample preparation might appear. The increments are those found on the movable microscope stage. Figure 4.11 shows the general pattern used where the rectangles show the area analyzed and the numbers indicate the stage increment numbers. Those numbers including an R on the Y axis represent the slide being rotated 180 degrees on the stage enabling the entire sample to be analyzed.

4.5 Raw data conversion for plane section analysis

Some image statistics were available through the CUE-2 system, but they were limited to the screen output and graphs. For these reasons processing of the raw data via

a spreadsheet was more appropriate. The Lotus formate file can be imported to various spreadsheets including Supercalc 5.0 and Excel. Supercalc 5.0 was chose for the work done here. The recorded data was imported as a 1-2-3 Lotus file to calculate additional parameters. The data on air void area, A; perimeter, Pm; and max Ferret diameter, Fe; were used to calculate the following parameters for each object: air void content, P_a; average area, A*; equivalent circle diameter, D_a; average equivalent circle diameter, D_a*; form factor, F; and weighted average form factor, F* [50]. Equations 4-1 through 4-6 found in Table 4.1 show these calculations.

During the image analysis some diffraction and irregularity of lighting commonly called noise was encountered and interpreted by the computer as objects. Most of these objects were small enough to be eliminated in the enhancement and preprocessing step. A key factor is how to eliminate the rest of this noise and not hurt the data collection. In previous work [50], voids or objects with equivalent diameters less than 50 microns were discarded and the void class interval from 0 to 100 microns was slightly distorted. This kind of noise reduction works, but observations were made showing some voids were also eliminated. It is still to be determined whether or not these voids have structural importance. All the parameters were calculated and collected for a determination of the best noise eliminating factor to be determined at a later time when enough data accumulates.

Table 4.1 - Image Analysis Equations

Air Void Content, P_a

$$P_A = \frac{\Sigma A}{Number\ of\ fields\ x\ field\ area} * 100\ Vol\% \qquad (4\text{-}1)$$

Average area of air void sections, A*

$$A^* = \frac{\Sigma A}{Number\ of\ air\ voids} \qquad (4\text{-}2)$$

Equivalent circle diameters, D_a

$$D_a = 2\sqrt{\frac{A}{\Pi}} \qquad (4\text{-}3)$$

Average equivalent circle diameter, D_a*

$$D_a^* = \frac{\Sigma D_a}{Number\ of\ air\ voids} \qquad (4\text{-}4)$$

Form factor, F

$$F = \frac{(D_a)^2}{Fe^2} * 100 \qquad (4\text{-}5)$$

Average form factor, F*

$$F^* = \frac{\Sigma F}{Number\ of\ air\ voids} \qquad (4\text{-}6)$$

4.6 Summary

Sample preparation of thin, plane, and fracture samples was similar. Thin and plane section samples allow investigation of void morphology and microstructure through microscopic and image analysis. Fracture samples allow investigation of crack propagation, fracture mechanisms, and locus of fracture through high speed photography and microscopic analysis. Thin and plane section samples were obtained as thin as 20 μm to investigate a single slice of an asphalt core or Marshall sample. Fracture samples, 1 to 1.5 mm thick, were tensile tested at room temperature under oblique lighting to enhance the asphalt-aggregate contrast, thereby allowing fracture to be seen and crack propagation followed.

Chapter Five

Results

This chapter consists of results and discussion of the four experimental methods: thin and plane section morphological and microstructure analysis; plane section air void image analysis; crack propagation of asphalt fracture samples; and microscopic analysis of fracture samples to determine their locus of fracture.

5.1 Morphological and microstructural analysis

Under normal lighting of the thin and plane sections the impregnated voids are yellow in color and hard to characterize in black and white, therefore samples have been viewed under UV lighting and through a two filter fluorescent system. The UV lighting condition allowed for visual observation of void distribution while the two filter system allowed quantitative results through optical microscopy and image analysis of plane sections. Figures 5.1, 5.2, 5.3, and 5.4 illustrate the difference between a good and bad sample plane section and their respective air void content. Good infers the sample shows signs of good adhesion while bad samples show signs of poor adhesion and adhesive failure. The good samples were made from Marshall samples and the bad samples were made from an aged road core, section 29, site 5. The black spots in Figures 5.2 and 5.4 illustrate the voids of the samples in Figures 5.1 and 5.3. These spots would be the colored voids visible under UV and fluorescent conditions.

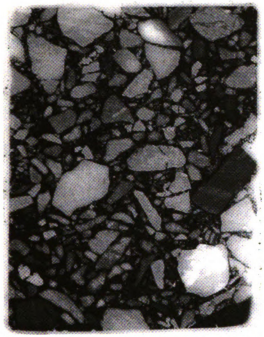

Figure 5.1 - Photograph under normal lighting of a 30 μm good plane section at 1.5X.

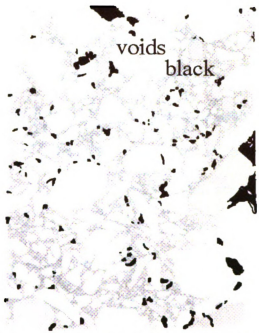

Figure 5.2 - Illustration of good section showing the voids at 1.5X.

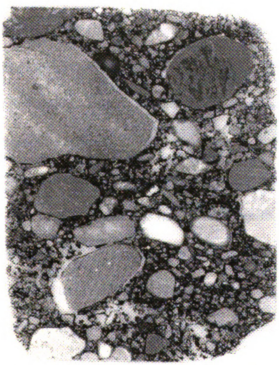

Figure 5.3 - Photograph under normal lighting of a 30 μm thick bad plane section at 1.5X.

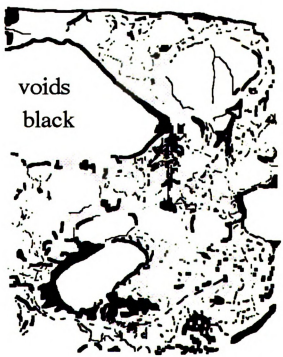

Figure 5.4 - Illustration of bad section showing the voids at 1.5X.

The two filter fluorescence emission system was used in conjunction with optical microscopy for micrographs and image analysis. The low magnification allowed investigation of the air voids in thin and plane sections. The thin sections are smaller than the plane sections and easier to make which serve well for morphological characterization. Figures 4.8, 5.5, and 5.6 illustrate small and large voids found in good asphalt samples, while Figures 5.7 and 5.8 illustrate voids found in bad samples. The light areas are the voids. In the bad samples, extra long voids were found formed along aggregate edges where adhesive failure had occurred. In both good and bad samples, voids were generally found associated with the aggregate surface where the surface was not completely wet.

Thin and plane sections offer good 2 dimensional void characterization of size, shape (morphology), and distribution which includes the enclosed voids not measurable through bulk testing. The test does have a problem being only 2 dimensional in analysis and not offering a means for 3 dimensional analysis of the interconnected void relationship. But, an incorporation of bulk testing with thin section analysis could solve the problems leading to a good void analysis. Relating the current testing on conventional asphalt to PMA's, microscopic sample observation allows characterization of the air void formation that occurred during the asphalt/aggregate wetting process. Sample preparation of conventional asphalts benefited when the processing temperatures were kept below the materials T_g through the application of ice in the saw's water bath and on the polisher. The cold temperature kept the saw blade's pores and the abrasive paper used for polishing from filling up with asphalt. Polymer modification will lower the asphalt T_g, thereby requiring sample preparation with colder temperatures.

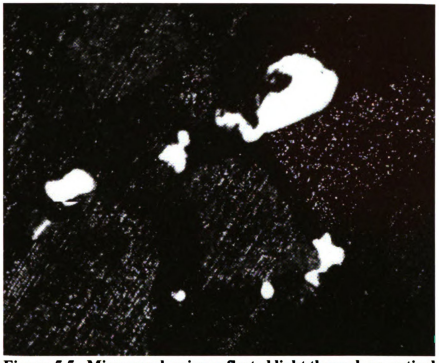

Figure 5.5 - Micrograph using reflected light through an optical microscope showing voids in a good sample at 41X.

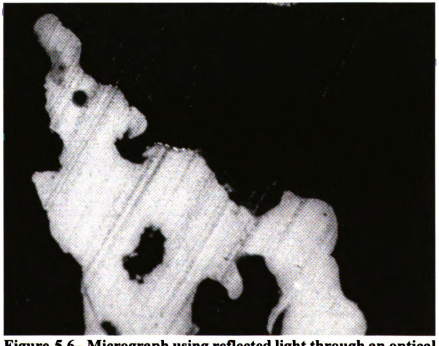

Figure 5.6 - Micrograph using reflected light through an optical microscope showing a void in a good sample at 38X.

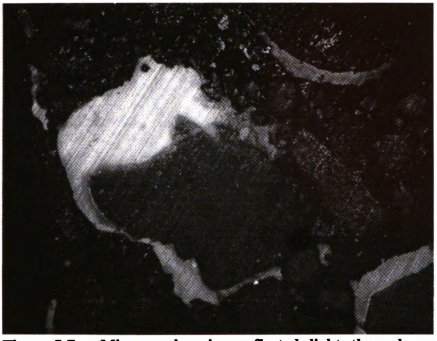

Figure 5.7 - Micrograph using reflected light through an optical microscope showing voids in a bad sample at 19X.

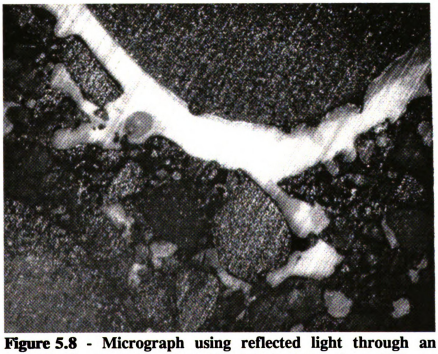

Figure 5.8 - Micrograph using reflected light through an optical microscope showing voids in a bad sample at 19X.

5.2 Plane section image analysis

Air void image analysis using the two filter system utilized fluorescence for high contrast between the voids and other material. Both a good and bad core were analyzed. The good core, Figure 5.9, was a Marshall specimen with five percent by weight asphalt cement and a bulk air void content of 3.6 percent as determined by the Michigan Department of Transportation. The bad core, Figure 5.10, was core 1 of section 29, site 5, flexible pavement which showed signs of stripping. The bad plane sections tested were taken from the middle section of the core where stripping was at a maximum.

Figures 5.11 and 5.12, a photograph and drawing, display the two good plane sections tested and analyzed. Table 5.1 presents a summary of the image analysis results. Figures 5.13 and 5.14 are graphical forms presenting the tabular data for the equivalent circle diameter and area of the voids showing void range distributions. Note the log scales showing the wide range of values detected and presented. Original and analyzed data sets from the good core are located in the appendix in Table A-3 and A-4, respectively. The air void content tested through image analysis is higher at 4.5 percent air void content as compared to its bulk testing measurement of 3.6 percent. A higher percentage would be expected with image analysis since the closed air voids are counted in the analysis. During data collection care must be taken so that the data is not skewed by unrepresentative or too few images that are not representative of the entire core.

The bad core was analyzed by the same method at two different thicknesses, 30 μm and 150 μm. The results for their analyses are presented in Figures 5.15 through 5.22 and Tables 5.2 and 5.3. The 30 μm bad sample gave a higher void content of 17.5

Figure 5.9 - Typical Marshall specimen of asphalt concrete at 2X.

Figure 5.10 - Asphalt core 1 of section 29, site 5 (used for bad samples) at 3.7X.

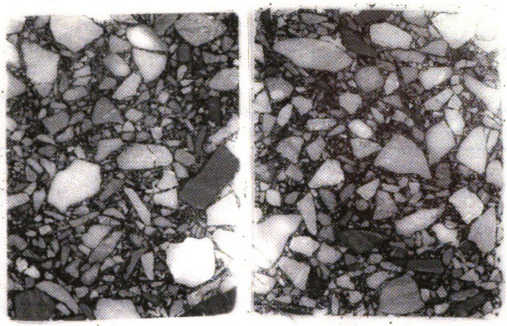

Figure 5.11 - Photograph of Sample: Good98 under normal light at 1.3X.

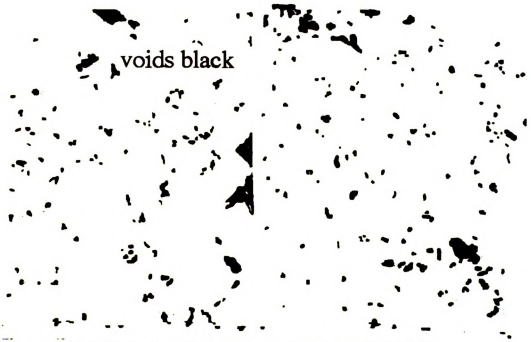

Figure 5.12 - Illustration of Good98 showing the voids at 1.3X.

Table 5.1 - Good98 plane section image analysis results.

	all voids	voids >50 μm eq._cir_dia
Air void content, P_a (vol %)	4.6	4.5
Average area of air void sections, A* (mm^2)	0.036	0.072
Average equivalent circle diameter (eq._cir_dia), D_a*(mm)	0.092	0.146
Average form factor, F*	58.3	53.7
Total area of plane section, (cm^2)	57.0	57.0
Total scan area, (cm^2)	7.0	7.0
Number of fields	40.0	40.0
Number of air voids	895.0	434.0

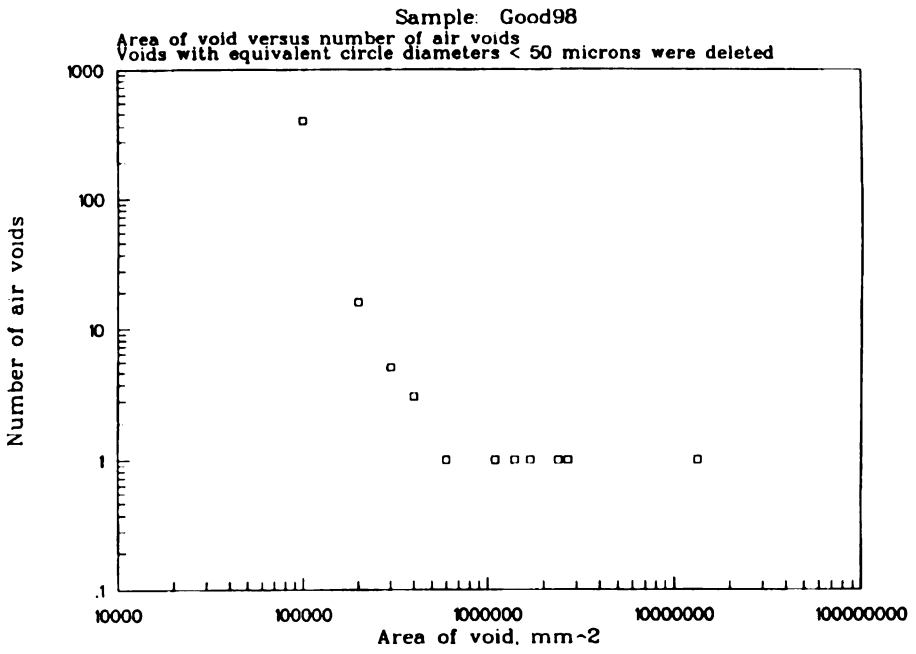

Figure 5.13 - Graphical results for air void area in sample Good98.

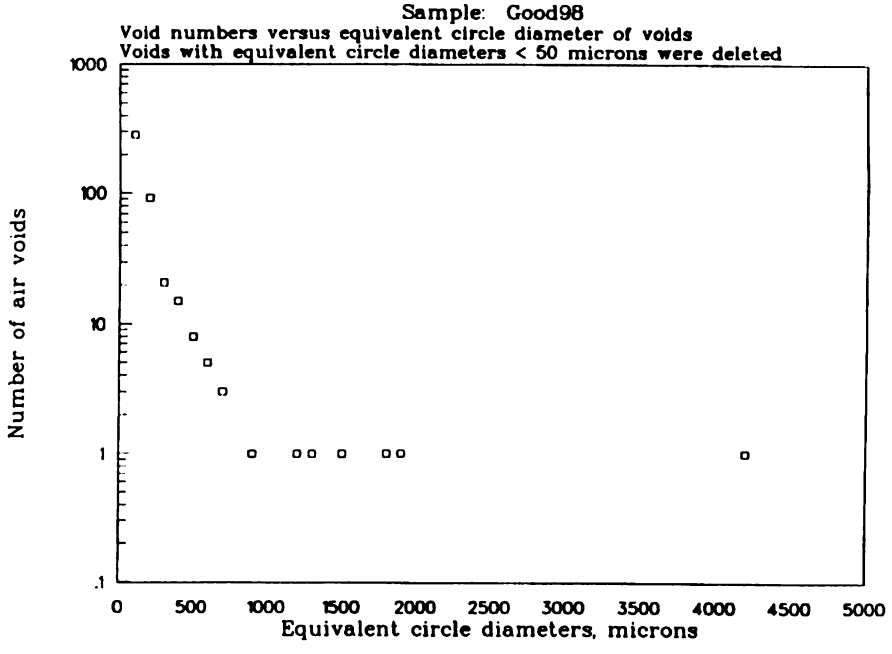

Figure 5.14 - Graphical results for air void equivalent diameters in sample Good98.

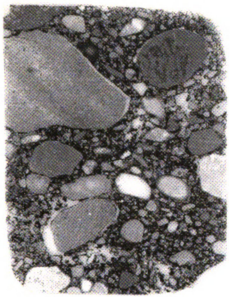

Figure 5.15 - Photograph of Sample: Bad30 under normal light at 1.2X.

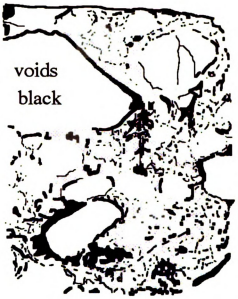

Figure 5.16 - Illustration of Bad30 showing the voids at 1.2X.

Table 5.2 - 30 μm thick bad plane section image analysis results.

	all voids	voids >50 μm eq._cir_dia
Air void content, P_a (vol %)	17.5	17.4
Average area of air void sections, A* (mm^2)	0.092	0.164
Average equivalent circle diameter (eq._cir_dia), D_a*(mm)	0.136	0.21
Average form factor, F*	57.1	53.0
Total area of plane section, (cm^2)	27.6	27.6
Total scan area, (cm^2)	3.5	3.5
Number of fields	20.0	20.0
Number of air voids	667.0	372.0

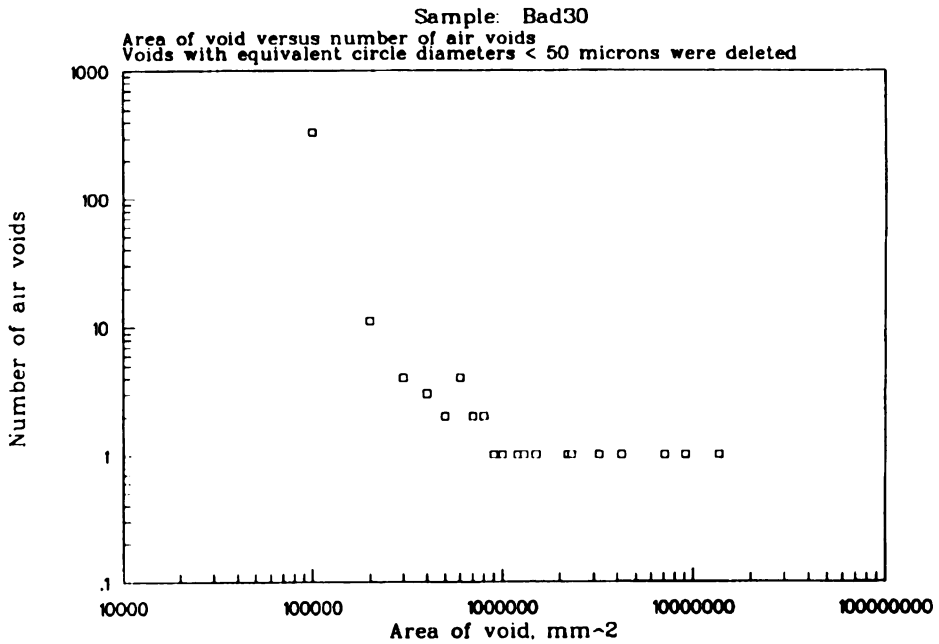

Figure 5.17 - Graphical results for air void area in sample Bad30.

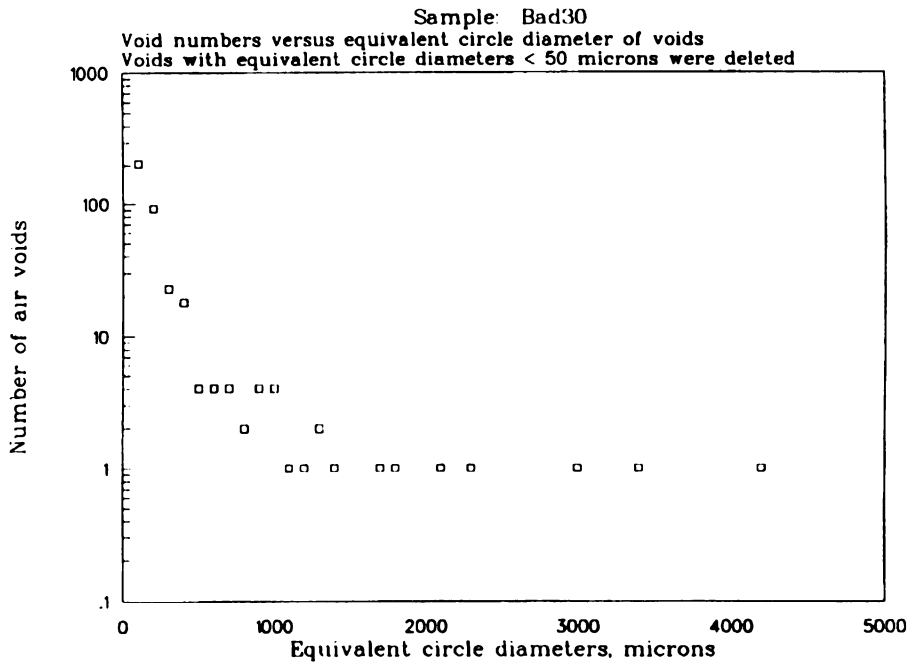

Figure 5.18 - Graphical results for air void equivalent diameters in sample Bad30.

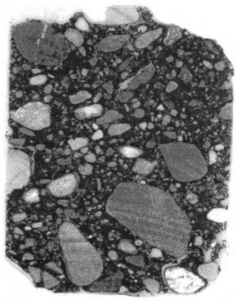

Figure 5.19 - Photograph of Sample: Bad150 under normal light at 1.2X.

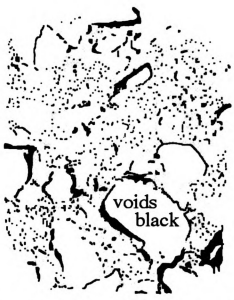

Figure 5.20 - Illustration of Bad150 showing the voids at 1.2X.

Table 5.3 - 150 μm bad plane section image analysis results.

	all voids	voids >50 μm eq._cir_dia
Air void content, P_a (vol %)	8.0	7.9
Average area of air void sections, A* (mm^2)	0.079	0.103
Average equivalent circle diameter (eq._cir_dia), D_a*(mm)	0.192	0.239
Average form factor, F*	52.6	49.8
Total area of plane section, (cm^2)	26.8	26.8
Total scan area, (cm^2)	3.5	3.5
Number of fields	20.0	20.0
Number of air voids	352.0	269.0

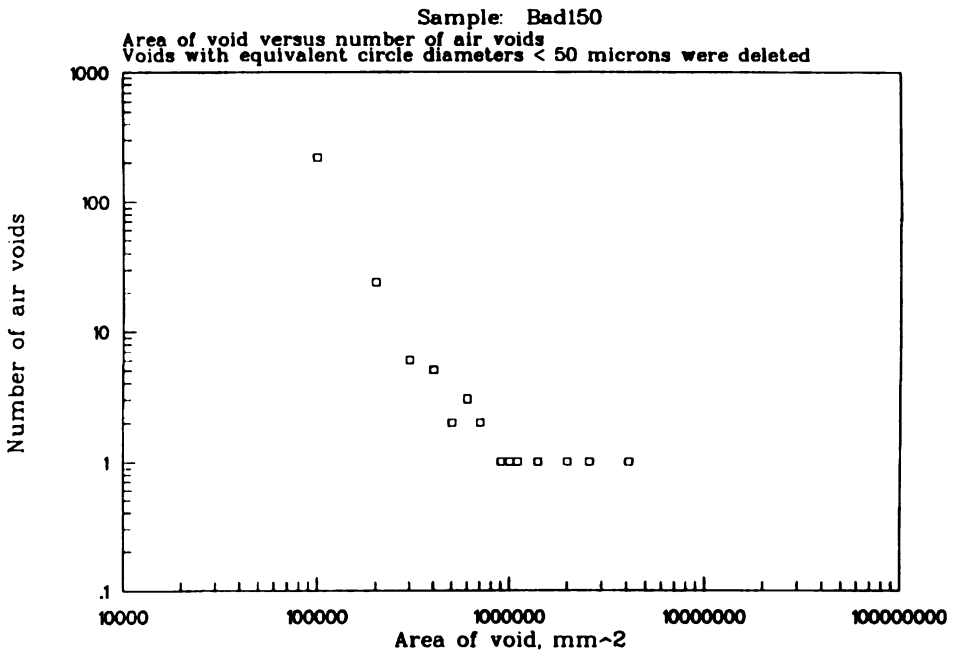

Figure 5.21 - Graphical results for air void area in sample Bad150.

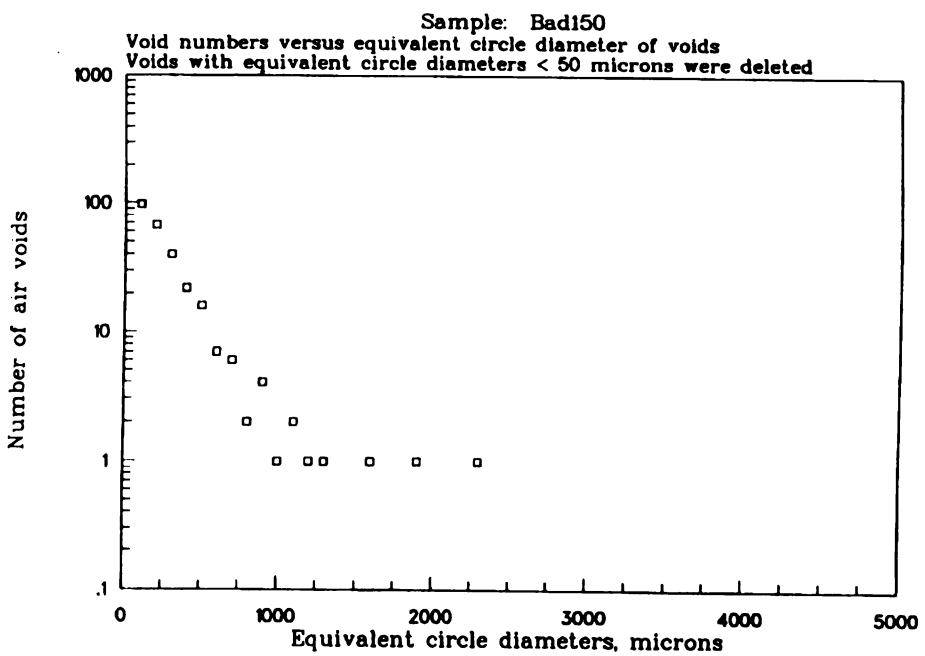

Figure 5.22 - Graphical results for air void equivalent diameters in sample Bad150.

percent while the 150 μm bad sample was only 8.0 percent. This large difference is attributed to sample section location, stripping effects, and the 150 μm bad sample not having all of the closed voids filled, thereby giving a smaller air void content. The 30 μm section sample allowed for an analysis of a single layer of asphalt a closer estimation to the correct air void content. In this case the stripping effects look to have skewed the data, but the stripping was representative of the small section investigated.

Plane image analysis quantizes the morphology data on size, shape, area, and density of air voids. These numbers give a means for future comparison of air voids in asphalts to asphalt compaction methods, stripping effects, and possibly pavement performance. The measurements are all representative of 2 dimensions and the interconnected voids in 3 dimension are not accounted for appropriately. Again the problem may be solved with bulk air void testing. Plane section sample testing is a lengthy process with sample preparation, testing, and data analysis currently lasting a few weeks. Some adhesive modification in sample preparation might allow samples to be prepared and analyzed in as little as 5 days.

5.3 Crack propagation of fracture sample

Crack propagation was observed when tensile testing fracture samples in front of a high speed recording camera. Figure 5.23 (a-h) highlights crack propagation from start to finish with photographs and drawings of a 1 mm thick sample. These photographs are of the high speed camera's video monitor taken with a 35 mm camera. This asphalt sample was made from a Marshall specimen. The sequence of pictures goes from top

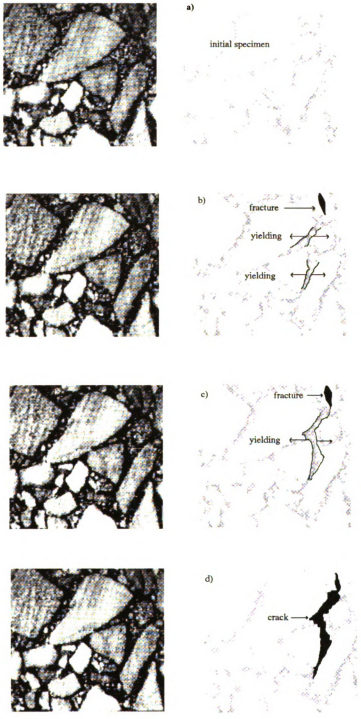

Figure 5.23 (a-d) - Crack propagation of a good sample with reflective oblique lighting and no background lighting at 2.4X.

to bottom with the highlights in the pictures on the right. Figure 5.23 a) is the initial specimen followed by pictures over a ten second period of tensile strain resulting in failure. The asphalt yielded throughout the entire sample illustrated in 5.23 b) and 5.23 c). Figures 5.23 b) and 5.23 c) also illustrate the start of fracture of a brittle aggregate, upper right hand corner. Continued yielding turned to crazing predominately around the larger aggregate where the stress concentrations were the largest, Figure 5.23 d), and then to fracture, Figures 5.23 e) through 5.23 h). During fracture the crack widens and the stresses increase, shown in Figure 5.23 e) and Figure 5.23 f). The crack takes another path shown in the left of Figure 5.23 g) along the large aggregate. Note the elastic effects of the asphalt where the crack to the right in Figure 5.23 f) shrinks in Figures 5.23 g) and 5.23 h) returning to its original position as the other crack grows.

When taking a closer look into a crack, fibrils were seen. Figure 5.24 illustrates a fibril representing good adhesive bonding and the viscoelastic property of asphalt. Observation of these fibrils during fracture shows that many break at the center and retract toward the aggregate as a result of their elastic properties. Fibrils are responsible for the elastic crack behavior in Figures 5.23 g) and 5.23 h) where the aggregate of one crack along the right hand side returned to its original position.

Figure 5.25 (a-f) shows a crack propagation series of a good asphalt sample with background lighting over a period of 12.9 seconds. The background lighting enabled the crazing stage with fibrils to be seen. Figure 5.25 a) is the initial specimen with one void present. Figure 5.25 b) shows crazing and the start of microvoids. These microvoids continue to grow and develop new ones with fibrils between them, Figure 5.25 c). Figures 5.25 d) through f) illustrate more of the crazing and crack development showing

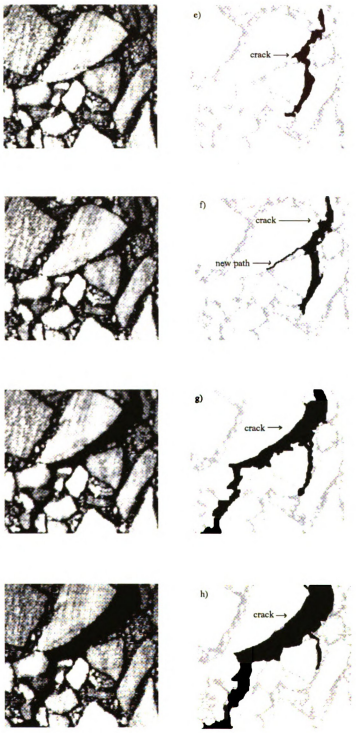

Figure 5.23 (e-h) - Crack propagation of a good sample with reflective oblique lighting and no background lighting at 2.4X.

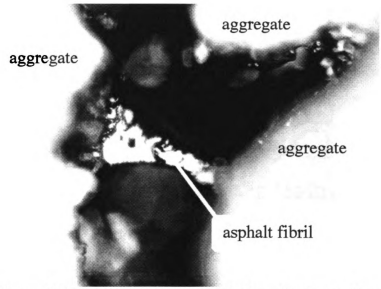

Figure 5.24 - Close up of fibril during fracture of an asphalt sample viewed through an optical microscope at 100X.

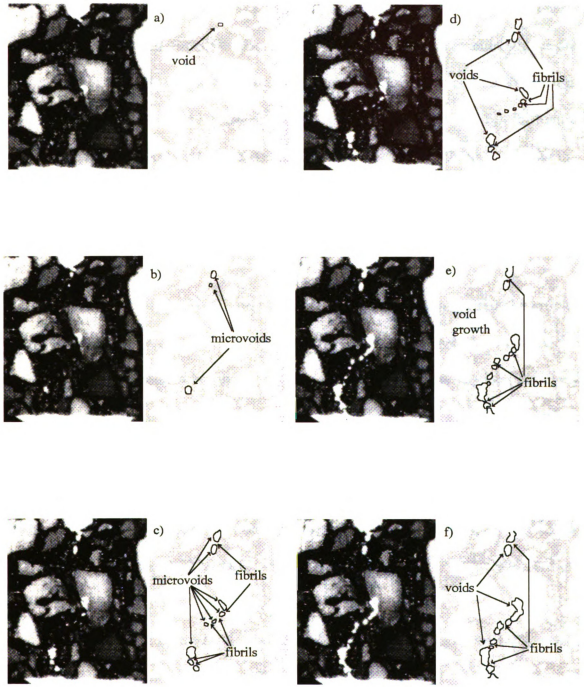

Figure 5.25 (a-f) - Crack propagation of 1st good sample with reflected oblique lighting and background lighting at 3X.

an overall joining of the voids.

Figure 5.26 (a-f) is another crack propagation series of a good asphalt sample with background lighting. In this series the fracture is more evident. The photographs are from two video camera recordings over a combined 18.9 second period. Again fracture starts with yielding and crazing in the larger aggregate planes, Figure 5.26 b). By Figure 5.26 c) crazing and microvoids were developing. Figures 5.26 d) through f) show the increased crack development and fibril formation which ultimately lead to total failure. Figure 5.26 e) also shows an elongated fibril and by Figure 5.26 f) the fibril had broken and started retracting.

Figure 5.27 (a-f) is a crack propagation series of a bad asphalt sample without background lighting over a 10.1 second period. The series shows evident fracture occurs along the aggregate boundaries and in the last figures some of the aggregate is clean showing adhesive failure. Adhesive failure is investigated more in the next section. Figure 5.27 a) is the initial specimen. Yielding is starting in b) and then fracture along the aggregate boundaries. Although not evident without the background lighting some fibrils did exist. In Figure 5.27 c) through e), crack development increased and the crack path changed in Figures 5.27 d) to e) and then again in f), following the path of least resistance.

Fracture testing offers determination of failure mechanisms of asphalt concrete during tensile failure and characterization of the cracking process. General failure of conventional asphalt concrete has been characterized by yielding, cracking, and then fracture of the specimen. Yielding was best determined using no background lighting and oblique lighting from each side to illuminate the front of the sample. Crazing was

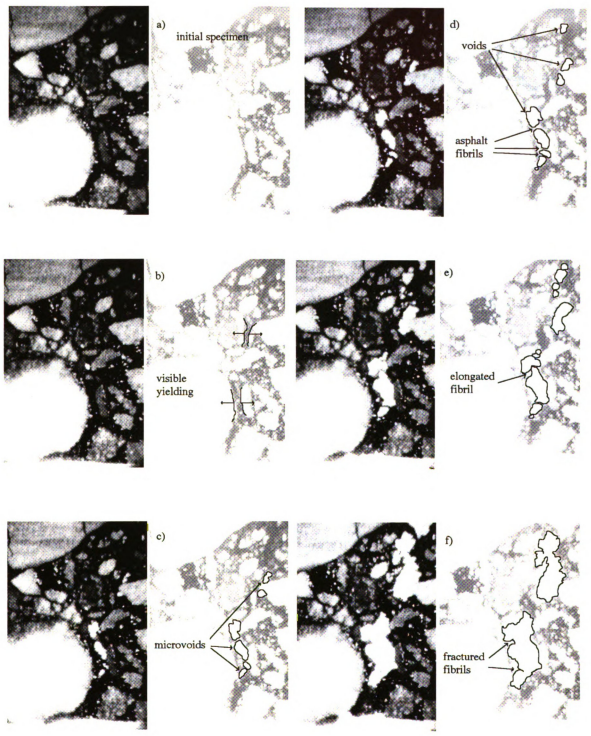

Figure 5.26 (a-f) - Crack propagation of 2nd good sample with reflected oblique lighting and background lighting at 3.8X.

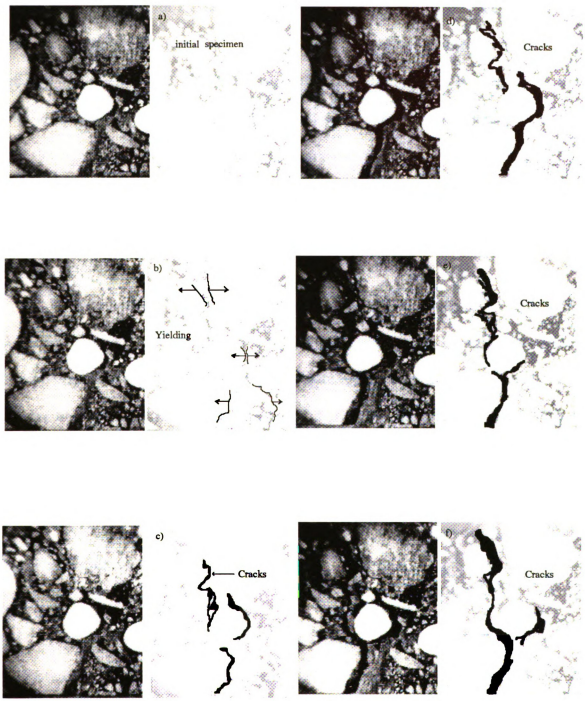

Figure 5.27 (a-f) - Crack propagation of bad sample using reflected oblique lighting without background lighting at 3.3X.

best determined using both background lighting and oblique lighting. Cracking was seen as a crazing process with the formation of microvoids and fibrils bridging the cracks. These fibrils serve as a means for healing effects to take place when the strains are reduced and/or eliminated. Fracture samples are currently prepared in 5 to 7 days and with an adhesive modification may be reduced to 3 or less days. Polymer modified asphalts should not pose a problem with this fracture test until: the elongation of the PMA increases past 12 percent, the elongation to necking of the polycarbonate film; or the asphalt concrete strength surpasses that of the epoxy bond holding the ends in place, an unlikely event.

Fracture testing was performed at room temperature and in an open room where the environmental conditions were not varied. Future work with ESE will allow various condiions such as; high temperatures, low temperatures, temperature cycling, and moisture effects, to be investigated. ESEM will also allow changing between high and low magnification of the cracking region during testing, a process difficult with the current high speed camera.

5.4 Microscopic analysis of fracture samples

Fracture samples were viewed under an optical microscope determining the locus of fracture. It was found adhesive and cohesive failure occurred together, but the degree of each differed. Figure 5.28 shows a common cohesive failure where the asphalt cement left a black film coating on the aggregate. This was the dominate type of failure common with most of the samples characteristic of good adhesion.

The samples with poor adhesive properties showed signs of adhesion failure. The degree of this type of failure varied from sample to sample with the greatest adhesion failure in core 1 of section 29, site 5 showing signs of stripping. Figures 5.29, 5.30, and 5.31 show different degrees of adhesion failure. Figure 5.29 shows an aggregate with strips of asphalt remaining behind after fracture revealing signs of cohesive failure also. Figure 5.30 illustrated a low surface energy aggregate where the asphalt cement had not spread over the surface, but beaded up similar to that of water on a waxed car. Figure 5.31 shows a clean adhesion failure where the aggregate surface can be seen quite well on the right side in the middle.

The micrographs presented here are only partly in focus because the depth of field of an optical microscope is limited to a few microns. Future work is planned for observations with ESEM that will eliminate this problem with its depth of field being 100 times greater than that of optical microscopy. This will allow the locus of fracture to be further characterized into degrees of each type of failure, adhesive and cohesive.

5.5 Summary

The tests and procedures developed and reported here collectively can provide a means for investigation of morphology, microstructure, and fracture of asphalt concrete. Thin and plane sections offer illustrative morphological and microstructural results while plane sections through auto image analysis offers numerical characterization of air void size, shape, and density. Thin fracture samples offer a means for investigating crack propagation and initiation of fracture by tensile testing through high speed camera

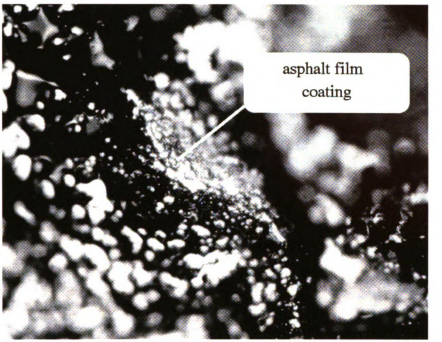

Figure 5.28 - Cohesive failure of asphalt cement shown at 50X.

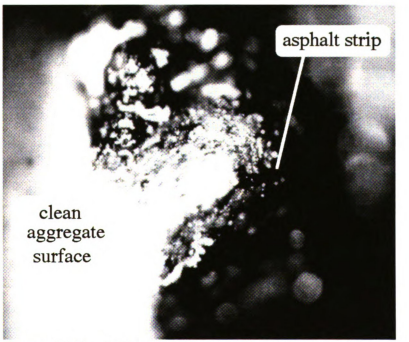

Figure 5.29 - Adhesive failure with cohesive strings at 50X.

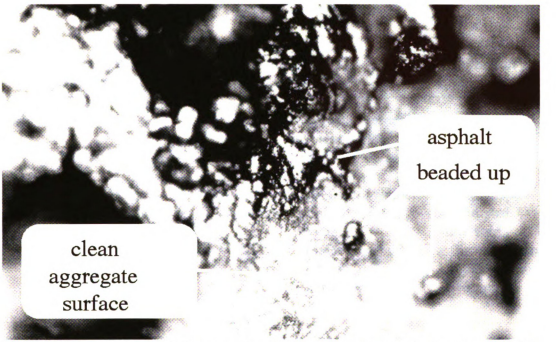

Figure 5.30 - Adhesive failure with a low energy aggregate beading up the asphalt at 69X.

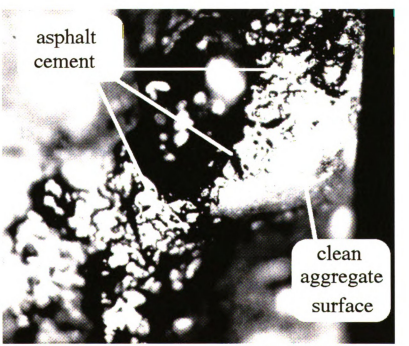

Figure 5.31 - Adhesive failure showing a clean aggregate surface in the center at 63X.

Table 5.4 - Experimental summary

Tests	sample configuration	environment	associated equipment	information to be gained
All tests			- optical microscope - diamond saw - polisher	
Thin section specimens	-15X40 mm asphalt sample - 30 μm thick - fully fixed to slide - filled voids	- open air - room temp. - dry - T < 30°C	- vacuum chamber - thin sectioning system - image analysis system - computer with spreadsheet	- void shape - void size - air void formation from asphalt aggregate wetting
Plane section specimens	- 50X70 mm asphalt sample - 30 μm thick - fully fixed to - filled voids	- open air - room temp. - dry - T < 30°C	- vacuum chamber - thin sectioning system - image analysis system - Computer with spreadsheet and large memory	- air void content including enclosed voids - void size - void shape - void distribution - void density - void area - numbers for comparison to compaction methods and stripping
Fracture specimens	- 15X40 mm asphalt sample - 1 mm thick - fixed to poly-carbonate at ends of asphalt sample - filled voids - unfilled voids	- room temp. - open air - tensile strain in frame by hand	- high speed camera system - tensile frame - background light - 35 mm camera - computer with laser scanner and enhancement	- crack mechanisms yielding crazing fibrils failure - crack propagation observations - locus of fracture adhesive cohesive

observations. These observations showed fracture occurred first by general yielding, crazing creating microvoids, and followed by ultimate failure. After failure the samples were then observed under optical microscopy determining the locus of fracture consisting of both adhesive and cohesive failures. Table 5.4 summarizes the experimentation with sample configuration, testing environment, associated equipment, and the information to be gained from each test.

Chapter Six

Proposed Experiments for the Measurement of Adhesion and Fracture Toughness

In the previous chapters, tests have been developed to investigate morphology, microstructure, fracture mechanisms, and locus of fracture for asphalt pavements. The information determined will give valued insight into predicting pavement performance and its relation to: air void content, size, shape, and distribution; aggregate size, shape, and content; and asphalt distribution, specifically the asphalt film thickness on the aggregate. The remaining critical parameter is the measurement of adhesion between the asphalt cement and the aggregate. An extensive body of literature which has been developed for the measurement of adhesion in polymeric systems can be used to provide a basis for either the selection or development of adhesion tests for asphalt concrete.

The best measure of adhesion is through torsional shear measurement [128]. There is a great degree of difficulty in such an experimental configuration for asphalt on aggregate. An adaptation for measuring the strength of adhesion through thick adherent lap-shear testing [128] has been proposed. Lap-shear testing gives a measurement of the adhesive bond strength between two flat parallel plates having an one inch overlap when pulled apart under tensile loading. Shear stress concentrations and cleavage stresses at the ends of the lap-shear plates may cause the adhesive to peel which could effect the results, but the adhesive industry has shown that reasonable agreement exists between lap-shear testing and shear measurements [128]. Applying this to an asphalt/aggregate bond a lap shear test would give the needed adhesion information. An experimental configuration similar to that shown in Figure 6.1 would be required. An aggregate

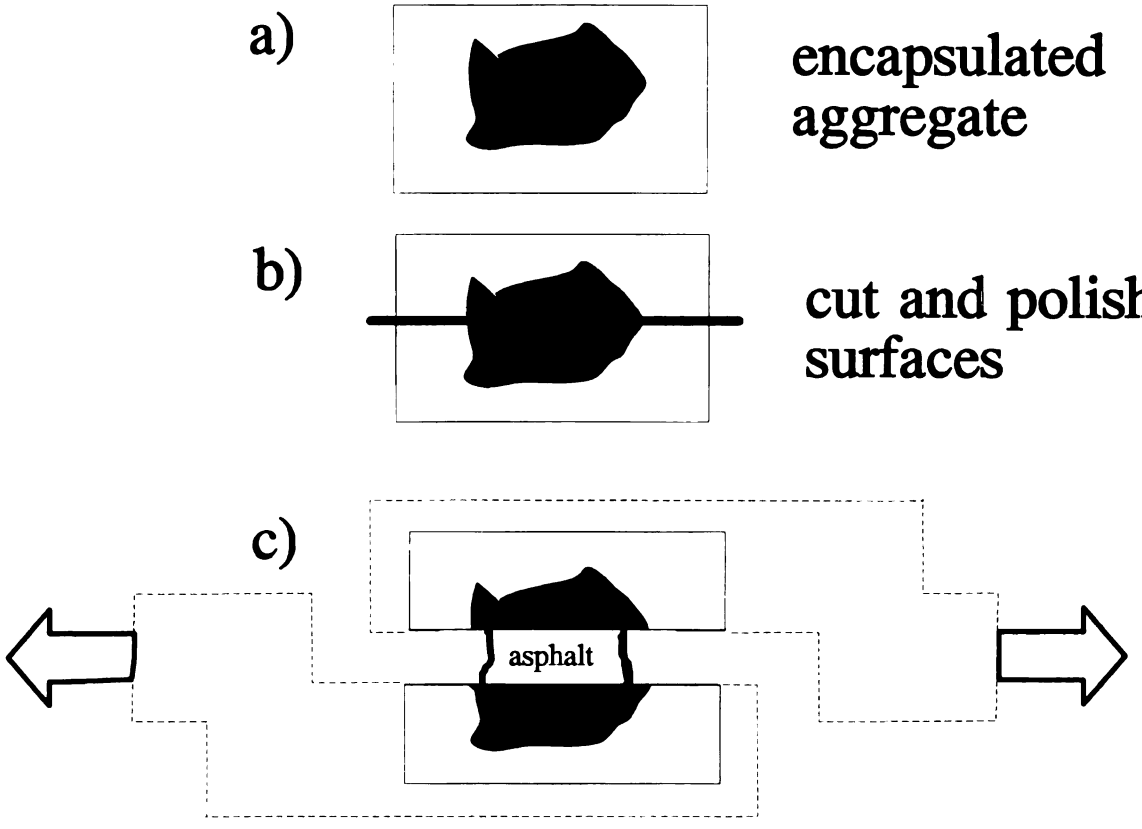

Figure 6.1 - Adhesive test preparation

would be encapsulated in a block of polymer, a) and cut into two pieces, b). This would give two flat surfaces for use as plates in a lap shear test. The surfaces would be prepared similar to conventional aggregate surfaces. The two surfaces would then be configured so that a tensile load could be applied to the specimen, c). This can be done with direct shear testing devices like those used in soil testing in the MSU Civil Engineering Department. Asphalt cement would then be applied with controlled thickness and confined to a fixed area between the two aggregates to create a specimen suitable for measuring the adhesive bond strength. The two aggregate plates give the capability to vary the asphalt cement film thickness of the asphalt adhesive bond which would allow for a determination and comparison of the plastic zone size to the aggregate's asphalt cement film thickness to determine their effects on the fracture toughness, as in the adhesive industry [78, 129]. After lap-shear testing, the test plate surfaces which failed can be examined through microscopy for the determination of the locus of fracture.

Fracture toughness should be used when characterizing polymer modified asphalt cement (PMAC) and polymer modified asphalt concrete (PMA). Technically, fracture toughness is the energy required per unit area to create a new crack surface [130] and will be considered theory 1. Fracture toughness is a difficult parameter to measure in heterogenous materials such as asphalt concrete, therefore by convention fracture toughness has been defined as the area under a stress-strain curve [10] which is equivalent to the total energy for specimen failure and will be considered theory 2.

PMAC has been analyzed by both theories. Theory 2 fracture toughness is most common with the new SHRP specification for direct tensile testing of a molded asphalt specimen [131]. This specimen is cast in the form of a dogbone with metal brackets at

the ends for Mode I (tensile) loading which can be applied through a tensile loading device. Theory 1 fracture toughness of asphalt cement has been analyzed by double cantilever beam (a Mode I direct tensile failure) and four point bending beam (a Mode II shear failure) [132]. Additional tests based on theory 1 from the polymer and adhesive industry could also be applied like the single edge notch (SEN) [78, 133-136], and three point bending beam tests (3PT-BEND) [133]. Of these tests the two already tested with asphalt, double cantilever beam (DCB) and four point bending beam seem most promising. Figure 6.2 shows an illustration of a double cantilever beam configuration where the asphalt cement is applied between the two beams and stressed while measuring the crack opening to obtain a fracture toughness value. Figure 6.3 shows a four point bending beam configuration where asphalt cement is applied between two plates and flexed to produce shear stresses for Mode II failure of the asphalt cement. The crack growth, stress, and strain would be measured for fracture toughness determination.

PMA fracture toughness has only been found to be studied based on theory 2 with Mode 1 (tensile) failure through indirect tensile [3, 10], triaxial [3], and flexural beam testing [3]. Of these three tests indirect tensile seems most promising and details on the new sample holding frame configuration are contained in Chapter Three. The indirect tensile test would measure the energy to failure starting with an intact Marshall or gyratory specimen.

For polymer and Portland cement, the use of three point bending beam [137] and four point bending beam configurations [138] are recommended for theory 1 fracture toughness measurement. Polymer concrete being a viscoelastic heterogeneous material has similar characteristics to that of asphalt concrete . Fracture toughness was evaluated

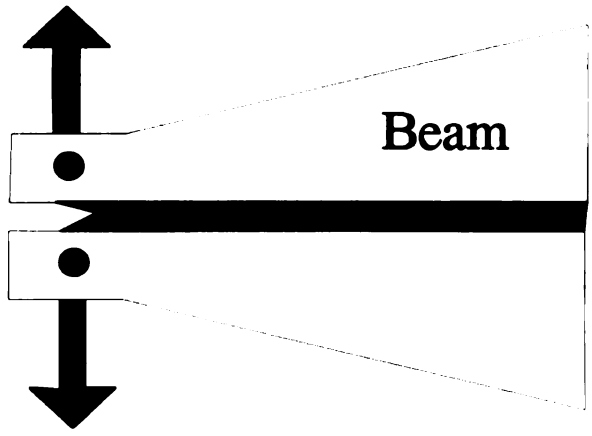

Figure 6.2 - Double cantilever beam test configuration.

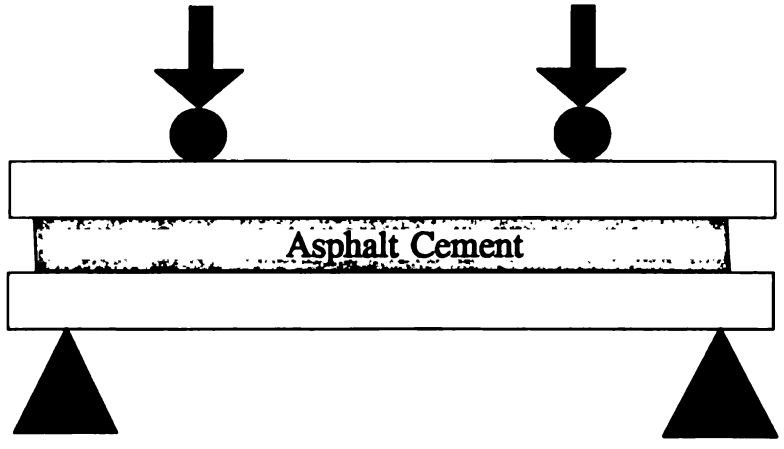

Figure 6.3 - Four point bending beam configuration for Mode II testing.

through a four point bending beam test configuration with equations adapted from the initial notch depth method, ASTM E399 and the CMOD Method, a relationship between linear elastic fracture mechanics (LEFM) and the crack mouth opening displacement to determine the stress intensity factor, K_I, in polymer concrete [138].

The initial notch depth method uses the beam cross section of b x d, thickness b, initial crack length a, and the applied pure bending moment M to calculate the stress intensity factor through equation 6.1 developed by Brown and Srawley presented in Vipulanandan [138]:

$$K_I = 6\, M\, a^{1/2}\, \frac{Y(a/d)}{bd^2} \qquad \textbf{6.1}$$

where

$$Y(a/d) = 1.97 - 2.47(a/d) + 12.97(a/d)^2 - 23.17(a/d)^3 + 24.80(a/d)^4$$

The CMOD method uses equation 6.2 to relate the elastic crack mouth opening to the crack length in four point bending [138].

$$CMOD^e = 4\, \sigma\, a\, \frac{V(\alpha)}{E'} \qquad \textbf{6.2}$$

where
- σ = net stress ($6\ M/\ bd^2$)
- a = crack length
- α = $(a + Ho)/(d + Ho)$
- Ho = clip gage holder thickness
- $V(\alpha)$ = $0.8 - 1.7(\alpha) + 2.4(\alpha)^2 + 0.66/(1-\alpha)^2$
- E' = modulus for plane stress
  = $E/(1-\upsilon^2)^{0.5}$
- υ = Poisson's ratio

This crack length, a, includes both inelastic and elastic crack growth of which the inelastic portion should be extracted to obtain the effective crack length, a_e. Equation 6.3, a numerical iterative procedure, is used where the compliance (CMOD/P) of the specimen unloaded at 95 percent of peak load (Cu) is compared to that of the initial loading compliance (Ci) where P is their respective loads.

$$a_e = a_i \frac{Cu}{Ci} \frac{V(\alpha_i)}{V(\alpha_e)} \qquad \textbf{6.3}$$

Using a_e, the stress intensity factor can be determined through equation 3.4, presented here again as equation 6.4.

$$K_I = \sigma \sqrt{\pi\, a} \qquad \textbf{6.4}$$

where σ = fracture strain

The polymer concrete approach system could be adapted for asphalt concrete as shown in Figure 6.4. An asphalt concrete beam would be notched with a diamond saw and fatigued lightly to initiate a microcrack. A continuous measurement of the crack opening would be done during loading through a crack opening displacement (COD) gage while monitoring the loading stress, thereby allowing theory 1 fracture toughness to be calculated.

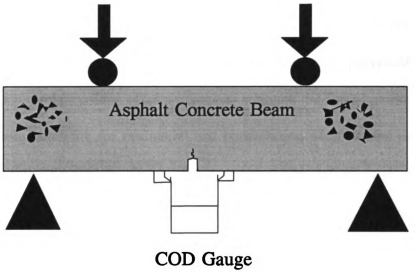

Figure 6.4 - Four point bending beam test configuration for asphalt concrete.

Chapter Seven

Recommendations for Characterization and Evaluation of Polymer Modified Asphalt Cement and Concrete

A linkage between polymer modified asphalt cement/concrete to asphalt pavement performance can be realized through a key fundamental understanding of microstructure, morphology, adhesion, locus of fracture, and fracture toughness. These basic elements are on a microscopic level with the exception of fracture toughness which must also be evaluated on a macroscopic level for the ultimate relationship to pavement performance. The microscopic relationships offer a means to evaluate the initial causes of pavement distress, thereby allowing for evaluation and optimization of pavement performance by the incorporation of polymers, fibers, and/or crumb rubber modifiers.

The recommended characterization and evaluation tests of polymer modified asphalt concrete (PMA) and polymer modified asphalt cement (PMAC) has been summarized in Table 7.1. The summary gives the existing and proposed tests with the information to be retrieved through each. The majority of tests are run on PMA because of the importance aggregate has on the results. These tests will supply the information necessary for characterization and evaluation in the following areas; voids, aggregate, stripping, crack mechanisms, crack propagation, locus of fracture, optimum asphalt cement film thickness (asphalt cement content), fracture toughness, plastic zone size, and adhesive bond strength. Therefore, characterization of conventional, polymer, and crumb rubber modified asphalts with respect to morphology, microstructure, adhesion, fracture

Table 7.1 - Comparative experimental summary

Type	Test	Information retrievable
PMA	Thin section specimens	- void shape and size - air void formation from asphalt aggregate wetting
	Plane section specimens	- air void content including enclosed voids - void size, shape, distribution, density, and area - comparison of voids to compaction methods and stripping
	Fracture specimens	- crack propagation and failure mechanisms (yielding, crazing, fibrils, and failure) - locus of fracture (adhesive and cohesive)
	Fracture toughness Methodology 1	- fracture toughness, K_I - crack growth mechanics - locus of fracture - relationship of adhesion to performance - Mode I (tensile) failures
	Fracture toughness Methodology 2	- bulk fracture toughness - optimum asphalt cement film thickness (partial) - locus of fracture - relationship of adhesion to performance - Mode I (tensile) failures
PMAC	Lap-shear	- adhesive bond strength - plastic zone size - optimum asphalt cement film thickness (partial) - locus of fracture
	Fracture toughness Methodology 1	- fracture toughness, K_I - Mode I (tensile) and Mode II (shear) failures - crack growth mechanics
	Fracture toughness Methodology 2	- bulk fracture toughness - Mode I (tensile) failures

mechanisms, locus of fracture, and fracture toughness will be possible using these existing and proposed testing techniques. This characterization will determine those polymer modifications necessary and beneficial for improvement in asphalt pavement performance. An incorporation of polymer modified asphalt will then allow evaluation of their pavement distresses in relation to pavement performance. From the results, an optimization of the PMAs can be done achieving the ultimate goal of improved pavement performance by solving/resisting pavement distresses.

APPENDIX

Table A-1 - Fatigue Cracking Damage Index [29]

Region	Binder	Time (Year) 1	5	10	15	20
	AC5	.93	4.68	9.36	14.04	18.73
	AC5+C	.12	.59	1.17	1.76	2.34
	AC5+P	.01	.05	.10	.15	.20
	AC10	.55	2.74	5.48	8.22	10.96
1	AC10+C	.09	.45	.91	1.36	1.82
	AC10+P	.004	.023	.046	.068	.091
	AC20	.073	.366	.731	.109	1.46
	AC20+C	.03	.15	.29	.44	.59
	AC20+P	.002	.009	.018	.026	.035
	AC5	1.15	5.77	11.54	17.32	23.05
	AC5+C	.09	.44	.88	1.32	1.75
	AC5+P	.11	.055	.110	.165	.220
	AC10	.675	3.37	6.74	10.12	13.49
2	AC10+C	.07	.35	.70	1.05	1.39
	AC10+P	.005	.025	.05	.075	.099
	AC20	.092	.45	.92	1.37	1.83
	AC20+C	.03	.13	.26	.40	.53
	AC20+P	.002	.010	.019	.028	.037
	AC5	3.54	17.74	35.48	53.22	70.96
	AC5+C	.39	1.94	3.87	5.81	7.75
	AC5+P	.039	.197	.394	.590	.78
	AC10	3.02	15.14	30.28	45.43	60.57
3	AC10+C	.31	1.57	3.13	4.70	6.26
	AC10+P	.027	.136	.272	.407	.543
	AC20	.561	2.80	5.60	8.40	11.21
	AC20+C	.18	.92	1.83	2.75	3.67
	AC20+P	.012	.058	.117	.175	.233
	AC5	*	*	*	*	*
	AC5+C	3.21	15.68	31.36	47.12	54.84
	AC5+P	1.75	8.79	17.5	26.38	35.17
	AC10	*	*	*	*	*
4	AC10+C	3.6	17.84	35.68	53.68	72.28
	AC10+P	1.24	6.20	12.41	18.61	24.82
	AC20	4.51	22.59	45.19	66.77	90.39
	AC20+C	2.80	14.00	28.08	42.08	56.8
	AC20+P	.85	4.27	8.54	12.82	17.09

* Not available

Table A-2 - Rut Depth in Inches [29]

Region	Binder	Time (Year) 1	5	10	15	20
	AC5	.26	.56	.78	.95	1.01
	AC5+C	.17	.39	.56	.69	.80
	AC5+P	.23	.47	.64	.77	.87
	AC10	.22	.48	.67	.82	.94
1	AC10+C	.16	.38	.55	.68	.79
	AC10+P	.21	.45	.61	.74	.84
	AC20	.20	.43	.60	.73	.84
	AC20+C	.15	.32	.52	.62	.72
	AC20+P	.18	.39	.55	.68	.78
	AC5	.31	.66	.92	1.1	1.3
	AC5+C	.18	.41	.58	.72	.83
	AC5+P	.24	.50	.68	.81	.92
	AC10	.28	.58	.80	.97	1.11
2	AC10+C	.18	.41	.58	.71	.77
	AC10+P	.22	.46	.63	.75	.86
	AC20	.23	.48	.66	.80	.92
	AC20+C	.17	.37	.54	.66	.77
	AC20+P	.18	.41	.58	.70	.81
	AC5	.37	.73	.98	1.18	1.34
	AC5+C	.20	.44	.63	.77	.89
	AC5+P	.25	.52	.71	.84	.95
	AC10	.35	.67	.89	1.06	1.21
3	AC10+C	.18	.41	.59	.73	.84
	AC10+P	.23	.48	.64	.80	.91
	AC20	.26	.52	.71	.84	.96
	AC20+C	.16	.37	.52	.65	.75
	AC20+P	.20	.44	.62	.73	.83
	AC5	*	*	*	*	*
	AC5+C	.21	.46	.65	.80	.92
	AC5+P	.27	.53	.72	.89	.98
	AC10	*	*	*	*	*
4	AC10+C	.20	.46	.65	.79	.92
	AC10+P	.24	.48	.66	.77	.87
	AC20	.36	.65	.80	.98	1.10
	AC20+C	.19	.42	.59	.73	.84
	AC20+P	.20	.46	.63	.76	.89

* Not Available

Table A-3

Sample: Good98 Original data for analysis of plane section

Date: 12/6/93

GALAI123 Microns 297.0 29.0

_A_r_e_a_	Perimeter Ú	0.00% Ú	45.00% Ú	90.00% Ú	135.00%	Min_Angle	Min_Feret	Max_Angle	Max_Feret	Avg_Feret	Asp_Ratio	Shape_Fac	Spec_Peri	Area_Frac	AvgRadius
1162.5	142.1	38.0	50.6	25.3	50.6	90.0	25.3	45.0	50.6	41.1	.500	.724	45.5	.0001	22.0
1550.0	167.4	50.6	50.6	25.3	50.6	90.0	25.3	.0	50.6	44.3	.500	.695	56.0	.0001	23.6
1162.5	142.1	38.0	50.6	25.3	50.6	90.0	25.3	45.0	50.6	41.1	.500	.724	45.5	.0001	22.0
2195.8	194.5	63.3	50.6	38.0	75.9	90.0	38.0	135.0	75.9	57.0	.500	.729	61.7	.0001	28.7
2454.1	199.8	50.6	63.3	50.6	63.3	.0	50.6	45.0	63.3	57.0	.800	.772	56.4	.0001	28.4
2712.5	238.4	75.9	88.6	50.6	63.3	90.0	50.6	45.0	88.6	69.6	.571	.600	88.6	.0002	29.0
3100.0	225.1	63.3	75.9	50.6	75.9	90.0	50.6	45.0	75.9	66.5	.667	.768	64.5	.0002	34.4
12658.2	467.8	126.6	151.9	126.6	151.9	.0	126.6	45.0	151.9	139.2	.833	.727	148.9	.0007	60.9
1323947.3	6669.2	1569.6	1797.5	1544.3	1354.4	135.0	1354.4	45.0	1797.5	1566.5	.754	.374	2873.9	.0739	601.5
30224.7	693.7	202.5	240.5	202.5	202.5	.0	202.5	45.0	240.5	212.0	.842	.789	240.5	.0017	97.5
1162.5	142.1	38.0	50.6	25.3	50.6	90.0	25.3	45.0	50.6	41.1	.500	.724	45.5	.0001	22.0
214931.5	2212.6	557.0	506.3	569.6	734.2	45.0	506.3	135.0	734.2	591.8	.690	.552	854.9	.0120	243.5
1162.5	142.1	38.0	50.6	25.3	50.6	90.0	25.3	45.0	50.6	41.1	.500	.724	45.5	.0001	22.0
2841.6	223.5	75.9	63.3	50.6	88.6	90.0	50.6	135.0	88.6	69.6	.571	.715	72.6	.0002	28.7
4391.6	294.5	101.3	113.9	75.9	63.3	135.0	63.3	45.0	113.9	88.6	.556	.636	105.7	.0002	33.8
1937.5	192.7	63.3	63.3	25.3	63.3	90.0	25.3	.0	63.3	53.8	.400	.656	67.8	.0001	25.2
2583.3	208.2	50.6	63.3	50.6	63.3	.0	50.6	45.0	63.3	57.0	.800	.749	63.3	.0001	30.6
1162.5	142.1	38.0	50.6	25.3	50.6	90.0	25.3	45.0	50.6	41.1	.500	.724	45.5	.0001	22.0
2841.6	208.4	63.3	75.9	50.6	63.3	90.0	50.6	45.0	75.9	63.3	.667	.822	75.9	.0002	32.2
4004.1	256.1	75.9	75.9	63.3	88.6	90.0	63.3	135.0	88.6	75.9	.714	.779	69.1	.0002	37.3
2712.5	223.7	38.0	75.9	75.9	75.9	.0	38.0	45.0	75.9	66.5	.500	.681	76.3	.0002	27.1
1162.5	142.1	38.0	50.6	25.3	50.6	90.0	25.3	45.0	50.6	41.1	.500	.724	45.5	.0001	22.0
1162.5	142.1	38.0	50.6	25.3	50.6	90.0	25.3	45.0	50.6	41.1	.500	.724	45.5	.0001	22.0
1550.0	167.4	50.6	50.6	25.3	50.6	90.0	25.3	.0	50.6	44.3	.500	.695	56.0	.0001	23.6
3745.8	247.4	63.3	75.9	75.9	88.6	.0	63.3	135.0	88.6	75.9	.714	.769	70.7	.0002	32.5
1162.5	142.1	38.0	50.6	25.3	50.6	90.0	25.3	45.0	50.6	41.1	.500	.724	45.5	.0001	22.0
1550.0	162.5	38.0	50.6	38.0	50.6	.0	38.0	45.0	50.6	44.3	.750	.738	50.6	.0001	23.3
4908.3	309.6	113.9	126.6	63.3	75.9	90.0	63.3	45.0	126.6	94.9	.500	.643	110.3	.0003	39.2
1162.5	142.1	38.0	50.6	25.3	50.6	90.0	25.3	45.0	50.6	41.1	.500	.724	45.5	.0001	22.0
52957.9	1024.3	291.1	253.2	291.1	367.1	45.0	253.2	135.0	367.1	300.6	.690	.634	368.4	.0030	123.7
12787.4	470.1	177.2	88.6	126.6	202.5	45.0	88.6	135.0	202.5	148.7	.438	.727	149.6	.0007	62.8
8266.6	404.6	126.6	151.9	101.3	88.6	135.0	88.6	45.0	151.9	117.1	.583	.635	145.5	.0005	49.4
15241.5	511.5	189.9	189.9	113.9	139.2	90.0	113.9	.0	189.9	158.2	.600	.732	161.2	.0009	63.1

Table A-3 (cont'd)

_A_r_e_a_	Perimeter Ú	0.00% Ú	45.00% Ú	90.00% Ú	135.00%	Min_Angle	Min_Feret	Max_Angle	Max_Feret	Avg_Feret	Asp_Ratio	Shape_Fac	Spec_Peri	Area_Frac	AvgRadius
171273.6	1886.6	519.0	506.3	468.4	506.3	90.0	468.4	.0	519.0	500.0	.902	.605	697.9	.0096	230.1
1550.0	167.4	50.6	50.6	25.3	50.6	90.0	25.3	.0	50.6	44.3	.500	.695	56.0	.0001	23.6
2712.5	214.9	63.3	75.9	50.6	63.3	90.0	50.6	45.0	75.9	63.3	.667	.738	67.0	.0002	30.6
20924.8	719.1	265.8	253.2	139.2	177.2	90.0	139.2	.0	265.8	208.9	.524	.508	286.5	.0012	71.7
5683.3	345.2	126.6	113.9	63.3	113.9	90.0	63.3	.0	126.6	104.4	.500	.599	128.3	.0003	42.3
1550.0	162.5	38.0	50.6	38.0	50.6	.0	38.0	45.0	50.6	44.3	.750	.738	50.6	.0001	23.3
4520.8	278.0	63.3	75.9	75.9	101.3	.0	63.3	135.0	101.3	79.1	.625	.735	87.1	.0003	38.3
3745.8	263.8	88.6	88.6	50.6	88.6	90.0	50.6	.0	88.6	79.1	.571	.677	90.5	.0002	35.4
2454.1	199.8	50.6	63.3	50.6	63.3	.0	50.6	45.0	63.3	57.0	.800	.772	56.4	.0001	28.4
1162.5	142.1	38.0	50.6	25.3	50.6	90.0	25.3	45.0	50.6	41.1	.500	.724	45.5	.0001	22.0
1162.5	142.1	38.0	50.6	25.3	50.6	90.0	25.3	45.0	50.6	41.1	.500	.724	45.5	.0001	22.0
1162.5	142.1	38.0	50.6	25.3	50.6	90.0	25.3	45.0	50.6	41.1	.500	.724	45.5	.0001	22.0
1550.0	162.5	38.0	50.6	38.0	50.6	.0	38.0	45.0	50.6	44.3	.750	.738	50.6	.0001	23.3
1808.3	171.0	50.6	63.3	38.0	50.6	90.0	38.0	45.0	63.3	50.6	.600	.777	47.2	.0001	22.6
2066.6	191.4	50.6	63.3	50.6	50.6	.0	50.6	45.0	63.3	53.8	.800	.709	62.8	.0001	26.1
1162.5	142.1	38.0	50.6	25.3	50.6	90.0	25.3	45.0	50.6	41.1	.500	.724	45.5	.0001	22.0
1550.0	162.5	38.0	50.6	38.0	50.6	.0	38.0	45.0	50.6	44.3	.750	.738	50.6	.0001	23.3
1162.5	142.1	38.0	50.6	25.3	50.6	90.0	25.3	45.0	50.6	41.1	.500	.724	45.5	.0001	22.0
1937.5	179.4	50.6	63.3	38.0	50.6	90.0	38.0	45.0	63.3	50.6	.600	.756	53.5	.0001	24.9
1162.5	142.1	38.0	50.6	25.3	50.6	90.0	25.3	45.0	50.6	41.1	.500	.724	45.5	.0001	22.0
1162.5	142.1	38.0	50.6	25.3	50.6	90.0	25.3	45.0	50.6	41.1	.500	.724	45.5	.0001	22.0
18470.7	662.5	227.8	265.8	177.2	139.2	135.0	139.2	45.0	265.8	202.5	.524	.529	260.3	.0010	62.4
1023120.6	6847.4	1949.4	2038.0	1367.1	1101.3	135.0	1101.3	45.0	2038.0	1613.9	.540	.274	3092.9	.0571	425.0
1162.5	142.1	38.0	50.6	25.3	50.6	90.0	25.3	45.0	50.6	41.1	.500	.724	45.5	.0001	22.0
1550.0	167.4	50.6	50.6	25.3	50.6	90.0	25.3	.0	50.6	44.3	.500	.695	56.0	.0001	23.6
2066.6	192.7	63.3	75.9	38.0	50.6	90.0	38.0	45.0	75.9	57.0	.500	.699	64.1	.0001	26.4
1162.5	142.1	38.0	50.6	25.3	50.6	90.0	25.3	45.0	50.6	41.1	.500	.724	45.5	.0001	22.0
1162.5	142.1	38.0	50.6	25.3	50.6	90.0	25.3	45.0	50.6	41.1	.500	.724	45.5	.0001	22.0
7620.8	413.5	88.6	88.6	126.6	151.9	.0	88.6	135.0	151.9	113.9	.583	.560	158.8	.0004	49.4
2325.0	233.5	63.3	50.6	63.3	88.6	45.0	50.6	135.0	88.6	66.5	.571	.536	91.3	.0001	25.8
381942.7	2702.6	797.5	746.8	772.2	848.1	45.0	746.8	135.0	848.1	791.1	.881	.657	948.7	.0213	330.7
1162.5	142.1	38.0	50.6	25.3	50.6	90.0	25.3	45.0	50.6	41.1	.500	.724	45.5	.0001	22.0
1937.5	179.4	50.6	50.6	38.0	63.3	90.0	38.0	135.0	63.3	50.6	.600	.756	53.5	.0001	27.1
3616.6	247.4	63.3	88.6	75.9	63.3	.0	63.3	45.0	88.6	72.8	.714	.743	76.3	.0002	33.5
21829.0	729.9	240.5	215.2	139.2	202.5	90.0	139.2	.0	240.5	199.4	.579	.515	289.6	.0012	79.0
1550.0	167.4	50.6	50.6	25.3	50.6	90.0	25.3	.0	50.6	44.3	.500	.695	56.0	.0001	23.6
5812.5	313.1	101.3	88.6	75.9	113.9	90.0	75.9	135.0	113.9	94.9	.667	.745	96.0	.0003	40.1
2325.0	202.9	63.3	63.3	38.0	75.9	90.0	38.0	135.0	75.9	60.1	.500	.710	66.5	.0001	28.7
1808.3	171.0	50.6	50.6	38.0	63.3	90.0	38.0	135.0	63.3	50.6	.600	.777	47.2	.0001	27.1
1162.5	142.1	38.0	50.6	25.3	50.6	90.0	25.3	45.0	50.6	41.1	.500	.724	45.5	.0001	22.0

Table A-3 (cont'd)

_A_r_e_a_	Perimeter Ú	0.00% Ú	45.00% Ú	90.00% Ú	135.00%	Min_Angle	Min_Feret	Max_Angle	Max_Feret	Avg_Feret	Asp_Ratio	Shape_Fac	Spec_Peri	Area_Frac	AvgRadius
3487.5	255.8	63.3	63.3	75.9	88.6	.0	63.3	135.0	88.6	72.8	.714	.670	88.5	.0002	34.7
1162.5	142.1	38.0	50.6	25.3	50.6	90.0	25.3	45.0	50.6	41.1	.500	.724	45.5	.0001	22.0
1162.5	142.1	38.0	50.6	25.3	50.6	90.0	25.3	45.0	50.6	41.1	.500	.724	45.5	.0001	22.0
7362.4	350.9	88.6	101.3	101.3	126.6	.0	88.6	135.0	126.6	104.4	.700	.752	105.9	.0004	46.9
4004.1	267.8	63.3	75.9	75.9	88.6	.0	63.3	135.0	88.6	75.9	.714	.702	88.8	.0002	36.7
1162.5	142.1	38.0	50.6	25.3	50.6	90.0	25.3	45.0	50.6	41.1	.500	.724	45.5	.0001	22.0
1550.0	167.4	50.6	50.6	25.3	50.6	90.0	25.3	.0	50.6	44.3	.500	.695	56.0	.0001	23.6
7879.1	394.4	126.6	126.6	75.9	126.6	90.0	75.9	.0	126.6	113.9	.600	.637	141.5	.0004	46.2
8137.4	409.2	75.9	139.2	139.2	126.6	.0	75.9	45.0	139.2	120.3	.545	.611	150.5	.0005	45.9
1162.5	142.1	38.0	50.6	25.3	50.6	90.0	25.3	45.0	50.6	41.1	.500	.724	45.5	.0001	22.0
6199.9	414.8	126.6	139.2	88.6	101.3	90.0	88.6	45.0	139.2	113.9	.636	.453	171.2	.0003	-1.0
1550.0	167.4	50.6	50.6	25.3	50.6	90.0	25.3	.0	50.6	44.3	.500	.695	56.0	.0001	23.6
4004.1	299.8	75.9	101.3	75.9	75.9	.0	75.9	45.0	101.3	82.3	.750	.560	115.1	.0002	31.5
8524.9	426.8	126.6	139.2	88.6	113.9	90.0	88.6	45.0	139.2	117.1	.636	.588	160.2	.0005	45.2
5683.3	306.4	88.6	101.3	75.9	101.3	90.0	75.9	45.0	101.3	91.8	.750	.761	90.2	.0003	42.4
16791.5	805.3	151.9	278.5	253.2	164.6	.0	151.9	45.0	278.5	212.0	.545	.325	355.4	.0009	57.1
3616.6	245.6	63.3	75.9	63.3	88.6	.0	63.3	135.0	88.6	72.8	.714	.754	73.7	.0002	35.7
1937.5	192.7	63.3	63.3	25.3	63.3	90.0	25.3	.0	63.3	53.8	.400	.656	67.8	.0001	25.2
1162.5	142.1	38.0	50.6	25.3	50.6	90.0	25.3	45.0	50.6	41.1	.500	.724	45.5	.0001	22.0
1162.5	142.1	38.0	50.6	25.3	50.6	90.0	25.3	45.0	50.6	41.1	.500	.724	45.5	.0001	22.0
5683.3	328.2	113.9	88.6	75.9	126.6	90.0	75.9	135.0	126.6	101.3	.600	.663	114.5	.0003	36.6
1162.5	142.1	38.0	50.6	25.3	50.6	90.0	25.3	45.0	50.6	41.1	.500	.724	45.5	.0001	22.0
1550.0	167.4	50.6	50.6	25.3	50.6	90.0	25.3	.0	50.6	44.3	.500	.695	56.0	.0001	23.6
1808.3	171.0	50.6	50.6	38.0	63.3	90.0	38.0	135.0	63.3	50.6	.600	.777	47.2	.0001	27.1
3100.0	233.5	63.3	88.6	63.3	63.3	.0	63.3	45.0	88.6	69.6	.714	.714	75.9	.0002	33.5
1162.5	142.1	38.0	50.6	25.3	50.6	90.0	25.3	45.0	50.6	41.1	.500	.724	45.5	.0001	22.0
2970.8	220.2	50.6	75.9	63.3	63.3	.0	50.6	45.0	75.9	63.3	.667	.770	62.9	.0002	31.9
2325.0	191.4	50.6	63.3	50.6	63.3	.0	50.6	45.0	63.3	57.0	.800	.797	63.3	.0001	26.1
2712.5	223.7	38.0	75.9	75.9	75.9	.0	38.0	45.0	75.9	66.5	.500	.681	76.3	.0002	27.1
1162.5	142.1	38.0	50.6	25.3	50.6	90.0	25.3	45.0	50.6	41.1	.500	.724	45.5	.0001	22.0
1162.5	142.1	38.0	50.6	25.3	50.6	90.0	25.3	45.0	50.6	41.1	.500	.724	45.5	.0001	22.0
2583.3	208.2	50.6	63.3	50.6	63.3	.0	50.6	45.0	63.3	57.0	.800	.749	63.3	.0001	30.6
2195.8	191.4	50.6	63.3	50.6	50.6	.0	50.6	45.0	63.3	53.8	.800	.753	57.6	.0001	26.1
1162.5	142.1	38.0	50.6	25.3	50.6	90.0	25.3	45.0	50.6	41.1	.500	.724	45.5	.0001	22.0
1550.0	162.5	38.0	50.6	38.0	50.6	.0	38.0	45.0	50.6	44.3	.750	.738	50.6	.0001	23.3
1162.5	142.1	38.0	50.6	25.3	50.6	90.0	25.3	45.0	50.6	41.1	.500	.724	45.5	.0001	22.0
4133.3	293.3	75.9	88.6	75.9	75.9	.0	75.9	45.0	88.6	79.1	.857	.604	108.6	.0002	-1.0
1162.5	142.1	38.0	50.6	25.3	50.6	90.0	25.3	45.0	50.6	41.1	.500	.724	45.5	.0001	22.0
2454.1	204.7	63.3	75.9	38.0	63.3	90.0	38.0	45.0	75.9	60.1	.500	.736	64.1	.0001	28.7
1162.5	142.1	38.0	50.6	25.3	50.6	90.0	25.3	45.0	50.6	41.1	.500	.724	45.5	.0001	22.0

Table A-3 (cont'd)

_A_r_e_a_	Perimeter Ú	0.00% Ú	45.00% Ú	90.00% Ú	135.00%	Min_Angle	Min_Feret	Max_Angle	Max_Feret	Avg_Feret	Asp_Ratio	Shape_Fac	Spec_Peri	Area_Frac	AvgRadius
4133.3	261.2	63.3	88.6	75.9	75.9	.0	63.3	45.0	88.6	75.9	.714	.761	76.8	.0002	36.0
2454.1	204.7	63.3	63.3	38.0	75.9	90.0	38.0	135.0	75.9	60.1	.500	.736	64.1	.0001	28.7
1162.5	142.1	38.0	50.6	25.3	50.6	90.0	25.3	45.0	50.6	41.1	.500	.724	45.5	.0001	22.0
1162.5	142.1	38.0	50.6	25.3	50.6	90.0	25.3	45.0	50.6	41.1	.500	.724	45.5	.0001	22.0
4779.1	276.2	63.3	101.3	75.9	88.6	.0	63.3	45.0	101.3	82.3	.625	.787	101.3	.0003	36.0
1162.5	142.1	38.0	50.6	25.3	50.6	90.0	25.3	45.0	50.6	41.1	.500	.724	45.5	.0001	22.0
6070.8	338.8	88.6	101.3	88.6	113.9	.0	88.6	135.0	113.9	98.1	.778	.665	117.9	.0003	45.9
8395.8	434.3	63.3	113.9	151.9	151.9	.0	63.3	90.0	151.9	120.3	.417	.559	166.8	.0005	34.7
7104.1	396.2	101.3	101.3	101.3	126.6	.0	101.3	135.0	126.6	107.6	.800	.569	151.1	.0004	48.1
6845.8	340.3	113.9	126.6	75.9	101.3	90.0	75.9	45.0	126.6	104.4	.600	.743	104.8	.0004	47.5
1162.5	142.1	38.0	50.6	25.3	50.6	90.0	25.3	45.0	50.6	41.1	.500	.724	45.5	.0001	22.0
3229.1	235.4	63.3	75.9	63.3	75.9	.0	63.3	45.0	75.9	69.6	.833	.733	74.1	.0002	31.2
22862.3	734.5	177.2	189.9	227.8	202.5	.0	177.2	90.0	227.8	199.4	.778	.533	287.8	.0013	82.6
31387.2	1061.4	240.5	278.5	202.5	227.8	90.0	202.5	45.0	278.5	237.3	.727	.350	462.9	.0018	86.6
1162.5	142.1	38.0	50.6	25.3	50.6	90.0	25.3	45.0	50.6	41.1	.500	.724	45.5	.0001	22.0
5683.3	352.1	101.3	88.6	88.6	113.9	45.0	88.6	135.0	113.9	98.1	.778	.576	133.5	.0003	40.5
4908.3	345.4	88.6	101.3	88.6	101.3	.0	88.6	45.0	101.3	94.9	.875	.517	136.8	.0003	40.5
4262.5	280.7	101.3	101.3	50.6	88.6	90.0	50.6	.0	101.3	85.4	.500	.680	95.9	.0002	34.7
1162.5	142.1	38.0	50.6	25.3	50.6	90.0	25.3	45.0	50.6	41.1	.500	.724	45.5	.0001	22.0
1162.5	142.1	38.0	50.6	25.3	50.6	90.0	25.3	45.0	50.6	41.1	.500	.724	45.5	.0001	22.0
8137.4	366.1	113.9	113.9	101.3	113.9	90.0	101.3	.0	113.9	110.8	.889	.763	107.1	.0005	50.0
1162.5	142.1	38.0	50.6	25.3	50.6	90.0	25.3	45.0	50.6	41.1	.500	.724	45.5	.0001	22.0
1162.5	142.1	38.0	50.6	25.3	50.6	90.0	25.3	45.0	50.6	41.1	.500	.724	45.5	.0001	22.0
5037.5	370.3	126.6	126.6	75.9	101.3	90.0	75.9	.0	126.6	107.6	.600	.462	152.0	.0003	40.1
2325.0	196.4	63.3	50.6	38.0	75.9	90.0	38.0	135.0	75.9	57.0	.500	.758	58.3	.0001	28.7
1162.5	142.1	38.0	50.6	25.3	50.6	90.0	25.3	45.0	50.6	41.1	.500	.724	45.5	.0001	22.0
10204.1	549.7	189.9	189.9	113.9	113.9	90.0	113.9	.0	189.9	151.9	.600	.424	230.6	.0006	44.0
3100.0	253.6	88.6	75.9	38.0	88.6	90.0	38.0	.0	88.6	72.8	.429	.606	93.7	.0002	30.6
1550.0	167.4	50.6	50.6	25.3	50.6	90.0	25.3	.0	50.6	44.3	.500	.695	56.0	.0001	23.6
6199.9	321.5	101.3	101.3	75.9	113.9	90.0	75.9	135.0	113.9	98.1	.667	.754	96.5	.0003	42.4
1162.5	142.1	38.0	50.6	25.3	50.6	90.0	25.3	45.0	50.6	41.1	.500	.724	45.5	.0001	22.0
11495.7	462.5	151.9	139.2	113.9	151.9	90.0	113.9	.0	151.9	139.2	.750	.675	158.9	.0006	59.9
25833.1	735.7	215.2	265.8	202.5	189.9	135.0	189.9	45.0	265.8	218.4	.714	.600	273.4	.0014	86.1
2066.6	191.4	50.6	50.6	50.6	63.3	.0	50.6	135.0	63.3	53.8	.800	.709	62.8	.0001	26.1
1162.5	142.1	38.0	50.6	25.3	50.6	90.0	25.3	45.0	50.6	41.1	.500	.724	45.5	.0001	22.0
3616.6	243.7	63.3	75.9	63.3	88.6	.0	63.3	135.0	88.6	72.8	.714	.765	70.7	.0002	37.9
1550.0	162.5	38.0	50.6	38.0	50.6	.0	38.0	45.0	50.6	44.3	.750	.738	50.6	.0001	23.3
3358.3	233.7	75.9	75.9	50.6	75.9	90.0	50.6	.0	75.9	69.6	.667	.773	65.9	.0002	31.5
56703.7	1183.3	316.5	253.2	329.1	405.1	45.0	253.2	135.0	405.1	325.9	.625	.509	471.4	.0032	134.2
14337.4	543.9	189.9	113.9	139.2	202.5	45.0	113.9	135.0	202.5	161.4	.563	.609	200.4	.0008	65.6

Table A-3 (cont'd)

A_r_e_a_	Perimeter Ú	0.00% Ú	45.00% Ú	90.00% Ú	135.00%	Min_Angle	Min_Feret	Max_Angle	Max_Feret	Avg_Feret	Asp_Ratio	Shape_Fac	Spec_Peri	Area_Frac	AvgRadius
1550.0	162.5	38.0	50.6	38.0	50.6	.0	38.0	45.0	50.6	44.3	.750	.738	50.6	.0001	23.3
11495.7	429.6	88.6	139.2	151.9	139.2	.0	88.6	90.0	151.9	129.7	.583	.783	113.5	.0006	57.1
4133.3	264.3	75.9	101.3	75.9	63.3	135.0	63.3	45.0	101.3	79.1	.625	.743	81.3	.0002	37.0
3745.8	273.1	50.6	101.3	88.6	75.9	.0	50.6	45.0	101.3	79.1	.500	.631	98.5	.0002	33.5
29837.3	705.1	189.9	189.9	240.5	253.2	.0	189.9	135.0	253.2	218.4	.750	.754	211.5	.0017	96.9
1162.5	142.1	38.0	50.6	25.3	50.6	90.0	25.3	45.0	50.6	41.1	.500	.724	45.5	.0001	22.0
1162.5	142.1	38.0	50.6	25.3	50.6	90.0	25.3	45.0	50.6	41.1	.500	.724	45.5	.0001	22.0
1614699.0	8123.8	1582.3	2949.4	2797.5	1202.5	135.0	1202.5	45.0	2949.4	2132.9	.408	.307	3615.2	.0901	611.3
1550.0	162.5	38.0	50.6	38.0	50.6	.0	38.0	45.0	50.6	44.3	.750	.738	50.6	.0001	23.3
1162.5	142.1	38.0	50.6	25.3	50.6	90.0	25.3	45.0	50.6	41.1	.500	.724	45.5	.0001	22.0
1162.5	142.1	38.0	50.6	25.3	50.6	90.0	25.3	45.0	50.6	41.1	.500	.724	45.5	.0001	22.0
9816.6	421.5	139.2	101.3	101.3	164.6	45.0	101.3	135.0	164.6	126.6	.615	.694	141.3	.0005	55.7
1162.5	142.1	38.0	50.6	25.3	50.6	90.0	25.3	45.0	50.6	41.1	.500	.724	45.5	.0001	22.0
1550.0	162.5	38.0	50.6	38.0	50.6	.0	38.0	45.0	50.6	44.3	.750	.738	50.6	.0001	23.3
1162.5	142.1	38.0	50.6	25.3	50.6	90.0	25.3	45.0	50.6	41.1	.500	.724	45.5	.0001	22.0
7104.1	393.5	75.9	126.6	126.6	126.6	.0	75.9	45.0	126.6	113.9	.600	.577	149.1	.0004	43.0
1937.5	179.4	50.6	50.6	38.0	63.3	90.0	38.0	135.0	63.3	50.6	.600	.756	53.5	.0001	27.1
63162.0	1479.6	316.5	329.1	303.8	329.1	90.0	303.8	45.0	329.1	319.6	.923	.363	641.3	.0035	95.5
14595.7	605.9	113.9	215.2	215.2	164.6	.0	113.9	45.0	215.2	177.2	.529	.500	242.9	.0008	62.5
1162.5	142.1	38.0	50.6	25.3	50.6	90.0	25.3	45.0	50.6	41.1	.500	.724	45.5	.0001	22.0
13691.6	523.2	151.9	202.5	126.6	126.6	90.0	126.6	45.0	202.5	151.9	.625	.629	189.2	.0008	62.5
15499.9	842.8	139.2	202.5	189.9	189.9	.0	139.2	45.0	202.5	180.4	.688	.274	380.7	.0009	61.8
1162.5	142.1	38.0	50.6	25.3	50.6	90.0	25.3	45.0	50.6	41.1	.500	.724	45.5	.0001	22.0
1162.5	142.1	38.0	50.6	25.3	50.6	90.0	25.3	45.0	50.6	41.1	.500	.724	45.5	.0001	22.0
41333.0	1046.9	291.1	291.1	253.2	265.8	90.0	253.2	.0	291.1	275.3	.870	.474	426.5	.0023	-1.0
1550.0	167.4	50.6	50.6	25.3	50.6	90.0	25.3	.0	50.6	44.3	.500	.695	56.0	.0001	23.6
9687.4	447.2	126.6	113.9	126.6	151.9	45.0	113.9	135.0	151.9	129.7	.750	.609	164.8	.0005	49.4
26737.3	892.9	265.8	265.8	202.5	227.8	90.0	202.5	.0	265.8	240.5	.762	.421	375.2	.0015	87.6
2454.1	204.7	63.3	75.9	38.0	63.3	90.0	38.0	45.0	75.9	60.1	.500	.736	64.1	.0001	28.7
1162.5	142.1	38.0	50.6	25.3	50.6	90.0	25.3	45.0	50.6	41.1	.500	.724	45.5	.0001	22.0
1162.5	142.1	38.0	50.6	25.3	50.6	90.0	25.3	45.0	50.6	41.1	.500	.724	45.5	.0001	22.0
10979.1	568.1	202.5	202.5	101.3	151.9	90.0	101.3	.0	202.5	164.6	.500	.440	232.9	.0006	55.0
1162.5	142.1	38.0	50.6	25.3	50.6	90.0	25.3	45.0	50.6	41.1	.500	.724	45.5	.0001	22.0
2195.8	191.4	50.6	50.6	50.6	63.3	.0	50.6	135.0	63.3	53.8	.800	.753	57.6	.0001	28.4
1550.0	167.4	50.6	50.6	25.3	50.6	90.0	25.3	.0	50.6	44.3	.500	.695	56.0	.0001	23.6
2325.0	199.8	50.6	63.3	50.6	63.3	.0	50.6	45.0	63.3	57.0	.800	.732	63.0	.0001	28.4
1550.0	162.5	38.0	50.6	38.0	50.6	.0	38.0	45.0	50.6	44.3	.750	.738	50.6	.0001	23.3
1550.0	167.4	50.6	50.6	25.3	50.6	90.0	25.3	.0	50.6	44.3	.500	.695	56.0	.0001	23.6
5037.5	284.9	88.6	88.6	75.9	88.6	90.0	75.9	.0	88.6	85.4	.857	.780	77.1	.0003	39.2
1550.0	162.5	38.0	50.6	38.0	50.6	.0	38.0	45.0	50.6	44.3	.750	.738	50.6	.0001	23.3

Table A-3 (cont'd)

_A_r_e_a_	Perimeter Û	0.00% Û	45.00% Û	90.00% Û	135.00%	Min_Angle	Min_Feret	Max_Angle	Max_Feret	Avg_Feret	Asp_Ratio	Shape_Fac	Spec_Peri	Area_Frac	AvgRadius
67295.3	1176.5	354.4	354.4	265.8	341.8	90.0	265.8	.0	354.4	329.1	.750	.611	432.8	.0038	138.9
1808.3	171.0	50.6	50.6	38.0	63.3	90.0	38.0	135.0	63.3	50.6	.600	.777	47.2	.0001	27.1
2325.0	218.0	75.9	75.9	25.3	75.9	90.0	25.3	.0	75.9	63.3	.333	.615	79.9	.0001	26.7
1162.5	142.1	38.0	50.6	25.3	50.6	90.0	25.3	45.0	50.6	41.1	.500	.724	45.5	.0001	22.0
2066.6	187.8	50.6	63.3	38.0	63.3	90.0	38.0	45.0	63.3	53.8	.600	.736	58.7	.0001	27.1
1162.5	142.1	38.0	50.6	25.3	50.6	90.0	25.3	45.0	50.6	41.1	.500	.724	45.5	.0001	22.0
1162.5	142.1	38.0	50.6	25.3	50.6	90.0	25.3	45.0	50.6	41.1	.500	.724	45.5	.0001	22.0
1808.3	171.0	50.6	63.3	38.0	50.6	90.0	38.0	45.0	63.3	50.6	.600	.777	47.2	.0001	22.6
137690.5	1543.4	569.6	531.6	329.1	443.0	90.0	329.1	.0	569.6	468.4	.578	.726	491.6	.0077	200.3
24799.8	783.5	253.2	177.2	215.2	291.1	45.0	177.2	135.0	291.1	234.2	.609	.508	312.3	.0014	74.9
4520.8	306.0	113.9	88.6	50.6	113.9	90.0	50.6	.0	113.9	91.8	.444	.607	113.0	.0003	39.5
2970.8	258.8	75.9	63.3	63.3	88.6	45.0	63.3	135.0	88.6	72.8	.714	.557	99.6	.0002	28.1
2325.0	191.4	50.6	50.6	50.6	63.3	.0	50.6	135.0	63.3	53.8	.800	.797	63.3	.0001	28.4
1162.5	142.1	38.0	50.6	25.3	50.6	90.0	25.3	45.0	50.6	41.1	.500	.724	45.5	.0001	22.0
1162.5	142.1	38.0	50.6	25.3	50.6	90.0	25.3	45.0	50.6	41.1	.500	.724	45.5	.0001	22.0
1162.5	142.1	38.0	50.6	25.3	50.6	90.0	25.3	45.0	50.6	41.1	.500	.724	45.5	.0001	22.0
1937.5	192.7	63.3	63.3	25.3	63.3	90.0	25.3	.0	63.3	53.8	.400	.656	67.8	.0001	25.2
1550.0	162.5	38.0	50.6	38.0	50.6	.0	38.0	45.0	50.6	44.3	.750	.738	50.6	.0001	23.3
1550.0	167.4	50.6	50.6	25.3	50.6	90.0	25.3	.0	50.6	44.3	.500	.695	56.0	.0001	23.6
1937.5	179.4	50.6	50.6	38.0	63.3	90.0	38.0	135.0	63.3	50.6	.600	.756	53.5	.0001	27.1
1162.5	142.1	38.0	50.6	25.3	50.6	90.0	25.3	45.0	50.6	41.1	.500	.724	45.5	.0001	22.0
2970.8	250.5	75.9	88.6	63.3	63.3	90.0	63.3	45.0	88.6	72.8	.714	.595	93.4	.0002	30.3
7104.1	391.5	101.3	126.6	101.3	101.3	.0	101.3	45.0	126.6	107.6	.800	.583	147.6	.0004	43.4
100749.2	2535.4	493.7	594.9	443.0	379.7	135.0	379.7	45.0	594.9	477.8	.638	.197	1182.5	.0056	73.6
1162.5	142.1	38.0	50.6	25.3	50.6	90.0	25.3	45.0	50.6	41.1	.500	.724	45.5	.0001	22.0
2325.0	218.0	75.9	75.9	25.3	75.9	90.0	25.3	.0	75.9	63.3	.333	.615	79.9	.0001	26.7
1550.0	162.5	38.0	50.6	38.0	50.6	.0	38.0	45.0	50.6	44.3	.750	.738	50.6	.0001	23.3
1162.5	142.1	38.0	50.6	25.3	50.6	90.0	25.3	45.0	50.6	41.1	.500	.724	45.5	.0001	22.0
2841.6	208.4	63.3	75.9	50.6	63.3	90.0	50.6	45.0	75.9	63.3	.667	.822	75.9	.0002	32.2
1937.5	192.7	63.3	63.3	25.3	63.3	90.0	25.3	.0	63.3	53.8	.400	.656	67.8	.0001	25.2
1162.5	142.1	38.0	50.6	25.3	50.6	90.0	25.3	45.0	50.6	41.1	.500	.724	45.5	.0001	22.0
1162.5	142.1	38.0	50.6	25.3	50.6	90.0	25.3	45.0	50.6	41.1	.500	.724	45.5	.0001	22.0
1162.5	142.1	38.0	50.6	25.3	50.6	90.0	25.3	45.0	50.6	41.1	.500	.724	45.5	.0001	22.0
1162.5	142.1	38.0	50.6	25.3	50.6	90.0	25.3	45.0	50.6	41.1	.500	.724	45.5	.0001	22.0
2583.3	206.6	63.3	75.9	50.6	50.6	90.0	50.6	45.0	75.9	60.1	.667	.761	60.8	.0001	26.4
1550.0	167.4	50.6	50.6	25.3	50.6	90.0	25.3	.0	50.6	44.3	.500	.695	56.0	.0001	23.6
1550.0	167.4	50.6	50.6	25.3	50.6	90.0	25.3	.0	50.6	44.3	.500	.695	56.0	.0001	23.6
1550.0	167.4	50.6	50.6	25.3	50.6	90.0	25.3	.0	50.6	44.3	.500	.695	56.0	.0001	23.6
7491.6	342.5	88.6	113.9	101.3	113.9	.0	88.6	45.0	113.9	104.4	.778	.803	113.9	.0004	48.4
1162.5	142.1	38.0	50.6	25.3	50.6	90.0	25.3	45.0	50.6	41.1	.500	.724	45.5	.0001	22.0

Table A-3 (cont'd)

_A_r_e_a_	Perimeter Ú	0.00% Ú	45.00% Ú	90.00% Ú	135.00%	Min_Angle	Min_Feret	Max_Angle	Max_Feret	Avg_Feret	Asp_Ratio	Shape_Fac	Spec_Peri	Area_Frac	AvgRadius
4650.0	296.2	88.6	75.9	75.9	101.3	45.0	75.9	135.0	101.3	85.4	.750	.666	102.9	.0003	38.9
2454.1	204.7	63.3	63.3	38.0	75.9	90.0	38.0	135.0	75.9	60.1	.500	.736	64.1	.0001	28.7
2970.8	243.3	88.6	88.6	38.0	75.9	90.0	38.0	.0	88.6	72.8	.429	.630	87.9	.0002	29.6
3487.5	264.3	63.3	75.9	75.9	88.6	.0	63.3	135.0	88.6	75.9	.714	.627	95.7	.0002	32.5
1550.0	167.4	50.6	50.6	25.3	50.6	90.0	25.3	.0	50.6	44.3	.500	.695	56.0	.0001	23.6
1808.3	171.0	50.6	63.3	38.0	50.6	90.0	38.0	45.0	63.3	50.6	.600	.777	47.2	.0001	22.6
2712.5	211.9	50.6	75.9	63.3	63.3	.0	50.6	45.0	75.9	63.3	.667	.759	62.6	.0002	29.6
1550.0	167.4	50.6	50.6	25.3	50.6	90.0	25.3	.0	50.6	44.3	.500	.695	56.0	.0001	23.6
1162.5	142.1	38.0	50.6	25.3	50.6	90.0	25.3	45.0	50.6	41.1	.500	.724	45.5	.0001	22.0
4908.3	343.3	126.6	126.6	63.3	101.3	90.0	63.3	.0	126.6	104.4	.500	.523	135.4	.0003	37.2
1162.5	142.1	38.0	50.6	25.3	50.6	90.0	25.3	45.0	50.6	41.1	.500	.724	45.5	.0001	22.0
2454.1	213.1	63.3	75.9	50.6	50.6	90.0	50.6	45.0	75.9	60.1	.667	.679	72.9	.0001	30.0
1550.0	167.4	50.6	50.6	25.3	50.6	90.0	25.3	.0	50.6	44.3	.500	.695	56.0	.0001	23.6
1162.5	142.1	38.0	50.6	25.3	50.6	90.0	25.3	45.0	50.6	41.1	.500	.724	45.5	.0001	22.0
1162.5	142.1	38.0	50.6	25.3	50.6	90.0	25.3	45.0	50.6	41.1	.500	.724	45.5	.0001	22.0
4908.3	343.7	75.9	88.6	88.6	101.3	.0	75.9	135.0	101.3	88.6	.750	.522	135.7	.0003	35.1
8912.4	512.0	202.5	177.2	63.3	151.9	90.0	63.3	.0	202.5	148.7	.313	.427	214.4	.0005	53.1
1937.5	179.4	50.6	50.6	38.0	63.3	90.0	38.0	135.0	63.3	50.6	.600	.756	53.5	.0001	27.1
3487.5	253.9	63.3	88.6	75.9	75.9	.0	63.3	45.0	88.6	75.9	.714	.680	86.8	.0002	34.7
2325.0	199.8	50.6	63.3	50.6	63.3	.0	50.6	45.0	63.3	57.0	.800	.732	63.0	.0001	26.1
1162.5	142.1	38.0	50.6	25.3	50.6	90.0	25.3	45.0	50.6	41.1	.500	.724	45.5	.0001	22.0
2841.6	242.1	75.9	50.6	63.3	88.6	45.0	50.6	135.0	88.6	69.6	.571	.609	89.2	.0002	27.7
1162.5	142.1	38.0	50.6	25.3	50.6	90.0	25.3	45.0	50.6	41.1	.500	.724	45.5	.0001	22.0
3100.0	243.7	63.3	88.6	63.3	63.3	.0	63.3	45.0	88.6	69.6	.714	.656	85.7	.0002	31.2
1162.5	142.1	38.0	50.6	25.3	50.6	90.0	25.3	45.0	50.6	41.1	.500	.724	45.5	.0001	22.0
3229.1	253.6	88.6	75.9	38.0	88.6	90.0	38.0	.0	88.6	72.8	.429	.631	91.5	.0002	34.1
1550.0	167.4	50.6	50.6	25.3	50.6	90.0	25.3	.0	50.6	44.3	.500	.695	56.0	.0001	23.6
21054.0	884.9	227.8	278.5	189.9	139.2	135.0	139.2	45.0	278.5	208.9	.500	.338	388.2	.0012	-1.0
1550.0	167.4	50.6	50.6	25.3	50.6	90.0	25.3	.0	50.6	44.3	.500	.695	56.0	.0001	23.6
19504.0	800.4	253.2	164.6	177.2	278.5	45.0	164.6	135.0	278.5	218.4	.591	.383	343.4	.0011	71.4
13820.7	676.2	151.9	177.2	164.6	164.6	.0	151.9	45.0	177.2	164.6	.857	.380	290.5	.0008	40.8
1162.5	142.1	38.0	50.6	25.3	50.6	90.0	25.3	45.0	50.6	41.1	.500	.724	45.5	.0001	22.0
3229.1	235.4	63.3	88.6	63.3	63.3	.0	63.3	45.0	88.6	69.6	.714	.733	74.1	.0002	31.2
2583.3	208.4	63.3	75.9	50.6	50.6	90.0	50.6	45.0	75.9	60.1	.667	.748	63.5	.0001	26.1
8137.4	476.2	126.6	177.2	126.6	75.9	135.0	75.9	45.0	177.2	126.6	.429	.451	196.7	.0005	37.3
1162.5	142.1	38.0	50.6	25.3	50.6	90.0	25.3	45.0	50.6	41.1	.500	.724	45.5	.0001	22.0
1550.0	167.4	50.6	50.6	25.3	50.6	90.0	25.3	.0	50.6	44.3	.500	.695	56.0	.0001	23.6
3100.0	231.9	75.9	63.3	50.6	88.6	90.0	50.6	135.0	88.6	69.6	.571	.725	74.1	.0002	33.8
32808.1	1001.5	227.8	316.5	303.8	177.2	135.0	177.2	45.0	316.5	256.3	.560	.411	423.3	.0018	90.2
3616.6	263.8	88.6	101.3	50.6	75.9	90.0	50.6	45.0	101.3	79.1	.500	.653	93.0	.0002	31.8

Table A-3 (cont'd)

_A_r_e_a_	Perimeter Ú	0.00% Ú	45.00% Ú	90.00% Ú	135.00%	Min_Angle	Min_Feret	Max_Angle	Max_Feret	Avg_Feret	Asp_Ratio	Shape_Fac	Spec_Peri	Area_Frac	AvgRadius
1550.0	167.4	50.6	50.6	25.3	50.6	90.0	25.3	.0	50.6	44.3	.500	.695	56.0	.0001	23.6
1162.5	142.1	38.0	50.6	25.3	50.6	90.0	25.3	45.0	50.6	41.1	.500	.724	45.5	.0001	22.0
1808.3	171.0	50.6	50.6	38.0	63.3	90.0	38.0	135.0	63.3	50.6	.600	.777	47.2	.0001	27.1
1162.5	142.1	38.0	50.6	25.3	50.6	90.0	25.3	45.0	50.6	41.1	.500	.724	45.5	.0001	22.0
1937.5	192.7	63.3	63.3	25.3	63.3	90.0	25.3	.0	63.3	53.8	.400	.656	67.8	.0001	25.2
2195.8	194.5	63.3	50.6	38.0	75.9	90.0	38.0	135.0	75.9	57.0	.500	.729	61.7	.0001	28.7
1162.5	142.1	38.0	50.6	25.3	50.6	90.0	25.3	45.0	50.6	41.1	.500	.724	45.5	.0001	22.0
1937.5	192.7	63.3	63.3	25.3	63.3	90.0	25.3	.0	63.3	53.8	.400	.656	67.8	.0001	25.2
1162.5	142.1	38.0	50.6	25.3	50.6	90.0	25.3	45.0	50.6	41.1	.500	.724	45.5	.0001	22.0
1550.0	162.5	38.0	50.6	38.0	50.6	.0	38.0	45.0	50.6	44.3	.750	.738	50.6	.0001	23.3
1162.5	142.1	38.0	50.6	25.3	50.6	90.0	25.3	45.0	50.6	41.1	.500	.724	45.5	.0001	22.0
1937.5	179.4	50.6	50.6	38.0	63.3	90.0	38.0	135.0	63.3	50.6	.600	.756	53.5	.0001	27.1
1937.5	179.4	50.6	63.3	38.0	50.6	90.0	38.0	45.0	63.3	50.6	.600	.756	53.5	.0001	24.9
1937.5	182.9	38.0	63.3	50.6	63.3	.0	38.0	45.0	63.3	53.8	.600	.728	58.1	.0001	26.6
1162.5	142.1	38.0	50.6	25.3	50.6	90.0	25.3	45.0	50.6	41.1	.500	.724	45.5	.0001	22.0
1937.5	182.9	38.0	63.3	50.6	63.3	.0	38.0	45.0	63.3	53.8	.600	.728	58.1	.0001	26.6
2454.1	204.7	63.3	63.3	38.0	75.9	90.0	38.0	135.0	75.9	60.1	.500	.736	64.1	.0001	28.7
1162.5	142.1	38.0	50.6	25.3	50.6	90.0	25.3	45.0	50.6	41.1	.500	.724	45.5	.0001	22.0
2454.1	213.1	63.3	50.6	50.6	75.9	45.0	50.6	135.0	75.9	60.1	.667	.679	72.9	.0001	28.7
1550.0	167.4	50.6	50.6	25.3	50.6	90.0	25.3	.0	50.6	44.3	.500	.695	56.0	.0001	23.6
2325.0	233.5	63.3	88.6	63.3	50.6	135.0	50.6	45.0	88.6	66.5	.571	.536	91.3	.0001	25.8
3358.3	240.6	50.6	75.9	75.9	88.6	.0	50.6	135.0	88.6	72.8	.571	.729	76.3	.0002	33.2
1162.5	142.1	38.0	50.6	25.3	50.6	90.0	25.3	45.0	50.6	41.1	.500	.724	45.5	.0001	22.0
2325.0	202.9	63.3	75.9	38.0	63.3	90.0	38.0	45.0	75.9	60.1	.500	.710	66.5	.0001	26.4
18212.3	812.0	291.1	265.8	113.9	215.2	90.0	113.9	.0	291.1	221.5	.391	.347	354.7	.0010	50.0
4004.1	295.8	113.9	101.3	38.0	101.3	90.0	38.0	.0	113.9	88.6	.333	.575	112.2	.0002	36.0
75949.4	1496.6	481.0	291.1	316.5	493.7	45.0	291.1	135.0	493.7	395.6	.590	.426	627.2	.0042	152.9
2325.0	191.4	50.6	63.3	50.6	50.6	.0	50.6	45.0	63.3	53.8	.800	.797	63.3	.0001	28.4
9299.9	528.5	151.9	126.6	113.9	164.6	90.0	113.9	135.0	164.6	139.2	.692	.418	222.4	.0005	37.0
7749.9	389.1	139.2	126.6	75.9	126.6	90.0	75.9	.0	139.2	117.1	.545	.643	138.6	.0004	46.2
24283.1	929.9	126.6	265.8	379.7	329.1	.0	126.6	90.0	379.7	275.3	.333	.353	405.0	.0014	62.5
18729.0	638.8	177.2	177.2	177.2	202.5	.0	177.2	135.0	202.5	183.5	.875	.577	242.0	.0010	76.5
25058.1	734.6	303.8	303.8	139.2	177.2	90.0	139.2	.0	303.8	231.0	.458	.584	276.7	.0014	77.0
1550.0	162.5	38.0	50.6	38.0	50.6	.0	38.0	45.0	50.6	44.3	.750	.738	50.6	.0001	23.3
27383.1	750.6	303.8	265.8	113.9	240.5	90.0	113.9	.0	303.8	231.0	.375	.611	276.1	.0015	83.7
1937.5	192.7	63.3	63.3	25.3	63.3	90.0	25.3	.0	63.3	53.8	.400	.656	67.8	.0001	25.2
1937.5	182.9	38.0	63.3	50.6	63.3	.0	38.0	45.0	63.3	53.8	.600	.728	58.1	.0001	24.6
3100.0	232.3	50.6	75.9	75.9	75.9	.0	50.6	45.0	75.9	69.6	.667	.722	74.6	.0002	33.2
154611.2	2474.0	278.5	658.2	772.2	594.9	.0	278.5	90.0	772.2	575.9	.361	.317	1095.9	.0086	188.8
23120.6	941.1	126.6	265.8	316.5	253.2	.0	126.6	90.0	316.5	240.5	.480	.328	414.8	.0013	84.2

Table A-3 (cont'd)

_A_r_e_a_	Perimeter Ú	0.00% Ú	45.00% Ú	90.00% Ú	135.00%	Min_Angle	Min_Feret	Max_Angle	Max_Feret	Avg_Feret	Asp_Ratio	Shape_Fac	Spec_Peri	Area_Frac	AvgRadius
2066.6	192.7	63.3	50.6	38.0	75.9	90.0	38.0	135.0	75.9	57.0	.500	.699	64.1	.0001	26.4
4004.1	281.5	50.6	88.6	88.6	101.3	.0	50.6	135.0	101.3	82.3	.500	.635	101.1	.0002	31.9
4520.8	290.0	63.3	101.3	88.6	88.6	.0	63.3	45.0	101.3	85.4	.625	.675	99.6	.0003	35.7
10462.4	419.0	101.3	151.9	126.6	126.6	.0	101.3	45.0	151.9	126.6	.667	.749	127.3	.0006	55.5
1162.5	142.1	38.0	50.6	25.3	50.6	90.0	25.3	45.0	50.6	41.1	.500	.724	45.5	.0001	22.0
1550.0	167.4	50.6	50.6	25.3	50.6	90.0	25.3	.0	50.6	44.3	.500	.695	56.0	.0001	23.6
1162.5	142.1	38.0	50.6	25.3	50.6	90.0	25.3	45.0	50.6	41.1	.500	.724	45.5	.0001	22.0
6458.3	378.0	75.9	126.6	113.9	101.3	.0	75.9	45.0	126.6	104.4	.600	.568	144.2	.0004	40.8
2325.0	199.8	50.6	63.3	50.6	63.3	.0	50.6	45.0	63.3	57.0	.800	.732	63.0	.0001	28.4
2325.0	203.3	38.0	63.3	63.3	63.3	.0	38.0	45.0	63.3	57.0	.600	.707	66.9	.0001	25.8
2325.0	203.3	38.0	63.3	63.3	63.3	.0	38.0	45.0	63.3	57.0	.600	.707	66.9	.0001	25.8
1550.0	162.5	38.0	50.6	38.0	50.6	.0	38.0	45.0	50.6	44.3	.750	.738	50.6	.0001	23.3
1162.5	142.1	38.0	50.6	25.3	50.6	90.0	25.3	45.0	50.6	41.1	.500	.724	45.5	.0001	22.0
1162.5	142.1	38.0	50.6	25.3	50.6	90.0	25.3	45.0	50.6	41.1	.500	.724	45.5	.0001	22.0
2454.1	211.9	50.6	75.9	63.3	63.3	.0	50.6	45.0	75.9	63.3	.667	.687	71.7	.0001	25.8
2841.6	220.2	50.6	75.9	63.3	63.3	.0	50.6	45.0	75.9	63.3	.667	.736	68.8	.0002	29.6
26091.4	943.8	202.5	202.5	253.2	215.2	.0	202.5	90.0	253.2	218.4	.800	.368	407.9	.0015	79.7
9687.4	517.0	113.9	151.9	139.2	126.6	.0	113.9	45.0	151.9	132.9	.750	.455	213.0	.0005	45.3
1162.5	142.1	38.0	50.6	25.3	50.6	90.0	25.3	45.0	50.6	41.1	.500	.724	45.5	.0001	22.0
30095.6	1087.5	139.2	253.2	316.5	278.5	.0	139.2	90.0	316.5	246.8	.440	.320	481.2	.0017	85.8
10204.1	495.6	151.9	151.9	101.3	151.9	90.0	101.3	.0	151.9	139.2	.667	.522	195.7	.0006	56.4
3100.0	270.9	63.3	63.3	75.9	88.6	.0	63.3	135.0	88.6	72.8	.714	.531	106.3	.0002	28.7
1550.0	167.4	50.6	50.6	25.3	50.6	90.0	25.3	.0	50.6	44.3	.500	.695	56.0	.0001	23.6
1550.0	167.4	50.6	50.6	25.3	50.6	90.0	25.3	.0	50.6	44.3	.500	.695	56.0	.0001	23.6
1162.5	142.1	38.0	50.6	25.3	50.6	90.0	25.3	45.0	50.6	41.1	.500	.724	45.5	.0001	22.0
1550.0	167.4	50.6	50.6	25.3	50.6	90.0	25.3	.0	50.6	44.3	.500	.695	56.0	.0001	23.6
1162.5	142.1	38.0	50.6	25.3	50.6	90.0	25.3	45.0	50.6	41.1	.500	.724	45.5	.0001	22.0
1162.5	142.1	38.0	50.6	25.3	50.6	90.0	25.3	45.0	50.6	41.1	.500	.724	45.5	.0001	22.0
19633.2	670.9	189.9	215.2	189.9	177.2	135.0	177.2	45.0	215.2	193.0	.824	.548	259.9	.0011	70.8
13380392.0	21283.3	4797.5	6240.5	4544.3	4316.5	135.0	4316.5	45.0	6240.5	4974.7	.692	.371	9184.8	.7469	2054.5
1162.5	142.1	38.0	50.6	25.3	50.6	90.0	25.3	45.0	50.6	41.1	.500	.724	45.5	.0001	22.0
1808.3	171.0	50.6	50.6	38.0	63.3	90.0	38.0	135.0	63.3	50.6	.600	.777	47.2	.0001	27.1
1162.5	142.1	38.0	50.6	25.3	50.6	90.0	25.3	45.0	50.6	41.1	.500	.724	45.5	.0001	22.0
2841.6	216.8	63.3	75.9	50.6	63.3	90.0	50.6	45.0	75.9	63.3	.667	.760	63.9	.0002	30.0
1162.5	142.1	38.0	50.6	25.3	50.6	90.0	25.3	45.0	50.6	41.1	.500	.724	45.5	.0001	22.0
1937.5	179.4	50.6	63.3	38.0	50.6	90.0	38.0	45.0	63.3	50.6	.600	.756	53.5	.0001	24.9
3229.1	253.6	88.6	75.9	38.0	88.6	90.0	38.0	.0	88.6	72.8	.429	.631	91.5	.0002	34.1
1162.5	142.1	38.0	50.6	25.3	50.6	90.0	25.3	45.0	50.6	41.1	.500	.724	45.5	.0001	22.0
1550.0	162.5	38.0	50.6	38.0	50.6	.0	38.0	45.0	50.6	44.3	.750	.738	50.6	.0001	23.3
7362.4	343.9	113.9	113.9	75.9	101.3	90.0	75.9	.0	113.9	101.3	.667	.782	91.4	.0004	46.8

Table A-3 (cont'd)

_A_r_e_a_	Perimeter Ú	0.00% Ú	45.00% Ú	90.00% Ú	135.00%	Min_Angle	Min_Feret	Max_Angle	Max_Feret	Avg_Feret	Asp_Ratio	Shape_Fac	Spec_Peri	Area_Frac	AvgRadius
4520.8	336.6	113.9	88.6	75.9	126.6	90.0	75.9	135.0	126.6	101.3	.600	.501	134.8	.0003	34.1
43658.0	1245.7	481.0	253.2	253.2	506.3	45.0	253.2	135.0	506.3	373.4	.500	.354	542.4	.0024	88.2
1162.5	142.1	38.0	50.6	25.3	50.6	90.0	25.3	45.0	50.6	41.1	.500	.724	45.5	.0001	22.0
1550.0	162.5	38.0	50.6	38.0	50.6	.0	38.0	45.0	50.6	44.3	.750	.738	50.6	.0001	23.3
2343322.0	15482.4	2481.0	2696.2	1607.6	1848.1	90.0	1607.6	45.0	2696.2	2158.2	.596	.123	7425.6	.1308	792.3
2841.6	238.4	75.9	63.3	50.6	88.6	90.0	50.6	135.0	88.6	69.6	.571	.628	86.3	.0002	29.0
1550.0	167.4	50.6	50.6	25.3	50.6	90.0	25.3	.0	50.6	44.3	.500	.695	56.0	.0001	23.6
2325.0	202.9	63.3	75.9	38.0	63.3	90.0	38.0	45.0	75.9	60.1	.500	.710	66.5	.0001	28.7
3229.1	247.4	63.3	88.6	75.9	63.3	.0	63.3	45.0	88.6	72.8	.714	.663	86.2	.0002	32.5
1162.5	142.1	38.0	50.6	25.3	50.6	90.0	25.3	45.0	50.6	41.1	.500	.724	45.5	.0001	22.0
17308.2	644.8	215.2	177.2	139.2	189.9	90.0	139.2	.0	215.2	180.4	.647	.523	254.4	.0010	72.0
1550.0	162.5	38.0	50.6	38.0	50.6	.0	38.0	45.0	50.6	44.3	.750	.738	50.6	.0001	23.3
3487.5	235.5	75.9	63.3	63.3	88.6	45.0	63.3	135.0	88.6	72.8	.714	.790	88.6	.0002	30.0
1550.0	167.4	50.6	50.6	25.3	50.6	90.0	25.3	.0	50.6	44.3	.500	.695	56.0	.0001	23.6
1162.5	142.1	38.0	50.6	25.3	50.6	90.0	25.3	45.0	50.6	41.1	.500	.724	45.5	.0001	22.0
42108.0	948.9	215.2	341.8	316.5	227.8	.0	215.2	45.0	341.8	275.3	.630	.588	356.2	.0024	115.1
19891.5	566.1	177.2	151.9	151.9	202.5	45.0	151.9	135.0	202.5	170.9	.750	.780	153.4	.0011	77.1
1162.5	142.1	38.0	50.6	25.3	50.6	90.0	25.3	45.0	50.6	41.1	.500	.724	45.5	.0001	22.0
117540.7	1447.2	481.0	417.7	316.5	481.0	90.0	316.5	.0	481.0	424.1	.658	.705	477.4	.0066	187.6
10333.2	465.3	113.9	101.3	164.6	177.2	45.0	101.3	135.0	177.2	139.2	.571	.600	172.8	.0006	50.4
328209.8	3149.9	924.1	974.7	898.7	797.5	135.0	797.5	45.0	974.7	898.7	.818	.416	1327.8	.0183	289.9
1808.3	171.0	50.6	50.6	38.0	63.3	90.0	38.0	135.0	63.3	50.6	.600	.777	47.2	.0001	27.1
1550.0	167.4	50.6	50.6	25.3	50.6	90.0	25.3	.0	50.6	44.3	.500	.695	56.0	.0001	23.6
2195.8	191.4	50.6	50.6	50.6	63.3	.0	50.6	135.0	63.3	53.8	.800	.753	57.6	.0001	28.4
1937.5	182.9	38.0	63.3	50.6	63.3	.0	38.0	45.0	63.3	53.8	.600	.728	58.1	.0001	24.6
5554.1	348.6	113.9	126.6	75.9	88.6	90.0	75.9	45.0	126.6	101.3	.600	.574	132.4	.0003	40.5
2454.1	204.7	63.3	63.3	38.0	75.9	90.0	38.0	135.0	75.9	60.1	.500	.736	64.1	.0001	28.7
1162.5	142.1	38.0	50.6	25.3	50.6	90.0	25.3	45.0	50.6	41.1	.500	.724	45.5	.0001	22.0
1162.5	142.1	38.0	50.6	25.3	50.6	90.0	25.3	45.0	50.6	41.1	.500	.724	45.5	.0001	22.0
3745.8	255.8	63.3	88.6	75.9	63.3	.0	63.3	45.0	88.6	72.8	.714	.720	82.4	.0002	32.5
1162.5	142.1	38.0	50.6	25.3	50.6	90.0	25.3	45.0	50.6	41.1	.500	.724	45.5	.0001	22.0
1937.5	192.7	63.3	63.3	25.3	63.3	90.0	25.3	.0	63.3	53.8	.400	.656	67.8	.0001	25.2
1162.5	142.1	38.0	50.6	25.3	50.6	90.0	25.3	45.0	50.6	41.1	.500	.724	45.5	.0001	22.0
2325.0	211.9	50.6	75.9	63.3	63.3	.0	50.6	45.0	75.9	63.3	.667	.651	74.9	.0001	25.8
1162.5	142.1	38.0	50.6	25.3	50.6	90.0	25.3	45.0	50.6	41.1	.500	.724	45.5	.0001	22.0
1162.5	142.1	38.0	50.6	25.3	50.6	90.0	25.3	45.0	50.6	41.1	.500	.724	45.5	.0001	22.0
3100.0	243.3	88.6	75.9	38.0	88.6	90.0	38.0	.0	88.6	72.8	.429	.658	85.4	.0002	31.8
1162.5	142.1	38.0	50.6	25.3	50.6	90.0	25.3	45.0	50.6	41.1	.500	.724	45.5	.0001	22.0
1162.5	142.1	38.0	50.6	25.3	50.6	90.0	25.3	45.0	50.6	41.1	.500	.724	45.5	.0001	22.0
1162.5	142.1	38.0	50.6	25.3	50.6	90.0	25.3	45.0	50.6	41.1	.500	.724	45.5	.0001	22.0

Table A-3 (cont'd)

_A_r_e_a_	Perimeter Û	0.00% Û	45.00% Û	90.00% Û	135.00%	Min_Angle	Min_Feret	Max_Angle	Max_Feret	Avg_Feret	Asp_Ratio	Shape_Fac	Spec_Peri	Area_Frac	AvgRadius
1937.5	179.4	50.6	50.6	38.0	63.3	90.0	38.0	135.0	63.3	50.6	.600	.756	53.5	.0001	27.1
1162.5	142.1	38.0	50.6	25.3	50.6	90.0	25.3	45.0	50.6	41.1	.500	.724	45.5	.0001	22.0
5166.6	325.1	101.3	113.9	75.9	75.9	90.0	75.9	45.0	113.9	91.8	.667	.614	119.2	.0003	36.0
2325.0	191.4	50.6	63.3	50.6	63.3	.0	50.6	45.0	63.3	57.0	.800	.797	63.3	.0001	30.6
1937.5	179.4	50.6	63.3	38.0	50.6	90.0	38.0	45.0	63.3	50.6	.600	.756	53.5	.0001	24.9
2970.8	216.8	63.3	75.9	50.6	75.9	90.0	50.6	45.0	75.9	66.5	.667	.795	75.9	.0002	32.2
1937.5	179.4	50.6	63.3	38.0	50.6	90.0	38.0	45.0	63.3	50.6	.600	.756	53.5	.0001	24.9
1162.5	142.1	38.0	50.6	25.3	50.6	90.0	25.3	45.0	50.6	41.1	.500	.724	45.5	.0001	22.0
1162.5	142.1	38.0	50.6	25.3	50.6	90.0	25.3	45.0	50.6	41.1	.500	.724	45.5	.0001	22.0
2325.0	202.9	63.3	63.3	38.0	75.9	90.0	38.0	135.0	75.9	60.1	.500	.710	66.5	.0001	28.7
1550.0	162.5	38.0	50.6	38.0	50.6	.0	38.0	45.0	50.6	44.3	.750	.738	50.6	.0001	23.3
1162.5	142.1	38.0	50.6	25.3	50.6	90.0	25.3	45.0	50.6	41.1	.500	.724	45.5	.0001	22.0
1162.5	142.1	38.0	50.6	25.3	50.6	90.0	25.3	45.0	50.6	41.1	.500	.724	45.5	.0001	22.0
1162.5	142.1	38.0	50.6	25.3	50.6	90.0	25.3	45.0	50.6	41.1	.500	.724	45.5	.0001	22.0
1162.5	142.1	38.0	50.6	25.3	50.6	90.0	25.3	45.0	50.6	41.1	.500	.724	45.5	.0001	22.0
1162.5	142.1	38.0	50.6	25.3	50.6	90.0	25.3	45.0	50.6	41.1	.500	.724	45.5	.0001	22.0
1550.0	162.5	38.0	50.6	38.0	50.6	.0	38.0	45.0	50.6	44.3	.750	.738	50.6	.0001	23.3
1162.5	142.1	38.0	50.6	25.3	50.6	90.0	25.3	45.0	50.6	41.1	.500	.724	45.5	.0001	22.0
1937.5	179.4	50.6	50.6	38.0	63.3	90.0	38.0	135.0	63.3	50.6	.600	.756	53.5	.0001	27.1
1550.0	167.4	50.6	50.6	25.3	50.6	90.0	25.3	.0	50.6	44.3	.500	.695	56.0	.0001	23.6
1550.0	167.4	50.6	50.6	25.3	50.6	90.0	25.3	.0	50.6	44.3	.500	.695	56.0	.0001	23.6
1162.5	142.1	38.0	50.6	25.3	50.6	90.0	25.3	45.0	50.6	41.1	.500	.724	45.5	.0001	22.0
1550.0	162.5	38.0	50.6	38.0	50.6	.0	38.0	45.0	50.6	44.3	.750	.738	50.6	.0001	23.3
2583.3	208.2	50.6	63.3	50.6	63.3	.0	50.6	45.0	63.3	57.0	.800	.749	63.3	.0001	30.6
1162.5	142.1	38.0	50.6	25.3	50.6	90.0	25.3	45.0	50.6	41.1	.500	.724	45.5	.0001	22.0
1550.0	167.4	50.6	50.6	25.3	50.6	90.0	25.3	.0	50.6	44.3	.500	.695	56.0	.0001	23.6
1162.5	142.1	38.0	50.6	25.3	50.6	90.0	25.3	45.0	50.6	41.1	.500	.724	45.5	.0001	22.0
1162.5	142.1	38.0	50.6	25.3	50.6	90.0	25.3	45.0	50.6	41.1	.500	.724	45.5	.0001	22.0
1162.5	142.1	38.0	50.6	25.3	50.6	90.0	25.3	45.0	50.6	41.1	.500	.724	45.5	.0001	22.0
1162.5	142.1	38.0	50.6	25.3	50.6	90.0	25.3	45.0	50.6	41.1	.500	.724	45.5	.0001	22.0
1162.5	142.1	38.0	50.6	25.3	50.6	90.0	25.3	45.0	50.6	41.1	.500	.724	45.5	.0001	22.0
1162.5	142.1	38.0	50.6	25.3	50.6	90.0	25.3	45.0	50.6	41.1	.500	.724	45.5	.0001	22.0
2583.3	238.4	75.9	63.3	50.6	88.6	90.0	50.6	135.0	88.6	69.6	.571	.571	90.8	.0001	29.3
1162.5	142.1	38.0	50.6	25.3	50.6	90.0	25.3	45.0	50.6	41.1	.500	.724	45.5	.0001	22.0
2325.0	202.9	63.3	63.3	38.0	75.9	90.0	38.0	135.0	75.9	60.1	.500	.710	66.5	.0001	28.7
11883.2	616.0	215.2	151.9	113.9	215.2	90.0	113.9	.0	215.2	174.1	.529	.393	262.8	.0007	43.0
4650.0	266.1	75.9	88.6	75.9	75.9	.0	75.9	45.0	88.6	79.1	.857	.825	88.6	.0003	38.6
2970.8	235.4	63.3	63.3	63.3	88.6	.0	63.3	135.0	88.6	69.6	.714	.674	81.0	.0002	31.2
1162.5	142.1	38.0	50.6	25.3	50.6	90.0	25.3	45.0	50.6	41.1	.500	.724	45.5	.0001	22.0
16016.5	747.9	253.2	202.5	126.6	189.9	90.0	126.6	.0	253.2	193.0	.500	.360	324.6	.0009	47.1

Table A-3 (cont'd)

_A_r_e_a_	Perimeter Ú	0.00% Ú	45.00% Ú	90.00% Ú	135.00%	Min_Angle	Min_Feret	Max_Angle	Max_Feret	Avg_Feret	Asp_Ratio	Shape_Fac	Spec_Peri	Area_Frac	AvgRadius
1162.5	142.1	38.0	50.6	25.3	50.6	90.0	25.3	45.0	50.6	41.1	.500	.724	45.5	.0001	22.0
2325.0	191.4	50.6	63.3	50.6	63.3	.0	50.6	45.0	63.3	57.0	.800	.797	63.3	.0001	30.6
18987.3	757.7	202.5	202.5	139.2	164.6	90.0	139.2	.0	202.5	177.2	.688	.416	319.4	.0011	71.7
1550.0	162.5	38.0	50.6	38.0	50.6	.0	38.0	45.0	50.6	44.3	.750	.738	50.6	.0001	23.3
3100.0	240.3	75.9	88.6	50.6	63.3	90.0	50.6	45.0	88.6	69.6	.571	.675	82.6	.0002	30.0
1937.5	179.4	50.6	50.6	38.0	63.3	90.0	38.0	135.0	63.3	50.6	.600	.756	53.5	.0001	27.1
3875.0	269.6	63.3	75.9	75.9	101.3	.0	63.3	135.0	101.3	79.1	.625	.670	93.2	.0002	34.4
44303.8	1826.7	379.7	227.8	341.8	468.4	45.0	227.8	135.0	468.4	354.4	.486	.167	861.9	.0025	83.4
7362.4	451.7	113.9	113.9	88.6	101.3	90.0	88.6	.0	113.9	104.4	.778	.453	186.4	.0004	36.3
2712.5	228.2	75.9	75.9	38.0	75.9	90.0	38.0	.0	75.9	66.5	.500	.654	80.4	.0002	30.3
19504.0	878.7	240.5	164.6	202.5	291.1	45.0	164.6	135.0	291.1	224.7	.565	.317	389.2	.0011	49.7
1162.5	142.1	38.0	50.6	25.3	50.6	90.0	25.3	45.0	50.6	41.1	.500	.724	45.5	.0001	22.0
3745.8	278.9	101.3	101.3	38.0	88.6	90.0	38.0	.0	101.3	82.3	.375	.605	103.1	.0002	33.4
3875.0	313.1	101.3	75.9	75.9	113.9	45.0	75.9	135.0	113.9	91.8	.667	.497	125.7	.0002	29.9
1162.5	142.1	38.0	50.6	25.3	50.6	90.0	25.3	45.0	50.6	41.1	.500	.724	45.5	.0001	22.0
2325.0	199.8	50.6	63.3	50.6	63.3	.0	50.6	45.0	63.3	57.0	.800	.732	63.0	.0001	28.4
2325.0	199.8	50.6	63.3	50.6	63.3	.0	50.6	45.0	63.3	57.0	.800	.732	63.0	.0001	26.1
1162.5	142.1	38.0	50.6	25.3	50.6	90.0	25.3	45.0	50.6	41.1	.500	.724	45.5	.0001	22.0
5166.6	345.7	101.3	75.9	88.6	126.6	45.0	75.9	135.0	126.6	98.1	.600	.543	134.4	.0003	31.3
1162.5	142.1	38.0	50.6	25.3	50.6	90.0	25.3	45.0	50.6	41.1	.500	.724	45.5	.0001	22.0
3875.0	286.0	88.6	75.9	63.3	101.3	90.0	63.3	135.0	101.3	82.3	.625	.595	106.7	.0002	31.9
2841.6	211.9	50.6	63.3	63.3	63.3	.0	50.6	45.0	63.3	60.1	.800	.796	63.3	.0002	31.9
5812.5	387.6	113.9	88.6	88.6	139.2	45.0	88.6	135.0	139.2	107.6	.636	.486	156.7	.0003	41.5
8137.4	463.6	139.2	164.6	88.6	113.9	90.0	88.6	45.0	164.6	126.6	.538	.476	188.7	.0005	49.7
8008.3	422.1	101.3	139.2	113.9	101.3	.0	101.3	45.0	139.2	113.9	.727	.565	161.4	.0004	43.3
1937.5	179.4	50.6	50.6	38.0	63.3	90.0	38.0	135.0	63.3	50.6	.600	.756	53.5	.0001	27.1
3358.3	240.8	63.3	63.3	75.9	88.6	.0	63.3	135.0	88.6	72.8	.714	.728	76.5	.0002	30.3
1162.5	142.1	38.0	50.6	25.3	50.6	90.0	25.3	45.0	50.6	41.1	.500	.724	45.5	.0001	22.0
2066.6	191.4	50.6	50.6	50.6	63.3	.0	50.6	135.0	63.3	53.8	.800	.709	62.8	.0001	26.1
10849.9	516.2	189.9	126.6	101.3	177.2	90.0	101.3	.0	189.9	148.7	.533	.512	205.2	.0006	53.2
3100.0	275.8	88.6	63.3	63.3	101.3	45.0	63.3	135.0	101.3	79.1	.625	.512	109.6	.0002	29.3
2325.0	199.8	50.6	63.3	50.6	63.3	.0	50.6	45.0	63.3	57.0	.800	.732	63.0	.0001	28.4
2454.1	199.8	50.6	63.3	50.6	63.3	.0	50.6	45.0	63.3	57.0	.800	.772	56.4	.0001	30.6
1162.5	142.1	38.0	50.6	25.3	50.6	90.0	25.3	45.0	50.6	41.1	.500	.724	45.5	.0001	22.0
4908.3	327.4	63.3	101.3	101.3	113.9	.0	63.3	135.0	113.9	94.9	.556	.576	124.1	.0003	37.0
9041.6	456.6	177.2	126.6	75.9	164.6	90.0	75.9	.0	177.2	136.1	.429	.545	177.3	.0005	50.3
2712.5	243.3	88.6	75.9	38.0	88.6	90.0	38.0	.0	88.6	72.8	.429	.576	92.3	.0002	28.3
1162.5	142.1	38.0	50.6	25.3	50.6	90.0	25.3	45.0	50.6	41.1	.500	.724	45.5	.0001	22.0
1162.5	142.1	38.0	50.6	25.3	50.6	90.0	25.3	45.0	50.6	41.1	.500	.724	45.5	.0001	22.0
1550.0	162.5	38.0	50.6	38.0	50.6	.0	38.0	45.0	50.6	44.3	.750	.738	50.6	.0001	23.3

Table A-3 (cont'd)

_A_r_e_a_	Perimeter Ú	0.00% Ú	45.00% Ú	90.00% Ú	135.00%	Min_Angle	Min_Feret	Max_Angle	Max_Feret	Avg_Feret	Asp_Ratio	Shape_Fac	Spec_Peri	Area_Frac	AvgRadius
1162.5	142.1	38.0	50.6	25.3	50.6	90.0	25.3	45.0	50.6	41.1	.500	.724	45.5	.0001	22.0
2325.0	203.3	38.0	63.3	63.3	63.3	.0	38.0	45.0	63.3	57.0	.600	.707	66.9	.0001	25.8
2454.1	204.7	63.3	63.3	38.0	75.9	90.0	38.0	135.0	75.9	60.1	.500	.736	64.1	.0001	28.7
1162.5	142.1	38.0	50.6	25.3	50.6	90.0	25.3	45.0	50.6	41.1	.500	.724	45.5	.0001	22.0
1550.0	167.4	50.6	50.6	25.3	50.6	90.0	25.3	.0	50.6	44.3	.500	.695	56.0	.0001	23.6
2712.5	208.4	63.3	63.3	50.6	75.9	90.0	50.6	135.0	75.9	63.3	.667	.785	53.3	.0002	30.0
2066.6	192.7	63.3	50.6	38.0	75.9	90.0	38.0	135.0	75.9	57.0	.500	.699	64.1	.0001	26.4
1937.5	182.9	38.0	63.3	50.6	63.3	.0	38.0	45.0	63.3	53.8	.600	.728	58.1	.0001	24.6
3745.8	245.7	75.9	63.3	63.3	88.6	45.0	63.3	135.0	88.6	72.8	.714	.780	66.7	.0002	35.7
1550.0	162.5	38.0	50.6	38.0	50.6	.0	38.0	45.0	50.6	44.3	.750	.738	50.6	.0001	23.3
3875.0	281.1	63.3	88.6	75.9	88.6	.0	63.3	45.0	88.6	79.1	.714	.616	102.9	.0002	33.8
1937.5	179.4	50.6	50.6	38.0	63.3	90.0	38.0	135.0	63.3	50.6	.600	.756	53.5	.0001	27.1
349263.8	2439.2	886.1	835.4	696.2	569.6	135.0	569.6	.0	886.1	746.8	.643	.738	760.1	.0195	325.0
1162.5	142.1	38.0	50.6	25.3	50.6	90.0	25.3	45.0	50.6	41.1	.500	.724	45.5	.0001	22.0
2970.8	220.2	50.6	63.3	63.3	75.9	.0	50.6	135.0	75.9	63.3	.667	.770	62.9	.0002	29.6
1162.5	142.1	38.0	50.6	25.3	50.6	90.0	25.3	45.0	50.6	41.1	.500	.724	45.5	.0001	22.0
1808.3	171.0	50.6	50.6	38.0	63.3	90.0	38.0	135.0	63.3	50.6	.600	.777	47.2	.0001	27.1
1808.3	171.0	50.6	50.6	38.0	63.3	90.0	38.0	135.0	63.3	50.6	.600	.777	47.2	.0001	27.1
13691.6	619.5	202.5	177.2	113.9	189.9	90.0	113.9	.0	202.5	170.9	.563	.448	256.3	.0008	56.7
1162.5	142.1	38.0	50.6	25.3	50.6	90.0	25.3	45.0	50.6	41.1	.500	.724	45.5	.0001	22.0
1162.5	142.1	38.0	50.6	25.3	50.6	90.0	25.3	45.0	50.6	41.1	.500	.724	45.5	.0001	22.0
1162.5	142.1	38.0	50.6	25.3	50.6	90.0	25.3	45.0	50.6	41.1	.500	.724	45.5	.0001	22.0
1937.5	192.7	63.3	63.3	25.3	63.3	90.0	25.3	.0	63.3	53.8	.600	.656	67.8	.0001	25.2
1162.5	142.1	38.0	50.6	25.3	50.6	90.0	25.3	45.0	50.6	41.1	.500	.724	45.5	.0001	22.0
3229.1	252.7	50.6	75.9	75.9	88.6	.0	50.6	135.0	88.6	72.8	.571	.636	90.8	.0002	30.6
1550.0	162.5	38.0	50.6	38.0	50.6	.0	38.0	45.0	50.6	44.3	.750	.738	50.6	.0001	23.3
1162.5	142.1	38.0	50.6	25.3	50.6	90.0	25.3	45.0	50.6	41.1	.500	.724	45.5	.0001	22.0
5941.6	358.8	113.9	126.6	75.9	101.3	90.0	75.9	45.0	126.6	104.4	.600	.580	135.6	.0003	42.7
5037.5	286.0	88.6	88.6	63.3	101.3	90.0	63.3	135.0	101.3	85.4	.625	.774	80.1	.0003	41.1
1162.5	142.1	38.0	50.6	25.3	50.6	90.0	25.3	45.0	50.6	41.1	.500	.724	45.5	.0001	22.0
1937.5	179.4	50.6	63.3	38.0	50.6	90.0	38.0	45.0	63.3	50.6	.600	.756	53.5	.0001	24.9
4004.1	284.2	88.6	75.9	63.3	101.3	90.0	63.3	135.0	101.3	82.3	.625	.623	103.3	.0002	34.1
6716.6	471.6	151.9	101.3	75.9	151.9	90.0	75.9	.0	151.9	120.3	.500	.380	202.6	.0004	-1.0
2970.8	225.1	63.3	75.9	50.6	63.3	90.0	50.6	45.0	75.9	63.3	.667	.736	70.3	.0002	34.4
1162.5	142.1	38.0	50.6	25.3	50.6	90.0	25.3	45.0	50.6	41.1	.500	.724	45.5	.0001	22.0
1937.5	179.4	50.6	63.3	38.0	50.6	90.0	38.0	45.0	63.3	50.6	.600	.756	53.5	.0001	24.9
1162.5	142.1	38.0	50.6	25.3	50.6	90.0	25.3	45.0	50.6	41.1	.500	.724	45.5	.0001	22.0
1550.0	167.4	50.6	50.6	25.3	50.6	90.0	25.3	.0	50.6	44.3	.500	.695	56.0	.0001	23.6
48824.6	998.6	265.8	278.5	291.1	316.5	.0	265.8	135.0	316.5	288.0	.840	.615	365.9	.0027	118.0
1162.5	142.1	38.0	50.6	25.3	50.6	90.0	25.3	45.0	50.6	41.1	.500	.724	45.5	.0001	22.0

Table A-3 (cont'd)

_A_r_e_a_	Perimeter Ù	0.00% Ù	45.00% Ù	90.00% Ù	135.00%	Min_Angle	Min_Feret	Max_Angle	Max_Feret	Avg_Feret	Asp_Ratio	Shape_Fac	Spec_Peri	Area_Frac	AvgRadius
1937.5	182.9	38.0	63.3	50.6	63.3	.0	38.0	45.0	63.3	53.8	.600	.728	58.1	.0001	24.6
1937.5	182.9	38.0	63.3	50.6	63.3	.0	38.0	45.0	63.3	53.8	.600	.728	58.1	.0001	24.6
2454.1	204.7	63.3	75.9	38.0	63.3	90.0	38.0	45.0	75.9	60.1	.500	.736	64.1	.0001	30.9
1550.0	167.4	50.6	50.6	25.3	50.6	90.0	25.3	.0	50.6	44.3	.500	.695	56.0	.0001	23.6
3487.5	257.2	88.6	75.9	50.6	101.3	90.0	50.6	135.0	101.3	79.1	.500	.663	89.7	.0002	35.4
1550.0	167.4	50.6	50.6	25.3	50.6	90.0	25.3	.0	50.6	44.3	.500	.695	56.0	.0001	23.6
2454.1	204.7	63.3	75.9	38.0	63.3	90.0	38.0	45.0	75.9	60.1	.500	.736	64.1	.0001	30.9
2712.5	228.2	75.9	75.9	38.0	75.9	90.0	38.0	.0	75.9	66.5	.500	.654	80.4	.0002	29.0
1162.5	142.1	38.0	50.6	25.3	50.6	90.0	25.3	45.0	50.6	41.1	.500	.724	45.5	.0001	22.0
1162.5	142.1	38.0	50.6	25.3	50.6	90.0	25.3	45.0	50.6	41.1	.500	.724	45.5	.0001	22.0
12012.4	507.0	126.6	164.6	151.9	126.6	.0	126.6	45.0	164.6	142.4	.769	.587	190.4	.0007	56.7
2841.6	216.8	63.3	63.3	50.6	75.9	90.0	50.6	135.0	75.9	63.3	.667	.760	63.9	.0002	30.0
1550.0	162.5	38.0	50.6	38.0	50.6	.0	38.0	45.0	50.6	44.3	.750	.738	50.6	.0001	23.3
1162.5	142.1	38.0	50.6	25.3	50.6	90.0	25.3	45.0	50.6	41.1	.500	.724	45.5	.0001	22.0
4004.1	259.0	88.6	88.6	50.6	75.9	90.0	50.6	.0	88.6	75.9	.571	.750	78.5	.0002	39.8
19504.0	587.6	189.9	202.5	151.9	164.6	90.0	151.9	45.0	202.5	177.2	.750	.710	192.5	.0011	76.8
12141.6	444.3	126.6	164.6	126.6	126.6	.0	126.6	45.0	164.6	136.1	.769	.773	125.1	.0007	58.6
1550.0	167.4	50.6	50.6	25.3	50.6	90.0	25.3	.0	50.6	44.3	.500	.695	56.0	.0001	23.6
152932.1	1770.6	341.8	569.6	620.3	506.3	.0	341.8	90.0	620.3	509.5	.551	.613	650.0	.0085	209.1
1550.0	162.5	38.0	50.6	38.0	50.6	.0	38.0	45.0	50.6	44.3	.750	.738	50.6	.0001	23.3
10849.9	490.2	113.9	164.6	126.6	126.6	.0	113.9	45.0	164.6	132.9	.692	.567	187.1	.0006	59.9
3616.6	252.7	50.6	75.9	75.9	75.9	.0	50.6	45.0	75.9	69.6	.667	.712	82.5	.0002	32.2
2712.5	228.2	75.9	75.9	38.0	75.9	90.0	38.0	.0	75.9	66.5	.500	.654	80.4	.0002	30.3
4004.1	266.1	63.3	88.6	75.9	88.6	.0	63.3	45.0	88.6	79.1	.714	.710	87.1	.0002	37.0
65099.5	1057.4	341.8	405.1	265.8	278.5	90.0	265.8	45.0	405.1	322.8	.656	.732	333.5	.0036	145.6
1162.5	142.1	38.0	50.6	25.3	50.6	90.0	25.3	45.0	50.6	41.1	.500	.724	45.5	.0001	22.0
57737.0	1152.1	392.4	303.8	265.8	405.1	90.0	265.8	135.0	405.1	341.8	.656	.547	446.9	.0032	132.5
7620.8	377.6	126.6	126.6	75.9	113.9	90.0	75.9	.0	126.6	110.8	.600	.672	130.3	.0004	50.6
1162.5	142.1	38.0	50.6	25.3	50.6	90.0	25.3	45.0	50.6	41.1	.500	.724	45.5	.0001	22.0
1550.0	162.5	38.0	50.6	38.0	50.6	.0	38.0	45.0	50.6	44.3	.750	.738	50.6	.0001	23.3
5554.1	299.8	88.6	88.6	75.9	88.6	90.0	75.9	.0	88.6	85.4	.857	.776	83.0	.0003	41.4
1162.5	142.1	38.0	50.6	25.3	50.6	90.0	25.3	45.0	50.6	41.1	.500	.724	45.5	.0001	22.0
1162.5	142.1	38.0	50.6	25.3	50.6	90.0	25.3	45.0	50.6	41.1	.500	.724	45.5	.0001	22.0
1162.5	142.1	38.0	50.6	25.3	50.6	90.0	25.3	45.0	50.6	41.1	.500	.724	45.5	.0001	22.0
1162.5	142.1	38.0	50.6	25.3	50.6	90.0	25.3	45.0	50.6	41.1	.500	.724	45.5	.0001	22.0
187677.6	2994.8	531.6	734.2	759.5	696.2	.0	531.6	90.0	759.5	680.4	.700	.263	1359.3	.0105	214.6
103203.3	2374.4	443.0	569.6	582.3	544.3	.0	443.0	90.0	582.3	534.8	.761	.230	1092.8	.0058	161.4
1162.5	142.1	38.0	50.6	25.3	50.6	90.0	25.3	45.0	50.6	41.1	.500	.724	45.5	.0001	22.0
1550.0	162.5	38.0	50.6	38.0	50.6	.0	38.0	45.0	50.6	44.3	.750	.738	50.6	.0001	23.3
1162.5	142.1	38.0	50.6	25.3	50.6	90.0	25.3	45.0	50.6	41.1	.500	.724	45.5	.0001	22.0

Table A-3 (cont'd)

_A_r_e_a_	Perimeter Ú	0.00% Ú	45.00% Ú	90.00% Ú	135.00%	Min_Angle	Min_Feret	Max_Angle	Max_Feret	Avg_Feret	Asp_Ratio	Shape_Fac	Spec_Peri	Area_Frac	AvgRadius
13820.7	594.2	177.2	189.9	139.2	164.6	90.0	139.2	45.0	189.9	167.7	.733	.492	239.4	.0008	64.0
1937.5	179.4	50.6	63.3	38.0	50.6	90.0	38.0	45.0	63.3	50.6	.600	.756	53.5	.0001	24.9
28674.8	929.0	253.2	177.2	240.5	291.1	45.0	177.2	135.0	291.1	240.5	.609	.418	391.2	.0016	86.0
3487.5	240.3	75.9	75.9	50.6	75.9	90.0	50.6	.0	75.9	69.6	.667	.759	71.0	.0002	33.8
4004.1	253.9	63.3	75.9	75.9	88.6	.0	63.3	135.0	88.6	75.9	.714	.780	68.6	.0002	39.2
4779.1	306.0	113.9	101.3	50.6	101.3	90.0	50.6	.0	113.9	91.8	.444	.641	109.3	.0003	38.5
1162.5	142.1	38.0	50.6	25.3	50.6	90.0	25.3	45.0	50.6	41.1	.500	.724	45.5	.0001	22.0
4262.5	321.5	101.3	75.9	75.9	113.9	45.0	75.9	135.0	113.9	91.8	.667	.518	127.3	.0002	28.7
1162.5	142.1	38.0	50.6	25.3	50.6	90.0	25.3	45.0	50.6	41.1	.500	.724	45.5	.0001	22.0
1162.5	142.1	38.0	50.6	25.3	50.6	90.0	25.3	45.0	50.6	41.1	.500	.724	45.5	.0001	22.0
85636.8	1468.9	493.7	278.5	392.4	544.3	45.0	278.5	135.0	544.3	427.2	.512	.499	589.1	.0048	144.1
187806.8	2567.5	1025.3	848.1	392.4	772.2	90.0	392.4	.0	1025.3	759.5	.383	.358	1115.4	.0105	210.3
1162.5	142.1	38.0	50.6	25.3	50.6	90.0	25.3	45.0	50.6	41.1	.500	.724	45.5	.0001	22.0
1162.5	142.1	38.0	50.6	25.3	50.6	90.0	25.3	45.0	50.6	41.1	.500	.724	45.5	.0001	22.0
211960.7	2120.6	721.5	670.9	506.3	569.6	90.0	506.3	.0	721.5	617.1	.702	.592	793.1	.0118	253.5
95970.0	1360.1	468.4	443.0	316.5	379.7	90.0	316.5	.0	468.4	401.9	.676	.652	480.2	.0054	174.5
2841.6	208.4	63.3	75.9	50.6	63.3	90.0	50.6	45.0	75.9	63.3	.667	.822	75.9	.0002	32.2
3616.6	235.5	75.9	75.9	63.3	75.9	90.0	63.3	.0	75.9	72.8	.833	.819	75.9	.0002	35.0
2195.8	194.5	63.3	50.6	38.0	75.9	90.0	38.0	135.0	75.9	57.0	.500	.729	61.7	.0001	28.7
2970.8	230.1	75.9	75.9	38.0	75.9	90.0	38.0	.0	75.9	66.5	.500	.705	75.9	.0002	32.5
1162.5	142.1	38.0	50.6	25.3	50.6	90.0	25.3	45.0	50.6	41.1	.500	.724	45.5	.0001	22.0
3487.5	263.8	88.6	75.9	50.6	101.3	90.0	50.6	135.0	101.3	79.1	.500	.630	95.3	.0002	34.1
1550.0	167.4	50.6	50.6	25.3	50.6	90.0	25.3	.0	50.6	44.3	.500	.695	56.0	.0001	23.6
77757.7	1211.8	443.0	367.1	240.5	417.7	90.0	240.5	.0	443.0	367.1	.543	.665	421.4	.0043	149.6
1162.5	142.1	38.0	50.6	25.3	50.6	90.0	25.3	45.0	50.6	41.1	.500	.724	45.5	.0001	22.0
1162.5	142.1	38.0	50.6	25.3	50.6	90.0	25.3	45.0	50.6	41.1	.500	.724	45.5	.0001	22.0
216869.0	2365.5	481.0	582.3	898.7	848.1	.0	481.0	90.0	898.7	702.5	.535	.487	955.8	.0121	224.8
5941.6	308.4	101.3	75.9	75.9	113.9	45.0	75.9	135.0	113.9	91.8	.667	.785	78.6	.0003	43.7
1162.5	142.1	38.0	50.6	25.3	50.6	90.0	25.3	45.0	50.6	41.1	.500	.724	45.5	.0001	22.0
4520.8	264.3	75.9	88.6	75.9	88.6	.0	75.9	45.0	88.6	82.3	.857	.813	88.6	.0003	38.6
1937.5	179.4	50.6	50.6	38.0	63.3	90.0	38.0	135.0	63.3	50.6	.600	.756	53.5	.0001	27.1
1162.5	142.1	38.0	50.6	25.3	50.6	90.0	25.3	45.0	50.6	41.1	.500	.724	45.5	.0001	22.0
2583.3	238.4	75.9	88.6	50.6	63.3	90.0	50.6	45.0	88.6	69.6	.571	.571	90.8	.0001	29.0
29191.4	1110.1	227.8	227.8	253.2	278.5	.0	227.8	135.0	278.5	246.8	.818	.298	496.2	.0016	71.4
1937.5	179.4	50.6	63.3	38.0	50.6	90.0	38.0	45.0	63.3	50.6	.600	.756	53.5	.0001	24.9
2454.1	199.8	50.6	63.3	50.6	63.3	.0	50.6	45.0	63.3	57.0	.800	.772	56.4	.0001	30.6
1162.5	142.1	38.0	50.6	25.3	50.6	90.0	25.3	45.0	50.6	41.1	.500	.724	45.5	.0001	22.0
1162.5	142.1	38.0	50.6	25.3	50.6	90.0	25.3	45.0	50.6	41.1	.500	.724	45.5	.0001	22.0
16920.7	781.1	215.2	240.5	177.2	151.9	135.0	151.9	45.0	240.5	196.2	.632	.349	340.9	.0009	43.7
1937.5	182.9	38.0	63.3	50.6	63.3	.0	38.0	45.0	63.3	53.8	.600	.728	58.1	.0001	24.6

Table A-3 (cont'd)

_A_r_e_a_	Perimeter Ú	0.00% Ú	45.00% Ú	90.00% Ú	135.00%	Min_Angle	Min_Feret	Max_Angle	Max_Feret	Avg_Feret	Asp_Ratio	Shape_Fac	Spec_Peri	Area_Frac	AvgRadius
1937.5	182.9	38.0	63.3	50.6	63.3	.0	38.0	45.0	63.3	53.8	.600	.728	58.1	.0001	24.6
2325.0	202.9	63.3	75.9	38.0	63.3	90.0	38.0	45.0	75.9	60.1	.500	.710	66.5	.0001	28.7
1162.5	142.1	38.0	50.6	25.3	50.6	90.0	25.3	45.0	50.6	41.1	.500	.724	45.5	.0001	22.0
2970.8	223.5	75.9	63.3	50.6	88.6	90.0	50.6	135.0	88.6	69.6	.571	.747	68.2	.0002	28.7
1937.5	179.4	50.6	50.6	38.0	63.3	90.0	38.0	135.0	63.3	50.6	.600	.756	53.5	.0001	27.1
1162.5	142.1	38.0	50.6	25.3	50.6	90.0	25.3	45.0	50.6	41.1	.500	.724	45.5	.0001	22.0
1162.5	142.1	38.0	50.6	25.3	50.6	90.0	25.3	45.0	50.6	41.1	.500	.724	45.5	.0001	22.0
4004.1	274.0	88.6	75.9	63.3	101.3	90.0	63.3	135.0	101.3	82.3	.625	.670	94.7	.0002	35.4
130844.7	1955.4	746.8	620.3	303.8	632.9	90.0	303.8	.0	746.8	575.9	.407	.430	817.7	.0073	172.3
2195.8	194.5	63.3	50.6	38.0	75.9	90.0	38.0	135.0	75.9	57.0	.500	.729	61.7	.0001	28.7
1808.3	171.0	50.6	50.6	38.0	63.3	90.0	38.0	135.0	63.3	50.6	.600	.777	47.2	.0001	27.1
1550.0	162.5	38.0	50.6	38.0	50.6	.0	38.0	45.0	50.6	44.3	.750	.738	50.6	.0001	23.3
5554.1	341.9	101.3	88.6	75.9	126.6	90.0	75.9	135.0	126.6	98.1	.600	.597	127.3	.0003	40.5
3229.1	228.8	63.3	75.9	63.3	63.3	.0	63.3	45.0	75.9	66.5	.833	.775	63.7	.0002	31.9
2970.8	216.8	63.3	63.3	50.6	75.9	90.0	50.6	135.0	75.9	63.3	.667	.795	75.9	.0002	32.2
2712.5	263.8	88.6	101.3	50.6	63.3	90.0	50.6	45.0	101.3	75.9	.500	.490	106.4	.0002	23.6
1162.5	142.1	38.0	50.6	25.3	50.6	90.0	25.3	45.0	50.6	41.1	.500	.724	45.5	.0001	22.0
10462.4	391.4	126.6	126.6	101.3	126.6	90.0	101.3	.0	126.6	120.3	.800	.858	126.6	.0006	55.4
4650.0	325.4	63.3	113.9	101.3	101.3	.0	63.3	45.0	113.9	94.9	.556	.552	125.7	.0003	30.9
1550.0	167.4	50.6	50.6	25.3	50.6	90.0	25.3	.0	50.6	44.3	.500	.695	56.0	.0001	23.6
116119.9	1501.6	455.7	481.0	417.7	405.1	135.0	405.1	45.0	481.0	439.9	.842	.647	532.9	.0065	179.0
119478.2	1451.8	405.1	367.1	455.7	493.7	45.0	367.1	135.0	493.7	430.4	.744	.712	473.7	.0067	191.2
4133.3	292.7	101.3	113.9	63.3	75.9	90.0	63.3	45.0	113.9	88.6	.556	.606	108.1	.0002	34.4
2325.0	203.3	38.0	63.3	63.3	63.3	.0	38.0	45.0	63.3	57.0	.600	.707	66.9	.0001	25.8
18212.3	571.4	177.2	202.5	177.2	151.9	135.0	151.9	45.0	202.5	177.2	.750	.701	189.7	.0010	71.1
1162.5	142.1	38.0	50.6	25.3	50.6	90.0	25.3	45.0	50.6	41.1	.500	.724	45.5	.0001	22.0
1162.5	142.1	38.0	50.6	25.3	50.6	90.0	25.3	45.0	50.6	41.1	.500	.724	45.5	.0001	22.0
1162.5	142.1	38.0	50.6	25.3	50.6	90.0	25.3	45.0	50.6	41.1	.500	.724	45.5	.0001	22.0
9687.4	464.1	139.2	151.9	126.6	113.9	135.0	113.9	45.0	151.9	132.9	.750	.565	177.5	.0005	50.0
111857.4	2543.9	455.7	367.1	683.5	797.5	45.0	367.1	135.0	797.5	575.9	.460	.217	1176.9	.0062	134.8
1162.5	142.1	38.0	50.6	25.3	50.6	90.0	25.3	45.0	50.6	41.1	.500	.724	45.5	.0001	22.0
1162.5	142.1	38.0	50.6	25.3	50.6	90.0	25.3	45.0	50.6	41.1	.500	.724	45.5	.0001	22.0
1162.5	142.1	38.0	50.6	25.3	50.6	90.0	25.3	45.0	50.6	41.1	.500	.724	45.5	.0001	22.0
1937.5	182.9	38.0	63.3	50.6	63.3	.0	38.0	45.0	63.3	53.8	.600	.728	58.1	.0001	24.6
1937.5	179.4	50.6	63.3	38.0	50.6	90.0	38.0	45.0	63.3	50.6	.600	.756	53.5	.0001	24.9
1162.5	142.1	38.0	50.6	25.3	50.6	90.0	25.3	45.0	50.6	41.1	.500	.724	45.5	.0001	22.0
2454.1	199.8	50.6	63.3	50.6	63.3	.0	50.6	45.0	63.3	57.0	.800	.772	56.4	.0001	28.4
1937.5	182.9	38.0	63.3	50.6	63.3	.0	38.0	45.0	63.3	53.8	.600	.728	58.1	.0001	24.6
1937.5	182.9	38.0	63.3	50.6	63.3	.0	38.0	45.0	63.3	53.8	.600	.728	58.1	.0001	24.6
17824.9	697.1	278.5	240.5	113.9	189.9	90.0	113.9	.0	278.5	205.7	.409	.461	286.3	.0010	66.5

Table A-3 (cont'd)

_A_r_e_a_	Perimeter Ú	0.00% Ú	45.00% Ú	90.00% Ú	135.00%	Min_Angle	Min_Feret	Max_Angle	Max_Feret	Avg_Feret	Asp_Ratio	Shape_Fac	Spec_Peri	Area_Frac	AvgRadius
21699.8	828.8	240.5	240.5	151.9	164.6	90.0	151.9	.0	240.5	199.4	.632	.397	352.9	.0012	78.0
49728.8	1297.7	265.8	253.2	329.1	329.1	45.0	253.2	90.0	329.1	294.3	.769	.371	560.1	.0028	116.7
2325.0	196.4	63.3	63.3	38.0	63.3	90.0	38.0	.0	63.3	57.0	.600	.758	58.3	.0001	30.9
1162.5	142.1	38.0	50.6	25.3	50.6	90.0	25.3	45.0	50.6	41.1	.500	.724	45.5	.0001	22.0
1162.5	142.1	38.0	50.6	25.3	50.6	90.0	25.3	45.0	50.6	41.1	.500	.724	45.5	.0001	22.0
10720.7	466.8	177.2	126.6	88.6	164.6	90.0	88.6	.0	177.2	139.2	.500	.618	170.6	.0006	56.7
1162.5	142.1	38.0	50.6	25.3	50.6	90.0	25.3	45.0	50.6	41.1	.500	.724	45.5	.0001	22.0
4262.5	306.0	113.9	126.6	63.3	88.6	90.0	63.3	45.0	126.6	98.1	.500	.572	116.4	.0002	35.0
1162.5	142.1	38.0	50.6	25.3	50.6	90.0	25.3	45.0	50.6	41.1	.500	.724	45.5	.0001	22.0
4650.0	301.1	101.3	101.3	63.3	88.6	90.0	63.3	.0	101.3	88.6	.625	.645	107.2	.0003	36.9
1162.5	142.1	38.0	50.6	25.3	50.6	90.0	25.3	45.0	50.6	41.1	.500	.724	45.5	.0001	22.0
1937.5	192.7	63.3	63.3	25.3	63.3	90.0	25.3	.0	63.3	53.8	.400	.656	67.8	.0001	25.2
1937.5	179.4	50.6	50.6	38.0	63.3	90.0	38.0	135.0	63.3	50.6	.600	.756	53.5	.0001	27.1
4908.3	306.9	75.9	75.9	88.6	113.9	.0	75.9	135.0	113.9	88.6	.667	.655	108.0	.0003	37.9
55412.0	1166.3	367.1	291.1	240.5	392.4	90.0	240.5	135.0	392.4	322.8	.613	.512	463.7	.0031	117.5
1162.5	142.1	38.0	50.6	25.3	50.6	90.0	25.3	45.0	50.6	41.1	.500	.724	45.5	.0001	22.0
1162.5	142.1	38.0	50.6	25.3	50.6	90.0	25.3	45.0	50.6	41.1	.500	.724	45.5	.0001	22.0
4908.3	288.2	63.3	101.3	88.6	88.6	.0	63.3	45.0	101.3	85.4	.625	.743	88.9	.0003	36.0
1162.5	142.1	38.0	50.6	25.3	50.6	90.0	25.3	45.0	50.6	41.1	.500	.724	45.5	.0001	22.0
1937.5	192.7	63.3	63.3	25.3	63.3	90.0	25.3	.0	63.3	53.8	.400	.656	67.8	.0001	25.2
7233.3	420.2	75.9	101.3	126.6	139.2	.0	75.9	135.0	139.2	110.8	.545	.515	166.7	.0004	38.9
18858.2	715.2	177.2	253.2	215.2	126.6	135.0	126.6	45.0	253.2	193.0	.500	.463	293.3	.0011	66.6
1162.5	142.1	38.0	50.6	25.3	50.6	90.0	25.3	45.0	50.6	41.1	.500	.724	45.5	.0001	22.0
3100.0	238.4	75.9	88.6	50.6	75.9	90.0	50.6	45.0	88.6	72.8	.571	.685	80.9	.0002	32.5
1162.5	142.1	38.0	50.6	25.3	50.6	90.0	25.3	45.0	50.6	41.1	.500	.724	45.5	.0001	22.0
6845.8	434.8	151.9	113.9	75.9	151.9	90.0	75.9	.0	151.9	123.4	.500	.455	179.2	.0004	41.7
30224.7	1150.3	215.2	253.2	303.8	316.5	.0	215.2	135.0	316.5	272.2	.680	.287	516.7	.0017	58.7
1162.5	142.1	38.0	50.6	25.3	50.6	90.0	25.3	45.0	50.6	41.1	.500	.724	45.5	.0001	22.0
6458.3	357.2	113.9	101.3	75.9	113.9	90.0	75.9	.0	113.9	101.3	.667	.636	128.2	.0004	42.0
3358.3	242.1	75.9	75.9	50.6	75.9	90.0	50.6	.0	75.9	69.6	.667	.720	78.0	.0002	36.0
1162.5	142.1	38.0	50.6	25.3	50.6	90.0	25.3	45.0	50.6	41.1	.500	.724	45.5	.0001	22.0
3487.5	228.8	63.3	75.9	63.3	75.9	.0	63.3	45.0	75.9	69.6	.833	.837	75.9	.0002	33.5
5037.5	287.8	88.6	101.3	75.9	88.6	90.0	75.9	45.0	101.3	88.6	.750	.764	83.8	.0003	40.1
1162.5	142.1	38.0	50.6	25.3	50.6	90.0	25.3	45.0	50.6	41.1	.500	.724	45.5	.0001	22.0
2583.3	211.9	50.6	63.3	63.3	75.9	.0	50.6	135.0	75.9	63.3	.667	.723	67.9	.0001	28.1
1550.0	167.4	50.6	50.6	25.3	50.6	90.0	25.3	.0	50.6	44.3	.500	.695	56.0	.0001	23.6
1162.5	142.1	38.0	50.6	25.3	50.6	90.0	25.3	45.0	50.6	41.1	.500	.724	45.5	.0001	22.0
1550.0	162.5	38.0	50.6	38.0	50.6	.0	38.0	45.0	50.6	44.3	.750	.738	50.6	.0001	23.3
2325.0	218.0	75.9	75.9	25.3	75.9	90.0	25.3	.0	75.9	63.3	.333	.615	79.9	.0001	26.7
1162.5	142.1	38.0	50.6	25.3	50.6	90.0	25.3	45.0	50.6	41.1	.500	.724	45.5	.0001	22.0

Table A-3 (cont'd)

_A_r_e_a_	Perimeter Ú	0.00% Ú	45.00% Ú	90.00% Ú	135.00%	Min_Angle	Min_Feret	Max_Angle	Max_Feret	Avg_Feret	Asp_Ratio	Shape_Fac	Spec_Peri	Area_Frac	AvgRadius
6329.1	370.3	126.6	126.6	75.9	113.9	90.0	75.9	.0	126.6	110.8	.600	.580	139.9	.0004	43.6
1162.5	142.1	38.0	50.6	25.3	50.6	90.0	25.3	45.0	50.6	41.1	.500	.724	45.5	.0001	22.0
2841.6	221.7	75.9	75.9	38.0	75.9	90.0	38.0	.0	75.9	66.5	.500	.727	70.6	.0002	30.3
1550.0	162.5	38.0	50.6	38.0	50.6	.0	38.0	45.0	50.6	44.3	.750	.738	50.6	.0001	23.3
143632.1	2213.4	303.8	645.6	848.1	632.9	.0	303.8	90.0	848.1	607.6	.358	.368	956.6	.0080	159.1
2325.0	191.4	50.6	63.3	50.6	63.3	.0	50.6	45.0	63.3	57.0	.800	.797	63.3	.0001	30.6
1162.5	142.1	38.0	50.6	25.3	50.6	90.0	25.3	45.0	50.6	41.1	.500	.724	45.5	.0001	22.0
2195.8	191.4	50.6	63.3	50.6	50.6	.0	50.6	45.0	63.3	53.8	.800	.753	57.6	.0001	26.1
1162.5	142.1	38.0	50.6	25.3	50.6	90.0	25.3	45.0	50.6	41.1	.500	.724	45.5	.0001	22.0
1550.0	167.4	50.6	50.6	25.3	50.6	90.0	25.3	.0	50.6	44.3	.500	.695	56.0	.0001	23.6
3358.3	238.4	75.9	75.9	50.6	75.9	90.0	50.6	.0	75.9	69.6	.667	.742	73.6	.0002	33.8
2454.1	199.8	50.6	63.3	50.6	63.3	.0	50.6	45.0	63.3	57.0	.800	.772	56.4	.0001	28.4
1162.5	142.1	38.0	50.6	25.3	50.6	90.0	25.3	45.0	50.6	41.1	.500	.724	45.5	.0001	22.0
1550.0	167.4	50.6	50.6	25.3	50.6	90.0	25.3	.0	50.6	44.3	.500	.695	56.0	.0001	23.6
4520.8	302.9	101.3	75.9	63.3	113.9	90.0	63.3	135.0	113.9	88.6	.556	.619	110.6	.0003	34.1
3616.6	262.5	75.9	63.3	75.9	101.3	45.0	63.3	135.0	101.3	79.1	.625	.660	91.9	.0002	31.9
3358.3	243.7	63.3	88.6	63.3	75.9	.0	63.3	45.0	88.6	72.8	.714	.710	79.8	.0002	33.5
94290.9	2473.9	481.0	632.9	506.3	417.7	135.0	417.7	45.0	632.9	509.5	.660	.196	1155.3	.0053	-1.0
2454.1	199.8	50.6	63.3	50.6	63.3	.0	50.6	45.0	63.3	57.0	.800	.772	56.4	.0001	28.4
1162.5	142.1	38.0	50.6	25.3	50.6	90.0	25.3	45.0	50.6	41.1	.500	.724	45.5	.0001	22.0
5941.6	335.4	88.6	113.9	75.9	101.3	90.0	75.9	45.0	113.9	94.9	.667	.664	116.8	.0003	40.5
1937.5	179.4	50.6	50.6	38.0	63.3	90.0	38.0	135.0	63.3	50.6	.600	.756	53.5	.0001	27.1
5425.0	369.4	88.6	88.6	113.9	139.2	.0	88.6	135.0	139.2	107.6	.636	.499	148.1	.0003	36.7
7620.8	342.1	113.9	126.6	75.9	101.3	90.0	75.9	45.0	126.6	104.4	.600	.818	126.6	.0004	46.8
1162.5	142.1	38.0	50.6	25.3	50.6	90.0	25.3	45.0	50.6	41.1	.500	.724	45.5	.0001	22.0
4262.5	279.4	88.6	101.3	75.9	75.9	90.0	75.9	45.0	101.3	85.4	.750	.686	94.7	.0002	36.3
14337.4	524.1	126.6	164.6	164.6	151.9	.0	126.6	45.0	164.6	151.9	.769	.656	184.2	.0008	69.2
1550.0	167.4	50.6	50.6	25.3	50.6	90.0	25.3	.0	50.6	44.3	.500	.695	56.0	.0001	23.6
1808.3	171.0	50.6	50.6	38.0	63.3	90.0	38.0	135.0	63.3	50.6	.600	.777	47.2	.0001	27.1
1162.5	142.1	38.0	50.6	25.3	50.6	90.0	25.3	45.0	50.6	41.1	.500	.724	45.5	.0001	22.0
2066.6	187.8	50.6	63.3	38.0	63.3	90.0	38.0	45.0	63.3	53.8	.600	.736	58.7	.0001	27.1
5037.5	319.9	113.9	126.6	75.9	88.6	90.0	75.9	45.0	126.6	101.3	.600	.619	116.8	.0003	39.2
2454.1	214.9	63.3	50.6	50.6	75.9	45.0	50.6	135.0	75.9	60.1	.667	.668	74.6	.0001	27.7
243864.6	2657.6	873.4	493.7	632.9	1000.0	45.0	493.7	135.0	1000.0	750.0	.496	.434	1108.9	.0136	234.8
1162.5	142.1	38.0	50.6	25.3	50.6	90.0	25.3	45.0	50.6	41.1	.500	.724	45.5	.0001	22.0
2634203.0	10377.0	2202.5	1949.4	2886.1	2759.5	45.0	1949.4	90.0	2886.1	2449.4	.675	.307	4618.1	.1470	804.0
110694.9	1939.8	848.1	683.5	240.5	594.9	90.0	240.5	.0	848.1	591.8	.284	.370	837.8	.0062	154.6
25962.3	627.9	177.2	202.5	202.5	202.5	.0	177.2	45.0	202.5	196.2	.875	.827	202.5	.0014	89.6
2712.5	228.2	75.9	75.9	38.0	75.9	90.0	38.0	.0	75.9	66.5	.500	.654	80.4	.0002	29.0
1162.5	142.1	38.0	50.6	25.3	50.6	90.0	25.3	45.0	50.6	41.1	.500	.724	45.5	.0001	22.0

Table A-3 (cont'd)

_A_r_e_e_	Perimeter Ú	0.00% Ú	45.00% Ú	90.00% Ú	135.00%	Min_Angle	Min_Feret	Max_Angle	Max_Feret	Avg_Feret	Asp_Ratio	Shape_Fac	Spec_Peri	Area_Frac	AvgRadius
541333.0	4619.6	1379.7	632.9	1113.9	1645.6	45.0	632.9	135.0	1645.6	1193.0	.385	.319	2045.1	.0302	335.9
1162.5	142.1	38.0	50.6	25.3	50.6	90.0	25.3	45.0	50.6	41.1	.500	.724	45.5	.0001	22.0
33841.4	1225.9	379.7	303.8	151.9	316.5	90.0	151.9	.0	379.7	288.0	.400	.283	551.6	.0019	-1.0
4650.0	299.3	101.3	101.3	50.6	101.3	90.0	50.6	.0	101.3	88.6	.500	.652	105.6	.0003	35.7
4779.1	294.9	75.9	75.9	75.9	113.9	.0	75.9	135.0	113.9	85.4	.667	.690	99.4	.0003	38.3
39395.5	1061.6	253.2	240.5	253.2	303.8	45.0	240.5	135.0	303.8	262.7	.792	.439	441.6	.0022	96.0
1162.5	142.1	38.0	50.6	25.3	50.6	90.0	25.3	45.0	50.6	41.1	.500	.724	45.5	.0001	22.0
11495.7	493.1	139.2	164.6	126.6	139.2	90.0	126.6	45.0	164.6	142.4	.769	.594	184.1	.0006	60.6
3358.3	255.8	63.3	88.6	75.9	63.3	.0	63.3	45.0	88.6	72.8	.714	.645	91.0	.0002	32.5
1162.5	142.1	38.0	50.6	25.3	50.6	90.0	25.3	45.0	50.6	41.1	.500	.724	45.5	.0001	22.0
4520.8	306.0	113.9	126.6	63.3	88.6	90.0	63.3	45.0	126.6	98.1	.500	.607	113.0	.0003	35.7
2970.8	223.3	63.3	75.9	50.6	75.9	90.0	50.6	45.0	75.9	66.5	.667	.749	67.9	.0002	34.4
2583.3	219.9	75.9	75.9	38.0	63.3	90.0	38.0	.0	75.9	63.3	.500	.672	75.9	.0001	30.3
1550.0	162.5	38.0	50.6	38.0	50.6	.0	38.0	45.0	50.6	44.3	.750	.738	50.6	.0001	23.3
3358.3	228.8	63.3	75.9	63.3	75.9	.0	63.3	45.0	75.9	69.6	.833	.806	75.9	.0002	35.7
1550.0	167.4	50.6	50.6	25.3	50.6	90.0	25.3	.0	50.6	44.3	.500	.695	56.0	.0001	23.6
3487.5	279.3	75.9	63.3	75.9	101.3	45.0	63.3	135.0	101.3	79.1	.625	.562	107.1	.0002	31.8
1937.5	182.9	38.0	63.3	50.6	63.3	.0	38.0	45.0	63.3	53.8	.600	.728	58.1	.0001	24.6
1937.5	179.4	50.6	50.6	38.0	63.3	90.0	38.0	135.0	63.3	50.6	.600	.756	53.5	.0001	27.1
1162.5	142.1	38.0	50.6	25.3	50.6	90.0	25.3	45.0	50.6	41.1	.500	.724	45.5	.0001	22.0
1550.0	167.4	50.6	50.6	25.3	50.6	90.0	25.3	.0	50.6	44.3	.500	.695	56.0	.0001	23.6
1550.0	162.5	38.0	50.6	38.0	50.6	.0	38.0	45.0	50.6	44.3	.750	.738	50.6	.0001	23.3
2325.0	196.4	63.3	75.9	38.0	50.6	90.0	38.0	45.0	75.9	57.0	.500	.758	58.3	.0001	28.7
1162.5	142.1	38.0	50.6	25.3	50.6	90.0	25.3	45.0	50.6	41.1	.500	.724	45.5	.0001	22.0
2454.1	214.9	63.3	75.9	50.6	50.6	90.0	50.6	45.0	75.9	60.1	.667	.668	74.6	.0001	23.9
33066.4	822.3	164.6	303.8	316.5	227.8	.0	164.6	90.0	316.5	253.2	.520	.614	301.5	.0018	99.5
1162.5	142.1	38.0	50.6	25.3	50.6	90.0	25.3	45.0	50.6	41.1	.500	.724	45.5	.0001	22.0
5812.5	375.6	113.9	75.9	88.6	139.2	45.0	75.9	135.0	139.2	104.4	.545	.518	148.7	.0003	39.8
1550.0	162.5	38.0	50.6	38.0	50.6	.0	38.0	45.0	50.6	44.3	.750	.738	50.6	.0001	23.3
66778.6	1006.8	303.8	303.8	341.8	291.1	135.0	291.1	90.0	341.8	310.1	.852	.828	341.8	.0037	145.0
8266.6	405.0	101.3	101.3	126.6	151.9	.0	101.3	135.0	151.9	120.3	.667	.633	165.8	.0005	46.9
1162.5	142.1	38.0	50.6	25.3	50.6	90.0	25.3	45.0	50.6	41.1	.500	.724	45.5	.0001	22.0
30999.7	717.7	215.2	202.5	227.8	253.2	45.0	202.5	135.0	253.2	224.7	.800	.756	214.0	.0017	94.7
109919.9	1576.9	443.0	607.6	481.0	278.5	135.0	278.5	45.0	607.6	452.5	.458	.555	607.6	.0061	185.8
1162.5	142.1	38.0	50.6	25.3	50.6	90.0	25.3	45.0	50.6	41.1	.500	.724	45.5	.0001	22.0
1550.0	162.5	38.0	50.6	38.0	50.6	.0	38.0	45.0	50.6	44.3	.750	.738	50.6	.0001	23.3
1162.5	142.1	38.0	50.6	25.3	50.6	90.0	25.3	45.0	50.6	41.1	.500	.724	45.5	.0001	22.0
1162.5	142.1	38.0	50.6	25.3	50.6	90.0	25.3	45.0	50.6	41.1	.500	.724	45.5	.0001	22.0
76595.2	1182.1	291.1	367.1	417.7	341.8	.0	291.1	90.0	417.7	354.6	.697	.689	399.1	.0043	155.5
2195.8	191.4	50.6	50.6	50.6	63.3	.0	50.6	135.0	63.3	53.8	.800	.753	57.6	.0001	28.4

Table A-3 (cont'd)

_A_r_e_a_	Perimeter Ú	0.00% Ú	45.00% Ú	90.00% Ú	135.00%	Min_Angle	Min_Feret	Max_Angle	Max_Feret	Avg_Feret	Asp_Ratio	Shape_Fac	Spec_Peri	Area_Frac	AvgRadius
18341.5	692.2	265.8	215.2	126.6	202.5	90.0	126.6	.0	265.8	202.5	.476	.481	280.7	.0010	66.1
1162.5	142.1	38.0	50.6	25.3	50.6	90.0	25.3	45.0	50.6	41.1	.500	.724	45.5	.0001	22.0
1162.5	142.1	38.0	50.6	25.3	50.6	90.0	25.3	45.0	50.6	41.1	.500	.724	45.5	.0001	22.0
4779.1	302.9	101.3	75.9	75.9	113.9	45.0	75.9	135.0	113.9	91.8	.667	.654	106.6	.0003	38.9
1162.5	142.1	38.0	50.6	25.3	50.6	90.0	25.3	45.0	50.6	41.1	.500	.724	45.5	.0001	22.0
1550.0	167.4	50.6	50.6	25.3	50.6	90.0	25.3	.0	50.6	44.3	.500	.695	56.0	.0001	23.6
1550.0	162.5	38.0	50.6	38.0	50.6	.0	38.0	45.0	50.6	44.3	.750	.738	50.6	.0001	23.3
1550.0	167.4	50.6	50.6	25.3	50.6	90.0	25.3	.0	50.6	44.3	.500	.695	56.0	.0001	23.6
4133.3	266.1	75.9	63.3	75.9	101.3	45.0	63.3	135.0	101.3	79.1	.625	.733	83.7	.0002	34.7
14208.2	624.6	227.8	189.9	126.6	177.2	90.0	126.6	.0	227.8	180.4	.556	.458	257.0	.0008	-1.0
1162.5	142.1	38.0	50.6	25.3	50.6	90.0	25.3	45.0	50.6	41.1	.500	.724	45.5	.0001	22.0
1162.5	142.1	38.0	50.6	25.3	50.6	90.0	25.3	45.0	50.6	41.1	.500	.724	45.5	.0001	22.0
1937.5	179.4	50.6	50.6	38.0	63.3	90.0	38.0	135.0	63.3	50.6	.600	.756	53.5	.0001	27.1
1162.5	142.1	38.0	50.6	25.3	50.6	90.0	25.3	45.0	50.6	41.1	.500	.724	45.5	.0001	22.0
1162.5	142.1	38.0	50.6	25.3	50.6	90.0	25.3	45.0	50.6	41.1	.500	.724	45.5	.0001	22.0
1808.3	171.0	50.6	63.3	38.0	50.6	90.0	38.0	45.0	63.3	50.6	.600	.777	47.2	.0001	22.6
1162.5	142.1	38.0	50.6	25.3	50.6	90.0	25.3	45.0	50.6	41.1	.500	.724	45.5	.0001	22.0
1162.5	142.1	38.0	50.6	25.3	50.6	90.0	25.3	45.0	50.6	41.1	.500	.724	45.5	.0001	22.0
2583.3	213.1	63.3	75.9	38.0	75.9	90.0	38.0	45.0	75.9	63.3	.500	.715	69.3	.0001	30.9
2325.0	202.9	63.3	63.3	38.0	75.9	90.0	38.0	135.0	75.9	60.1	.500	.710	66.5	.0001	28.7
3745.8	284.2	88.6	75.9	75.9	101.3	45.0	75.9	135.0	101.3	85.4	.750	.583	107.1	.0002	32.2
1162.5	142.1	38.0	50.6	25.3	50.6	90.0	25.3	45.0	50.6	41.1	.500	.724	45.5	.0001	22.0
1162.5	142.1	38.0	50.6	25.3	50.6	90.0	25.3	45.0	50.6	41.1	.500	.724	45.5	.0001	22.0
2841.6	216.8	63.3	75.9	50.6	63.3	90.0	50.6	45.0	75.9	63.3	.667	.760	63.9	.0002	34.4
59545.3	1037.9	354.4	329.1	215.2	329.1	90.0	215.2	.0	354.4	307.0	.607	.695	347.7	.0033	131.2
1162.5	142.1	38.0	50.6	25.3	50.6	90.0	25.3	45.0	50.6	41.1	.500	.724	45.5	.0001	22.0
32162.2	866.0	265.8	253.2	189.9	253.2	90.0	189.9	.0	265.8	240.5	.714	.539	337.8	.0018	101.9
1937.5	179.4	50.6	63.3	38.0	50.6	90.0	38.0	45.0	63.3	50.6	.600	.756	53.5	.0001	24.9
1162.5	142.1	38.0	50.6	25.3	50.6	90.0	25.3	45.0	50.6	41.1	.500	.724	45.5	.0001	22.0
1162.5	142.1	38.0	50.6	25.3	50.6	90.0	25.3	45.0	50.6	41.1	.500	.724	45.5	.0001	22.0
1162.5	142.1	38.0	50.6	25.3	50.6	90.0	25.3	45.0	50.6	41.1	.500	.724	45.5	.0001	22.0
14337.4	466.4	113.9	164.6	139.2	139.2	.0	113.9	45.0	164.6	139.2	.692	.828	164.6	.0008	65.7
4520.8	331.3	113.9	101.3	50.6	101.3	90.0	50.6	.0	113.9	91.8	.444	.518	131.2	.0003	39.5
1162.5	142.1	38.0	50.6	25.3	50.6	90.0	25.3	45.0	50.6	41.1	.500	.724	45.5	.0001	22.0
1162.5	142.1	38.0	50.6	25.3	50.6	90.0	25.3	45.0	50.6	41.1	.500	.724	45.5	.0001	22.0
1162.5	142.1	38.0	50.6	25.3	50.6	90.0	25.3	45.0	50.6	41.1	.500	.724	45.5	.0001	22.0
1937.5	192.7	63.3	63.3	25.3	63.3	90.0	25.3	.0	63.3	53.8	.400	.656	67.8	.0001	25.2
1550.0	162.5	38.0	50.6	38.0	50.6	.0	38.0	45.0	50.6	44.3	.750	.738	50.6	.0001	23.3
1937.5	179.4	50.6	63.3	38.0	50.6	90.0	38.0	45.0	63.3	50.6	.600	.756	53.5	.0001	24.9
1162.5	142.1	38.0	50.6	25.3	50.6	90.0	25.3	45.0	50.6	41.1	.500	.724	45.5	.0001	22.0

Table A-3 (cont'd)

_A_r_e_a_	Perimeter Ú	0.00% Ú	45.00% Ú	90.00% Ú	135.00%	Min_Angle	Min_Feret	Max_Angle	Max_Feret	Avg_Feret	Asp_Ratio	Shape_Fac	Spec_Peri	Area_Frac	AvgRadius
1162.5	142.1	38.0	50.6	25.3	50.6	90.0	25.3	45.0	50.6	41.1	.500	.724	45.5	.0001	22.0
1550.0	162.5	38.0	50.6	38.0	50.6	.0	38.0	45.0	50.6	44.3	.750	.738	50.6	.0001	23.3
1162.5	142.1	38.0	50.6	25.3	50.6	90.0	25.3	45.0	50.6	41.1	.500	.724	45.5	.0001	22.0
7362.4	386.4	88.6	126.6	113.9	126.6	.0	88.6	45.0	126.6	113.9	.700	.620	141.0	.0004	44.6
1937.5	182.9	38.0	63.3	50.6	63.3	.0	38.0	45.0	63.3	53.8	.600	.728	58.1	.0001	24.6
1937.5	192.7	63.3	63.3	25.3	63.3	90.0	25.3	.0	63.3	53.8	.400	.656	67.8	.0001	25.2
1162.5	142.1	38.0	50.6	25.3	50.6	90.0	25.3	45.0	50.6	41.1	.500	.724	45.5	.0001	22.0
1550.0	167.4	50.6	50.6	25.3	50.6	90.0	25.3	.0	50.6	44.3	.500	.695	56.0	.0001	23.6
1550.0	162.5	38.0	50.6	38.0	50.6	.0	38.0	45.0	50.6	44.3	.750	.738	50.6	.0001	23.3
3100.0	238.4	75.9	88.6	50.6	75.9	90.0	50.6	45.0	88.6	72.8	.571	.685	80.9	.0002	32.5
4133.3	257.6	63.3	75.9	75.9	88.6	.0	63.3	135.0	88.6	75.9	.714	.783	68.1	.0002	34.7
1162.5	142.1	38.0	50.6	25.3	50.6	90.0	25.3	45.0	50.6	41.1	.500	.724	45.5	.0001	22.0
9429.1	471.4	139.2	164.6	126.6	101.3	135.0	101.3	45.0	164.6	132.9	.615	.533	184.7	.0005	53.2
1937.5	182.9	38.0	63.3	50.6	63.3	.0	38.0	45.0	63.3	53.8	.600	.728	58.1	.0001	24.6
10591.6	440.1	139.2	139.2	101.3	139.2	90.0	101.3	.0	139.2	129.7	.727	.687	148.9	.0006	55.4
2454.1	211.9	50.6	75.9	63.3	63.3	.0	50.6	45.0	75.9	63.3	.667	.687	71.7	.0001	27.4
5812.5	399.3	139.2	101.3	75.9	151.9	90.0	75.9	135.0	151.9	117.1	.500	.458	164.3	.0003	37.6
1550.0	167.4	50.6	50.6	25.3	50.6	90.0	25.3	.0	50.6	44.3	.500	.695	56.0	.0001	23.6
1550.0	167.4	50.6	50.6	25.3	50.6	90.0	25.3	.0	50.6	44.3	.500	.695	56.0	.0001	23.6
2066.6	187.8	50.6	63.3	38.0	63.3	90.0	38.0	45.0	63.3	53.8	.600	.736	58.7	.0001	27.1
14595.7	469.2	164.6	151.9	126.6	139.2	90.0	126.6	.0	164.6	145.6	.769	.833	164.6	.0008	65.9
1937.5	192.7	63.3	63.3	25.3	63.3	90.0	25.3	.0	63.3	53.8	.400	.656	67.8	.0001	25.2
2325.0	191.4	50.6	50.6	50.6	63.3	.0	50.6	135.0	63.3	53.8	.800	.797	63.3	.0001	28.4
2066.6	187.8	50.6	63.3	38.0	63.3	90.0	38.0	45.0	63.3	53.8	.600	.736	58.7	.0001	27.1
2066.6	187.8	50.6	63.3	38.0	63.3	90.0	38.0	45.0	63.3	53.8	.600	.736	58.7	.0001	27.1
6199.9	367.4	113.9	126.6	75.9	88.6	90.0	75.9	45.0	126.6	101.3	.600	.577	139.1	.0003	35.4
1162.5	142.1	38.0	50.6	25.3	50.6	90.0	25.3	45.0	50.6	41.1	.500	.724	45.5	.0001	22.0
1550.0	167.4	50.6	50.6	25.3	50.6	90.0	25.3	.0	50.6	44.3	.500	.695	56.0	.0001	23.6
1550.0	162.5	38.0	50.6	38.0	50.6	.0	38.0	45.0	50.6	44.3	.750	.738	50.6	.0001	23.3
1162.5	142.1	38.0	50.6	25.3	50.6	90.0	25.3	45.0	50.6	41.1	.500	.724	45.5	.0001	22.0
6716.6	337.6	75.9	126.6	113.9	88.6	.0	75.9	45.0	126.6	101.3	.600	.741	104.5	.0004	43.7
1162.5	142.1	38.0	50.6	25.3	50.6	90.0	25.3	45.0	50.6	41.1	.500	.724	45.5	.0001	22.0
3229.1	237.2	63.3	63.3	63.3	88.6	.0	63.3	135.0	88.6	69.6	.714	.721	76.2	.0002	29.6
1937.5	179.4	50.6	50.6	38.0	63.3	90.0	38.0	135.0	63.3	50.6	.600	.756	53.5	.0001	27.1
21958.2	846.3	316.5	227.8	126.6	278.5	90.0	126.6	.0	316.5	237.3	.400	.385	362.6	.0012	65.5
5166.6	334.8	113.9	101.3	63.3	101.3	90.0	63.3	.0	113.9	94.9	.556	.579	126.6	.0003	40.8
1550.0	162.5	38.0	50.6	38.0	50.6	.0	38.0	45.0	50.6	44.3	.750	.738	50.6	.0001	23.3
5683.3	310.0	88.6	101.3	75.9	88.6	90.0	75.9	45.0	101.3	88.6	.750	.743	95.5	.0003	39.2
3100.0	243.3	88.6	88.6	38.0	75.9	90.0	38.0	.0	88.6	72.8	.429	.658	85.4	.0002	31.8
1550.0	162.5	38.0	50.6	38.0	50.6	.0	38.0	45.0	50.6	44.3	.750	.738	50.6	.0001	23.3

Table A-3 (cont'd)

_A_r_e_a_	Perimeter Ú	0.00% Ú	45.00% Ú	90.00% Ú	135.00%	Min_Angle	Min_Feret	Max_Angle	Max_Feret	Avg_Feret	Asp_Ratio	Shape_Fac	Spec_Peri	Area_Frac	AvgRadius
1162.5	142.1	38.0	50.6	25.3	50.6	90.0	25.3	45.0	50.6	41.1	.500	.724	45.5	.0001	22.0
1937.5	179.4	50.6	63.3	38.0	50.6	90.0	38.0	45.0	63.3	50.6	.600	.756	53.5	.0001	24.9
9299.9	429.0	88.6	126.6	126.6	151.9	.0	88.6	135.0	151.9	123.4	.583	.635	154.2	.0005	51.0
1937.5	182.9	38.0	63.3	50.6	63.3	.0	38.0	45.0	63.3	53.8	.600	.728	58.1	.0001	24.6
1162.5	142.1	38.0	50.6	25.3	50.6	90.0	25.3	45.0	50.6	41.1	.500	.724	45.5	.0001	22.0
1162.5	142.1	38.0	50.6	25.3	50.6	90.0	25.3	45.0	50.6	41.1	.500	.724	45.5	.0001	22.0
277835.2	2752.4	683.5	721.5	569.6	645.6	90.0	569.6	45.0	721.5	655.1	.789	.461	1130.4	.0155	297.3
1162.5	142.1	38.0	50.6	25.3	50.6	90.0	25.3	45.0	50.6	41.1	.500	.724	45.5	.0001	22.0
1162.5	142.1	38.0	50.6	25.3	50.6	90.0	25.3	45.0	50.6	41.1	.500	.724	45.5	.0001	22.0
1550.0	167.4	50.6	50.6	25.3	50.6	90.0	25.3	.0	50.6	44.3	.500	.695	56.0	.0001	23.6
3229.1	231.9	75.9	75.9	50.6	75.9	90.0	50.6	.0	75.9	69.6	.667	.755	69.4	.0002	31.5
1162.5	142.1	38.0	50.6	25.3	50.6	90.0	25.3	45.0	50.6	41.1	.500	.724	45.5	.0001	22.0
3875.0	269.1	75.9	88.6	63.3	75.9	90.0	63.3	45.0	88.6	75.9	.714	.673	92.7	.0002	37.3
6329.1	352.7	88.6	75.9	113.9	126.6	45.0	75.9	135.0	126.6	101.3	.600	.639	126.2	.0004	45.3
1162.5	142.1	38.0	50.6	25.3	50.6	90.0	25.3	45.0	50.6	41.1	.500	.724	45.5	.0001	22.0
1937.5	179.4	50.6	63.3	38.0	50.6	90.0	38.0	45.0	63.3	50.6	.600	.756	53.5	.0001	24.9
1162.5	142.1	38.0	50.6	25.3	50.6	90.0	25.3	45.0	50.6	41.1	.500	.724	45.5	.0001	22.0
76207.7	1332.8	443.0	367.1	227.8	379.7	90.0	227.8	.0	443.0	354.4	.514	.539	519.8	.0043	147.1
1162.5	142.1	38.0	50.6	25.3	50.6	90.0	25.3	45.0	50.6	41.1	.500	.724	45.5	.0001	22.0
20279.0	643.9	215.2	202.5	164.6	189.9	90.0	164.6	.0	215.2	193.0	.765	.615	236.0	.0011	75.2
4004.1	262.7	88.6	101.3	63.3	63.3	90.0	63.3	45.0	101.3	79.1	.625	.729	83.2	.0002	35.0
1162.5	142.1	38.0	50.6	25.3	50.6	90.0	25.3	45.0	50.6	41.1	.500	.724	45.5	.0001	22.0
1550.0	167.4	50.6	50.6	25.3	50.6	90.0	25.3	.0	50.6	44.3	.500	.695	56.0	.0001	23.6
1808.3	171.0	50.6	50.6	38.0	63.3	90.0	38.0	135.0	63.3	50.6	.600	.777	47.2	.0001	27.1
1937.5	179.4	50.6	50.6	38.0	63.3	90.0	38.0	135.0	63.3	50.6	.600	.756	53.5	.0001	27.1
1550.0	162.5	38.0	50.6	38.0	50.6	.0	38.0	45.0	50.6	44.3	.750	.738	50.6	.0001	23.3
1162.5	142.1	38.0	50.6	25.3	50.6	90.0	25.3	45.0	50.6	41.1	.500	.724	45.5	.0001	22.0
2970.8	216.8	63.3	63.3	50.6	75.9	90.0	50.6	135.0	75.9	63.3	.667	.795	75.9	.0002	32.2
1162.5	142.1	38.0	50.6	25.3	50.6	90.0	25.3	45.0	50.6	41.1	.500	.724	45.5	.0001	22.0
46499.6	1128.5	341.8	227.8	291.1	417.7	45.0	227.8	135.0	417.7	319.6	.565	.459	464.0	.0026	98.4
3100.0	228.8	63.3	63.3	63.3	75.9	.0	63.3	135.0	75.9	66.5	.833	.744	70.3	.0002	31.9
1162.5	142.1	38.0	50.6	25.3	50.6	90.0	25.3	45.0	50.6	41.1	.500	.724	45.5	.0001	22.0
1162.5	142.1	38.0	50.6	25.3	50.6	90.0	25.3	45.0	50.6	41.1	.500	.724	45.5	.0001	22.0
3358.3	253.6	88.6	88.6	38.0	75.9	90.0	38.0	.0	88.6	72.8	.429	.656	89.1	.0002	34.1
1162.5	142.1	38.0	50.6	25.3	50.6	90.0	25.3	45.0	50.6	41.1	.500	.724	45.5	.0001	22.0
1550.0	167.4	50.6	50.6	25.3	50.6	90.0	25.3	.0	50.6	44.3	.500	.695	56.0	.0001	23.6
1550.0	162.5	38.0	50.6	38.0	50.6	.0	38.0	45.0	50.6	44.3	.750	.738	50.6	.0001	23.3
1162.5	142.1	38.0	50.6	25.3	50.6	90.0	25.3	45.0	50.6	41.1	.500	.724	45.5	.0001	22.0
7749.9	422.3	88.6	126.6	139.2	139.2	.0	88.6	90.0	139.2	123.4	.636	.546	163.8	.0004	50.1
1162.5	142.1	38.0	50.6	25.3	50.6	90.0	25.3	45.0	50.6	41.1	.500	.724	45.5	.0001	22.0

Table A-3 (cont'd)

_A_r_e_a_	Perimeter Û	0.00% Û	45.00% Û	90.00% Û	135.00%	Min_Angle	Min_Feret	Max_Angle	Max_Feret	Avg_Feret	Asp_Ratio	Shape_Fac	Spec_Peri	Area_Frac	AvgRadius
1162.5	142.1	38.0	50.6	25.3	50.6	90.0	25.3	45.0	50.6	41.1	.500	.724	45.5	.0001	22.0
1162.5	142.1	38.0	50.6	25.3	50.6	90.0	25.3	45.0	50.6	41.1	.500	.724	45.5	.0001	22.0
1550.0	162.5	38.0	50.6	38.0	50.6	.0	38.0	45.0	50.6	44.3	.750	.738	50.6	.0001	23.3
2454.1	214.9	63.3	50.6	50.6	75.9	45.0	50.6	135.0	75.9	60.1	.667	.668	74.6	.0001	28.4
1550.0	162.5	38.0	50.6	38.0	50.6	.0	38.0	45.0	50.6	44.3	.750	.738	50.6	.0001	23.3
2841.6	216.8	63.3	75.9	50.6	63.3	90.0	50.6	45.0	75.9	63.3	.667	.760	63.9	.0002	30.0
1162.5	142.1	38.0	50.6	25.3	50.6	90.0	25.3	45.0	50.6	41.1	.500	.724	45.5	.0001	22.0
1162.5	142.1	38.0	50.6	25.3	50.6	90.0	25.3	45.0	50.6	41.1	.500	.724	45.5	.0001	22.0
1162.5	142.1	38.0	50.6	25.3	50.6	90.0	25.3	45.0	50.6	41.1	.500	.724	45.5	.0001	22.0
1162.5	142.1	38.0	50.6	25.3	50.6	90.0	25.3	45.0	50.6	41.1	.500	.724	45.5	.0001	22.0
1162.5	142.1	38.0	50.6	25.3	50.6	90.0	25.3	45.0	50.6	41.1	.500	.724	45.5	.0001	22.0
1162.5	142.1	38.0	50.6	25.3	50.6	90.0	25.3	45.0	50.6	41.1	.500	.724	45.5	.0001	22.0
3100.0	240.8	63.3	88.6	75.9	50.6	135.0	50.6	45.0	88.6	69.6	.571	.672	83.1	.0002	33.2
1162.5	142.1	38.0	50.6	25.3	50.6	90.0	25.3	45.0	50.6	41.1	.500	.724	45.5	.0001	22.0
5554.1	330.8	63.3	113.9	113.9	101.3	.0	63.3	45.0	113.9	98.1	.556	.638	118.6	.0003	37.6
1162.5	142.1	38.0	50.6	25.3	50.6	90.0	25.3	45.0	50.6	41.1	.500	.724	45.5	.0001	22.0
23120.6	678.9	240.5	240.5	164.6	189.9	90.0	164.6	.0	240.5	208.9	.684	.630	245.1	.0013	87.2
11754.1	555.2	139.2	139.2	126.6	177.2	90.0	126.6	135.0	177.2	145.6	.714	.479	225.5	.0007	56.4
1162.5	142.1	38.0	50.6	25.3	50.6	90.0	25.3	45.0	50.6	41.1	.500	.724	45.5	.0001	22.0
6716.6	347.0	126.6	101.3	75.9	126.6	90.0	75.9	.0	126.6	107.6	.600	.701	115.2	.0004	41.7
1162.5	142.1	38.0	50.6	25.3	50.6	90.0	25.3	45.0	50.6	41.1	.500	.724	45.5	.0001	22.0
1162.5	142.1	38.0	50.6	25.3	50.6	90.0	25.3	45.0	50.6	41.1	.500	.724	45.5	.0001	22.0

Table A-4

Sample: Good98 Sorted data

Number of fields data taken form -> 40.0 fields
Field area-> 17.511 mm^2

values below in microns unless otherwise noted

Calculated values	all voids	voids > 50 eq. cir_dia
Air void content,Pa(vol %)	4.6	4.5
Average area of air void sections, A* (mm^2)	.036	.072
Average equivalent circle diameter, Da* (mm)	.092	.146
Average form factor, F*	58.3	53.7
Total area of plane section, (cm^2)	57.0	57.0
Total scan area, (cm^2)	7.0	7.0
Number of fields	40.0	40.0
Number of air voids	895.0	434.0

_A_r_e_a_	Perimeter	Shape_Fac	Max_Feret	Eq._cir_d	Form_fact
13380392.0	21283.3	.371	6240.5	4127.5	43.7
2634203.0	10377.0	.307	2886.1	1831.4	40.3
2343322.0	15482.4	.123	2696.2	1727.3	41.0
1614699.0	8123.8	.307	2949.4	1433.8	23.6
1323947.3	6669.2	.374	1797.5	1298.3	52.2
1023120.6	6847.4	.274	2038.0	1141.3	31.4
541333.0	4619.6	.319	1645.6	830.2	25.5
381942.7	2702.6	.657	848.1	697.4	67.6
349263.8	2439.2	.738	886.1	666.9	56.6
328209.8	3149.9	.416	974.7	646.4	44.0
277835.2	2752.4	.461	721.5	594.8	68.0
243864.6	2657.6	.434	1000.0	557.2	31.0
216869.0	2365.5	.487	898.7	525.5	34.2
214931.5	2212.6	.552	734.2	523.1	50.8
211960.7	2120.6	.592	721.5	519.5	51.8
187806.8	2567.5	.358	1025.3	489.0	22.7
187677.6	2994.8	.263	759.5	488.8	41.4
171273.6	1886.6	.605	519.0	467.0	81.0
154611.2	2474.0	.317	772.2	443.7	33.0
152932.1	1770.6	.613	620.3	441.3	50.6
143632.1	2213.4	.368	848.1	427.6	25.4
137690.5	1543.4	.726	569.6	418.7	54.0
130844.7	1955.4	.430	746.8	408.2	29.9
119478.2	1451.8	.712	493.7	390.0	62.4
117540.7	1447.2	.705	481.0	386.9	64.7
116119.9	1501.6	.647	481.0	384.5	63.9
111857.4	2543.9	.217	797.5	377.4	22.4
110694.9	1939.8	.370	848.1	375.4	19.6
109919.9	1576.9	.555	607.6	374.1	37.9
103203.3	2374.4	.230	582.3	362.5	38.8
100749.2	2535.4	.197	594.9	358.2	36.2
95970.0	1360.1	.652	468.4	349.6	55.7
94290.9	2473.9	.194	632.9	346.5	30.0
85636.8	1468.9	.499	544.3	330.2	36.8
77757.7	1211.8	.665	443.0	314.6	50.4
76595.2	1182.1	.689	417.7	312.3	55.9
76207.7	1332.8	.539	443.0	311.5	49.4
75949.4	1496.6	.426	493.7	311.0	39.7
67295.3	1176.5	.611	354.4	292.7	68.2

Table A-4 (cont'd)

A_r_e_a_	Perimeter	Shape_Fac	Max_Feret	Eq._cir_d	Form_Factor
66778.6	1006.8	.828	341.8	291.6	72.8
65099.5	1057.4	.732	405.1	287.9	50.5
63162.0	1479.6	.363	329.1	283.6	74.2
59545.3	1037.9	.695	354.4	275.3	60.4
57737.0	1152.1	.547	405.1	271.1	44.8
56703.7	1183.3	.509	405.1	268.7	44.0
55412.0	1166.3	.512	392.4	265.6	45.8
52957.9	1024.3	.634	367.1	259.7	50.0
49728.8	1297.7	.371	329.1	251.6	58.5
48824.6	998.6	.615	316.5	249.3	62.1
46499.6	1128.5	.459	417.7	243.3	33.9
44303.8	1826.7	.167	468.4	237.5	25.7
43658.0	1245.7	.354	506.3	235.8	21.7
42108.0	948.9	.588	341.8	231.5	45.9
41333.0	1046.9	.474	291.1	229.4	62.1
39395.5	1061.6	.439	303.8	224.0	54.3
33841.4	1225.9	.283	379.7	207.6	29.9
33066.4	822.3	.614	316.5	205.2	42.0
32808.1	1001.5	.411	316.5	204.4	41.7
32162.2	866.0	.539	265.8	202.4	58.0
31387.2	1061.4	.350	278.5	199.9	51.5
30999.7	717.7	.756	253.2	198.7	61.6
30224.7	693.7	.789	240.5	196.2	66.5
30224.7	1150.3	.287	316.5	196.2	38.4
30095.6	1087.5	.320	316.5	195.8	38.3
29837.3	705.1	.754	253.2	194.9	59.3
29191.4	1110.1	.298	278.5	192.8	47.9
28674.8	929.0	.418	291.1	191.1	43.1
27383.1	750.6	.611	303.8	186.7	37.8
26737.3	892.9	.421	265.8	184.5	48.2
26091.4	943.8	.368	253.2	182.3	51.8
25962.3	627.9	.827	202.5	181.8	80.6
25833.1	735.7	.600	265.8	181.4	46.5
25058.1	734.6	.584	303.8	178.6	34.6
24799.8	783.5	.508	291.1	177.7	37.3
24283.1	929.9	.353	379.7	175.8	21.4
23120.6	941.1	.328	316.5	171.6	29.4
23120.6	678.9	.630	240.5	171.6	50.9
22862.3	734.5	.533	227.8	170.6	56.1
21958.2	846.3	.385	316.5	167.2	27.9
21829.0	729.9	.515	240.5	166.7	48.0
21699.8	828.8	.397	240.5	166.2	47.8
21054.0	884.9	.338	278.5	163.7	34.6
20924.8	719.1	.508	265.8	163.2	37.7
20279.0	643.9	.615	215.2	160.7	55.8
19891.5	566.1	.780	202.5	159.1	61.7
19633.2	670.9	.548	215.2	158.1	54.0
19504.0	800.4	.383	278.5	157.6	32.0
19504.0	878.7	.317	291.1	157.6	29.3
19504.0	587.6	.710	202.5	157.6	60.5
18987.3	757.7	.416	202.5	155.5	58.9
18858.2	715.2	.463	253.2	155.0	37.5
18729.0	638.8	.577	202.5	154.4	58.1
18470.7	662.5	.529	265.8	153.4	33.3
18341.5	692.2	.481	265.8	152.8	33.0
18212.3	812.0	.347	291.1	152.3	27.4
18212.3	571.4	.701	202.5	152.3	56.5
17824.9	697.1	.461	278.5	150.6	29.3
17308.2	644.8	.523	215.2	148.5	47.6
16920.7	781.1	.349	240.5	146.8	37.2

Table A-4 (cont'd)

A_r_e_a_	Perimeter	Shape_Fac	Max_Feret	Eq._cir_d	Form_Factor
16791.5	805.3	.325	278.5	146.2	27.6
16016.5	747.9	.360	253.2	142.8	31.8
15499.9	842.8	.274	202.5	140.5	48.1
15241.5	511.5	.732	189.9	139.3	53.8
14595.7	605.9	.500	215.2	136.3	40.1
14595.7	469.2	.833	164.6	136.3	68.6
14337.4	543.9	.609	202.5	135.1	44.5
14337.4	524.1	.656	164.6	135.1	67.4
14337.4	466.4	.828	164.6	135.1	67.4
14208.2	624.6	.458	227.8	134.5	34.8
13820.7	676.2	.380	177.2	132.7	56.0
13820.7	594.2	.492	189.9	132.7	48.8
13691.6	523.2	.629	202.5	132.0	42.5
13691.6	619.5	.448	202.5	132.0	42.5
12787.4	470.1	.727	202.5	127.6	39.7
12658.2	467.8	.727	151.9	127.0	69.9
12141.6	444.3	.773	164.6	124.3	57.1
12012.4	507.0	.587	164.6	123.7	56.5
11883.2	616.0	.393	215.2	123.0	32.7
11754.1	555.2	.479	177.2	122.3	47.7
11495.7	462.5	.675	151.9	121.0	63.4
11495.7	429.6	.783	151.9	121.0	63.4
11495.7	493.1	.594	164.6	121.0	54.1
10979.1	560.1	.440	202.5	118.2	34.1
10849.9	516.2	.512	189.9	117.5	38.3
10849.9	490.2	.567	164.6	117.5	51.0
10720.7	466.8	.618	177.2	116.8	43.5
10591.6	440.1	.687	139.2	116.1	69.6
10462.4	419.0	.749	151.9	115.4	57.7
10462.4	391.4	.858	126.6	115.4	83.1
10333.2	465.3	.600	177.2	114.7	41.9
10204.1	549.7	.424	189.9	114.0	36.0
10204.1	495.6	.522	151.9	114.0	56.3
9816.6	421.5	.694	164.6	111.8	46.2
9687.4	447.2	.609	151.9	111.1	53.5
9687.4	517.0	.455	151.9	111.1	53.5
9687.4	464.1	.565	151.9	111.1	53.5
9429.1	471.4	.533	164.6	109.6	44.3
9299.9	528.5	.418	164.6	108.8	43.7
9299.9	429.0	.635	151.9	108.8	51.3
9041.6	456.6	.545	177.2	107.3	36.7
8912.4	512.0	.427	202.5	106.5	27.7
8524.9	426.8	.588	139.2	104.2	56.0
8395.8	434.3	.559	151.9	103.4	46.3
8266.6	404.6	.635	151.9	102.6	45.6
8266.6	405.0	.633	151.9	102.6	45.6
8137.4	409.2	.611	139.2	101.8	53.4
8137.4	366.1	.763	113.9	101.8	79.8
8137.4	476.2	.451	177.2	101.8	33.0
8137.4	463.6	.476	164.6	101.8	38.3
8008.3	422.1	.565	139.2	101.0	52.6
7879.1	394.4	.637	126.6	100.2	62.6
7749.9	389.1	.643	139.2	99.3	50.9
7749.9	422.3	.546	139.2	99.3	50.9
7620.8	413.5	.560	151.9	98.5	42.1
7620.8	377.6	.672	126.6	98.5	60.6
7620.8	342.1	.818	126.6	98.5	60.6
7491.6	342.5	.803	113.9	97.7	73.5
7362.4	350.9	.752	126.6	96.8	58.5
7362.4	343.9	.782	113.9	96.8	72.2

Table A-4 (cont'd)

A_r_e_a_	Perimeter	Shape_Fac	Max_Feret	Eq._cir_d	Form_Factor
7362.4	451.7	.453	113.9	96.8	72.2
7362.4	386.4	.620	126.6	96.8	58.5
7233.3	420.2	.515	139.2	96.0	47.5
7104.1	396.2	.569	126.6	95.1	56.5
7104.1	393.5	.577	126.6	95.1	56.5
7104.1	391.5	.583	126.6	95.1	56.5
6845.8	340.3	.743	126.6	93.4	54.4
6845.8	434.8	.455	151.9	93.4	37.8
6716.6	471.6	.380	151.9	92.5	37.1
6716.6	337.6	.741	126.6	92.5	53.4
6716.6	347.0	.701	126.6	92.5	53.4
6458.3	378.0	.568	126.6	90.7	51.3
6458.3	357.2	.636	113.9	90.7	63.4
6329.1	370.3	.580	126.6	89.8	50.3
6329.1	352.7	.639	126.6	89.8	50.3
6199.9	414.8	.453	139.2	88.8	40.7
6199.9	321.5	.754	113.9	88.8	60.8
6199.9	367.4	.577	126.6	88.8	49.3
6070.8	338.8	.665	113.9	87.9	59.6
5941.6	358.8	.580	126.6	87.0	47.2
5941.6	308.4	.785	113.9	87.0	58.3
5941.6	335.4	.664	113.9	87.0	58.3
5812.5	313.1	.745	113.9	86.0	57.0
5812.5	387.6	.486	139.2	86.0	38.2
5812.5	375.6	.518	139.2	86.0	38.2
5812.5	399.3	.458	151.9	86.0	32.1
5683.3	345.2	.599	126.6	85.1	45.2
5683.3	306.4	.761	101.3	85.1	70.6
5683.3	328.2	.663	126.6	85.1	45.2
5683.3	352.1	.576	113.9	85.1	55.8
5683.3	310.0	.743	101.3	85.1	70.6
5554.1	348.6	.574	126.6	84.1	44.1
5554.1	299.8	.776	88.6	84.1	90.1
5554.1	341.9	.597	126.6	84.1	44.1
5554.1	330.8	.638	113.9	84.1	54.5
5425.0	369.4	.499	139.2	83.1	35.6
5166.6	325.1	.614	113.9	81.1	50.7
5166.6	345.7	.543	126.6	81.1	41.1
5166.6	334.8	.579	113.9	81.1	50.7
5037.5	370.3	.462	126.6	80.1	40.0
5037.5	284.9	.780	88.6	80.1	81.7
5037.5	286.0	.774	101.3	80.1	62.5
5037.5	287.8	.764	101.3	80.1	62.5
5037.5	319.9	.619	126.6	80.1	40.0
4908.3	309.6	.643	126.6	79.1	39.0
4908.3	345.4	.517	101.3	79.1	60.9
4908.3	343.3	.523	126.6	79.1	39.0
4908.3	343.7	.522	101.3	79.1	60.9
4908.3	327.4	.576	113.9	79.1	48.2
4908.3	306.9	.655	113.9	79.1	48.2
4908.3	288.2	.743	101.3	79.1	60.9
4779.1	276.2	.787	101.3	78.0	59.3
4779.1	306.0	.641	113.9	78.0	46.9
4779.1	294.9	.690	113.9	78.0	46.9
4779.1	302.9	.654	113.9	78.0	46.9
4650.0	296.2	.666	101.3	76.9	57.7
4650.0	266.1	.825	88.6	76.9	75.4
4650.0	325.4	.552	113.9	76.9	45.6
4650.0	301.1	.645	101.3	76.9	57.7
4650.0	299.3	.652	101.3	76.9	57.7

Table A-4 (cont'd)

A_r_e_a_	Perimeter	Shape_Fac	Max_Feret	Eq._cir_d	Form_Factor
4520.8	278.0	.735	101.3	75.9	56.1
4520.8	306.0	.607	113.9	75.9	44.4
4520.8	290.0	.675	101.3	75.9	56.1
4520.8	336.6	.501	126.6	75.9	35.9
4520.8	264.3	.813	88.6	75.9	73.3
4520.8	302.9	.619	113.9	75.9	44.4
4520.8	306.0	.607	126.6	75.9	35.9
4520.8	331.3	.518	113.9	75.9	44.4
4391.6	294.5	.636	113.9	74.8	43.1
4262.5	280.7	.680	101.3	73.7	52.9
4262.5	321.5	.518	113.9	73.7	41.8
4262.5	306.0	.572	126.6	73.7	33.9
4262.5	279.4	.686	101.3	73.7	52.9
4133.3	293.3	.604	88.6	72.5	67.0
4133.3	261.2	.761	88.6	72.5	67.0
4133.3	264.3	.743	101.3	72.5	51.3
4133.3	292.7	.606	113.9	72.5	40.5
4133.3	266.1	.733	101.3	72.5	51.3
4133.3	257.6	.783	88.6	72.5	67.0
4004.1	254.1	.779	88.6	71.4	64.9
4004.1	267.8	.702	88.6	71.4	64.9
4004.1	299.8	.560	101.3	71.4	49.7
4004.1	295.8	.575	113.9	71.4	39.3
4004.1	281.5	.635	101.3	71.4	49.7
4004.1	284.2	.623	101.3	71.4	49.7
4004.1	259.0	.750	88.6	71.4	64.9
4004.1	266.1	.710	88.6	71.4	64.9
4004.1	253.9	.780	88.6	71.4	64.9
4004.1	274.0	.670	101.3	71.4	49.7
4004.1	262.7	.729	101.3	71.4	49.7
3875.0	269.6	.670	101.3	70.2	48.1
3875.0	313.1	.497	113.9	70.2	38.0
3875.0	286.0	.595	101.3	70.2	48.1
3875.0	281.1	.616	88.6	70.2	62.8
3875.0	269.1	.673	88.6	70.2	62.8
3745.8	247.4	.769	88.6	69.1	60.7
3745.8	263.8	.677	88.6	69.1	60.7
3745.8	273.1	.631	101.3	69.1	46.5
3745.8	255.8	.720	88.6	69.1	60.7
3745.8	278.9	.605	101.3	69.1	46.5
3745.8	245.7	.780	88.6	69.1	60.7
3745.8	284.2	.583	101.3	69.1	46.5
3616.6	247.4	.743	88.6	67.9	58.7
3616.6	245.6	.754	88.6	67.9	58.7
3616.6	243.7	.765	88.6	67.9	58.7
3616.6	263.8	.653	101.3	67.9	44.9
3616.6	252.7	.712	75.9	67.9	79.8
3616.6	235.5	.819	75.9	67.9	79.8
3616.6	262.5	.660	101.3	67.9	44.9
3487.5	255.8	.670	88.6	66.6	56.6
3487.5	264.3	.627	88.6	66.6	56.6
3487.5	253.9	.680	88.6	66.6	56.6
3487.5	235.5	.790	88.6	66.6	56.6
3487.5	257.2	.663	101.3	66.6	43.3
3487.5	240.3	.759	75.9	66.6	77.0
3487.5	263.8	.630	101.3	66.6	43.3
3487.5	228.8	.837	75.9	66.6	77.0
3487.5	279.3	.562	101.3	66.6	43.3
3358.3	233.7	.773	75.9	65.4	74.1
3358.3	240.6	.729	88.6	65.4	54.5

Table A-4 (cont'd)

A_r_e_a_	Perimeter	Shape_Fac	Max_Feret	Eq._cir_d	Form_Factor
3358.3	240.8	.728	88.6	65.4	54.5
3358.3	242.1	.720	75.9	65.4	74.1
3358.3	238.4	.742	75.9	65.4	74.1
3358.3	243.7	.710	88.6	65.4	54.5
3358.3	255.8	.645	88.6	65.4	54.5
3358.3	228.8	.806	75.9	65.4	74.1
3358.3	253.6	.656	88.6	65.4	54.5
3229.1	235.4	.733	75.9	64.1	71.3
3229.1	253.6	.631	88.6	64.1	52.4
3229.1	235.4	.733	88.6	64.1	52.4
3229.1	253.6	.631	88.6	64.1	52.4
3229.1	247.4	.663	88.6	64.1	52.4
3229.1	252.7	.636	88.6	64.1	52.4
3229.1	228.8	.775	75.9	64.1	71.3
3229.1	237.2	.721	88.6	64.1	52.4
3229.1	231.9	.755	75.9	64.1	71.3
3100.0	225.1	.768	75.9	62.8	68.4
3100.0	233.5	.714	88.6	62.8	50.3
3100.0	253.6	.606	88.6	62.8	50.3
3100.0	243.7	.656	88.6	62.8	50.3
3100.0	231.9	.725	88.6	62.8	50.3
3100.0	232.3	.722	75.9	62.8	68.4
3100.0	270.9	.531	88.6	62.8	50.3
3100.0	243.3	.658	88.6	62.8	50.3
3100.0	240.3	.675	88.6	62.8	50.3
3100.0	275.8	.512	101.3	62.8	38.5
3100.0	238.4	.685	88.6	62.8	50.3
3100.0	238.4	.685	88.6	62.8	50.3
3100.0	243.3	.658	88.6	62.8	50.3
3100.0	228.8	.744	75.9	62.8	68.4
3100.0	240.8	.672	88.6	62.8	50.3
2970.8	220.2	.770	75.9	61.5	65.6
2970.8	258.8	.557	88.6	61.5	48.2
2970.8	250.5	.595	88.6	61.5	48.2
2970.8	243.3	.630	88.6	61.5	48.2
2970.8	216.8	.795	75.9	61.5	65.6
2970.8	235.4	.674	88.6	61.5	48.2
2970.8	220.2	.770	75.9	61.5	65.6
2970.8	225.1	.736	75.9	61.5	65.6
2970.8	230.1	.705	75.9	61.5	65.6
2970.8	223.5	.747	88.6	61.5	48.2
2970.8	216.8	.795	75.9	61.5	65.6
2970.8	223.3	.749	75.9	61.5	65.6
2970.8	216.8	.795	75.9	61.5	65.6
2841.6	223.5	.715	88.6	60.2	46.1
2841.6	208.4	.822	75.9	60.2	62.7
2841.6	208.4	.822	75.9	60.2	62.7
2841.6	242.1	.609	88.6	60.2	46.1
2841.6	220.2	.736	75.9	60.2	62.7
2841.6	216.8	.760	75.9	60.2	62.7
2841.6	238.4	.628	88.6	60.2	46.1
2841.6	211.9	.796	63.3	60.2	90.3
2841.6	216.8	.760	75.9	60.2	62.7
2841.6	208.4	.822	75.9	60.2	62.7
2841.6	221.7	.727	75.9	60.2	62.7
2841.6	216.8	.760	75.9	60.2	62.7
2841.6	216.8	.760	75.9	60.2	62.7
2712.5	238.4	.600	88.6	58.8	44.0
2712.5	223.7	.681	75.9	58.8	59.9
2712.5	214.9	.738	75.9	58.8	59.9

Table A-4 (cont'd)

A_r_e_a_	Perimeter	Shape_Fac	Max_Feret	Eq._cir_d	Form_Factor
2712.5	223.7	.681	75.9	58.8	59.9
2712.5	211.9	.759	75.9	58.8	59.9
2712.5	228.2	.654	75.9	58.8	59.9
2712.5	243.3	.576	88.6	58.8	44.0
2712.5	208.4	.785	75.9	58.8	59.9
2712.5	228.2	.654	75.9	58.8	59.9
2712.5	228.2	.654	75.9	58.8	59.9
2712.5	263.8	.490	101.3	58.8	33.7
2712.5	228.2	.654	75.9	58.8	59.9
2583.3	208.2	.749	63.3	57.4	82.1
2583.3	208.2	.749	63.3	57.4	82.1
2583.3	206.6	.761	75.9	57.4	57.0
2583.3	208.4	.748	75.9	57.4	57.0
2583.3	208.2	.749	63.3	57.4	82.1
2583.3	238.4	.571	88.6	57.4	41.9
2583.3	238.4	.571	88.6	57.4	41.9
2583.3	211.9	.723	75.9	57.4	57.0
2583.3	219.9	.672	75.9	57.4	57.0
2583.3	213.1	.715	75.9	57.4	57.0
2454.1	199.8	.772	63.3	55.9	78.0
2454.1	199.8	.772	63.3	55.9	78.0
2454.1	204.7	.736	75.9	55.9	54.2
2454.1	204.7	.736	75.9	55.9	54.2
2454.1	204.7	.736	75.9	55.9	54.2
2454.1	204.7	.736	75.9	55.9	54.2
2454.1	213.1	.679	75.9	55.9	54.2
2454.1	204.7	.736	75.9	55.9	54.2
2454.1	213.1	.679	75.9	55.9	54.2
2454.1	211.9	.687	75.9	55.9	54.2
2454.1	204.7	.736	75.9	55.9	54.2
2454.1	199.8	.772	63.3	55.9	78.0
2454.1	204.7	.736	75.9	55.9	54.2
2454.1	204.7	.736	75.9	55.9	54.2
2454.1	204.7	.736	75.9	55.9	54.2
2454.1	199.8	.772	63.3	55.9	78.0
2454.1	199.8	.772	63.3	55.9	78.0
2454.1	199.8	.772	63.3	55.9	78.0
2454.1	199.8	.772	63.3	55.9	78.0
2454.1	214.9	.668	75.9	55.9	54.2
2454.1	214.9	.668	75.9	55.9	54.2
2454.1	211.9	.687	75.9	55.9	54.2
2454.1	214.9	.668	75.9	55.9	54.2
2325.0	233.5	.536	88.6	54.4	37.7
2325.0	202.9	.710	75.9	54.4	51.3
2325.0	191.4	.797	63.3	54.4	73.9
2325.0	196.4	.758	75.9	54.4	51.3
2325.0	199.8	.732	63.3	54.4	73.9
2325.0	218.0	.615	75.9	54.4	51.3
2325.0	191.4	.797	63.3	54.4	73.9
2325.0	218.0	.615	75.9	54.4	51.3
2325.0	199.8	.732	63.3	54.4	73.9
2325.0	233.5	.536	88.6	54.4	37.7
2325.0	202.9	.710	75.9	54.4	51.3
2325.0	191.4	.797	63.3	54.4	73.9
2325.0	199.8	.732	63.3	54.4	73.9
2325.0	203.3	.707	63.3	54.4	73.9
2325.0	203.3	.707	63.3	54.4	73.9
2325.0	202.9	.710	75.9	54.4	51.3
2325.0	211.9	.651	75.9	54.4	51.3
2325.0	191.4	.797	63.3	54.4	73.9

Table A-4 (cont'd)

A_r_e_a_	Perimeter	Shape_Fac	Max_Feret	Eq._cir_d	Form_Factor
2325.0	202.9	.710	75.9	54.4	51.3
2325.0	202.9	.710	75.9	54.4	51.3
2325.0	191.4	.797	63.3	54.4	73.9
2325.0	199.8	.732	63.3	54.4	73.9
2325.0	199.8	.732	63.3	54.4	73.9
2325.0	199.8	.732	63.3	54.4	73.9
2325.0	203.3	.707	63.3	54.4	73.9
2325.0	202.9	.710	75.9	54.4	51.3
2325.0	203.3	.707	63.3	54.4	73.9
2325.0	196.4	.758	63.3	54.4	73.9
2325.0	218.0	.615	75.9	54.4	51.3
2325.0	191.4	.797	63.3	54.4	73.9
2325.0	196.4	.758	75.9	54.4	51.3
2325.0	202.9	.710	75.9	54.4	51.3
2325.0	191.4	.797	63.3	54.4	73.9
2195.8	194.5	.729	75.9	52.9	48.5
2195.8	191.4	.753	63.3	52.9	69.8
2195.8	191.4	.753	63.3	52.9	69.8
2195.8	194.5	.729	75.9	52.9	48.5
2195.8	191.4	.753	63.3	52.9	69.8
2195.8	194.5	.729	75.9	52.9	48.5
2195.8	194.5	.729	75.9	52.9	48.5
2195.8	191.4	.753	63.3	52.9	69.8
2195.8	191.4	.753	63.3	52.9	69.8
2066.6	191.4	.709	63.3	51.3	65.7
2066.6	192.7	.699	75.9	51.3	45.6
2066.6	191.4	.709	63.3	51.3	65.7
2066.6	187.8	.736	63.3	51.3	65.7
2066.6	192.7	.699	75.9	51.3	45.6
2066.6	191.4	.709	63.3	51.3	65.7
2066.6	192.7	.699	75.9	51.3	45.6
2066.6	187.8	.736	63.3	51.3	65.7
2066.6	187.8	.736	63.3	51.3	65.7
2066.6	187.8	.736	63.3	51.3	65.7
2066.6	187.8	.736	63.3	51.3	65.7
1937.5	192.7	.656	63.3	49.7	61.6
1937.5	179.4	.756	63.3	49.7	61.6
1937.5	179.4	.756	63.3	49.7	61.6
1937.5	192.7	.656	63.3	49.7	61.6
1937.5	179.4	.756	63.3	49.7	61.6
1937.5	192.7	.656	63.3	49.7	61.6
1937.5	179.4	.756	63.3	49.7	61.6
1937.5	192.7	.656	63.3	49.7	61.6
1937.5	179.4	.756	63.3	49.7	61.6
1937.5	192.7	.656	63.3	49.7	61.6
1937.5	192.7	.656	63.3	49.7	61.6
1937.5	179.4	.756	63.3	49.7	61.6
1937.5	179.4	.756	63.3	49.7	61.6
1937.5	182.9	.728	63.3	49.7	61.6
1937.5	182.9	.728	63.3	49.7	61.6
1937.5	192.7	.656	63.3	49.7	61.6
1937.5	182.9	.728	63.3	49.7	61.6
1937.5	179.4	.756	63.3	49.7	61.6
1937.5	182.9	.728	63.3	49.7	61.6
1937.5	192.7	.656	63.3	49.7	61.6
1937.5	179.4	.756	63.3	49.7	61.6
1937.5	179.4	.756	63.3	49.7	61.6
1937.5	179.4	.756	63.3	49.7	61.6
1937.5	179.4	.756	63.3	49.7	61.6
1937.5	179.4	.756	63.3	49.7	61.6

Table A-4 (cont'd)

A_r_e_a_	Perimeter	Shape_Fac	Max_Feret	Eq._cir_d	Form_Factor
1937.5	179.4	.756	63.3	49.7	61.6
1937.5	182.9	.728	63.3	49.7	61.6
1937.5	179.4	.756	63.3	49.7	61.6
1937.5	192.7	.656	63.3	49.7	61.6
1937.5	179.4	.756	63.3	49.7	61.6
1937.5	179.4	.756	63.3	49.7	61.6
1937.5	182.9	.728	63.3	49.7	61.6
1937.5	182.9	.728	63.3	49.7	61.6
1937.5	179.4	.756	63.3	49.7	61.6
1937.5	179.4	.756	63.3	49.7	61.6
1937.5	179.4	.756	63.3	49.7	61.6
1937.5	182.9	.728	63.3	49.7	61.6
1937.5	182.9	.728	63.3	49.7	61.6
1937.5	179.4	.756	63.3	49.7	61.6
1937.5	182.9	.728	63.3	49.7	61.6
1937.5	179.4	.756	63.3	49.7	61.6
1937.5	182.9	.728	63.3	49.7	61.6
1937.5	182.9	.728	63.3	49.7	61.6
1937.5	192.7	.656	63.3	49.7	61.6
1937.5	179.4	.756	63.3	49.7	61.6
1937.5	192.7	.656	63.3	49.7	61.6
1937.5	179.4	.756	63.3	49.7	61.6
1937.5	182.9	.728	63.3	49.7	61.6
1937.5	179.4	.756	63.3	49.7	61.6
1937.5	179.4	.756	63.3	49.7	61.6
1937.5	179.4	.756	63.3	49.7	61.6
1937.5	192.7	.656	63.3	49.7	61.6
1937.5	179.4	.756	63.3	49.7	61.6
1937.5	182.9	.728	63.3	49.7	61.6
1937.5	192.7	.656	63.3	49.7	61.6
1937.5	182.9	.728	63.3	49.7	61.6
1937.5	192.7	.656	63.3	49.7	61.6
1937.5	179.4	.756	63.3	49.7	61.6
1937.5	179.4	.756	63.3	49.7	61.6
1937.5	182.9	.728	63.3	49.7	61.6
1937.5	179.4	.756	63.3	49.7	61.6
1937.5	179.4	.756	63.3	49.7	61.6
1808.3	171.0	.777	63.3	48.0	57.5
1808.3	171.0	.777	63.3	48.0	57.5
1808.3	171.0	.777	63.3	48.0	57.5
1808.3	171.0	.777	63.3	48.0	57.5
1808.3	171.0	.777	63.3	48.0	57.5
1808.3	171.0	.777	63.3	48.0	57.5
1808.3	171.0	.777	63.3	48.0	57.5
1808.3	171.0	.777	63.3	48.0	57.5
1808.3	171.0	.777	63.3	48.0	57.5
1808.3	171.0	.777	63.3	48.0	57.5
1808.3	171.0	.777	63.3	48.0	57.5
1808.3	171.0	.777	63.3	48.0	57.5
1808.3	171.0	.777	63.3	48.0	57.5
1808.3	171.0	.777	63.3	48.0	57.5
1808.3	171.0	.777	63.3	48.0	57.5
1550.0	167.4	.695	50.6	44.4	77.0
1550.0	167.4	.695	50.6	44.4	77.0
1550.0	162.5	.738	50.6	44.4	77.0
1550.0	167.4	.695	50.6	44.4	77.0
1550.0	162.5	.738	50.6	44.4	77.0
1550.0	162.5	.738	50.6	44.4	77.0
1550.0	162.5	.738	50.6	44.4	77.0
1550.0	167.4	.695	50.6	44.4	77.0

Table A-4 (cont'd)

A_r_e_a_	Perimeter	Shape_Fac	Max_Feret	Eq._cir_d	Form_Factor
1550.0	167.4	.695	50.6	44.4	77.0
1550.0	167.4	.695	50.6	44.4	77.0
1550.0	167.4	.695	50.6	44.4	77.0
1550.0	167.4	.695	50.6	44.4	77.0
1550.0	162.5	.738	50.6	44.4	77.0
1550.0	167.4	.695	50.6	44.4	77.0
1550.0	162.5	.738	50.6	44.4	77.0
1550.0	162.5	.738	50.6	44.4	77.0
1550.0	162.5	.738	50.6	44.4	77.0
1550.0	162.5	.738	50.6	44.4	77.0
1550.0	167.4	.695	50.6	44.4	77.0
1550.0	167.4	.695	50.6	44.4	77.0
1550.0	162.5	.738	50.6	44.4	77.0
1550.0	167.4	.695	50.6	44.4	77.0
1550.0	162.5	.738	50.6	44.4	77.0
1550.0	162.5	.738	50.6	44.4	77.0
1550.0	167.4	.695	50.6	44.4	77.0
1550.0	162.5	.738	50.6	44.4	77.0
1550.0	167.4	.695	50.6	44.4	77.0
1550.0	167.4	.695	50.6	44.4	77.0
1550.0	167.4	.695	50.6	44.4	77.0
1550.0	167.4	.695	50.6	44.4	77.0
1550.0	167.4	.695	50.6	44.4	77.0
1550.0	167.4	.695	50.6	44.4	77.0
1550.0	167.4	.695	50.6	44.4	77.0
1550.0	167.4	.695	50.6	44.4	77.0
1550.0	167.4	.695	50.6	44.4	77.0
1550.0	167.4	.695	50.6	44.4	77.0
1550.0	162.5	.738	50.6	44.4	77.0
1550.0	167.4	.695	50.6	44.4	77.0
1550.0	162.5	.738	50.6	44.4	77.0
1550.0	167.4	.695	50.6	44.4	77.0
1550.0	162.5	.738	50.6	44.4	77.0
1550.0	167.4	.695	50.6	44.4	77.0
1550.0	167.4	.695	50.6	44.4	77.0
1550.0	167.4	.695	50.6	44.4	77.0
1550.0	162.5	.738	50.6	44.4	77.0
1550.0	162.5	.738	50.6	44.4	77.0
1550.0	167.4	.695	50.6	44.4	77.0
1550.0	162.5	.738	50.6	44.4	77.0
1550.0	167.4	.695	50.6	44.4	77.0
1550.0	167.4	.695	50.6	44.4	77.0
1550.0	162.5	.738	50.6	44.4	77.0
1550.0	162.5	.738	50.6	44.4	77.0
1550.0	167.4	.695	50.6	44.4	77.0
1550.0	167.4	.695	50.6	44.4	77.0
1550.0	162.5	.738	50.6	44.4	77.0
1550.0	167.4	.695	50.6	44.4	77.0
1550.0	162.5	.738	50.6	44.4	77.0
1550.0	162.5	.738	50.6	44.4	77.0
1550.0	167.4	.695	50.6	44.4	77.0
1550.0	162.5	.738	50.6	44.4	77.0
1550.0	162.5	.738	50.6	44.4	77.0
1550.0	167.4	.695	50.6	44.4	77.0
1550.0	167.4	.695	50.6	44.4	77.0
1550.0	167.4	.695	50.6	44.4	77.0
1550.0	162.5	.738	50.6	44.4	77.0
1550.0	167.4	.695	50.6	44.4	77.0
1550.0	162.5	.738	50.6	44.4	77.0
1550.0	162.5	.738	50.6	44.4	77.0

Table A-4 (cont'd)

A_r_e_a_	Perimeter	Shape_Fac	Max_Feret	Eq._cir_d	Form_Factor
1550.0	162.5	.738	50.6	44.4	77.0
1550.0	167.4	.695	50.6	44.4	77.0
1550.0	162.5	.738	50.6	44.4	77.0
1550.0	167.4	.695	50.6	44.4	77.0
1550.0	167.4	.695	50.6	44.4	77.0
1550.0	162.5	.738	50.6	44.4	77.0
1550.0	162.5	.738	50.6	44.4	77.0
1550.0	167.4	.695	50.6	44.4	77.0
1550.0	167.4	.695	50.6	44.4	77.0
1550.0	167.4	.695	50.6	44.4	77.0
1550.0	162.5	.738	50.6	44.4	77.0
1550.0	167.4	.695	50.6	44.4	77.0
1550.0	167.4	.695	50.6	44.4	77.0
1550.0	162.5	.738	50.6	44.4	77.0
1550.0	162.5	.738	50.6	44.4	77.0
1550.0	162.5	.738	50.6	44.4	77.0
1550.0	167.4	.695	50.6	44.4	77.0
1550.0	162.5	.738	50.6	44.4	77.0
1550.0	167.4	.695	50.6	44.4	77.0
1550.0	162.5	.738	50.6	44.4	77.0
1550.0	162.5	.738	50.6	44.4	77.0
1550.0	167.4	.695	50.6	44.4	77.0
1550.0	162.5	.738	50.6	44.4	77.0
1550.0	167.4	.695	50.6	44.4	77.0
1550.0	167.4	.695	50.6	44.4	77.0
1550.0	167.4	.695	50.6	44.4	77.0
1550.0	162.5	.738	50.6	44.4	77.0
1550.0	162.5	.738	50.6	44.4	77.0
1550.0	162.5	.738	50.6	44.4	77.0
1550.0	167.4	.695	50.6	44.4	77.0
1550.0	167.4	.695	50.6	44.4	77.0
1550.0	162.5	.738	50.6	44.4	77.0
1550.0	167.4	.695	50.6	44.4	77.0
1550.0	162.5	.738	50.6	44.4	77.0
1550.0	162.5	.738	50.6	44.4	77.0
1550.0	162.5	.738	50.6	44.4	77.0
1162.5	142.1	.724	50.6	38.5	57.7
1162.5	142.1	.724	50.6	38.5	57.7
1162.5	142.1	.724	50.6	38.5	57.7
1162.5	142.1	.724	50.6	38.5	57.7
1162.5	142.1	.724	50.6	38.5	57.7
1162.5	142.1	.724	50.6	38.5	57.7
1162.5	142.1	.724	50.6	38.5	57.7
1162.5	142.1	.724	50.6	38.5	57.7
1162.5	142.1	.724	50.6	38.5	57.7
1162.5	142.1	.724	50.6	38.5	57.7
1162.5	142.1	.724	50.6	38.5	57.7
1162.5	142.1	.724	50.6	38.5	57.7
1162.5	142.1	.724	50.6	38.5	57.7
1162.5	142.1	.724	50.6	38.5	57.7
1162.5	142.1	.724	50.6	38.5	57.7
1162.5	142.1	.724	50.6	38.5	57.7
1162.5	142.1	.724	50.6	38.5	57.7
1162.5	142.1	.724	50.6	38.5	57.7
1162.5	142.1	.724	50.6	38.5	57.7
1162.5	142.1	.724	50.6	38.5	57.7
1162.5	142.1	.724	50.6	38.5	57.7
1162.5	142.1	.724	50.6	38.5	57.7
1162.5	142.1	.724	50.6	38.5	57.7
1162.5	142.1	.724	50.6	38.5	57.7

Table A-4 (cont'd)

A_r_e_a_	Perimeter	Shape_Fac	Max_Feret	Eq._cir_d	Form_Factor
1162.5	142.1	.724	50.6	38.5	57.7
1162.5	142.1	.724	50.6	38.5	57.7
1162.5	142.1	.724	50.6	38.5	57.7
1162.5	142.1	.724	50.6	38.5	57.7
1162.5	142.1	.724	50.6	38.5	57.7
1162.5	142.1	.724	50.6	38.5	57.7
1162.5	142.1	.724	50.6	38.5	57.7
1162.5	142.1	.724	50.6	38.5	57.7
1162.5	142.1	.724	50.6	38.5	57.7
1162.5	142.1	.724	50.6	38.5	57.7
1162.5	142.1	.724	50.6	38.5	57.7
1162.5	142.1	.724	50.6	38.5	57.7
1162.5	142.1	.724	50.6	38.5	57.7
1162.5	142.1	.724	50.6	38.5	57.7
1162.5	142.1	.724	50.6	38.5	57.7
1162.5	142.1	.724	50.6	38.5	57.7
1162.5	142.1	.724	50.6	38.5	57.7
1162.5	142.1	.724	50.6	38.5	57.7
1162.5	142.1	.724	50.6	38.5	57.7
1162.5	142.1	.724	50.6	38.5	57.7
1162.5	142.1	.724	50.6	38.5	57.7
1162.5	142.1	.724	50.6	38.5	57.7
1162.5	142.1	.724	50.6	38.5	57.7
1162.5	142.1	.724	50.6	38.5	57.7
1162.5	142.1	.724	50.6	38.5	57.7
1162.5	142.1	.724	50.6	38.5	57.7
1162.5	142.1	.724	50.6	38.5	57.7
1162.5	142.1	.724	50.6	38.5	57.7
1162.5	142.1	.724	50.6	38.5	57.7
1162.5	142.1	.724	50.6	38.5	57.7
1162.5	142.1	.724	50.6	38.5	57.7
1162.5	142.1	.724	50.6	38.5	57.7
1162.5	142.1	.724	50.6	38.5	57.7
1162.5	142.1	.724	50.6	38.5	57.7
1162.5	142.1	.724	50.6	38.5	57.7
1162.5	142.1	.724	50.6	38.5	57.7
1162.5	142.1	.724	50.6	38.5	57.7
1162.5	142.1	.724	50.6	38.5	57.7
1162.5	142.1	.724	50.6	38.5	57.7
1162.5	142.1	.724	50.6	38.5	57.7
1162.5	142.1	.724	50.6	38.5	57.7
1162.5	142.1	.724	50.6	38.5	57.7
1162.5	142.1	.724	50.6	38.5	57.7
1162.5	142.1	.724	50.6	38.5	57.7
1162.5	142.1	.724	50.6	38.5	57.7
1162.5	142.1	.724	50.6	38.5	57.7
1162.5	142.1	.724	50.6	38.5	57.7
1162.5	142.1	.724	50.6	38.5	57.7
1162.5	142.1	.724	50.6	38.5	57.7
1162.5	142.1	.724	50.6	38.5	57.7
1162.5	142.1	.724	50.6	38.5	57.7
1162.5	142.1	.724	50.6	38.5	57.7
1162.5	142.1	.724	50.6	38.5	57.7
1162.5	142.1	.724	50.6	38.5	57.7
1162.5	142.1	.724	50.6	38.5	57.7
1162.5	142.1	.724	50.6	38.5	57.7
1162.5	142.1	.724	50.6	38.5	57.7
1162.5	142.1	.724	50.6	38.5	57.7
1162.5	142.1	.724	50.6	38.5	57.7
1162.5	142.1	.724	50.6	38.5	57.7

Table A-4 (cont'd)

A_r_e_a_	Perimeter	Shape_Fac	Max_Feret	Eq._cir_d	Form_Factor
1162.5	142.1	.724	50.6	38.5	57.7
1162.5	142.1	.724	50.6	38.5	57.7
1162.5	142.1	.724	50.6	38.5	57.7
1162.5	142.1	.724	50.6	38.5	57.7
1162.5	142.1	.724	50.6	38.5	57.7
1162.5	142.1	.724	50.6	38.5	57.7
1162.5	142.1	.724	50.6	38.5	57.7
1162.5	142.1	.724	50.6	38.5	57.7
1162.5	142.1	.724	50.6	38.5	57.7
1162.5	142.1	.724	50.6	38.5	57.7
1162.5	142.1	.724	50.6	38.5	57.7
1162.5	142.1	.724	50.6	38.5	57.7
1162.5	142.1	.724	50.6	38.5	57.7
1162.5	142.1	.724	50.6	38.5	57.7
1162.5	142.1	.724	50.6	38.5	57.7
1162.5	142.1	.724	50.6	38.5	57.7
1162.5	142.1	.724	50.6	38.5	57.7
1162.5	142.1	.724	50.6	38.5	57.7
1162.5	142.1	.724	50.6	38.5	57.7
1162.5	142.1	.724	50.6	38.5	57.7
1162.5	142.1	.724	50.6	38.5	57.7
1162.5	142.1	.724	50.6	38.5	57.7
1162.5	142.1	.724	50.6	38.5	57.7
1162.5	142.1	.724	50.6	38.5	57.7
1162.5	142.1	.724	50.6	38.5	57.7
1162.5	142.1	.724	50.6	38.5	57.7
1162.5	142.1	.724	50.6	38.5	57.7
1162.5	142.1	.724	50.6	38.5	57.7
1162.5	142.1	.724	50.6	38.5	57.7
1162.5	142.1	.724	50.6	38.5	57.7
1162.5	142.1	.724	50.6	38.5	57.7
1162.5	142.1	.724	50.6	38.5	57.7
1162.5	142.1	.724	50.6	38.5	57.7
1162.5	142.1	.724	50.6	38.5	57.7
1162.5	142.1	.724	50.6	38.5	57.7
1162.5	142.1	.724	50.6	38.5	57.7
1162.5	142.1	.724	50.6	38.5	57.7
1162.5	142.1	.724	50.6	38.5	57.7
1162.5	142.1	.724	50.6	38.5	57.7
1162.5	142.1	.724	50.6	38.5	57.7
1162.5	142.1	.724	50.6	38.5	57.7
1162.5	142.1	.724	50.6	38.5	57.7
1162.5	142.1	.724	50.6	38.5	57.7
1162.5	142.1	.724	50.6	38.5	57.7
1162.5	142.1	.724	50.6	38.5	57.7
1162.5	142.1	.72	50.6	38.5	57.7
1162.5	142.1	.72	50.6	38.5	57.7
1162.5	142.1	.724	50.6	38.5	57.7
1162.5	142.1	.724	50.6	38.5	57.7
1162.5	142.1	.724	50.6	38.5	57.7
1162.5	142.1	.724	50.6	38.5	57.7
1162.5	142.1	.724	50.6	38.5	57.7
1162.5	142.1	.724	50.6	38.5	57.7
1162.5	142.1	.724	50.6	38.5	57.7
1162.5	142.1	.724	50.6	38.5	57.7
1162.5	142.1	.724	50.6	38.5	57.7
1162.5	142.1	.724	50.6	38.5	57.7
1162.5	142.1	.724	50.6	38.5	57.7
1162.5	142.1	.724	50.6	38.5	57.7
1162.5	142.1	.724	50.6	38.5	57.7

Table A-4 (cont'd)

A_r_e_a_	Perimeter	Shape_Fac	Max_Feret	Eq._cir_d	Form_Factor
1162.5	142.1	.724	50.6	38.5	57.7
1162.5	142.1	.724	50.6	38.5	57.7
1162.5	142.1	.724	50.6	38.5	57.7
1162.5	142.1	.724	50.6	38.5	57.7
1162.5	142.1	.724	50.6	38.5	57.7
1162.5	142.1	.724	50.6	38.5	57.7
1162.5	142.1	.724	50.6	38.5	57.7
1162.5	142.1	.724	50.6	38.5	57.7
1162.5	142.1	.724	50.6	38.5	57.7
1162.5	142.1	.724	50.6	38.5	57.7
1162.5	142.1	.724	50.6	38.5	57.7
1162.5	142.1	.724	50.6	38.5	57.7
1162.5	142.1	.724	50.6	38.5	57.7
1162.5	142.1	.724	50.6	38.5	57.7
1162.5	142.1	.724	50.6	38.5	57.7
1162.5	142.1	.724	50.6	38.5	57.7
1162.5	142.1	.724	50.6	38.5	57.7
1162.5	142.1	.724	50.6	38.5	57.7
1162.5	142.1	.724	50.6	38.5	57.7
1162.5	142.1	.724	50.6	38.5	57.7
1162.5	142.1	.724	50.6	38.5	57.7
1162.5	142.1	.724	50.6	38.5	57.7
1162.5	142.1	.724	50.6	38.5	57.7
1162.5	142.1	.724	50.6	38.5	57.7
1162.5	142.1	.724	50.6	38.5	57.7
1162.5	142.1	.724	50.6	38.5	57.7
1162.5	142.1	.724	50.6	38.5	57.7
1162.5	142.1	.724	50.6	38.5	57.7
1162.5	142.1	.724	50.6	38.5	57.7
1162.5	142.1	.724	50.6	38.5	57.7
1162.5	142.1	.724	50.6	38.5	57.7
1162.5	142.1	.724	50.6	38.5	57.7
1162.5	142.1	.724	50.6	38.5	57.7
1162.5	142.1	.724	50.6	38.5	57.7
1162.5	142.1	.724	50.6	38.5	57.7
1162.5	142.1	.724	50.6	38.5	57.7
1162.5	142.1	.724	50.6	38.5	57.7
1162.5	142.1	.724	50.6	38.5	57.7
1162.5	142.1	.724	50.6	38.5	57.7
1162.5	142.1	.724	50.6	38.5	57.7
1162.5	142.1	.724	50.6	38.5	57.7
1162.5	142.1	.724	50.6	38.5	57.7
1162.5	142.1	.724	50.6	38.5	57.7
1162.5	142.1	.724	50.6	38.5	57.7
1162.5	142.1	.724	50.6	38.5	57.7
1162.5	142.1	.724	50.6	38.5	57.7
1162.5	142.1	.724	50.6	38.5	57.7
1162.5	142.1	.724	50.6	38.5	57.7
1162.5	142.1	.724	50.6	38.5	57.7
1162.5	142.1	.724	50.6	38.5	57.7
1162.5	142.1	.724	50.6	38.5	57.7
1162.5	142.1	.724	50.6	38.5	57.7
1162.5	142.1	.724	50.6	38.5	57.7
1162.5	142.1	.724	50.6	38.5	57.7
1162.5	142.1	.724	50.6	38.5	57.7
1162.5	142.1	.724	50.6	38.5	57.7
1162.5	142.1	.724	50.6	38.5	57.7
1162.5	142.1	.724	50.6	38.5	57.7
1162.5	142.1	.724	50.6	38.5	57.7
1162.5	142.1	.724	50.6	38.5	57.7

Table A-4 (cont'd)

A_r_e_a_	Perimeter	Shape_Fac	Max_Feret	Eq._cir_d	Form_Factor
1162.5	142.1	.724	50.6	38.5	57.7
1162.5	142.1	.724	50.6	38.5	57.7
1162.5	142.1	.724	50.6	38.5	57.7
1162.5	142.1	.724	50.6	38.5	57.7
1162.5	142.1	.724	50.6	38.5	57.7
1162.5	142.1	.724	50.6	38.5	57.7
1162.5	142.1	.724	50.6	38.5	57.7
1162.5	142.1	.724	50.6	38.5	57.7
1162.5	142.1	.724	50.6	38.5	57.7
1162.5	142.1	.724	50.6	38.5	57.7
1162.5	142.1	.724	50.6	38.5	57.7
1162.5	142.1	.724	50.6	38.5	57.7
1162.5	142.1	.724	50.6	38.5	57.7
1162.5	142.1	.724	50.6	38.5	57.7
1162.5	142.1	.724	50.6	38.5	57.7
1162.5	142.1	.724	50.6	38.5	57.7
1162.5	142.1	.724	50.6	38.5	57.7
1162.5	142.1	.724	50.6	38.5	57.7
1162.5	142.1	.724	50.6	38.5	57.7
1162.5	142.1	.724	50.6	38.5	57.7
1162.5	142.1	.724	50.6	38.5	57.7
1162.5	142.1	.724	50.6	38.5	57.7
1162.5	142.1	.724	50.6	38.5	57.7
1162.5	142.1	.724	50.6	38.5	57.7
1162.5	142.1	.724	50.6	38.5	57.7
1162.5	142.1	.724	50.6	38.5	57.7
1162.5	142.1	.724	50.6	38.5	57.7
1162.5	142.1	.724	50.6	38.5	57.7
1162.5	142.1	.724	50.6	38.5	57.7
1162.5	142.1	.724	50.6	38.5	57.7
1162.5	142.1	.724	50.6	38.5	57.7
1162.5	142.1	.724	50.6	38.5	57.7
1162.5	142.1	.724	50.6	38.5	57.7
1162.5	142.1	.724	50.6	38.5	57.7
1162.5	142.1	.724	50.6	38.5	57.7
1162.5	142.1	.724	50.6	38.5	57.7
1162.5	142.1	.724	50.6	38.5	57.7
1162.5	142.1	.724	50.6	38.5	57.7
1162.5	142.1	.724	50.6	38.5	57.7
1162.5	142.1	.724	50.6	38.5	57.7
1162.5	142.1	.724	50.6	38.5	57.7
1162.5	142.1	.724	50.6	38.5	57.7
1162.5	142.1	.724	50.6	38.5	57.7
1162.5	142.1	.724	50.6	38.5	57.7
1162.5	142.1	.724	50.6	38.5	57.7
1162.5	142.1	.724	50.6	38.5	57.7
1162.5	142.1	.724	50.6	38.5	57.7
1162.5	142.1	.724	50.6	38.5	57.7
1162.5	142.1	.724	50.6	38.5	57.7
1162.5	142.1	.724	50.6	38.5	57.7
1162.5	142.1	.724	50.6	38.5	57.7
1162.5	142.1	.724	50.6	38.5	57.7
1162.5	142.1	.724	50.6	38.5	57.7
1162.5	142.1	.724	50.6	38.5	57.7
1162.5	142.1	.724	50.6	38.5	57.7
1162.5	142.1	.724	50.6	38.5	57.7
1162.5	142.1	.724	50.6	38.5	57.7
1162.5	142.1	.724	50.6	38.5	57.7
1162.5	142.1	.724	50.6	38.5	57.7
1162.5	142.1	.724	50.6	38.5	57.7

Table A-4 (cont'd)

A_r_e_a_	Perimeter	Shape_Fac	Max_Feret	Eq._cir_d	Form_Factor
1162.5	142.1	.724	50.6	38.5	57.7
1162.5	142.1	.724	50.6	38.5	57.7
1162.5	142.1	.724	50.6	38.5	57.7
1162.5	142.1	.724	50.6	38.5	57.7
1162.5	142.1	.724	50.6	38.5	57.7
1162.5	142.1	.724	50.6	38.5	57.7
1162.5	142.1	.724	50.6	38.5	57.7
1162.5	142.1	.724	50.6	38.5	57.7
1162.5	142.1	.724	50.6	38.5	57.7
1162.5	142.1	.724	50.6	38.5	57.7
1162.5	142.1	.724	50.6	38.5	57.7
1162.5	142.1	.724	50.6	38.5	57.7
1162.5	142.1	.724	50.6	38.5	57.7
1162.5	142.1	.724	50.6	38.5	57.7
1162.5	142.1	.724	50.6	38.5	57.7
1162.5	142.1	.724	50.6	38.5	57.7

LIST OF REFERENCES

LIST OF REFERENCES

1. Hugo, F. and T. Kennedy, *Surface Cracking of Asphalt Mixtures in Southern Africa*, in Association of Asphalt Paving Technology, 1985. **54**. pp. 454-491.

2. Bouldin, M.G., J.H. Collins, and A. Berker, *Rheology and Microstructure of Polymer / Asphalt Blends.* Rubber Chemistry And Technology, 1991. **64** No. 4, September-October. pp. 577-600.

3. Baladi, G.Y., *Integrated Material and Structural Design Method for Flexible Pavements*. 1988. Federal Highway Administration.

4. Geiger, F.W., ed. *Equipment Operator 3&2, NAVEDTRA 10640-J1*. 1987. Naval Education and Training Program Management Support Activity: Washington, D.C. 11.1.

5. *Material Reference Library Asphalt Data,* in *Strategic Highway Research Program, National Research Council, Washington, D.C.* 1992.

6. *Highway Materials Engineering - Asphalt Materials and Paving Mixtures*. Vol. FHWA-HI-90-008, Washington, D.C. 1990. U.S.D.O.T, Federal Highway Administration, National Highway Institute.

7. Newcomb, D.E., M. Stroup-Gardiner, and J.A. Epps, *Laboratory and Field Studies of Polyolefin and Latex Modifiers for Asphalt Mixtures,* in *Polymer Modified Asphalt Binders, ASTM STP 1108,* K.R. Wardlaw and S. Shuler, Editor. 1992. American Society For Testing Materials: Philadelphia. pp. 129-50.

8. Jain, P.K., Sangita, S. Bose, and I.R. Arya, *Characterization of Polymer Modified Asphalt Binders for Roads and Airfields,* in *Polymer Modified Asphalt Binders, ASTM STP 1108,* K.R. Wardlaw and S. Shuler, Editor. 1992. American Society For Testing Materials: Philadelphia. pp. 341-356.

9. Hesp, S.A. and R.T. Woodhams, *Stabilization Mechanisms in Polyolefin-Asphalt Emulsions,* in *Polymer Modified Asphalt Binders, ASTM STP 1108,* K.R. Wardlaw and S. Shuler, Editor. 1992. American Society For Testing and Materials: Philadelphia. pp. 1-19.

10. Little, D., *Performance Assessment of Binder-Rich Polyethylene-Modified Asphalt Concrete Mixtures (Novophalt).* Transportation Research Record - Transportation Research Board, 1991. **1317.**

11. Anderson, D.A., *et al., Rheological Properties Of Polymer Modified Emulsion Residue,* in *Polymer Modified Asphalt Binders, ASTM STP 1108,* K.R. Wardlaw and S. Shuler, Editor. 1992. American Society For Testing Materials: Philadelphia. pp. 20-34.

12. Bouldin, M.G. and J.H. Collins, *Influence of Binder Rheology on Rut Resistance of Polymer Modified and Unmodified Hot Mix Asphalt,* in *Polymer Modified Asphalt Binders, ASTM STP 1108,* K.R. Wardlaw and S. Shuler, Editor. 1992. American Society For Testing and Materials: Philadelphia. pp. 50-60.

13. Linde, S. and U. Johansson, *Thermo-Oxidative Degradation of Polymer Modified Bitumen,* in *Polymer Modified Asphalt Binders, ASTM STP 1108,* K.R. Wardlaw and S. Shuler, Editor. 1992. American Society For Testing Materials: Philadelphia. pp. 244-253.

14. Schwager, B.P., *Viscosity Measurements of Polymer Modified Asphalt,* in *Polymer Modified Asphalt Binders, ASTM STP 1108,* K.R. Wardlaw and S. Shuler, Editor. 1992. American Society For Testing Materials: Philadelphia. pp. 254-280.

15. Rogge, D.F., R.L. Terrel, and A.J. George, *Polymer Modified Hot Mix Asphalt - Oregon Experience,* in *Polymer Modified Asphalt Binders, ASTM STP 1108,* K.R. Wardlaw and S. Shuler, Editor. 1992. American Society for Testing and Materials: Philadelphia. pp. 151-172.

16. Moore, E., *Personal Communication.* 1992.

17. Stewart, L., *Polymers: Pavement's Miracle Additive? Experience portends powerful performance, but the perfect mix design remains illusive.* Highway & Heavy Construction, 1989. pp. 48-50.

18. Farrar, M. and R. Harvey, *Performance of Binder-Modifiers in Recycled Asphalt Pavement.* Transportation Research Board 72nd Annual Meeting, January, 1993. pp. 1-25.

19. Mayama, M., M. Yshino, and K. Hasegawa, *An Evaluation Of Heavy Duty Binders in the Laboratory,* in *Polymer Modified Asphalt Binders, ASTM STP 1108,* K.R. Wardlaw and S. Shuler, Editor. 1992. American Society For Testing Materials: Philadelphia. pp. 61-76.

20. Goodrich, J.L., *Polymer and Asphalt Reaction Process and Polymer-Linked Asphalt Product.* 1991. Chevron Research and Technology Company.

21. Chollar, B.H., *et al.*, *Characteristics of the Furfural Modified Asphalt Reaction.* Transportation Research Board 72nd Annual Meeting January 10-14, 1993. Washington, D.C., pp. 1-24.

22. Stuart, K.D., *Asphalt Mixtures Containing Chemically Modified Binders.* Transportation Research Board 72nd Annual Meeting January 10-14, 1993. Washington, D.C., pp. 1-34.

23. Schwager, B.P., *Personal Communication.* 1993.

24. Statz, B., *Personal Communication.* 1993.

25. Ishai, I., Y.A. Tuffour, and J. Craus, *Some Aspects of the effect of Asphalt Chemical Composition on Material Behavior and Pavement Performance.* Transportation Research Board 72nd Annual Meeting January 10-14, 1993. Washington, D.C., pp. 1-38.

26. Jones, D.R., T.W. Kennedy, and H.F. Torshizi, *Field Performance of Polymer-Modified Asphalts.* Transportation Research Board 72nd Annual Meeting January 10-14, 1993. Washington, D.C., pp. 1-18.

27. Peltonen, P.V., *Characterization and testing of fibre-modified bitumen composites.* Journal of Materials Science, 1991. **26**. pp. 5618-5622.

28. Khosla, N.P. *Laboratory Characterization of Crumb Rubber Modified Mixtures*, in *72nd TRB Annual Meeting.* 1993. Washington, D.C.

29. Khosla, N.P., *Effect of the Use of Modifiers on Performance of Asphaltic Pavements.* Transportation Research Record, 1991. **1317**: pp. 10-22.

30. Tayebali, A.A., *et al.*, *Influence of Rheological Properties of Modified Asphalt Binders on the Load Deformation Characteristics of the Binder-Aggregate Mixtures,* in *Polymer Modified Asphalt Binders, ASTM STP 1108,* K.R. Wardlaw and S. Shuler, Editor. 1992. American Society For Testing Materials: Philadelphia.

31. Huang, S.-C., *et al.*, *Effects Of Modifiers On The Temperature Susceptibility And Aging Characteristics Of Typical Asphalt Cements Used In Florida.* Transportation Research Board 72nd Annual Meeting January 10-14, 1993. Washington, D.C., pp. 1-24.

32. Stroup-Gardiner, M., D.E. Newcomb, and B. Tanquist, *Asphalt-Rubber Interactions.* Transportation Research Board 72nd Annual Meeting January 10-14, 1993. Washington, D.C., pp. 1-30.

33. Aurilio, V., *Crumb Rubber Modified Asphalt Materials, Recycling Crumb Rubber Modified Mixtures*, in 72nd TRB Annual Meeting. 1993. Washington, D.C.

34. Brock, D.J., *Crumb Rubber Modified Asphalt Materials, Construction Considerations*, in 72nd TRB Annual Meeting. 1993. Washington, D.C.

35. Kandhal, P.S., *Crumb Rubber Modified Asphalt Materials, Specification Quality Control and Quality Assurance*, in 72nd TRB Annual Meeting. 1993. Washington, D.C.

36. Grulke, E.A., *Polymer Process Engineering*. 1994, New Jersey: PTR Prentice Hall. p. 119.

37. Gloaguen, J.M., *et al.*, *Plasticity and Fracture Initiation in Rubber-Toughened Poly(MethylMethacrylate)*. Polymer Engineering and Science, 1993. **33** (No. 12): pp. 748-753.

38. Daly, W.H., Z. Qiu, and I. Negulescu, *Preparation and Characterization of Polyethylene Modified Asphalt.* Transportation Research Board 72nd Annual Meeting January 10-14, 1993. Washington, D.C., pp. 1-17.

39. Bouldin, M.G., *Results Of Repetitive Creep Experiments Carried Out On Polymer Modified Hot Mix Asphalts Used On The Mesquite Nevada Job - Shell Development Company*. 1991, Shell Development Company.

40. Bouldin, M.G. and J.H. Collins, *Wheel Tracking Experiments with Polymer Modified and Unmodified Hot Mix Asphalt,* in *Polymer Modified Asphalt Binders, ASTM STP 1108,* K.R. Wardlaw and S. Shuler, Editor. 1990, American Society For Testing and Materials: Philadelphia.

41. Luckenbach, T.A. *Rheological Testing of Asphalt Using a Cup and Plate Geometry*. in *Petersen Asphalt Research Conference*. 1992. Western Research Institute, Laramie, Wyoming: American Society For Testing and Materials.

42. Billmeyer, F.W.J., *Textbook of Polymer Science*. 3rd ed. 1984, New York: John Wiley & Sons. p. 312.

43. Billmeyer, F.W.J., *Textbook of Polymer Science*. 3rd ed. 1984, New York: John Wiley & Sons. p. 314.

44. Hesp, S., *Personal Communication*. 1992.

45. ASM Handbook,. Vol. 12. Fractography, 1992. p. 473: fig. 1290, 1291, 1292, 1293.

46. Khosla, N.P., *Crumb Rubber Modified Asphalt Materials, Laboratory Characterization of Crumb Rubber Modified Mixtures*, in 72nd TRB Annual Meeting. 1993. Washington, D.C.

47. He, L.Y. and J.W. Button, *Methods To Determine Polymer Content Of Modified Asphalt.* Transportation Research Record - Transportation Research Board, 1991. **1317**.

48. Terrel, R.L. and S. Al-Swailmi, *The Role of Pessimum Voids Concept in Understanding Moisture Damage to Asphalt Concrete Mixtures.* Transportation Research Board 72nd Annual Meeting January 10-14, 1993. Washington, D.C. pp. 1-28.

49. Eriksen, K. *Summary Report on Specimen Preparation.* in *SHRP Symposium.* 1990. Washington, D.C.

50. Eriksen, K., *Air Void Characteristics in Asphalt-Concrete Samples from the Compaction Study.* 1992. Strategic Highway Research Program, National Research Council.

51. Eriksen, K. and A. Neidel., *Thin Sections of Asphalt Concrete Preparation Techniques*, in *SHRP Symposium.* 1990. Washington, D.C.

52. Eriksen, K. and A. Neidel., *Plane Sections of Asphalt Concrete Preparation Techniques*, in *SHRP Symposium.* 1990. Washington, D.C.

53. Eriksen, K., *Microscopical Analysis of Asphalt-Aggregate Mixture Related to Pavement Performance*, in 72nd TRB Annual Meeting. 1993. Washington, D.C.

54. Kalantar, J. and L.T. Drzal, *The Bonding Mechanism of Aramid Fibers to Epoxy Matrices, Part I A Review of the Literature.* J. Mat. Sci., 1990. **25**: pp. 4186-4193.

55. King, G.N., *et al.*, *Influence Of Asphalt Grade And Polymer Concentration On The Low Temperature Performance Of Polymer Modified Asphalt.* Prepared for Presentation at the Annual Meeting of the Association of Asphalt Paving Technologists, 1993.

56. Shuler, T.S., D.L. Hanson, and R.G. McKeen, *Design and Construction of Asphalt Concrete Using Polymer Modified Asphalt Binders,* in *Polymer Modified Asphalt Binders, ASTM STP 1108,* K.R. Wardlaw and S. Shuler, Editor. 1992, American Society For Testing Materials: Philadelphia. pp.97-128.

57. Kandhal, P.S., *et al.*, *Low Temperature Properties of Paving Asphalt Cements.* Report, Transportation Research Board, 1988. Washington, D.C.

58. Van der poel, C., *A General System Describing the Viscoelastic Properties of Bitumens and its Relation to Routine Test Data.* J. Appl. Chem., 1964. **4**.

59. Gaw, W.J., ed. *Measurement and Prediction of Asphalt Stiffness.* Technical Publication, ASTM, Vol. 628. 1977. Philadelphia, PA. pp. 57-67.

60. Readshow, E., *Asphalt Specifications in British Columbia for Low Temperature Performance.* Proc., Association of Asphalt Paving Technologists, 1972. **41**.

61. McLeod, N.W. *"A 4-Year Survey of Low Temperature Transverse Pavement Cracking on Three Ontario Test Roads.* 1972. Proceedings from Association of Asphalt Paving Technologists.

62. Serfass, J.P., A. Joly, and J. Samanos, *SBS-Modified Asphalt for Surface Dressing - A comparison Between Hot-Applied and Emulsified Binders,* in *Polymer Modified Asphalt Binders, ASTM STP 1108,* K.R. Wardlaw and S. Shuler, Editor. 1992, American Society For Testing Materials: Philadelphia. pp. 281-308.

63. King, G., *et al., Influence of Asphalt Grade and Polymer Concentration on the High Temperature Performance of Polymer Modified Asphalt.*, in *Association of Asphalt Paving Technology*, 1992. **61**, pp. 29-66.

64. Ruth, B., L. Bloy, and A. Avital, *Prediction of Pavement Cracking at Low Temperatures,* in *Association of Asphalt Paving Technology*, 1982. **51**, pp. 53-103.

65. Kausch, H.H., *Polymer Fracture.* 2nd ed. 1987, Berlin Heidelberg: Springer-Verlag. pp. 416-426.

66. Majdzadah, K., E.M. Kauffmann, and C.L. Saraf, ed. *Analysis of Fatigue of Paving Mixtures From the Fracture Mechanics Viewpoint.* Fatigue of Compacted Bituminous Aggregates Mixture, ASTM STP 508. 1972. American Society for Testing and Materials. p. 67.

67. Nahas, N.C., *et al. Polymer Modified Asphalts For High Performance Hot Mix Pavement Binders*, in *Association of Asphalt Paving Technology.* 1990.

68. Kinloch, A.J., *Adhesion and Adhesives.* 1987. New York: Chapman and Hall. pp. 280, 306-309.

69. Williams, J.G., *Fracture Mechanics of Polymers.* 1984. New York: John Wiley & Sons. p. 98.

70. Kennedy, T.W., *Use of Hydrated Lime in Asphalt Paving Mixtures,* in *Bulletin No. 325.* 1984. National Lime Association.

71. Chawla, K.K., *Composite Materials, Science and Engineering.* ed. B. Ilschner and N.J. Grant. 1987, New York: Springer-Verlag. 235.

72. Studt, T., *New Advances Revive Interest in Cement-Based Materials.* R&D Magazine, 1992. (November), pp. 74-78.

73. Speakman, J.D., *Performance Characteristics of Polypropylene (Monofilament) FRC*, in 72nd TRB Annual Meeting. 1993. Washington, D.C.

74. MacDonald, C.N. *Experiences with Steel Fiber and Expansive Cement for Concrete Slab on Ground*, in 72nd TRB Annual Meeting. 1993. Washington, D.C.

75. Yalamanchi, S.S., *Influence of Loading Type, Specimen Size, and Fiber Content on Flexural Toughness of FRC*, , in 72nd TRB Annual Meeting. 1993. Washington, D.C.

76. Larson, B.K., L.T. Drzal, and P. Soroushian, *Carbon fibre-cement adhesion in carbon fibre reinforced cement composites.* Composites, 1990. **21**(No. 3): pp. 205-215.

77. Andrews, E.H., ed. *Developments in Polymer Fracture - 1.* 1979, Applied Science Publishers LTD: London. pp. 264-265.

78. Trantina, G.G., *Fracture Mechanics Approach to Adhesive Joints.* 1971, Department of the Navy, Naval Air Systems Command.

79. Williams, J.G., *Fracture Mechanics of Polymers.* 1984, New York: John Wiley & Sons. pp. 55-58.

80. Menges, G., *Attempt to Explain Crazing in Amorphous Thermoplastics and Adhesion Fractures in Semicrystalline Thermoplastics and Filled Polymers*, in *Deformation and Fracture of High Polymers.* 1972. Kronberg, Germany: Plenum Press.

81. Katz, H.S. and J.V. Milewski, ed. *Handbook of Fillers for Plastics.* 2nd ed. 1987, Van Nostrand Reinhold Company: Chapman & Hall, New York. p. 41.

82. Kinloch, A.J. and R.J. Young, *Fracture Behaviour of Polymers.* 1983, New York: Applied Science Publishers. pp. 242-245.

83. Hellan, K., *Introduction of Fracture Mechanics.* 1984, New York: McGraw-Hill Book Company. pp. 60-61.

84. Andrews, E.H., ed. *Developments in Polymer Fracture - 1.* 1979, Applied Science Publishers LTD: London. pp. 100-103.

85. Kinloch, A.J., *Adhesion and Adhesives.* 1987, New York: Chapman and Hall. pp. 265-266, 360.

86. Williams, J.G., *Fracture Mechanics of Polymers.* 1984, New York: John Wiley & Sons. pp. 41, 175-189, 226.

87. Kausch, H.H., *Polymer Fracture.* 2nd ed. 1987, Berlin Heidelberg: Springer-Verlag. pp. 62, 224, 256, 306-312.

88. Kinloch, A.J. and R.J. Young, *Fracture Behaviour of Polymers*. 1983, New York: Applied Science Publishers. pp. 88-92, 276.

89. Andrews, E.H., ed. *Developments in Polymer Fracture - 1*. 1979, Applied Science Publishers LTD: London. p. 273.

90. Kausch, H.H., *Polymer Fracture*. 2nd ed. 1987, Berlin Heidelberg: Springer-Verlag. pp. 306-312, 393.

91. Barenblatt, G.I., *Methods of Combustion Theory in the Mechanics of Deformation, Flow, and Fracture of Polymers*, in *Deformation and Fracture of High Polymers*. 1972. Kronberg, Germany: Plenum Press.

92. Vincent, P.I., *Load-Extension Curves and Fracture Toughness*, in *Deformation and Fracture of High Polymers*. 1972. Kronberg, Germany: Plenum Press.

93. Rolland, L., *et al.*, *A Fracture Mechanics Approach to Surface Embrittlement in Ductile Polymers*, in *Fifth International Conference on Deformation, yield and fracture of polymers*. 1982. Churchill College, Cambridge: The Plastics and Rubber Institute.

94. Anderson, G.P., J.S. Bennett, and L.K. DeVries, *Analysis and Testing of Adhesive Bonds*. 1977. New York: Academic Press. p. 213.

95. Knott, J.F., *Fundamentals of Fracture Mechanics*. 1973. London: Butterworth. pp. 120, 123-125, 239-241.

96. Kausch, H.H., *Polymer Fracture*. 2nd ed. 1987. Berlin Heidelberg: Springer-Verlag. p. 61.

97. Knott, J.F., *Fundamentals of Fracture Mechanics*. 1973. London: Butterworth. pp. 211-216.

98. Hellan, K., *Introduction of Fracture Mechanics*. 1984. New York: McGraw-Hill Book Company. p. 125.

99. Kausch, H.H., *Polymer Fracture*. 2nd ed. 1987. Berlin Heidelberg: Springer-Verlag. p. 306.

100. Broek, D., *Elementary Engineering Fracture Mechanisms*. 3rd ed. 1982. Boston: Martinus Nijhoff. pp. 12-13.

101. Chawla, K.K., *Composite Materials, Science and Engineering*. ed. B. Ilschner and N.J. Grant. 1987. New York: Springer-Verlag. p. 237.

102. Knott, J.F., *Fundamentals of Fracture Mechanics*. 1973. London: Butterworth. pp. 204-206.

103. Friedrich, K., *Microstructure and Fracture Mechanical Properties of Short Fiber Reinforced Thermoplastic P.E.T*, in *Fifth International Conference on Deformation, yield and fracture of polymers*. 1982. Churchill College, Cambridge: The Plastics and Rubber Institute.

104. Wells, J.K. and P.W. Beaumont, *The Use of Fracture Maps on Failure Analysis of Fibre Composite Materials*, in *Fifth International Conference on Deformation, yield and fracture of polymers*. 1982. Churchill College, Cambridge: The Plastics and Rubber Institute.

105. Andrews, E.H., ed. *Developments in Polymer Fracture - 1*. 1979. Applied Science Publishers LTD: London. pp. 280-310.

106. Chawla, K.K., *Composite Materials, Science and Engineering*. ed. B. Ilschner and N.J. Grant. 1987. New York: Springer-Verlag. pp. 232-233.

107. Milewski, J.V. and H.S. Katz, ed. *Handbook of Reinforcements for Plastics*. 2nd ed. 1987. Van Nostrand Reinhold Company: New York. pp. 6-7.

108. Kinloch, A.J. and R.J. Young, *Fracture Behaviour of Polymers*. 1983. New York: Applied Science Publishers. p. 70.

109. Williams, J.G., *Fracture Mechanics of Polymers*. 1984. New York: John Wiley & Sons. p. 165.

110. Bucknall, C.B. and D.P. Jones, *Deformation and Fracture of Thermoplastics containing Spherical Particles*, in *Fifth International Conference on Deformation, yield and fracture of polymers*. 1982. Churchill College, Cambridge: The Plastics and Rubber Institute.

111. Kinloch, A.J. and R.J. Young, *Fracture Behaviour of Polymers*. 1983. New York: Applied Science Publishers. pp. 448-451.

112. Kinloch, A.J. and R.J. Young, *Fracture Behaviour of Polymers*. 1983. New York: Applied Science Publishers. pp. 442-448.

113. Kinloch, A.J., S.J. Shaw, and D.L. Hunston, *Crack Propagation in a Rubber-Toughened Epoxy*, in *Fifth International Conference on Deformation, yield and fracture of polymers*. 1982. Churchill College, Cambridge: The Plastics and Rubber Institute.

114. Oliphant, K. and W.E. Baker, *The Use of Cryogenically Ground Rubber Tires as a Filler in Polyolefin Blends.* Polymer Engineering and Science, 1993. **33**, No. 3: pp. 166-174.

115. Williams, J.G., *Fracture Mechanics of Polymers.* 1984. New York: John Wiley & Sons. p. 143.

116. Katz, H.S. and J.V. Milewski, ed. *Handbook of Fillers for Plastics.* 2nd ed. 1987. Van Nostrand Reinhold Company: Chapman & Hall, New York. pp. 390, 402-404.

117. Kinloch, A.J. and R.J. Young, *Fracture Behaviour of Polymers.* 1983. New York: Applied Science Publishers. p. 423.

118. Andrews, E.H., ed. *Developments in Polymer Fracture - 1.* 1979. Applied Science Publishers LTD: London. pp. 157-172.

119. Kinloch, A.J. and R.J. Young, *Fracture Behaviour of Polymers.* 1983. New York: Applied Science Publishers. pp. 451-452.

120. Katz, H.S. and J.V. Milewski, ed. *Handbook of Fillers for Plastics.* 2nd ed. 1987. Van Nostrand Reinhold Company: Chapman & Hall, New York. pp. 70-74.

121. Kinloch, A.J. and R.J. Young, *Fracture Behaviour of Polymers.* 1983. New York: Applied Science Publishers. p. 20.

122. Williams, J.G., *Fracture Mechanics of Polymers.* 1984. New York: John Wiley & Sons. p. 124.

123. Andrews, E.H., ed. *Developments in Polymer Fracture - 1.* 1979. Applied Science Publishers LTD: London. p. 114.

124. Kinloch, A.J. and R.J. Young, *Fracture Behaviour of Polymers.* 1983. New York: Applied Science Publishers. pp. 35-36.

125. Broek, D., *Elementary Engineering Fracture Mechanisms.* 3rd ed. 1982. Boston: Martinus Nijhoff. pp. 15-17.

126. Kodak, E., *Kodak EKTAPRO EM Motion Analyzer Operating Manual, Manual part number 91000022-001.* 1990.

127. Olympus, *Cue 2 Image Analyzer Operation Manual.* Version 3.0, 1989.

128. Kinloch, A.J., *Adhesion and Adhesives.* 1987. New York: Chapman and Hall. pp. 200-204.

129. Kinloch, A.J. and R.J. Young, *Fracture Behaviour of Polymers*. 1983. New York: Applied Science Publishers. pp. 93-97.

130. Williams, J.G., *Fracture Mechanics of Polymers*. 1984. New York: John Wiley & Sons. p. 18.

131. Kennedy, T., *Personal Communication*. 1992.

132. Buchman, A., *Personal Communication at 206th American Chemical Society National Meeting and Exposition, Chicago, IL*. 1993.

133. Kausch, H.H., *Polymer Fracture*. 2nd ed. 1987. Berlin Heidelberg: Springer-Verlag. p. 323.

134. Aglan, H., *et al.*, *Structure-Fracture Toughness Relationships of Asphalt Concrete Mixtures*. Transportation Research Record - Transportation Research Board, 1992. **1353** pp. 24-30.

135. Kinloch, A.J. and R.J. Young, *Fracture Behaviour of Polymers*. 1983. New York: Applied Science Publishers. p. 343.

136. ASTM_E813, *Standard Test Method for J_{IC}, A Measure of Fracture Toughness*. Annual Book of ASTM Standards, 1993. **3.01**, pp. 738-752.

137. ASTM_D5045, *Standard Test Methods for Plane-Strain Fracture Toughness and Strain Energy Release Rate of Plastic Materials*. Annual Book of ASTM Standards, 1993. **8.03**, pp. 314-322.

138. Vipulanandan, C. and N. Dharmarajan, *Fracture Toughness of Polymer Concrete*, in *Fracture Mechanics: Application to Concrete*, C.L. Victor and P.B. Zdenek, Editor. 1989. American Concrete Institute: Detroit, MI. pp. 69-90.